Role of Homotypic Membrane Fusions in Size Control Mechanism of Golgi Apparatus

By

Madhura Bhave

LIFE09200904009

Tata Memorial Centre

A thesis submitted to the Board of Studies in Life Sciences

In partial fulfillment of requirements for the Degree of

DOCTOR OF PHILOSOPHY

of

HOMI BHABHA NATIONAL INSTITUTE

JUNE,2015

Homi Bhabha National Institute

Recommendations of the Viva Voce Committee

As members of the Viva Voce Committee, we certify that we have read the dissertation prepared by **Ms. Madhura Bhave** entitled "**Role of homotypic membrane fusions in size control mechanism of Golgi apparatus**" and recommend that it may be accepted as fulfilling the thesis requirement for the award of Degree of Doctor of Philosophy.

Chairman – Dr. Rajiv Kalraiya R Kalraiya **Date:** 29/06/2015

Guide / Convener – Dr. Dibyendu Bhattacharyya Dibyendu Bhattacharyya **Date:** 29/06/2015

Member 1 – Dr. Prasanna Venkatraman **Date:** 29/06/15

Member 2- Dr. Milind Vaidya **Date:**

External Examiner- Dr. Suman Kumar Dhar Suman Kumar Dhar **Date:** 29/06/15

Final approval and acceptance of this thesis is contingent upon the candidate's submission of the final copies of the thesis to HBNI.

I/We hereby certify that I/we have read this thesis prepared under my/our direction and recommend that it may be accepted as fulfilling the thesis requirement.

Date: 29/6/2015

Place: ACTREC, Kharghar

Guide Dibyendu Bhattacharyya

STATEMENT BY AUTHOR

This dissertation has been submitted in partial fulfillment of requirements for an advanced degree at Homi Bhabha National Institute (HBNI) and is deposited in the Library to be made available to borrowers under rules of the HBNI.

Brief quotations from this dissertation are allowable without special permission, provided that accurate acknowledgement of source is made. Requests for permission for extended quotation from or reproduction of this manuscript in whole or in part may be granted by the Competent Authority of HBNI when in his or her judgment the proposed use of the material is in the interests of scholarship. In all other instances, however, permission must be obtained from the author.

Madhura Bhave

DECLARATION

I, hereby declare that the investigation presented in the thesis has been carried out by me. The work is original and has not been submitted earlier as a whole or in part for a degree / diploma at this or any other Institution / University.

Madhura Bhave

List of Publications arising from the thesis

1. **Madhura Bhave**, Effrosyni Papanikou, Prasanna Iyer, Koushal Pandya, Bhawik Kumar Jain, Abira Ganguly, Chandrakala Sharma, Ketakee Pawar, Jotham Austin II, Kasey J. Day, Olivia W. Rossanese, Benjamin S. Glick and Dibyendu Bhattacharyya, Golgi enlargement in Arf1 depleted yeast cells is due to altered dynamics of cisternal maturation. **J Cell Sci**, 2014.127(Pt 1): p. 250-7.
2. Elisabeth A. Montegna, **Madhura Bhave**, Yang Liu, Dibyendu Bhattacharyya, Benjamin S. Glick, Sec12 binds to Sec16 at transitional ER sites. **PLoS One**, 2012. **7**(2): p. e31156

Conferences

1. **Won 1nd prize** for poster presentation on ‘Size control mechanism of Golgi apparatus: Role of Arf1’ at Indian Association for Cancer Research, held in ACTREC, Jan 2012.
2. **Presented Poster** on ‘intracellular intelligence : Size control mechanism of organelles’ in All India Cell Biology conference held in Kolkata, Dec 2010
3. **Presented Poster**on ‘COPI recruitment function as a decision making step for the size control mechanism of Golgi apparatus’ in meeting of Society for Biological Chemists, India held in Indian Institute of Sciences (IISc) Bangalore, Dec 2010.
4. **Presented poster** on ‘Molecular supervisors of Golgi size regulation’ in international conference of American Society for Cell Biology, held in Philadelphia, December 2014.

Madhura Bhave

To my mother,

Your innumerable sacrifices, love & faith in me have made this possible for me.

ACKNOWLEDGEMENTS

I wish to express my gratitude to my mentor Dr. Dibyendu Bhattacharyya for giving me an opportunity to work on this interesting project and for introducing me the intriguing field of Organelle biology.

I thank Dr. Chiplunkar (Director, ACTREC), Dr. Rajiv Sarin (ex-Director, ACTREC), Dr. Surekha Zingde (ex-Dy. Director, ACTREC), for providing the entire research infrastructure. I am thankful to all my doctoral committee members, Dr. Rita Mulherkar (Ex-Chairperson), Dr. Rajiv Kalraiya (Chairperson), Dr. Prasanna Venkatraman, Dr. Milind Vaidya for their critical and valuable suggestions for improving the thesis. I owe my sincere thanks to our collaborator Dr. Benjamin Glick (University of Chicago) for his valuable inputs and for some of the constructs and yeast strains used in this study.

In addition, I thank Dr. Gajanan Zore (Assistant Professor, Biotechnology, SRTM University, Nanded) for introducing me to the world of science and for encouraging me to join PhD program.

My sincere thanks to all the following imaging facilities I had access to, for completing my PhD work. ADIF (ACTREC Digital Imaging Facility), Imaging facility-IISER Pune, Microscopy facility-University of Chicago, Central Imaging and Flow Cytometry Facility (CIFF)- NCBS and Dr. Sudipta Maiti- TIFR for his suggestions for challenging 4D microscopy experiments.

I take this opportunity to thank ADIF staff, especially Vaishali, Tanuja, Jairaj for their constant help.

I am also thankful to staff in CIR- Mr. Dandekar, Mr. Kulkarni who were always very helpful to solve any instrument related problems.

I would also like to thank staff from Photography, and library for their help whenever needed.

With constant support, valuable inputs from scientific discussions my dear lab members have helped me through thick and thin, during my entire PhD tenure. I would say thanks to all Organelle Biology lab members Abira Ganguly, Prasanna Iyer, Kaushal Pandya, Ketki Pawar, Bhawik Kumar Jain and Pravin Marathe. They really made difficult times easier for me with tons of jokes, funny fights and laughter. Countless amazing food parties and tea sessions will always be cherished.

I would also like to take this opportunity to thank the past lab members Rincy, Muthu, Munmun, Janhvi for their help towards completing this project.

Without excellent technical help, I could not have completed this study and I cannot forget to thank Mansi Samarth, Sanjay Dabholkar, Vinit Yadav for their timely help.

Batchmates for sure have been the strongest pillars during the entire PhD journey. Right from course work up to thesis writing they have been wonderful companions. I enjoyed discussing work problems, all the batch outings, birthday parties. Special thanks to Rupa, Pooja, Snehal, Sushmita, Shrikanta, Shafqat, Tanmoy for keeping the atmosphere so lively.

I would also like to thank seniors Dr. Ajit Chande, Dr. Amitabha Mukhopadhyaya and Dr. Padma Nannaware and Monika Tyagi from whom I got to learn many things.

Finally, I dedicate my warmest gratitude to all my family members for their love and constant faith in me. Thank you so much for your endless support and tolerating my absence in most of the occasions.

Thank you all

Madhura

INDEX

Synopsis

Homi Bhabha National Institute

Ph. D. PROGRAMME

1. Name of the Student: **Ms. Madhura Bhave**
2. Name of the Constituent Institution: **ACTREC**
3. Enrolment No. **LIFE09200904009**
4. Title of the Thesis: **Role of homotypic membrane fusions in size control mechanism of Golgi apparatus**
5. Board of Studies: **Life Sciences**

SYNOPSIS

Role of homotypic membrane fusions in size control mechanism of Golgi apparatus.

Introduction:

Regulation of sizes of intracellular organelles is one of the fundamental problem of cell biology[2]. Each type of cell maintains its size or volume at a constant value. In the same way, sizes of various intracellular organelles are also maintained in a much regulated manner. In spite of being such a fundamental question, the mechanism by which a cell senses changes in organelle size and regulates the same is not yet clearly understood. It is also observed that perturbation in organelle size is often linked to diseases like cancer and others.

The Golgi apparatus is essential for protein sorting and transport. The Golgi apparatus is known for its characteristic structure which is conserved in species specific manner. If membrane budding is inhibited from trans Golgi network, there is expansion of TGN [3]. Size and organization of Golgi apparatus is altered in various neurological disorders as well as some type of cancers [4, 5]. Apart from diseases, Golgi size is also altered in some physiological conditions, for example, during hormonal changes at parturition, there is a rapid expansion of the Golgi. But how size of this organelle is controlled in normal case is not known.

The Golgi apparatus is not a stable structure; instead, new cisternae are continuously being formed at cis face and late cisternae are continuously being disintegrated at trans face of the Golgi apparatus. The secretory vesicles known as COPII coated vesicles emerge from specialized sub-domains of ER, called ER exit sites (ERES) or transitional ER sites. They carry cargo that needs to be modified and transported through Golgi apparatus. Once budded from ERES, these vesicles fuse to each other by homotypic membrane fusion. These fusions of COPII vesicles continue

and lead to formation of pre-Golgi elements which later on develop into cis-Golgi cisternae. According to cisternal maturation model [6, 7], these cisternae then mature to medial and then trans Golgi by acquiring new marker enzymes specific to type of cisternae. So basically ERES are the birth places of Golgi apparatus. For this reason to understand the size control mechanism of Golgi it is also essential to study ERES, especially the factors that controls it size.

In present dissertation, role of Sec12 in regulation of size of ERES was studied. The study also included systematic characterization of a Golgi size mutant, and role of Arf1 in Golgi size control. The contribution of homotypic membrane fusion in size control of Golgi was also assessed.

Aims and Objectives:

1. Role of Sec12 in regulation of size and dynamics of ERES.
2. Characterization of CMOSS-G-1(Ts Golgi size mutant)
3. Studying role of ARF1 in regulation of Golgi size.
4. To visualize the homotypic membrane fusion in real time in altered ARF1 function background.

Materials and methods:

Preparation of ultra-competent cell: *E.coli* strain DH5α MCR was made ultra-competent for the transformation of ligated DNA or plasmid vectors. A single colony was inoculated in 250 ml SOB broth and incubated at 18°C /250 rpm till O.D.600 reached ~0.4. The cells were harvested by pelleting down at 4°C and re-suspended in 80 ml of Transformation buffer (TB) followed by incubation on ice for 10 min and centrifugation. The cell pellet was re-suspended in 18.6 ml TB. 1.4 ml (7%) DMSO was added to the cells and mixed completely. 200µl aliquots of the cells were made in sterile microfuge tubes and snap frozen in liquid nitrogen followed by storage at -80°C.

Plasmid miniprep: Minipreps for cloning and expression purpose was mostly done by kit based on column purification (Qiagen miniprep kit).

Growing yeast cultures: All experiments were performed with derivatives of the haploid S. cerevisiae strain JK9-3d, which has the genotype leu2-3,112 ura3-52 rme1 trp1 his4 [8]. Yeast were grown in rich glucose medium (YPD) or minimal glucose medium (SD) (Sherman, 1991), with shaking at 200 r.p.m. in baffled flasks. Wild-type strains were grown at 30°C unless otherwise indicated. Thermo sensitive mutants were grown at 25°C, and then shifted to 37°C for 30 minutes before analysis.

Yeast transformation: The yeast strain was grown overnight to an OD_{6oo} of 0.5 - 1.0 with good aeration in 50 mI YPD. The cells were spun for 3 min at 3000 rpm at room temperature in a tabletop centrifuge. The pellet was re-suspended in 20 ml sterile ddH_2O. Cells were spun again, and re-suspended in 0.5 ml 0.1M LiAc. Cell suspension was transferred to a sterile Eppendorf tube. The cell suspension was incubated for 15 min at 30^0C in a water bath. Meanwhile, an aliquot of single-stranded carrier DNA (Bio 101 #2200-205) was boiled for 10 min, and then cooled in an ice/water bath. For each transformation, 5 µl boiled carrier DNA and approximately 100 ng transforming DNA (in 5 µl or less) were added to a sterile Eppendorf tube at room temperature. The cell suspension was vortexed briefly, and 50 µl cell suspensions were added to each transformation tube. Mixture was vortexed briefly. To each tube, 300 µl PEG/LiAc was added and mixed by repeated gentle pipetting with a P-1000. The tubes were incubated 30 min at 30^0C. Heat shock was given to cells for 15 min at 42^0C. Cells were spun l-0 sec in a microfuge at top speed, and PEG/LiAc supernatant was removed. The cell pellet was gently re-suspended in 200 µl sterile ddH_2O. 100 µl of cells were spread onto a selective plate. Plates were incubated until colonies appeared.

Genomic DNA isolation from yeast: 10ml yeast culture was grown overnight. The culture was spun for 5min, 3000 rpm. R.T. Supernatant was removed and pellet was re-suspended in 0.5 ml MQ.

Again cells were spun at room temperature and supernatant was removed carefully. The pellet was disrupted by vortexing briefly. Cells were re-suspended in 200 µl breaking buffer (2% Triton X-100, 1% SDS, 100mM NaCl, 10mM Tris-Cl pH8, 1mM EDTA, pH 8). 0.3 g (200µl in vol.) glass beads and 200 µl phenol (cold)/chloroform was added. The mixture is vortexed at highest speed for 3min. 200 µl T.E buffer is added, vortexed briefly. Micro centrifuged for 5 min, highest speed/R.T. The aqueous layer is transferred to fresh tube. 1 ml 100% ethanol (ice cold) is added, mixed by inversion. The vials centrifuged for 3 min at high speed at room temperature. Supernatant is removed and re-suspended pellet in 0.4 ml 1 XT.E. Buffer. 3 µl of 1mg/ml DNase-free RNase A is added, mixed and incubated 5 min at 37°C. 10 µl of 4M Ammonium acetate and 1ml of 100% ethanol is added. The contents of vials were mixed by inversion, again incubated at -20°C and centrifuged 10-15 min, room temperature. Supernatant is discarded and pellet is allowed to air dry. DNA is dissolved in 100 µl TE buffer and stored in -20°C.

Live cell imaging yeast mutants in laser confocal microscope: Confocal imaging was performed with either a Leica SP5 or a Zeiss LSM 780 for 4D imaging, or a Zeiss LSM 510 META or LSM 710 for single time-point measurements, equipped with 1006 or 63X 1.4 NA objectives. Cells grown to log phase at 25°C or 30°C in non-fluorescent or minimally fluorescent SD medium were immobilized on glass-bottomed dishes (Cell EandG, Houston, TX, USA) using Concanavalin A (Sigma-Aldrich) as previously described [9], and were imaged at room temperature. Single- or dual-color data sets were obtained using separate excitation and capture of red and

green signals, with a pinhole of 1.0–1.2 AU and with line averaging of 4 to improve the signal-to-noise ratio. The pixel size was 70–90 nm. Optical sections were 0.25–0.40 mm apart, and, 15–20 optical sections were collected to span an entire cell. Z-stacks were collected at intervals of 2–4 seconds. To limit photo damage, laser illumination was minimized and confocal scans were carried out as quickly as possible.

Image processing: Fluorescence micrographs were assembled using Adobe Photoshop, with uniform adjustments of brightness where appropriate. Projected movies of 4D confocal data sets were generated and quantified using ImageJ as follows. To remove shot noise, individual optical sections were processed with a custom plugin that implemented a 3D version of a 3*3 hybrid median filter[10]. The processed optical sections were then average projected and corrected for exponential photo bleaching [9], and the fluorescence and transmitted light channels were merged

Quantification of statistical parameters from confocal images: Images were opened in IMARIS software for 3D visualization. The number of cisternae was calculated in every frame. Homotypic fusion events were calculated per minute. Maturation frequency was calculated as events of green cisternae turning red per minute. Persistence time was calculated as time taken for green cisternae from first appearing until it turned into red cisternae. For red cisternae, persistence time was calculated as time period from appearance of red cisternae until it completely disappeared.

Mammalian cell culture: Adherent cell lines were cultured in DMEM. The media was supplemented with 10% fetal bovine serum (FBS) and 1% antibiotics. The cells were maintained in a humidified CO2 incubator at 37°C and 5% CO2. Cell lines were stored in freezing medium (medium + 10% DMSO) in liquid Nitrogen. Transfection

of cells was done in ~60 % confluent monolayer of cells with standard CaPO4 method.

Cell lysis and immunoprecipitation: The cells were harvested at 24 h post-transfection, and lysed in 50 mM Tris- HCl, pH 7.9, 50 mM NaCl, 1 mM phenylmethylsulfonyl fluoride, 0.5% NP-40 supplemented with the Complete mini protease inhibitor cocktail (Roche). Approximately 3 mg of cell lysate was used for each immunoprecipitation. Protein A-agarose beads (Calbiochem) were pre-blocked with 1% bovine serum albumin and then incubated at 4^0C with polyclonal rabbit anti-FLAG antibody (Sigma). Immunoprecipitation was performed overnight at 4^0C. Then the beads were washed three times with 20 mM Na^+-HEPES, pH 7.9, 100 mM NaCl, 0.1% NP-40. Finally, bound material was eluted by boiling in SDS-PAGE sample buffer.

Immunoblotting: Proteins were resolved mostly by denaturing SDS-PAGE and transferred onto a PVDF membrane. The blot was blocked with 5% nonfat milk/BSA in Tris buffered saline and subjected to incubation with primary antibody followed by 3 washings with TBST. Post incubation of blot with secondary antibody and 5 washings with TBST, it was analyzed with a chemiluminescent substrate detection system.

Immunofluorescence: Improved immunofluorescence protocol was used to detect Sec12[11]. Human Sec12 was detected using an affinity purified goat anti-human PREB antibody from RandD Systems (cat. #AF5557, diluted 1:50), and Sec16A was detected using a rabbit polyclonal anti-KIAA0310 antibody from Bethyl Laboratories (cat. No. #BL2467, diluted 1:50). These primary antibodies were detected with Alexa Fluor 594 donkey anti-goat and Alexa Fluor 488 chicken anti-rabbit IgG secondary antibodies (Invitrogen), respectively.

Results:

1. Role of Sec12 in regulation of size and dynamics of ERES or tER. It was known that Sec12 localizes to general ER in mammalian cells but immunofluorescence data described before were not adequately conclusive. Improved method of immunofluorescence can preserve delicate structures like ERES; even in harsh fixation treatments[11]. By using improved immunofluorescence method, we observed that Sec12 concentrates at ERES along with general ER. It was also observed that Sec12 cytosolic domain interacts with C-terminal conserved domain of Sec16 which is well known marker of ER exit sites. Sec12 and Sec16 also co-localize in live cell condition as observed by confocal microscopy. Over expression of Sec12 GFP causes enlargement of ERES. It was observed that Sec12 at low expression level localizes to ERES giving normal size distribution of ERES punctae; but as expression level increases, Sec12 punctae become larger and after a threshold level, Sec12 can no longer be held at ER exit sites and then falls back to general ER. On the contrary, if Sec12 and Sec16 (binding partner at ER exit sites) are over expressed in same proportion, although ERES become larger in size, Sec12 still localizes to ERES presumably does not fall back to general ER as evidenced standard light microscopy.

2. Characterization of Temperature sensitive Golgi size mutant: A temperature sensitive Golgi size yeast mutant [12] showed larger Golgi cisterna size as measured from Sec7 GFP punctae compared to wild type. The total number of Golgi cisternae was also reduced compared to wild type. The mutation was found out by complementing with wild type genomic library. Two clones from wild type genomic library rescued temperature sensitive phenotype. Both clones shared ORF of NMT1 gene. Wild type NMT1 was then cloned and expressed in Golgi size mutant. Wild type NMT1 gene was able to complement the large Golgi phenotype. The sequencing

data showed T400I mutation in NMT1 gene. When T400I mutation was corrected in the genome of Golgi size mutant, the large Golgi phenotype was rescued.

3. Studying role of ARF1 in regulation of Golgi size: ARF1 is one of the substrate of NMT1. To check if NMT1 regulates size of Golgi spots through ARF1, WT ARF1 was over expressed in Golgi size mutant. Over expression of WT ARF1 rescued the large Golgi phenotype. To further study role of ARF1 on Golgi size, ARF1 was completely deleted from wild type background by PCR based gene disruption method. Deletion of ARF1 resulted in further enlargement of Golgi size compared to NMT1 mutant background and severe reduction in number of Golgi cisternae.

4. To visualize the homotypic membrane fusion in real time in altered ARF1 function background: Golgi cisternae are formed by homotypic fusions of COPII vesicles coming out from ER. These vesicles are around 50nm structures which are beyond scope of detection by light microscopy. So to actually visualize these fusion events in live cell condition, we used arf1 deletion background in which size of Golgi cisternae is already enlarged. Different early Golgi markers were then tagged with GFP that mark different stage of maturation of vesicles fusion to all the way up to Golgi to identify the marker which represents the exact stage of homotypic fusions. It was found that Vrg4 a well-known early Golgi marker and Gea2 were able to show homotypic fusion events in arf1Δ background. Vrg4 showed lesser homotypic fusion frequency compared to Gea2.From the 4D movies taken for Vrg4-Sec7 strain, it was found out that number of late Golgi cisternae were dramatically reduced in arf1 deletion background. It was also observed that persistence time of early Golgi cisternae was specifically increased. Along with this, frequency of maturation of early cisternae to late cisternae was reduced in arf1deletion background.

Discussion:

In the first part of study, the objective was to find out role of Sec12 in size control of ERES. We found out Sec12 over expression creates larger ERES. In case of Golgi size study, large Golgi phenotype shown by NMT1 mutation further pointed possible role of Arf1 in Golgi size control as Arf1 is well known substrate of NMT1. Arf1 was also previously reported to play role in altered Golgi phenotype [13]. As expected, deletion of Arf1 resulted in further enlarged Golgi phenotype. According to our study, arf1 deletion specifically increases persistence time of early Golgi cisternae and also decreases frequency of early to late maturation events. Slow maturation of Golgi cisternae explains delay observed in secretion [13].

Although the mechanistic details of how exactly arf1 deletion specifically slows down maturation of early cisternae, needs to be determined, we have provided a simplistic model of maturation kinetics alteration. The decrease in Arf1 may compromise the recruitment or function of the COPI vesicle coat, since a thermo sensitive COPI allele was reported to slow Golgi maturation at the restrictive temperature [6]. Arf1 deletion may perturb lipid metabolism [13]. Arf1 deletion is known to induce the unfolded protein response [14], which in turn alters phospholipid biosynthesis and other aspects of the secretory pathway [15]. Two reports in past implicated Arf as a factor for regulation of Golgi size [13, 16] and our study although started with an unbiased approach, through NMT1, also points to Arf1 as a key regulator of maturation and morphology of Golgi cisternae in *S. cerevisiae*.

To conclude, in this study we found out that over expression of Sec12 creates larger ERES possibly because of inhibiting export from ERES. Through unbiased approach, we have been able find out a key gene that is regulating Golgi size in *S. cerevisiae.* We first found out that mutation in NMT1 gene leads to larger Golgi

phenotype. Deletion of Arf1 led to further enlarged Golgi phenotype. We also discovered that deletion of Arf1 causes slower maturation of early Golgi cisternae thus affecting number and size of early as well as late Golgi cisternae. We were also able to capture homotypic fusions in live cell condition giving rise to new Golgi cisternae in altered arf1 background.

References:

1. Chan, Y.H. and W.F. Marshall, *Scaling properties of cell and organelle size.* Organogenesis, 2010. **6**(2): p. 88-96.
2. Wang, Y.J., et al., *Phosphatidylinositol 4 phosphate regulates targeting of clathrin adaptor AP-1 complexes to the Golgi.* Cell, 2003. **114**(3): p. 299-310.
3. Baloyannis, S.J., et al., *The acoustic cortex in frontotemporal dementia: a Golgi and electron microscope study.* Acta Otolaryngol, 2011. **131**(4): p. 359-61.
4. Kellokumpu, S., R. Sormunen, and I. Kellokumpu, *Abnormal glycosylation and altered Golgi structure in colorectal cancer: dependence on intra-Golgi pH.* FEBS Lett, 2002. **516**(1-3): p. 217-24.
5. Losev, E., et al., *Golgi maturation visualized in living yeast.* Nature, 2006. **441**(7096): p. 1002-6.
6. Matsuura-Tokita, K., et al., *Live imaging of yeast Golgi cisternal maturation.* Nature, 2006. **441**(7096): p. 1007-10.
7. Kunz, J., et al., *Target of rapamycin in yeast, TOR2, is an essential phosphatidylinositol kinase homolog required for G1 progression.* Cell, 1993. **73**(3): p. 585-96.
8. Bevis, B.J., et al., *De novo formation of transitional ER sites and Golgi structures in Pichia pastoris.* Nat Cell Biol, 2002. **4**(10): p. 750-6.
9. Hammond, A.T. and B.S. Glick, *Raising the speed limits for 4D fluorescence microscopy.* Traffic, 2000. **1**(12): p. 935-40.
10. Bhattacharyya, D., A.T. Hammond, and B.S. Glick, *High-quality immunofluorescence of cultured cells.* Methods Mol Biol, 2010. **619**: p. 403-10.
11. Rossanese, O.W., et al., *A role for actin, Cdc1p, and Myo2p in the inheritance of late Golgi elements in Saccharomyces cerevisiae.* J Cell Biol, 2001. **153**(1): p. 47-62.
12. Gaynor, E.C., et al., *ARF is required for maintenance of yeast Golgi and endosome structure and function.* Mol Biol Cell, 1998. **9**(3): p. 653-70.
13. Jonikas, M.C., et al., *Comprehensive characterization of genes required for protein folding in the endoplasmic reticulum.* Science, 2009. **323**(5922): p. 1693-7.
14. Travers, K.J., et al., *Functional and genomic analyses reveal an essential coordination between the unfolded protein response and ER-associated degradation.* Cell, 2000. **101**(3): p. 249-58.
15. Peyroche, A., et al., *The ARF exchange factors Gea1p and Gea2p regulate Golgi structure and function in yeast.* J Cell Sci, 2001. **114**(Pt 12): p. 2241-53.

Publications from thesis

1. Madhura Bhave, Effrosyni Papanikou, Prasanna Iyer, Koushal Pandya, Bhawik Kumar Jain, Abira Ganguly, Chandrakala Sharma, Ketakee Pawar, Jotham Austin II, Kasey J. Day, Olivia W. Rossanese, Benjamin S. Glick and Dibyendu Bhattacharyya, Golgi enlargement in Arf1 depleted yeast cells is due to altered dynamics of cisternal maturation. J Cell Sci, 2014.127(Pt 1): p. 250-7.

2. Elisabeth A. Montegna1, **Madhura Bhave**, Yang Liu, Dibyendu Bhattacharyya, Benjamin S.Glick, Sec12 binds to Sec16 at transitional ER sites. PLoS One, 2012. **7**(2): p. e31156.

Conferences

1. **Won 1nd prize** for poster presentation on 'Size control mechanism of Golgi apparatus: Role of Arf1' at Indian Association for Cancer Research, held in ACTREC, Jan 2012.
2. **Presented Poster** on 'intracellular intelligence : Size control mechanism of organelles' in All India Cell Biology conference held in Kolkata, Dec 2010.
3. **Presented Poster** on 'COPI recruitment function as a decision making step for the size control mechanism of Golgi apparatus' in meeting of Society for Biological Chemists, India held in Indian Institute of Sciences (IISc) Bangalore, Dec 2010.

4. **Presented poster** on 'Molecular supervisors of Golgi size regulation' in international conference of American Society for Cell Biology, held in Philadelphia, December 2014.

Signature of Student:

Date: 18/9/2014

Doctoral Committee:

S. No.	Name	Designation	Signature	Date
1.	Dr. Rajiv Kalaraiya	Chairman		18.9.14
2.	Dr. Dibyendu Bhattacharyya	Guide/ Convener		18.9.14
4.	Dr. Prasanna Venkatraman	Member		18.9.14
5.	Dr. Milind Vaidya	Member		18.9.14

Forwarded through:

18/9/14

Dr. S. V. Chiplunkar
Director,
Chairperson,
Academics and Training Programme,
ACTREC

Dr. K.S. Sharma
Director Academics,
Tata Memorial Centre

Prof. K.S. Sharma
DIRECTOR - ACADEMICS, TMC
Mumbai - 400 012

Abbreviations

ER	Endoplasmic reticulum
ERES	ER exit sites
tER	Transitional ER exit sites
COPII	Coat protein complex II
COPI	Coat protein complexI
EM	Electron microscopy
VSV-G	Vesicular stomatitis virus glycoprotein
NSF	N-ethylmaleimide sensitive factor
SNAP	Soluble NSF attachment proteins
SNARE	Soluble NSF Attachment Protein receptor
ERGIC	ER-Golgi intermediate compartment
GEF	guanine nucleotide exchange factor
GAP	GTPase-activating protein
SOB	Super optimal broth
GTP	Guanosine triphosphate
GDP	Guanosine diphosphate
PREB	prolactin regulatory element binding protein
FRAP	Fluorescence recovery after photobleaching
MTOC	Microtubule organizing center
VTC	Vesicular-tubular cluster
GT	Glycosyl transferase
TGN	Trans Golgi network
GFP	Green fluorescent protein
DMEM	Dulbecco's Modified Eagle's Medium
Ts	Temperature sensitive
WT	Wild type

List of figures

List of tables:

Chapter 1

Introduction and Review of Literature

This introduction will brief about the organelles of intracellular secretory pathway and their size regulation. Initially the introduction focusses on general speculations of organelle size control which is followed by introduction to the early secretory pathway. Finally the structure and function of ER exit sites (ERES) as well as Golgi apparatus and existing knowledge on their size control mechanisms will be summarized. A short description about function of some of the proteins involved in size control mechanism of the ERES and Golgi apparatus is also included.

Organelle size control:

Size of a cell varies considerably among different organisms. Even within the same organism, different tissue types and different developmental stages show cell size variation. In spite of these cell size variations, cells always maintain a constant ratio of their size with the size of organelles within it. Natural modulation of the organelle size during changing developmental stages is an intriguing phenomenon. Many examples show that organelles inside a cell are always being scaled up or down with reference to cell size. But how this scaling is achieved at molecular level is not completely understood. Organelle size is important because of its immediate connection with the function of organelle. For example it is important to have sufficient flagellar length in order to swim efficiently [17].

The presence of different organelles in a cell serves an important purpose. Biochemical reactions are segregated from cytoplasm in order to carry them out more efficiently in controlled conditions. For example, beta oxidation of fatty acids occurs inside mitochondria while fatty acid chain elongation takes place on the endoplasmic reticulum (ER) membrane. Thus organelles also separate different cellular reactions from each other. In a way, each organelle can be considered as a reaction vessel which provides controlled conditions under which the desired reaction can take place [18]. If this is true, then the size of the reaction vessel will be very important as it will directly decide the amount of the product being formed. The significance of organelle size on the function of cell is indicated by the fact

that in specialized cells, the organelles important for performing its specialized function are found to be enlarged compared to other cell types. For example, in secretory cells the requirement for a high rate of flux of secreted proteins is achieved by a massive over proliferation of ER and Golgi apparatus. Other examples include changes in mitochondrial abundance as a function of respiratory state, proliferation of microvilli on the surface of cells lining the intestine, increased surface area and volume of rhodopsin containing vesicles in rods versus cone cells, and enlarged lipid droplets in adipose cells. But how is this organelle size regulated in the first place?

Hypothetically, there could be many ways of organelle size control mechanisms existing in the cell. Some of them are discussed here [18].

1. Limiting precursor: One way to regulate organelle size can be to produce a fixed amount of a critical structural precursor so that the amount of available precursor will define size of the organelle. In this model, number of a particular organelle will be inversely proportional to size of that organelle[19]. An example of this is size regulation of centrosomes [20].

2. Constant growth: Cell and organelles both might grow at a constant rate. In this model, without measuring organelle size time to time, the cell and organelle will both grow at constant rate.

3. Feedback based on size measurement: According to this, a cell can have various sensor molecules which have to be capable of measuring organelle size. Based on the measurements by sensor, the desired control of organelle size can be achieved. For linear structures, there are ruler molecules whose length matches the length of organelle [21, 22].

4. Feedback based on organelle function: An organelle which synthesizes a particular product might increase its size if there is a need for increased quantities of that product by the cell. Organelle function-based feedback control allows organelle size

to be automatically adjusted to the physiological needs of the cell. Such a control mechanism can be considered to be followed by ER in which unfolded protein response determines the synthesis of ER resident proteins and inositol response governs synthesis of membrane lipids [23, 24].

5. Self-balancing of opposing influences: In case of a dynamic organelle, size of an organelle at steady state is the result of constant rate of assembly and disassembly of the organelle structure. In such a case if any of the rates is altered, that will result in the alteration of size of that organelle. Such a control mechanism can explain size control of eukaryotic flagella, whose axonemal microtubules undergo continuous disassembly at a constant rate which is balanced by continuous assembly. The assembly is dependent on transport from the cell body up to the tip of the flagella which makes the assembly rate a decreasing function of length [25]. So there is only one value that matches the disassembly and assembly rate which defines the length of flagella [26].

6. Structural scaffold – The size of organelle might be shaped by a molecular scaffold. The scaffold's size will itself depend on the other regulatory mechanisms. An example of this mechanism is the clathrin coat, which sterically constrains the size and curvature of endocytic vesicles while it is assembled.

Recently several groups gave insight about regulation of size of different organelles. For example, nuclear transport can be considered as a major means of scaling nuclear size [27]. Results of some preliminary studies to find out how the flagellar length is controlled, showed that cells use a constitutive method to maintain correct flagellar length by using constant turnover of flagellar components so that flagellar length remains sensitive to the available pool of precursor, which is regulated in the cytoplasm [28]. In order to regulate size of membrane bound dynamic organelles, rates of vesicle fusion and vesicle fission play crucial role to determine size at steady state [29].

Need to study organelle size control: The scaling of organelle size to cell size is very important for the normal functioning of cells. If the scaling is disturbed, it often leads to an altered function of the organelle. There are several reports supporting the importance of organelle size regulation. Many cancer cells have an enlarged nucleus. Pap smear test, used for the detection of cervical cancers even today, is based on the presence of abnormally large nuclei. The enlarged vacuole found in fab1 mutants leads to improper karyogamy and fitness defects [30]. Defects in the length of mitotic spindle can result in improper chromosome separation [31]. Enlarged size of Golgi cisternae in arf1Δ leads to decreased rates of secretion [32]. The size and morphology of the Golgi apparatus in endothelial cells determines the size and functionality of a medically important secretory granule. The size of Golgi cisternae is directly proportional to the size of a secreted particle, the Weibel-Palade body (WPB) in endothelial cells. The size of WPB in turn is directly proportional to the length of the Willebrand factor (vWF) which serve as tethers to capture platelets during injury [33]. The size of cilia and flagella is also critically regulated to achieve efficient motility [34, 35]. Such findings stress upon the importance of studying the mechanism behind the regulation of organelle size in normal circumstances.

The Secretory Pathway: An overview

George Palade, a founding father of cell biology, established the ultrastructural framework for an understanding how cargo proteins are secreted and membranes are assembled in eukaryotic cells. He used the techniques to preserve membranes for ultrastructural analysis by transmission electron microscopy. George Palade used the technique of pulse-chase autoradiographic tracing of newly synthesized zymogen proteins. He observed the labeled proteins marching progressively from the endoplasmic reticulum (ER) through the Golgi complex and storage granules to the cell surface [36]. In every cell, proteins once synthesized on rough ER pass through several post translational modifications steps and sorting before they can be functionally active at the desired location inside or outside the cell. To achieve this, cells use a secretory pathway which involves the passage of newly

synthesized proteins through a series of cellular compartments where sequential post translational modifications are done on the proteins and finally they are sorted in different types of transport vesicles which deliver proteins to their correct locations. The proteins are synthesized on the ribosomes on rough ER membrane. Once synthesized, these proteins enter the lumen of ER. Soluble proteins in this class are first localized in the ER lumen and are then transported to the lumen of other organelles in the secretory pathway or are secreted from the cell. Similarly, the integral membrane proteins in this class are initially inserted into the rough ER membrane; some remain there, but many eventually localize to the plasma membrane or membranes of other cellular compartments.

All the proteins that enter the secretory pathway have an ER signal sequence, generally at the N-terminus. This sequence directs the proteins being synthesized to the rough ER. Most newly synthesized proteins in the ER lumen or membrane are incorporated into small transport vesicles emerging from specialized sub-domains of ER called ER exit sites (ERES) [36, 37].

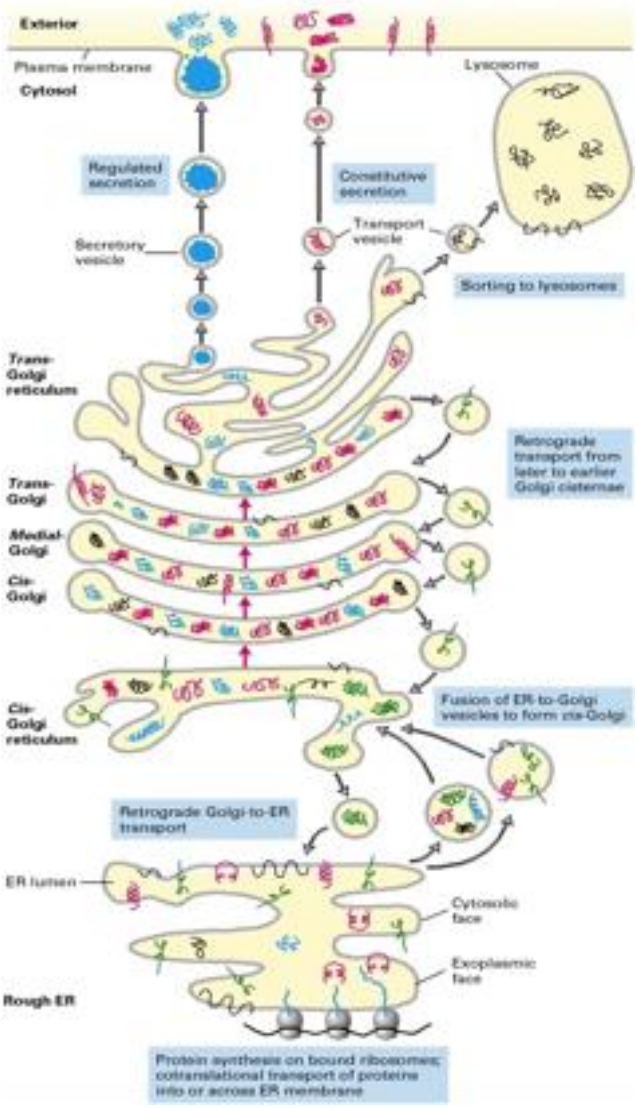

Fig1.1: The secretory pathway: A schematic diagram explaining the secretory pathway inside a cell. Adapted from Molecular cell biology by Lodish H, Berk A, Zipursky SL, et al.

The vesicles that carry newly synthesized proteins from ER to Golgi apparatus are COPII coated vesicles. Sec12, a guanine nucleotide exchange factor for GTPase Sar1 triggers formation of COPII vesicles by activating Sar1. Activated Sar1 gets recruited to ER membrane and induces membrane curvature. It also recruits coat protein complexes Sec23-24 and Sec13-31. These vesicles either fuse with each other and with early Golgi vesicles to form the membranous structure known as the cis-Golgi network. Trafficking between ER and Golgi apparatus is bidirectional. Transport from ER to Golgi is called anterograde transport and the traffic from Golgi to ER is called retrograde transport. An important complex

involved in the retrograde transport is the COPI coated vesicles. From the cis-Golgi certain proteins, mainly ER-localized proteins, are retrieved to the ER via COPI vesicles. COPI vesicles are also important in intra-Golgi transport in retrograde direction. Initiation of COPI vesicle formation is similar to that of COPII vesicle formation. But biogenesis of COPI vesicle takes place on Golgi membranes. A cargo protein after reaching cis cisterna, travels towards trans face of Golgi apparatus. While it is being transported to trans face, the cargo undergoes through various post translational modification steps. When cargo proteins reach trans Golgi network, they are sorted and packaged into different type of transport vesicles. Depending on where the final destination of protein lies, the cargo proteins are then delivered to their respective location within the cell or plasma membrane or are secreted outside the cell. In all cell types, at least some of the secretory proteins are secreted continuously. Examples of such constitutive (or continuous) secretion include collagen secretion by fibroblasts and secretion of serum proteins by hepatocytes.

The history of two major organelles of secretory system:

First existence of Golgi apparatus was reported by Camillo Golgi while studying cerebellum of owl [38]. Camillo Golgi was studying nerve cells stained by the metal impregnation technique, when he noticed a basket-like network surrounding the nucleus in Purkinje cells (Fig1.2). Golgi published the first report of Golgi structure in 1898, and called it the ‘apparato reticolare interno’ or ‘internal reticular apparatus” [39].

Fig 1.2: First drawing of Golgi in Purkinje cells

The existence of Golgi apparatus as a bona fide organelle was controversial for long time as it could not be seen in living cells and needed heavy metal staining for visualization. It was believed that this could be just an artifact of the black reaction used to visualize Golgi apparatus. The existence of this organelle was not confirmed until supported by electron microscopy data that was available in 1950s [40, 41]. EM data by Dalton and Felix in 1954 gave clear picture of existence of this organelle having a regular structure with flattened disc like lamellae, later on called as cisternae [40]. The function of this organelle as important organelle for glycosylation and protein secretion was uncovered by Neutra & Leblond and also by Palade, Jamieson & coworkers in 1966, 1967 [42, 43]. Compartmentalization of Golgi resident enzymes was reported by Novikoff & Goldfischer in 1961 from classic histochemistry data. Erik Fries & Rothman reconstituted the vesicle transport in cell-free extracts of tissue culture cells for the first time in 1980 [44]. In vitro reconstitution of ER-to-Golgi transport was done by Becker and Balch in 1987 [45]. Dunphy and Rothman discovered that glycosylation pathway is compartmentalized within the Golgi stack in the cis to transdirection in 1983 [46]. Purification of cytosolic components required for the cell free transport reaction led to discovery of NSF, soluble NSF attachment proteins (SNAPs), Soluble NSF Attachment Protein receptor (SNAREs) by Rothman and colleagues [47, 48].

These experiments also resulted in discovering COPI vesicles 1986 by Orci and Glick et al [49]. Involvement of KDEL receptors in retention of ER resident proteins was reported by Munro and Pelham in 1987 [50]. Pierre Cosson & Francois Letourneur discovered that retrograde traffic is carried by COPI vesicles [51]. ER-Golgi intermediate compartment (ERGIC) was isolated by Schweizer et al in 1988 [52]. COPII coat was discovered in 1994 by Barlow et al [53]. Lippincott-Schwartz and colleagues for the first time in 1990, made use of Brefeldin A, a fungal metabolite to study ER to Golgi transport and revealed that Golgi resident glycosyl transferases are not statically localized to Golgi [54]. In 2006 direct evidences to support cisternal maturation came from 2 groups simultaneously [6, 7]. This model supported that Golgi cisternae are continuously being formed at cis face. A cis cisterna acquires respective glycosyl transferases & gets converted to medial or late Golgi cisterna while carrying cargo proteins within themselves. Many modifications of vesicular transport and cisternal maturation models are still being proposed. Nevertheless, many of the observations still need to be explained before general acceptance of any particular model for explaining Golgi functioning. A majority of the researchers presently accept the cisternal maturation model.

The Endoplasmic Reticulum Exit Sites

ERESs were first discovered and characterized by electron microscopic studies of mammalian cells [55]. ER exit sites (ERES) are specialized subdomains of ER. They are also called transitional ER sites. These are ribosome free domains of ER where secretory cargo gets accumulated and it is packaged in COat Protein II (COPII) vesicles [56, 57]. Usually ERES are distributed randomly throughout the ER but recently it was shown that the membrane curvature is a key geometric feature for the regulation of ERES localization [58]. In *S. cerevisiae,* budding appears to occur stochastically across the entire ER membrane. In *P. pastoris* and metazoans, the budding event is highly organized, occurring at discrete sites on the ribosome-free ER, called transitional ER (tER) or ER exit sites [37, 55]. Typical vertebrate cells have several hundreds of ERES inside a cell. The ERES are stable and long

lived structures as demonstrated by live cell fluorescence microscopy [59, 60]. Although when Sec13 labeled mammalian cells were treated by nocodazol, Sec13 labeled ERES formed clusters near Golgi structures. This meant that although individual ERES are long lived and stable structures, their localization is quite dynamic. Even in the budding yeast, ERES were found to be stable and they rarely moved [1]. *Pichia pastoris* often has 4-5 Sec13 labeled ERES spots which are present to adjacent Sec7 labeled Golgi cisternae. It was also demonstrated in *Pichia pastoris* that these ERES form de novo. These ERES spots in *Pichia pastoris* also fused with each other occasionally creating larger ERES spot [1]. ERES were often observed by labeling one of the COPII coat marker. In order to understand clearly if COPII coat forms vesicles at ERES or they just form sub-domains on ER membrane, Zeuschner and colleagues used 3D tomography and immunogold labeling [61]. This data establish the existence of free, bona fide COPII-coated transport carriers at the ER to Golgi interface, suggesting that assembly of COPII coats *in vivo* can result in vesicle formation[61].

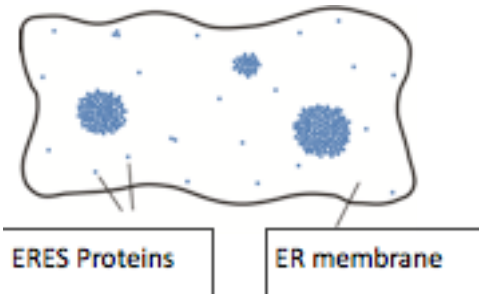

Fig 1.3 Model of de novo ERES formation in *Pichia pastoris*

Bevis and colleagues also proposed a model (fig 1.3) for self-organization of ERES in which they proposed that ERES are patches of self-associating membrane components [1]. Individual ERES proteins can diffuse throughout the whole ER and have a weak, cooperative affinity for one another. When the local concentration of these ERES exceeds a certain threshold, they spontaneously associate and nucleate a new patch. This patch then captures additional ERES proteins until it grows large enough to produce COPII vesicles. The COPII vesicles remove ERES proteins and thereby limit the growth of the ERES site. ERES are diffused in the plane of the ER and on collision they fuse with each other. Later on, it was

believed that in mammalian cells, Sec16 localizes to cup-like structures of ERES that are spatially distinct from the localization of other COPII coat components and Sec16 recruitment at ERES is not dependent on recruitment of other COPII proteins at ERES and that it is required for export from ERES and ERES organization [62], [63], [64], [65]. Recently with help of studies of COPII turnover in Pichia pastoris, it was proposed that Sec16 does not in fact organize COPII. Instead, regulation of COPII turnover can account for the influence of Sec16 on ERES sites [66]. With this knowledge, a new model was proposed for ERES-Golgi secretory unit in *Pichia pastoris* which suggested that ERES are created by tethering to Golgi membranes and are regulated by Sec16. The COPII vesicles that bud from ERES are thought to nucleate new Golgi cisternae. Thus, an integrated self-organization process may generate ERES-Golgi units[67].

Size regulation of ERES:

In mammalian cells ERES are formed *de novo.* The mammalian ERES can also undergo fusion to form larger ERES and they also undergo fission. Even in P. pastoris, ERES form de novo and undergo fusions which create larger ERES. But they shrink after fusion to control their size and after de novo formation; they increase in size to attain a typical threshold. So in general, ERES seem to maintain their size with help of fusion of existing ERES and fission of larger ERES [1, 68]. The amount of cargo flow from ERES can definitely influence the number of ERES in mammalian cells as seen from many protein export inhibitor studies [69, 70]. Since Sec16 was earlier thought to be a scaffold protein which recruited other components of COPII machinery at ERES, Sec16 was suspected to regulate size of ERES. But 10 folds overproduction of Sec16 didn't result in any detectable change in number and size of ERES in *P. pastoris* [65]. Thermo sensitive mutants namely sec12-4 and sec16-2 (which inhibit cargo export from ER) showed larger ERES punctae as labeled by Sec13 and Sec23. When unfolded protein response was induced by treating cells with DTT, it resulted in initial enlargement of Sec13 labeled structures but the effect didn't persist after 2 hours. Inhibition of *de novo* fatty acid synthesis also blocked budding of COPII

vesicles from ERES and showed larger size of Sec23 punctae. Continuous fatty acid synthesis is required for maintenance of ERES size [71]. When protein synthesis was blocked in case of thermo-sensitive mutants of Sec12, Sec16 or in case of fatty acid synthesis, the enlarged Sec13 punctae were not observed. In general, continuation of cargo assembly and defects in COPII assembly can only result in enlarged ERES structures in *S. cerevisiae.* In higher organisms it is proposed that fusion and fission of ERES might regulate ERES size, but molecular mechanisms that regulate size of ERES remains to be identified.

COPII vesicles:

COPII was first described in *S. cerevisiae* by in vitro reconstitution experiments [53] but their basic function is conserved in all eukaryotes. Production of COPII vesicles occurs at specific sites of ER called ERES in mostly all eukaryotes except *S. cerevisiae* where COPII production occurs throughout ER [72, 73]. The sorting of cargo proteins which are to be transported out of ER towards Golgi apparatus or retained at ER takes place at ERES. This sorting and incorporation of selected cargo for further transport in vesicles is achieved by the coat protein complex II (COPII).

The very first step of COPII coat assembly begins with the recruitment of the small GTPase switch Sar1 to the ERES [74]. This event is promoted by guanine nucleotide exchange factor (GEF) Sec12 [75], that catalyzes GDP/GTP exchange on Sar1. Upon activation, Sar1 rearranges its conformation by swinging out N-terminal helix and exposes its hydrophobic amino acids that will probably be embedded in the bilayer [76-79]. Sar1 performs multiple functions in COPII vesicle formation: it provides a GTP-activated switch that serves to mediate vesicle morphogenesis, scission and uncoating [80-82], and it also interacts with Sec23 and Sec31. Insertion of N-terminal helix of Sar1 into the ER membrane induces initial curvature, and also the recruitment of the Sec23–24 heterodimer [80-82]. Sec23 and Sec24 form a bow-tie-shaped complex which forms inner coat of the COPII vesicles. This has a basic concave surface that contacts the membrane and may contribute to

the induction of curvature [77]. Sec24 binds transport cargo while Sec23 interacts with Sar1 and recruits Sec13/31. Sec24 can bind a variety of cargoes and cargo adaptors. Binding of Sec24 to a wide variety of cargos is achieved by using different paralogues of Sec24 in mammals. Sec24 interacts with ER export motifs present on the cargo that has to be transported to Golgi apparatus [83-86]. The complex between Sar1–Sec23–24 and cargo is captured by the Sec13–31 hetero-tetramer. This Sec13-Sec31 hetero-tetramer forms the outer cage of COPII coated vesicle [87-89].

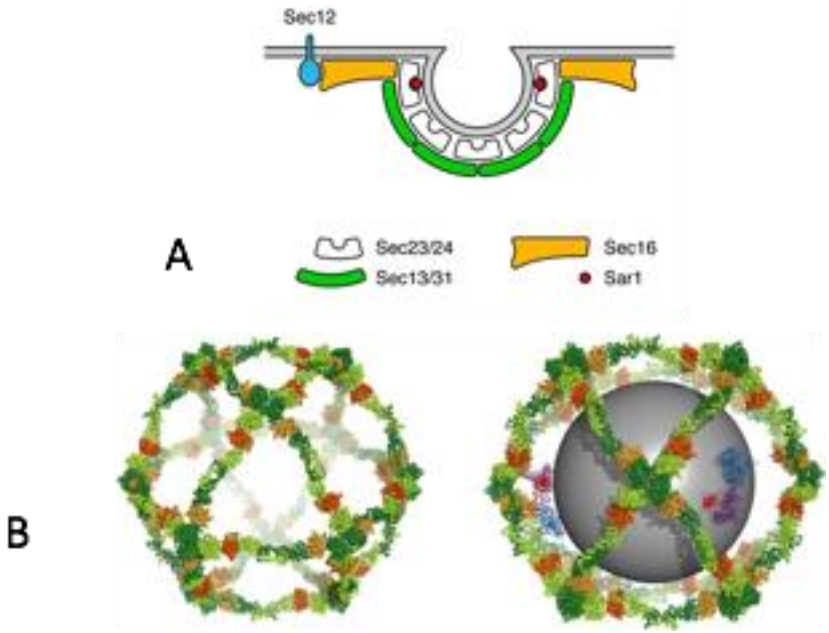

Fig 1.4: Components and structure of COPII coat A] Components of COPII coat assembly [66], B] Molecular model of COPII cage [88]

Structural studies showed that the Sec13–31 hetero-tetramer forms a rod-shaped complex [88] that assembles *in vitro* into cuboctahedral geometrical cages [89-91]. The inner and outer coat of COPII vesicles can interact flexibly to accommodate various cargo proteins[92].

The GTP hydrolysis of Sar1 is the primary mode of regulation, known to govern initiation of coat assembly/disassembly. Sar1 GTP hydrolysis is stimulated by the GTPase-activating protein (GAP) Sec23, and is further accelerated by Sec31, necessary for vesicle

fission [37, 82, 93]. The effect of this autonomous GAP in minimal systems is that as soon as the coat fully assembles, GTP is hydrolyzed and the coat is rapidly released. This raises a question as to how coat assembly is sustained for a sufficient length of time to generate vesicles. A GAP inhibitory function contributed by the peripheral ER protein, Sec16 has been reported to modulate the activity of the coat. Sec16 inhibits the GAP activity of Sec23 and Sec31. [94]. Upon coat depolymerization, COPII proteins are recycled back to the ER, ready for a new round of cargo export [95].

Sec12:

Yeast Sec12p is a 70kD glycoprotein having a 40kD N-terminal cytosolic catalytic domain, a single transmembrane domain, and a 30kD glycosylated luminal domain [96]. ScSec12 uses a potassium-stabilized loop at the catalytic site for catalyzing guanine nucleotide exchange for Sar1 [97]. If in vitro reconstitution of COPII vesicle generation assay is performed in presence of all other COPII components along with Sar1, GTP except Sec12, it leads to unstable COPII coat. Sec12 is a guanine nucleotide exchange factor which exchanges GDP with GTP on Sar1 GTPase leading to recruitment of other coat proteins at ERES [98]. Thus activation of Sar1 by Sec12 is the first step of COPII vesicle biogenesis at ERES [99]. Sec12 is exclusively present in ER but it is modified by an enzyme present in early Golgi cisterna which suggests that Sec12 cycles between ER and Golgi. Rer1p is responsible for retention of Sec12 at ER as observed from genetic analysis [100].

In all eukaryotes, all components of COPII machinery localize to punctate structures on the ER which define ERES [101]. But although Sec12 initiates COPII vesicle budding, Sec12 localization is found to be variable in different species. In *Pichia pastoris*, Sec12 is concentrated at ERES [73, 102]. But in *S. cerevisiae*, Sec12 is found to be present throughout ER [73, 100]. Sec12 has a paralog in *S. cerevisiae* named as Sed4 [106]. Sed4 is also known to stimulate Sar1 GTP hydrolysis and bind to Sec16p [105]. Mammalian Sec12 has a large cytosolic domain. A fragment of this has previously been reported to be the

transcription factor 'prolactin regulatory element binding protein' (PREB). In humans, Sec12 was found throughout the ER [103], but the immunofluorescence data were ambiguous. PpSec12 is associated with ERES reversibly as observed from FRAP experiments. Over expression of PpSec12 in *P. pastoris* results in its localization to general ER which points to the fact that PpSec12 localizes at ERES by binding to a partner protein & this binding is saturable [73, 102]. Oligomerization of PpSec12 luminal domain is required for its interaction with its binding partner [102]. The candidate binding partner for Sec12 at ERES could be Sec16 as it is known to be present at ERES and it also interacts with other COPII proteins [104, 105]. Another finding pointing that Sec16 could be the binding partner comes from studies in *P. pastoris*. In a mutant Sec16 strain of *P. pastoris*, most of the mutant Sec16 protein is displaced from ERES sites at the non-permissive temperature, and most of the PpSec12 is also delocalized to the general ER [65].

Sec16:

A genetic screen for *P. pastoris* mutants having disrupted ERES organization uncovered a role of Sec16 protein [65]. Sec16 was first identified as an essential protein required for protein secretion in a mutant screen in *S. cerevisiae* [107]. In *S. cerevisiae*, Sec16 is a 240-kDa peripheral membrane protein that is essential for ER-to-Golgi transport and cell viability [104]. Sec16 was subsequently implicated in ERES organization and maintenance in various species [62, 63, 65, 108]. Immunofluorescence studies have identified Sec16 as a component of ERES, where it colocalizes with other COPII proteins [62, 64, 65, 71, 109]. To understand exact localization of Sec16 with reference to other components of COPII machinery, high-resolution fluorescence and electron microscopy studies were carried out in HeLa cells. These studies suggested that Sec16 and COPII proteins localize adjacent to each other but mark distinct areas of ERES at steady state. Sec16 localizes to cup-like structures of ERES that are spatially distinct from the localization of other COPII coat components.

Steady-state localization of Sec16 is independent of the localization of downstream

COPII components. The FRAP studies on fluorescently labeled Sec16 and other COPII components showed that rate of association and dissociation of Sec16 from the membrane is slower than other COPII components. Sec16 also interacts with other components of COPII machinery like Sec13, Sec23, Sec24, and Sec31 [63, 104, 110]. Because of these observations, Sec16 was believed to be a scaffold protein which recruits other COPII proteins.

Comparison of the sequences of Sec16 protein from *P. pastoris* and *S. cerevisiae* revealed the presence of a central conserved domain and a C-terminal conserved domain of Sec16 [65]. Two orthologues of *S. cerevisiae* Sec16 were found in case of mammalian cells, namely Sec16A and Sec16B. [64]. Sec16A is a longer ortholog and it is similar to *S. cerevisiae* Sec16 which has C-terminal conserved domain that also interacts with Sec23, and other is a shorter protein Sec16B, which lacks the Sec23-interacting C-terminal domain. Knockdown of Sec16L or Sec16S, or both, disrupts ERES and blocks cargo export from the ER and normal ERES organization. Overexpression of Sec16A also disrupts the normal ERES organization suggesting important stoichiometry of Sec16 molecules at ERES [64]. Also, these proteins are present as heteromeric complexes. The similar functions of Sec16 were also proved in another organism *D. melanogaster* [108].

Apart from just providing scaffold for COPII vesicle biogenesis and interacting with COPII subunits, recent reports uncover regulatory roles of Sec16. Sec16 was found to negatively regulate the GAP stimulation activity of Sec31 [111]. Another report revealed that displacing Sec16 from ERES to cytoplasm in fact accelerated ERES dynamics [66].

Golgi structure and function:

The Golgi apparatus resides at the heart of secretory pathway. This organelle is the place where most of the post translational modification and sorting of proteins and lipids takes place. In many of the eukaryotes, Golgi is made up of one or more stacks of disc shaped cisternae which gives appearance like a stack of pancakes. In *S. cerevisiae* Golgi cisternae are not stacked together but they are freely dispersed in cytoplasm. In another budding yeast *P.*

pastoris, Golgi cisternae are stacked and each stack has 3-5 cisternae. Each of the stacks is present just next to ERES which might give rise to corresponding Golgi cisterna [112]. This arrangement is called as a 'secretory unit'. In case of *Drosophila melanogaster*, the individual Golgi stacks are present as ERES-Golgi secretory units throughout the cytoplasm. Each stack consists of 2–3 cisternae [113]. The plant Golgi apparatus is composed of many stacks of cisternae dispersed throughout cytoplasm. They are also present as secretory units as in Pichia and Drosophila. The number of stacks and their distribution within the cell depends on the cell type. Maize root cap cells, which are actively secreting large amounts of mucopolysaccharides, contain between 300 and 600 Golgi stacks per cell but as few as 25 stacks are present in the apical meristem cells of the hairy-willow herb *Epilobium hirsutum* [114].

The function of organelle reflects from its structure. A true example of this is Golgi apparatus. Despite of such diverse structural arrangement of Golgi apparatus in different species, the basic principle of functioning of this organelle is much conserved across all species. The cargo proteins are carried in COPII vesicles. The cargo enters cis face of Golgi and leaves from trans face [115]. These COPII vesicles fuse with each other and merge to form ER-Golgi intermediate compartment (ERGIC) / vesicular tubular cluster (VTC) [116, 117]. This further develops into cis cisternae having early acting modifying enzymes. Cargo then travels through all Golgi cisternae from cis to trans direction while being modified by Golgi resident glycosyl transferases in a sequential manner [118]. Then after trans cisternae there comes trans Golgi network (TGN) where cargo is sorted into different types of vesicles for their further transport to ultimate destination [119].

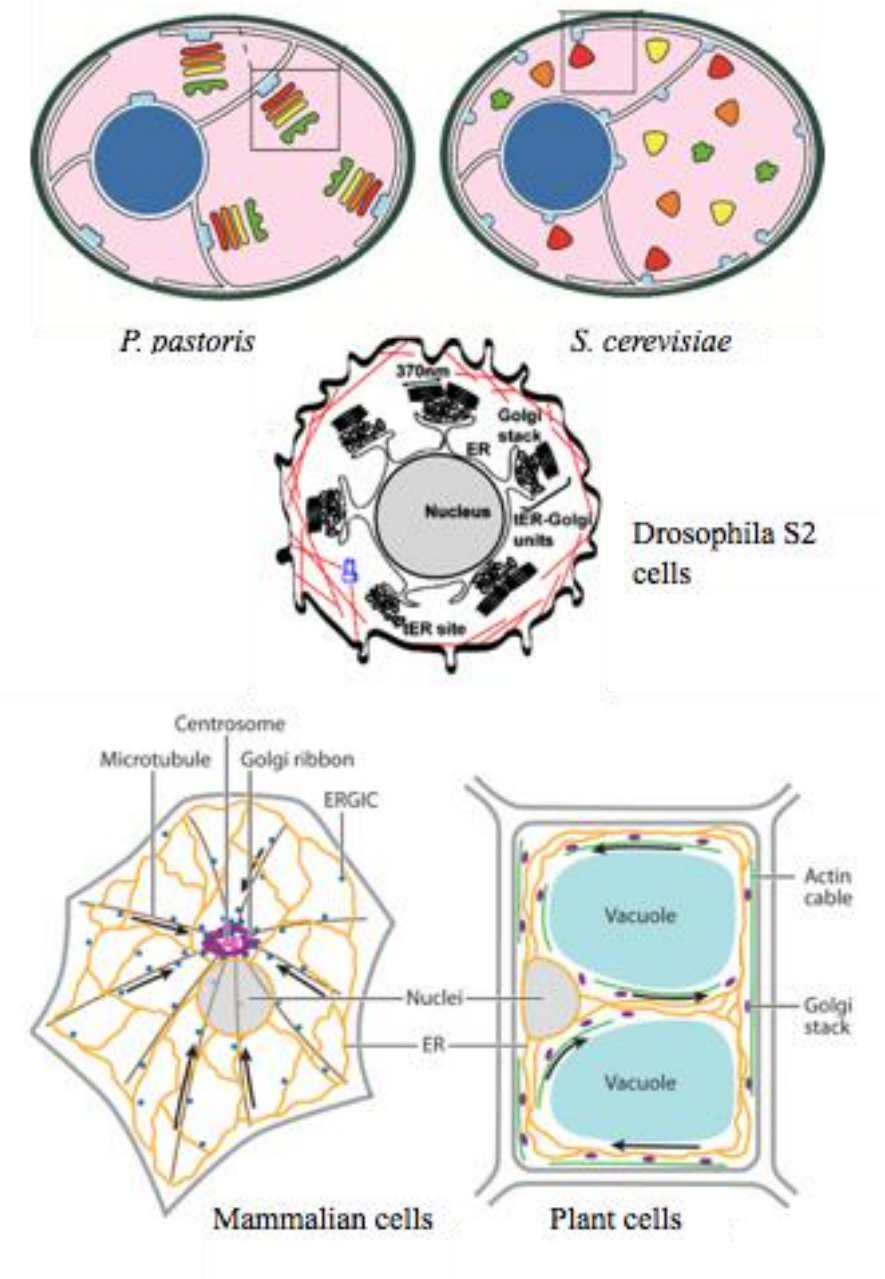

Fig 1.5: Arrangement of Golgi cisternae in different organisms [112, 113, 120]

Recently, to give a consistent idea of Golgi functioning in different Golgi cisternal arrangements, a three stage model was proposed. According to this model, in all the eukaryotic cells, the Golgi apparatus has 3 different types of membrane compartments [121]. First compartment that the cargo enters after budding from ERES is the cisternal assembly compartment. These compartments receive the COPII vesicles coming out of ERES and the recycling COPI vesicles that carry proteins to be transported back to ER within them. During

this stage, a new cisterna is being formed. The next stage is carbohydrate synthesis stage. The cisternae in this stage acquire corresponding enzymes with help of COPI vesicles. In this stage, cargo proteins are glycosylated in sequential manner. The third stage is the carrier formation stage. In this stage, cargo proteins are packaged into different types of transport vesicles like clathrin coated vesicle, secretory vesicles. During this stage the cisternae also disassemble. This model can explain Golgi structure and function in various species having different inherent Golgi structure.

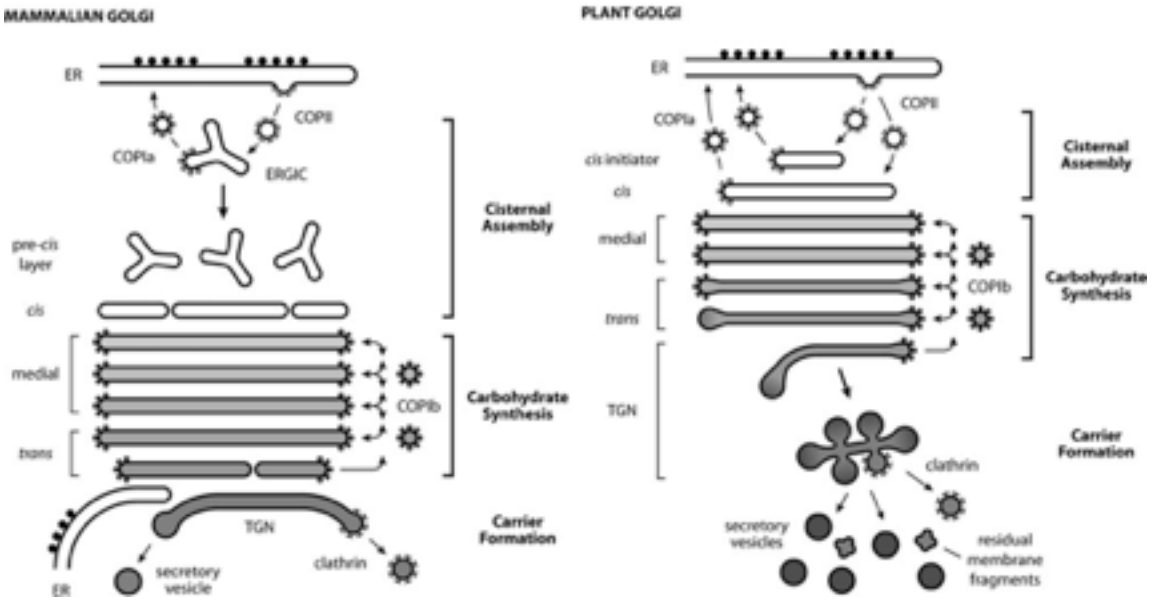

Fig 1.6: 3 stage model of Golgi structure and function[121]

Transport through the Golgi apparatus:

More than 30% of the proteins encoded by human genome are processed by Golgi apparatus [122]. But the pathway or mechanism of transport of cargo through the Golgi apparatus is still a debated topic. Several models were developed to explain transport of cargo through Golgi but each had its own weakness to explain all the observed facts. These models are briefly discussed below.

Vesicular transport model: This was the most accepted model of cargo transport through Golgi cisternae until 1990s. According to this model, the Golgi cisternae are stable

compartments [115, 123]. The newly synthesized cargo is transported to cis-Golgi via COPII vesicles. Then the cargo is transported from cis to medial to trans cisternae via COPI vesicles [124]. The Golgi resident enzymes are retained in particular cisternae by their exclusion from cargo carrying COPI vesicles. In the modified version of this model, presence of two types of COPI vesicles was proposed. Anterograde COPI vesicles carried cargo, whereas retrograde COPI vesicles carried recycling components [125, 126].

This model could explain the existence of polarized Golgi cisternae and could explain functions of two classes of COPI vesicles observed. This explained the presence of cargo proteins like VSV-G in the COPI vesicles observed by immunoelectron microscopy and biochemical analysis [127]. This model could also explain very fast intra-Golgi traffic of small secretory cargo with help of percolating COPI vesicles carrying cargo [125]. But the major point that could not be explained by this model is the passage of large cargo through Golgi cisternae which are impossible to fit in the COPI sized vesicles [128, 129]. Many studies could not locate presence of secretory cargo in COPI vesicles by immunoelectron microscopy or proteomics; instead COPI vesicles were enriched in recycling components [130-132]. The model also failed to explain the formation of new Golgi cisternae and disassembly of old cisternae as well as transient nature of yeast Golgi cisternae and mobility of Golgi resident enzymes between compartments.

Cisternal maturation model: In this model, cisternae are viewed as transient structures. Cisternae are formed at cis-face by fusion of ER derived COPII vesicles [116]. Once new cis cisterna is formed, it matures into medial and then trans by acquisition of respective resident enzymes with help of retrograde COPI vesicles carrying Golgi resident enzymes. Gradually when it matures into trans Golgi network, the cisternae disassembles by packaging cargo into secretory vesicles or other transport vesicles. According to this model cargo is carried within the cisternae from cis to trans end [129]. Recently it was postulated that the various Golgi compartments represent discrete kinetic stages of maturation, with the transition from one stage to the next being regulated by Rab GTPases [120].

This model can readily explain the existence of distinct and polarized Golgi compartments, the existence of secretory cargo within cisternae, the transport of large secretory cargoes, the apparent formation and disassembly of Golgi cisternae, the mobility of resident Golgi enzymes between compartments, and the transient nature of yeast Golgi cisternae. It also included COPI vesicles as retrograde carriers. There is general agreement that mammalian COPI vesicles contain the KDEL receptor [127, 133]. Not only this but the resident Golgi glycosylation enzymes were also found to be concentrated in COPI vesicles [130, 132]. But this model cannot explain existence of heterotypic tubular connections between cisternae, the rapid intra-Golgi traffic of small secretory cargoes, or the exponential kinetics of secretory cargo exit from the Golgi region. In a cisternal maturation model, all secretory cargoes should pass through the Golgi at the same rate and should exit the Golgi with linear kinetics. Recent findings challenge this key assumption of cisternal maturation model [134]. Also, some immunoelectron microscopy studies have not found significant levels of Golgi glycosylation enzymes in COPI vesicles [125, 135, 136].

Cisternal maturation with heterotypic tubular transport: This model is an extension of existing cisternal maturation model with addition of tubular connections between cisternae. In mammalian Golgi, two neighboring cisternae are known to be connected horizontally by homotypic tubular connections to form the Golgi ribbon[137]. There is also a possibility that Golgi cisternae within a stack might also be linked "vertically" by heterotypic tubular connections. Recent electron tomography studies have supported the idea of the presence of such heterotypic tubular connections [138, 139].

This model has all advantages of cisternal maturation and in addition it also explains homotypic and heterotypic tubular connections between cisternae. Narrow tubular connections may provide a fast route that allows small secretory cargoes to traverse the Golgi without requiring extensive membrane transport. These connections may also allow Golgi glycosylation enzymes to recycle independently of COPI vesicles [140]. This model still cannot explain exponential kinetics of procollagen which is too big to be transported through

tubular connections. Heterotypic tubular connections are not yet described for other species like fungus or plants. How the compartments are able to maintain their identity in presence of such heterotypic tubular connections is not known yet.

Rapid partitioning in mixed Golgi: A recent paper suggested a completely different model to explain Golgi functioning. This was based on the observation from fluorescent microscopic analysis of VSVG (Vesicular stomatitis virus glycoprotein) which was segregated from Golgi glycosyl transferases [134, 141]. This model suggested that Golgi operates as a single compartment having processing and export domain.

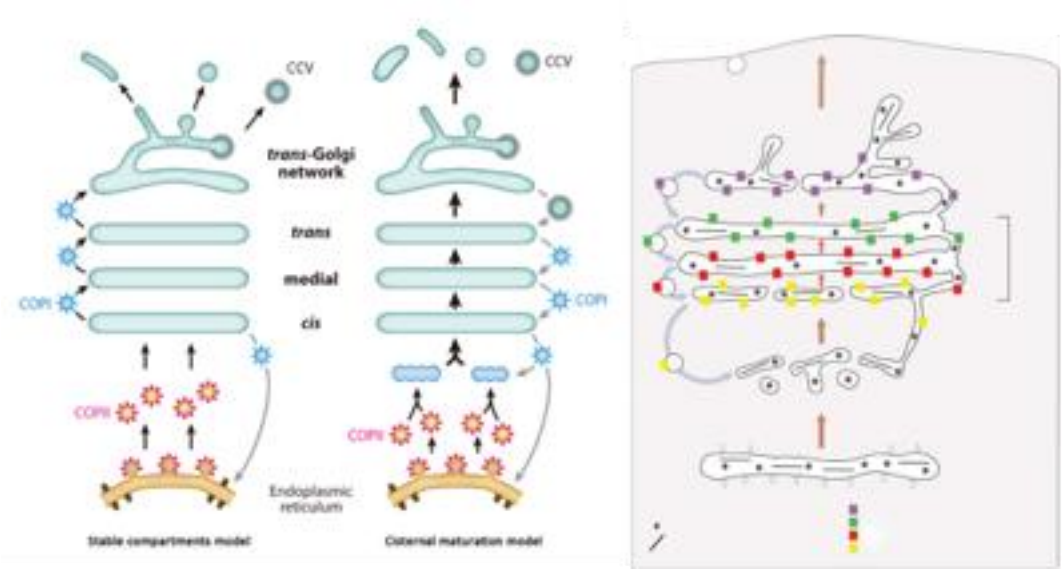

Fig 1.7: Models of transport through Golgi: Stable compartment, cisternal maturation model and Cisternal maturation with heterotypic tubular transport [120, 142]

Cargo arrives at Golgi, gets partitioned and exits from each stage to their final destinations. Although this model explains exponential kinetics of cargo, this couldn't explain discrete nature of Golgi cisternae and their formation and disassembly.

Stable compartment as cisternal progenitors: This model is an extension of stable compartment model. This still views Golgi cisternae as stable compartments but they are segregated into domains which are defined by Rab GTPase [122]. As observed for

endosomes, it is believed that Golgi cisternae might undergo Rab conversion which will be followed by homotypic fusion with matching Rab domain of older cisternae of adjacent Golgi stack [143, 144]. Or else, alternatively, a Rab domain can simply pinch off from a cisterna which would then fuse with a later cisterna from the same Golgi stack. This model could explain the existence of distinct and polarized Golgi compartments, the transport of large secretory cargoes, the mobility of resident Golgi enzymes, the existence of heterotypic tubular connections between cisternae, the rapid intra-Golgi traffic of small secretory cargoes. This also explained presence of mega vesicles for transport of large cargo which was described earlier [145]. This model fails to explain formation and disassembly of Golgi cisternae, the transient nature of yeast Golgi cisternae. Moreover, this model provides no specific role for COPI vesicles. In plants, algae, and fungi, individual Golgi stacks are found, making domain transfer between stacks improbable.

After comparing all available models for explaining transport through Golgi, cisternal maturation and cisternal maturation with heterotypic tubular connection models seem to answer majority of observations if not all. Today, cisternal maturation model is the most accepted model to explain Golgi function in various species.

COPI complex:

COPI complex is an important player in early secretory pathway. This helps both in intra-Golgi as well as Golgi to ER retrograde transport. The architecture of COPI coat is similar to that of clathrin coat but there are significant differences when it comes to cargo sorting and vesicle formation. COPI is also known as 'coatomer'. COPI complex consists of following 7 subunits, namely Sec27, Sec28, Ret1, Ret2, Ret3, Sec21, Sec26. All of these except Sec28 are essential genes for *S. cerevisiae*. Mammalian names of the subunits are β', ε, α, δ, ζ, γ, β-COP respectively. According to EM data, COPI is localized to Golgi membranes [146]. Major function of COPI complex is to retrieve proteins from Golgi to ER [149] and from older Golgi cisternae to newer cisternae [146]. Initially it was believed that COPI also

participates in anterograde transport but there are no strong evidences of the fact.

Apart from roles in vesicular transport, COPI also functions during mitosis for causing breakdown of Golgi apparatus into vesicles [150]. COPI is also known to interact with cdc42 and dynein to help Golgi positioning [151, 152]. Coatomer has also been implicated to take part in the maturation of early endosomes [153].

COPI complex is made up of two sub complexes. First is made up of a trimer composed of α-COP, β'- COP, and ε-COP. Second is a tetramer of β-COP, γ-COP, δ-COP, and ζ-COP[154].

The Golgi associated Arf1 GTPase when activated by binding to GTP gets inserted into lipid bilayer and initiates COPI coat recruitment. Activation of Arf1 and its membrane recruitment is pre-requisite for recruitment of COPI coat to membrane. The COPI complex is recruited *en block* onto Golgi membrane [155].

Three to four Arf1 molecules bind to one COPI complex [147]. γ-COP binds to p24 dimer and stabilizes coatomer on Golgi membranes. This results in a conformational change in γ-COP which is transmitted to α-COP. This rearrangement leads to coat polymerization [156]. Another important part of COPI machinery is KDEL/HDEL receptor. Its cytoplasmic domain interacts with coatomer and luminal domain interacts with soluble cargo having KDEL motif at their C-terminus. Thus KDEL-proteins are included into COPI vesicles and transported back to the ER [157].

Glycosylation at Golgi:

The transfer of initial sugars to glycoproteins or glycolipids occurs in the ER. But the subsequent addition of the many different sugars that generates a fully functional glycan is accomplished in the Golgi cisternae.

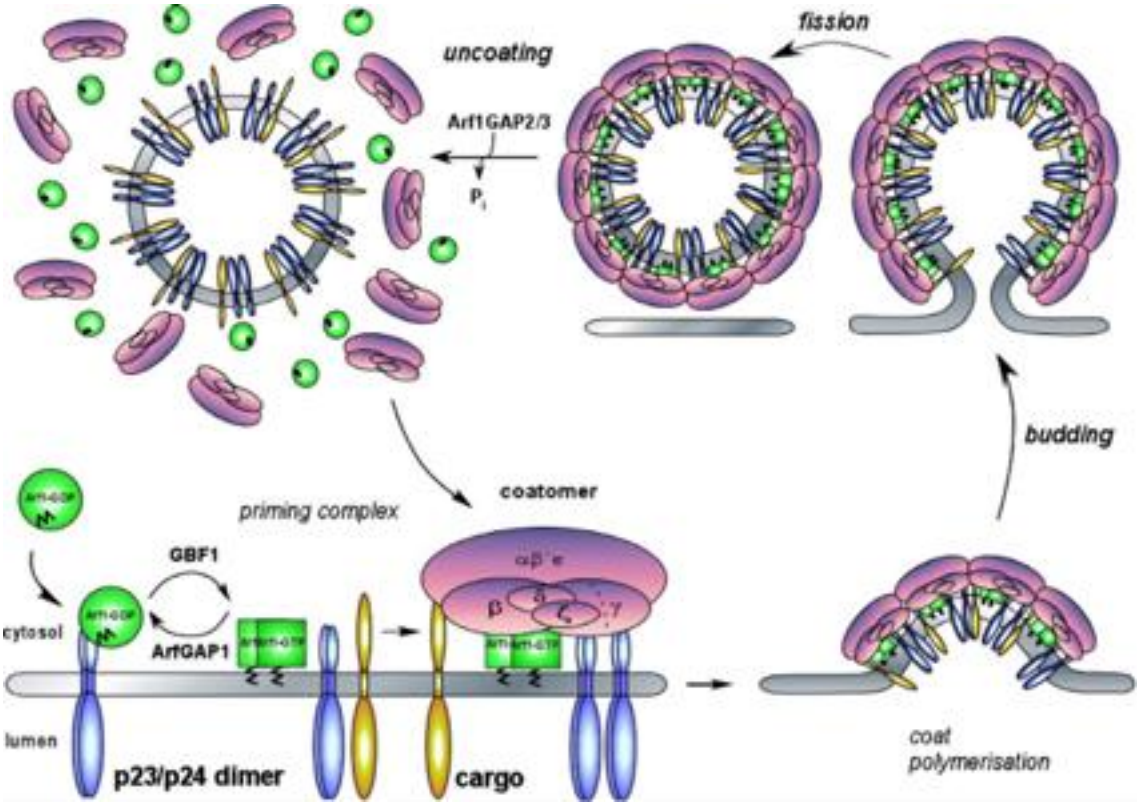

Fig 1.8:Individual steps in the formation of a COPI vesicle [158].

In mammalian cells, there are more than 250 glycosyl transferases (GTs) that catalyze the transfer of one sugar to another sugar on a glycan acceptor, which is usually covalently attached to protein or a lipid. The Golgi GT is a type II transmembrane protein with a short amino-terminal cytoplasmic tail, a transmembrane domain with a stalk-like stem region, and a catalytic domain that faces the Golgi lumen. Golgi residents GTs are arranged in an ordered manner from the cis-Golgi to the TGN, such that each GT is able to act on specific substrate which is generated in an earlier step of the glycosylation pathway. To achieve this, Golgi GTs must be appropriately localized in sequential manner of their action to cis-, medial-, trans-Golgi, or the TGN [118]. In 1990s, it was demonstrated that membrane spanning domain is important for compartmental identity of glycosyl transferases [159]. Another model for explaining sorting of glycosyl transferases depends on intra-membrane domain thickness and its composition. For localization of proteases of trans Golgi network, the short sequence in cytoplasmic tail is important for conferring TGN localization [160, 161].

Synthesis of all N-linked oligosaccharides starts in ER by transfer of pre-formed 14 residues to Asn residue in nascent polypeptide. Only asparagine residues in the tripeptide sequences Asn-X-Ser and Asn-X-Thr (where X is any amino acid except proline) are substrates for oligosaccharyl transferase, the enzyme that catalyzes this reaction. This pre-formed 14 residues is a branched oligosaccharide, containing three glucose (Glc), nine mannose (Man), and two N-acetyl glucosamine (GlcNAc) molecules, which can be written as $Glc_3Man_9(GlcNAc)_2$[162]. This structure is further modified in ER first and then in Golgi cisternae (Fig 1.9).

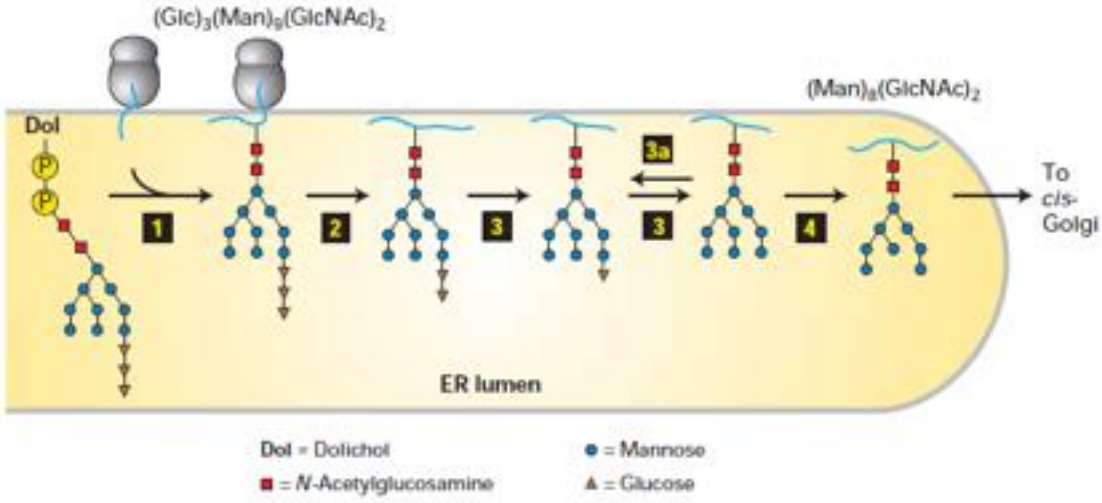

Fig 1.9: Initial processing of N-linked oligosaccharides in ER (Adapted from Molecular cell biology by Lodish H, Berk A, Zipursky SL, et al.)

Further processing of N-linked oligosaccharides occurs in Golgi cisternae in sequential manner. In cis Golgi, 3 mannose residues are first removed. After removal of three mannose residues in the *cis*-Golgi, the protein moves to the *medial*-Golgi.

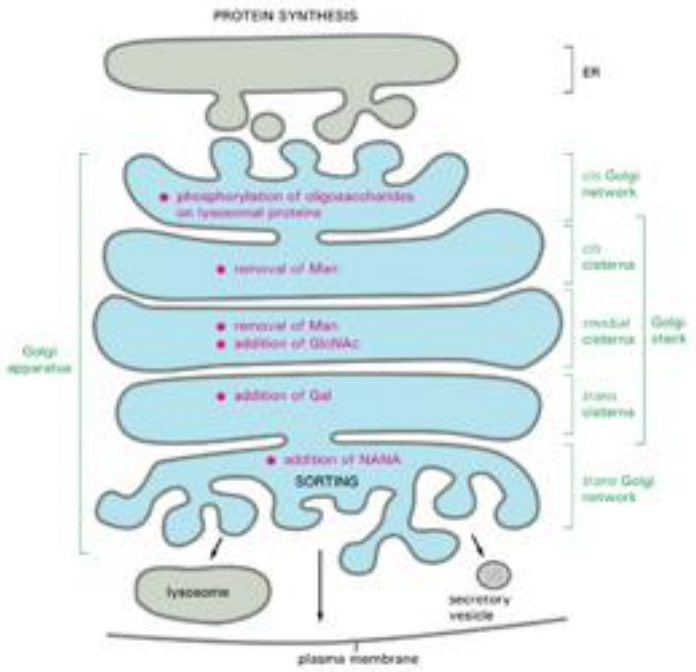

Fig 1.10: Sequential steps of post translational modification of cargo proteins in Golgi cisternae. (Adopted from Molecular biology of Cell by Bruce Alberts)

Here, three GlcNAc residues are added, two more mannose residues are removed, and a single fucose is added. Processing is completed in the *trans*-Golgi by addition of three galactose residues and finally by linkage of an *N*-acetylneuraminic acid residue to each of the galactose residues. Specific transferase enzymes add sugars to the oligosaccharide, one at a time, from sugar nucleotide precursors imported from the cytosol. This pathway represents the Golgi processing events for a typical mammalian glycoprotein. For glycoproteins, the N-linked core carbohydrate chain is extended by addition of α-1,6-mannose residues in the cis-Golgi. Then in medial Golgi, by addition of α-1,2- andα-1,3-mannose residues. Kex2-dependent proteolytic processing of certain secretory cargo occurs in the trans-Golgi compartment[163]. In plant Golgi apparatus, complex polysaccharides which form cell wall are also synthesized at Golgi apparatus.

Size control of Golgi apparatus:

Understanding size control mechanism of dynamic organelles like Golgi apparatus is a very important question. In various species, there exists a peculiar structure of Golgi apparatus. Variations involve different number and shape of cisternae, different arrangements of cisternae (stacked or unstacked or ribbon). Although there are differences in Golgi size and structure among different species, for one particular species, size, shape and organization of cisternae is usually observed to be maintained constant.

But in certain scenario, the Golgi size can be changed by cells to meet demands of protein secretion. Following conditions show alteration of Golgi size to meet cellular demands: during hormonal changes at parturition, Golgi apparatus is known to be enlarged in mammary epithelial cells. [164, 165]. Stimulated pancreatic exocrine cells show enlarged Golgi apparatus with numerous stacked cisternae vesicles [43]. Thus, depending on cellular needs for protein secretion, Golgi apparatus size and number of cisternae can be altered by cells.

Apart from such normal physiological conditions, in several diseases, Golgi size and structure is known to get altered. It is known that the size of Golgi is altered in case of some cancers [5]. Some viral infections cause fragmentation of Golgi apparatus [166, 167]. Many neurological disorders like Parkinson's disease, Pelizaeus-Merzbacher disease, Alzheimer's disease involve fragmentation of Golgi apparatus [168, 169]. Smith-McCort dysplasia which is a skeletal muscle dysplasia and RIN2 syndrome (connective tissue disorder) lead to swollen, fragmented Golgi and dilated Golgi cisternae respectively [170, 171].

The Golgi size change can occur in form of following options: 1) Changes in the volume of individual cisternae 2) Increase in the number of cisternae per stack, 3) In case of mammalian Golgi, the number of ministacks in the ribbon.

The size of the Golgi complex is greatly dependent on the balanced flux of material to and fro from the Golgi complex. Inhibition of Golgi to ER pathway by knockdown of Scyl1, a

protein involved in KDEL receptor trafficking from the Golgi to the ER resulted in increase in Golgi cisternal luminal width [172]. Inhibition of ER to Golgi transport results in the disintegration of the Golgi complex. Similarly, inhibition of membrane budding from the trans-Golgi network results in the enlargement of the TGN and a size reduction of the Golgi complex [173].

Upon glucose stimulation of pancreatic β cells, the surface area of cisternae increases as a result of altered trafficking [174]. After antigen stimulation of B cells, Golgi complex size increases three fold when cells need to differentiate and produce and secrete huge amounts of immunoglobulin [175]. Golgi size is also known to be increased during differentiation of neuroblasts and myoblasts [173].

Every species usually have fixed number of Golgi cisternae. Mammalian cells normally have 5-8 cisternae per stack. Usually cis, medial and trans acting enzymes are present in cisternae in overlapping fashion. So if there is increased number of cisternae, it might lead to precise compartmentalization which might improve complex glycosylation events. Apparently to support this idea, green algal cells which synthesize very complex glycosylated proteins contain 20 cisternae per stack [176].

In summary, if we study all examples mentioned above, it is very clear that Golgi complex modulates its size according to cellular needs to meet the secretory requirements of the cell. But nothing is known at molecular level about how exactly cells bring about the alterations in size of Golgi complex.

Yeast Golgi apparatus:

The yeast Golgi apparatus came into limelight by very first discovery of identification of 23 complementation groups important for secretory pathway in *S. cerevisiae* [107]. Like all other eukaryotes, yeast Golgi can be divided into functionally different cis, medial and trans cisternae which carry out different steps of post translational modification. Early acting enzymes like α-1,6-mannosyltransferases (Och1, Mnn9) localize to cis cisternae. Also, Golgi-

ER retrieval enzymes like Erd2, Rer1 localize to early cisternae. Later acting enzymes such as -1,2-mannosyltransferases (Mnn2) and α-1,3-mannosyltransferases (Mnn1) localize to medial and trans cisternae.

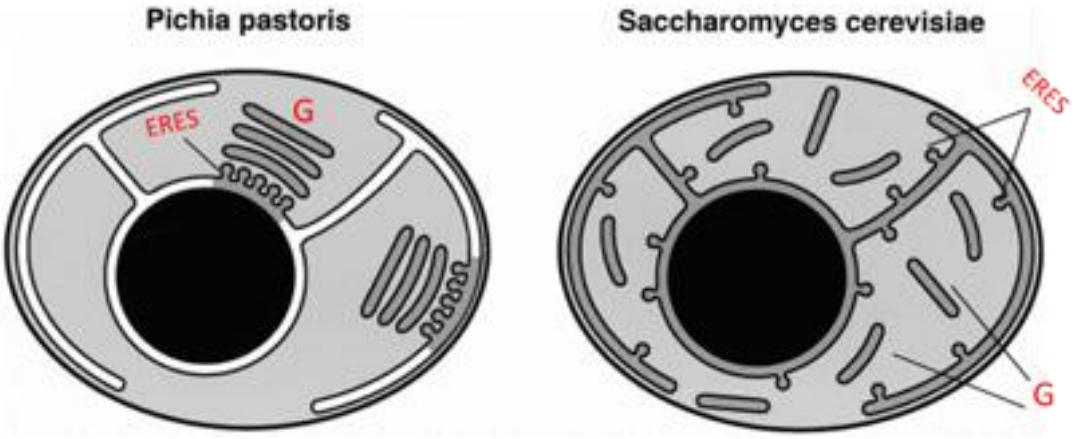

Fig 1.11: Golgi cisternae arrangement in two budding yeasts [73]

Many yeast species like *P. pastoris, Schizosaccharomyces pombe* show stacked Golgi cisternae like higher eukaryotes. But *S. cerevisiae* shows a unique Golgi structure in which the Golgi cisternae are unstacked and they are seen floating throughout the cytoplasm. *S. cerevisiae* Golgi cisternae are not flattened membrane sacs but they are present as elaborate network of tubules [177, 178]. Although this yeast has unstacked Golgi, when it comes to functioning; it follows same rules like other higher eukaryotes. *P. pastoris* Golgi cisternae are bigger in size compared to cisternae of *S. cerevisiae.* Also they are stacked and are located just next to ERES sites [1, 73] indicating that vesicles formed from ERES immediately lead to formation of new Golgi cisternae.

Yeast Golgi shows some unique features. For example, during subcellular fractionation by density gradient ultra-centrifugation, late cisternae tend to be denser compared to early cisternae [179]. Immunofluorescence studies show non-overlapping pattern of different Golgi proteins which indicate that yeast Golgi cisternae behave as individual, separate entities. This provided great opportunity to test cisternal maturation model in *S. cerevisiae.* Two different Golgi resident proteins localizing to distinct compartments were

labeled with different fluorescent proteins. Individual cisterna was followed using high end confocal microscopy by two different groups separately. In this study, it was observed that a Golgi cisterna forms *de novo*, changes its nature from cis to trans over the time and then disappears. This gave a very strong result in support of cisternal maturation model to explain transport of cargo through Golgi cisterna [6, 7].

N-myristoyl transferase1 (Nmt1):

Nmt1 catalyzes co-translational transfer of myristic acid (C14:0) to N-terminus Glycine residue of substrate proteins. Peptides with Asn, Gln, Ser, Val, or Leu penultimate to the amino-terminal Glycine are substrates of Nmt1 but peptides with Asp, D-Asn, Phe, or Tyr at this position cannot be myristoylated [180]. Substrates of Nmt1 include proteins involved in cell growth and signal transduction as well as some viral proteins. Myristoylation of Golgi localized Arf1 at Glycine 2 is important for function of Arf1 [181]. Because of this, Nmt1 has become a target for developing anti-viral, anti-fungal drugs. Nmt1 is essential for vegetative growth of *S. cerevisiae.* Localization of Nmt1 was confirmed to be cytosolic from fractionation, EM, immunocytochemical analysis [182]. Nmt1p has a sequential ordered mechanism. The apo-enzyme first forms myristoyl CoA:Nmt binary complex. The substrate peptide then binds to form a ternary complex. This is followed by catalytic transfer of myristate from CoA to substrate peptide, then release of CoA, and subsequently release of myristoylpeptide [183]. Examples of NMT1 substrates include protein kinases such as the catalytic subunit of protein kinase (PK-A), phosphatases such as calcineurin B**,** proteins involved in transmembrane signaling such as several guanine nucleotide-binding α subunits of heterotrimeric G proteins, the gag polyprotein precursors of a number of retroviruses e.g. HIV-I and Moloney murine leukemiavirus) as well as the capsid proteins of some papovaviruses and picornaviruses.

ADP Ribosylation Factor 1 (Arf1):

Arf1 encodes for a small Ras family GTPase. Arf1 is important for coated vesicle

budding from Golgi and for regulation of vesicle trafficking. Arf1 has a paralog Arf2. Yeast Arf1 encodes 181 amino acid proteins with molecular weight of 21KD. Deletion of Arf1 causes mild defects of secretion and arf mutants show altered Golgi cisternal structure [32]. Arf1 and Arf2 share 96% identical sequence. They also have interchangeable functions although Arf1 accounts for 90% of Golgi associated Arfs [184]. N-terminal Myristoylation at Glycine 2 is a conserved feature of Arfs and is important for their GTP dependent membrane binding function [185]. Arf1 is a GTPase switch. Arf1 contains Golgi localization sequence. Arf1-GDP binds to p24 dimeric complex at Golgi membrane. Arf1 GEFs of GBF1 (Gea1 and 2) and BIG (Sec7) activate Arf1 at Golgi membrane. Once Arf1 and its GEF both are recruited to membrane, Sec7 domain of GEF carries out activation of Arf1. When it is bound to GTP a conformational change is induced in Arf1 where its N-terminal amphipathic myristoylated helix gets exposed. By insertion of this helix into bilayer, Arf1 secures its membrane anchorage [80]. A recent report contradicts this and says that after exposure of N-term helix, instead of being inserted within the bilayer parallel to the phospholipid-acyl chains, the myristic fattyacyl chain appears on top of the bicelles, perpendicular to the phospholipids [186]. This needs to be further evaluated. The well-known Arf effectors include coat complexes, such as the cis-Golgi-localized COPI (coat protein complex I) coat, and trans-Golgi network-endosomal clathrin coats.

Vrg4:

Vrg4 (Vandate Resistance Glycosylation) is a cis Golgi localized GDP mannose transporter that is essential for vegetative growth of *S. cerevisiae*. It has a paralog named Hvg1. The function of this protein is to transport the GDP-mannose inside the lumen of Golgi apparatus. The mutations in Vrg4 cause defects in N-linked, O-linked glycosylation of proteins and mannosylation of sphingolipids [187]. Along with this, other function of Vrg4 is to retrieve ER localized BiP from Golgi and maintaining normal membrane morphology [188]. Vrg4 localizes to early Golgi membrane with help of several transmembrane domains. Vrg4 is present as oligomer. C terminal domain of Vrg4 is required for its assembly into

oligomers. Vrg4 lacking N-terminal domain are stable and multimerize but are mislocalized to ER. This suggested that N-terminal domain is important for correct localization of the protein to Golgi membranes [189]. Golgi mannosyl transferases are type II membrane proteins having a short cytosolic N-terminal domain followed by a transmembrane domain to anchor the enzymes to the Golgi membrane. The transmembrane domain is followed by a non-conserved stem and a more conserved C-terminal globular catalytic domain. To label Vrg4 with fluorescent protein like GFP, GFP is often attached to N-terminus of Vrg4 so as to achieve proper folding of GFP which is much better in cytosol than in Golgi lumen [6, 190].

Gea2:

Gea2 (Guanine nucleotide Exchange on ARF) is a guanine nucleotide exchange factor required for Arfs activation at early Golgi cisternae. Other than this, Gea2 also functions to organize actin cytoskeleton in S. cerevisiae. It has a paralog Gea1. Gea2 was initially identified as multicopy suppressor of *sec21-3*mutant. Gea1 and Gea2 have partially overlapping functions as deletion of any of the two genes has no obvious phenotype change. But the double deletion is not viable. Gea2 is present as free soluble as well as membrane bound form. Membrane bound form localizes to Golgi membranes and is required for Golgi to ER transport [191]. Like all GEFs, catalytic activity of Gea2 localizes to amino terminal 200 amino acids which is also called as Sec7 domain. Gea2 localization is a matter of debate. Fractionation studies have shown that Gea2 co-fractionates with late Golgi protein Kex2 and Drs2 but some fraction of Gea2 also overlaps with early Golgi markers [192]. Some fractionation studies showed that Gea2 co-migrates with other cis Golgi markers [191]. Other reports have shown that the Gea1p/Gea2p pair is required in the early secretory pathway [193, 194]. Gea2 is also known to interact with early Golgi localized Gmh1 from co-immunofluorescence experiments [195].

Sec7:

Sec7 is a BIG family guanine nucleotide exchange factor required for activation of Arfs. It's a very large protein having 2009 amino acids. Sec7 was first identified from the mutation study that caused secretion defects [107]. This gene is essential for vegetative growth of yeast cells. The catalytic activity of Sec7p resides in a 200 amino acid domain called the Sec7 domain [196]. This domain is conserved in proteins from yeast and many other species. Sec7 is sensitive to a drug Brefeldin A, a fungal metabolite which is known to inhibit secretion. An important feature of catalytic domain of Sec7 is its "glutamic finger" [197]. Sec7 localizes to membranes via its HDS1 domain by interaction with its product, activated Arf1 thus forming a positive feedback loop and stabilizing its localization. Also the auto inhibition caused by Sec7 C-terminus is relieved after its stable recruitment to membrane [198]. A recent report suggests that Arf1, Arl1, Ypt1 affect the membrane localization of Sec7 and ypt31/32 can stimulate GEF activity of Sec7 [199].

Sec7 localizes to late Golgi cisternae [200]. Sec7 is peripheral membrane protein abundantly present on the late Golgi membrane. This was used as a marker to label late Golgi in many studies. Late Golgi cisternae can be labeled by Sec7 GFP or Sec7 DsRed very well [6, 201].

Chapter 2

Role of Sec12 in Size Control Mechanism of Endoplasmic Reticulum Exit Site

2.1. Introduction:

Proteins are synthesized on endoplasmic reticulum membranes (ER) and then translocated in ER lumen. Once they are correctly folded, they are exported out from ER. Specialized subdomains of ER that specifically carry out this function are called as ER exit sites (ERES). These are ribosome free domains of ER. The cargo proteins that are ready for export are accumulated near ERES. Secretory vesicles containing cargo proteins are formed at ERES. These vesicles are coated with COPII coat proteins. Components of COPII coat include subunits like Sar1 GTPase, Sec23, Sec24 and Sec13, and Sec31. After emerging from ER, secretory COPII vesicles fuse with each other by homotypic membrane fusion creating pre-Golgi elements. In essence, ERES are birthplaces of Golgi apparatus. Thus to understand the size control mechanism of Golgi it is essential to study ER exit sites, specially the factors that control their size or dynamics.

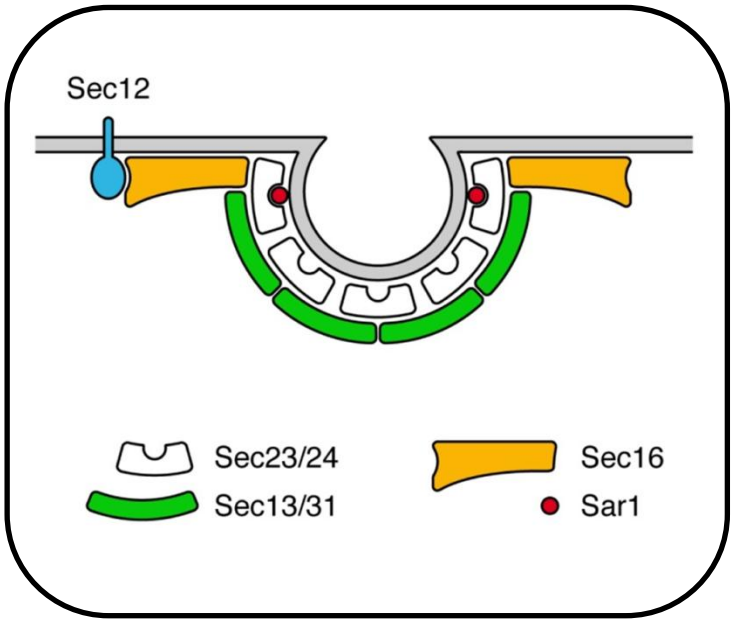

Fig 2.1: Schematic representation of COPII vesicle formation [66]

Fig 2.1 shows schematic representation of vesicle budding at ERES. Sec12 is a trans membrane ER protein that initiates COPII vesicle formation by catalyzing

guanine nucleotide exchange on the GTPase Sar1 which has been shown to possess membrane curvature induction capability [79, 82]. Once Sar1 is bound to GTP, it gets recruited to ER membrane near a scaffolding protein called Sec16. Recruitment of active Sar1 to membrane induces membrane curvature and also recruits Sec23-24 complex at ERES. This in turn recruits the Sec13-31 complex at ERES. Thus formation of COPII vesicles is triggered by activation of Sar1 GTPase by its GEF Sec12. Since Sec12 functions at very early stage of COPII assembly pathway we chose to study Sec12 in the context of studying size and dynamics of ERES. Also in different species, there are different localization patterns found for Sec12. We also intended to study the exact localization of Sec12 in mammalian cells. In addition, Sec16 and Sec12 are reported to be very important factors that were implicated separately before in the dynamics of ER exit sites. [62, 70, 202, 203]. However it was not known if these two proteins interact with each other at ER exit sites.

Hence the objective of current study is to investigate the role of Sec12 in size regulation of ERES and also to study if Sec12 and Sec16 interact with each other in mammalian cells. The specific questions answered in this study are as follows:

1. Where does the Sec12 protein localize in mammalian cells?
2. What is the effect of over expression of Sec12 on size of ERES?
3. Does Sec12 interact with Sec16?

2.2 Materials and Methods:

2.2.1 Source of reagents:

1] Bacterial cell culture: Luria broth/agar powder (HiMedia), Kanamycin (Sigma Aldrich), Glycerol (SRL), Lysozyme (Sigma), Sterile disposable 90mm petri plates (Genetix); 12ml round bottom tubes (Genetix), Baffled flasks (Allied Scientfic), Host strain: *E. coli* DH5α (Glick lab), glass beads (Sigma), SOC, 1.5ml eppendorfs, tips - 1ml, 200µl (Tarsons), tips-0.2 µl (Axygen), T50, T15 tubes (Genetix)

2] Common salts, buffers, detergents, organic reagents Sigma, USB, Merck, HiMedia, SRL, Qualigens

3] Plasmids: pCMV 3X FLAG-1A (Stratagene), pmGFP-C1 (Clonetech), pmYFP-C1 (Clonetech) (fig 2.2)

4] Oligos: Oligonucleotide primers: Sigma Aldrich (Appendix 1)

5] Cloning: Restriction enzymes (New England Biolabs), DNA polymerase (Phusion high fidelity DNA polymerase, NEB), DNA modifying enzymes (New England Biolabs, Fermentas), DNA Ligase (New England Biolabs), PCR tubes (Axygen)

6] Plasmid DNA extraction: CsCl density gradient ultra-centrifugation- Salts and buffers (mentioned later), absolute alcohol, Syringes (Dispovan), Needles (BD),Butanol, Plasmid miniprep kit (Qiagen), TELT buffer method.

7] DNA gel electrophoresis: Agarose (HiMedia), Ethidium bromide (Sigma), 6X Gel loading dye (Bromophenol blue, glycerol, SDS, EDTA, nuclease free water), DNA molecular weight markers (New England Biolabs)

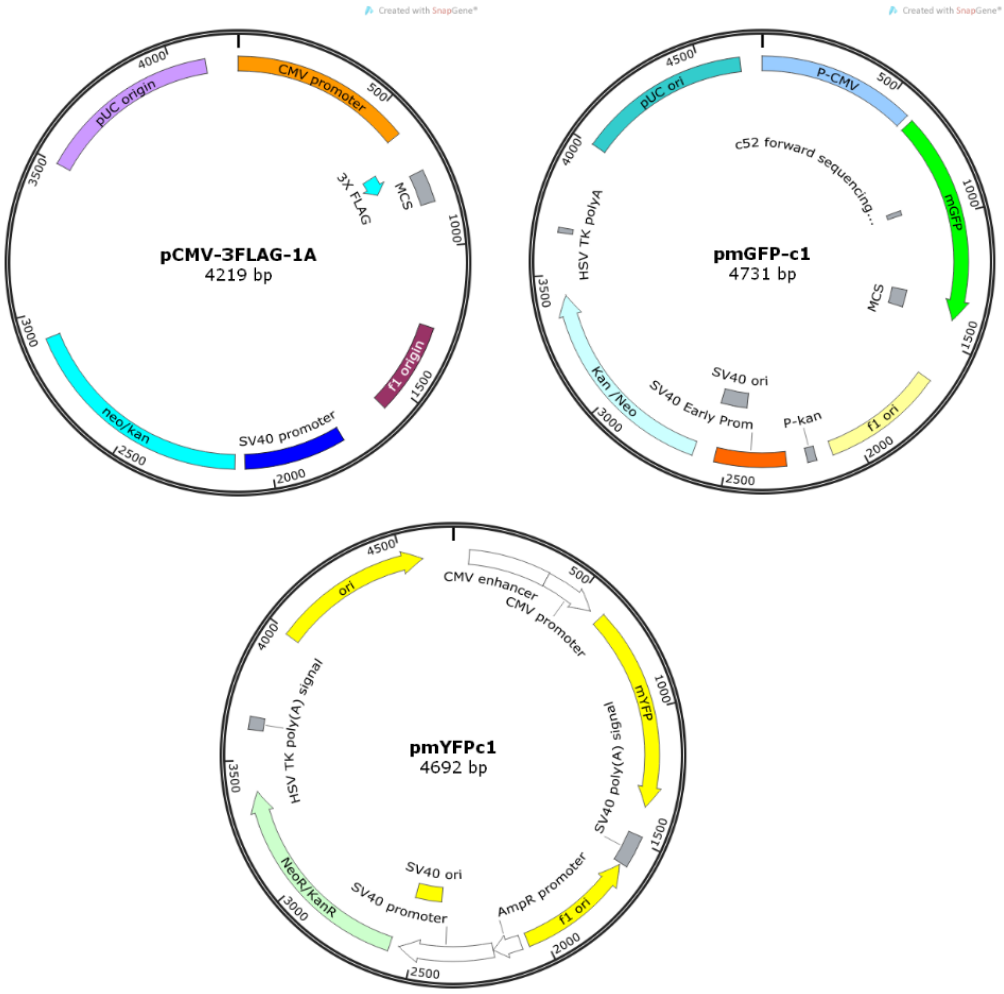

Fig 2.2 Maps of commercial mammalian expression Vectors

8] DNA fragment preparation: Nucleotide removal kit(Qiagen), Gel extraction kit (Sigma)

9] Mammalian cell culture: DMEM (HiMedia), FBS (Gibco), Anti-bacterial Anti-mycotic (Gibco), Trypsin-EDTA (Gibco), Tissue culture plastic ware (Nunc), cryovials (Tarsons, Corning) and centrifuge tubes (Nunc, BD Falcon, Thermo-Fisher, Greiner, Genetix), Glass bottom plates with cover glass no 1.5 (Cell E and G), DMEM without Phenol Red for live cell imaging (HiMedia), DMSO (Sigma), Filters for sterilization (Millipore)

10] Transfection: Calcium Phosphate mediated transfection- NaCl, KCl, $Na_2HPO_4.2H_2O$, dextrose, HEPES, Tris.Cl, EDTA, $CaCl_2$.

11] Cell lysis: Tris, NaCl, PMSF (Sigma), NP40 (Sigma), Complete mini protease inhibitor cocktail (Roche)

12] Immunoprecipitation, Protein electrophoresis/detection: Protein Assasy (Bio-Rad), Acrylamide (USB), Bis-acrylamide (USB), SDS (Sigma), Tris (Sigma), TEMED (Sigma), APS (Qualigens), BSA (Sigma) β-mercapto ethanol (Sigma), Protein A agarose (Calbiochem), Protein pre-stained ladder (Fermentas), ECL+ detection system (GE Healthcare), PolyvinylideneDifluoride (PVDF) membranes (Amersham), membrane filters(Millipore), X-ray films (Kodak), Filter papers (Whatman), cut-tips for handling protein A-agarose beads.

13] Immunofluorescence: Methanol (SRL, Merck), Normal horse serum (Vector Laboratories, Burlingame, CA), PBS, BS^3 ((Pierce, Rockford, IL), *n*-propyl gallate (), SecureSlip™ Coverslips (Grace Biolabs), Ethylenediamine.

14] Antibodies: GFP immunoblotting- rabbit polyclonal antibody (Abcam cat. #ab290, FLAG immunoblotting- mouse monoclonal antibody (Sigma cat.#F1804, FLAG Immunoprecipitation- polyclonal rabbit anti-FLAG antibody (Sigma cat.#F7425), Sec12-Goat anti hPREB (RandD Systems cat.#AF5557), Sec16- Rabbit polyclonal anti-KIAA0310 antibody from (Bethyl Laboratories cat. #BL2467), Alexa Fluor 594 donkey anti-goat- A-11058, Alexa Fluor 488 chicken anti-rabbit IgG- A-21441(Invitrogen)

2.2.2 Instruments:

37^0C Bacterial incubator (Trishul Equipments), 37^0C Bacterial shaker incubator (Trishul Equipments),Table top centrifuge (eppendorf Centrifuge 5418), Refrigerated centrifuge (eppendorf Centrifuge 5430R), Bacto hood (Micro-filt), ultra-centrifuge (Beckman Coulter/Sorvall), Weighing balance (AND), pH meter (Eutech), Magnetic stirrer (Spinot), Autoclave, Vortex mixer (Genei), -80^0C refrigerator (Sanyo), -20^0C refrigerator (Sanyo), 4^0C refrigerator (Godrej), 37^0C and 42^0C water-bath (TrishulEquipments), NanoDrop, Agarose gel electrophoresis apparatus (Hoefer), Gel Doc system (EC3 Imaging System), CO_2 incubator (Thermo), inverted microscope(Nikon), Laminar air flow unit (Esco), Vacuum pump (Welch), Spectrophotometer (Shimadzu), Cell scraper (Genetix), Protein gel electrophoresis apparatus (Bio-Rad), transfer apparatus (Bio-Rad), rotator (Trishul Equipments), rocker (Trishul Equipments), Thermo mixer comfort (eppendorf), Confocal microscope- Zeiss LSM 510 Meta

2.2.3 Materials:

Bacterial culture

Luria-Bertani (LB),) medium A minimal growth medium used for culture and maintenance of different *E. coli* strains harboring desired plasmids. Powdered Luria Broth (20g) was dissolved in 800 ml deionized 'MilliQ' (D/W) and the volume was adjusted to 1 litre (L) with D/W and sterilized by autoclaving. For making LB-agar plates, 20g bacteriological grade agar powder was dissolved/ L sterilized by autoclaving and poured in 90 mm sterile plates.

Antibiotics Ampicillin and Kanamycin were used for selection of clones or propagation of plasmids carrying the respective antibiotic markers. Stock solutions (100 mg/ml) were prepared and stored at -20°C. Antibiotics were added to the media (broth/agar plates) at 50 μg/ml final concentration for ampicillin and 30μg/ml for kanamycin. For making plates, antibiotics were added to molten agar medium after autoclaving when it was about to solidify to prevent the loss of activity.

Ultra-competent cells SOB (Super Optimal Broth): Following components were mixed in the required volume of D/W: 2% Bactotryptone, 0.5%Yeast extract, 10 mM NaCl, 2.5 mM KCl, 10 mM $MgCl_2$, 10mM $MgSO_4$

Transformation buffer (TB): The following components were added to 100 ml of D/W; 10 mM PIPES, 15 mM $CaCl_2$, 250 mM KCl, adjusted pH to 6.7 with 5N KOH, later added 55 mM $MnCl_2$, filter sterilized through 0.2 μ membrane filter and stored at 4C.

Bacterial freezedowns: overnight grown bacterial culture, sterile 50% glycerol in distilled water.

Plasmid DNA preparation

Plasmid Isolation: For cloning purpose, miniprep was done using Qiagen miniprep kit.

Plasmid isolation for screening of clones: TELT buffer (50mM TrisCL pH7.5, 62.5mM EDTA pH-8, 0.4% Triton X100, 2.5M LiCl), Lysozyme (50mg/ml), 70% ethanol, absolute alcohol, TE buffer.

Large scale plasmid DNA isolation: CsCl density gradient centrifugation method

(Solution I): 50 mM Glucose, 25 mMTris.Cl (pH 8.0), 10 mM EDTA.$2H_2O$; D/W to make up the total volume; *Lysis solution* (Solution II) freshly prepared: 0.2 N NaOH, 1% SDS; D/W to make up the total volume; *Neutralization solution* (Solution III): 5M Potassium Acetate 60 ml, Glacial acetic acid 11.5 ml, D/W 28.5 ml; Tris*/EDTA* (TE): 10 mM/1 mM, pH 8.0, D/W to make up the total volume. *Lysozyme solution*: (50mg/ml in 20mM Tris-HCl pH 7). *Cesium chloride*: 1 g/ml in TE buffer; isopropanol, absolute ethanol, 70% ethanol, water saturated butanol; *Ethidium bromide* (EtBr)*:* 10 mg/ml in D/W

Cloning

Polymerase Chain Reaction: 10X Phusion HF buffer/ 10X Phusion GC buffer, 10mM dNTPs (dATP, dCTP, dTTP, dGTP), oligonucleotide primers, nuclease free water, Phusion high fidelity DNA polymerase, Pfu Turbo polymerase, DMSO (if required), template DNA (plasmid or cDNA)

Restriction digestion: 10X buffer for respective restriction enzyme, nuclease free water, template DNA for digestion, restriction enzyme, BSA (if required)

Ligation: Vector and insert fragment (digested with suitable enzyme), 10X T4 DNA ligase buffer, T4 DNA ligase, 50% PEG (if required), nuclease free water to make up volume to 10µl.

Transformation: ligation mixture (10µl), plasmid (100ng), ultra competent *E.coli* cells (DH5α), Sterile SOC broth (SOB-98ml, 2M $MgCl_2$-1, 2M glucose-1ml), LB agar plates with 50 µg/ml of ampicillin, or kanamycin, sterile toothpicks.

Agarose gel electrophoresis:

Sodium Borate (SB) buffer: To 800 ml MiliQ water 8g NaOH was dissolved.35 g boric acid was added. Later boric acid was added to make pH 8. The volume was made to 1L to make it 20X solution. Using this stock dilution was done to prepare 1X working solution. *6X gel loading dye*: (1.2ml glycerol, 1.2ml 0.3mM EDTA, 300µl of 20% SDS, 160 µl of 0.5% Bromophenol blue stock, nuclease free water to make volume to 10ml);

EtBr: 0.5 µg/ml; agarose, 100 bp and 1 Kb ladder (NEB)

Mammalian cell culture

Cell lines used:

Name	Tissue origin	Medium
U2OS	Human Bone Osteosarcoma Cells	DMEM
HeLa	Human Cervical cancer Cells	DMEM

Table 2.1: Cell lines used

Dulbecco's Modified Eagle Medium (DMEM) 13.5g powdered medium was dissolved in~900 ml autoclaved distilled water, supplemented further with 3.7 g sodium bicarbonate(NaHCO3). pH was adjusted to 7.1-7.2 with concentrated HCL or 0.5N NaOH and volume made up to 1 L. The medium was filtered through 0.22 µ sterile filter and stored at 4°C.

Fetal bovine serum (FBS): Serum was aliquoted in sterile T50 tubes (50 ml/ sterile tube) and stored at -80°C.

Complete medium (CM): DMEM supplemented with 10% FBS and 1% antibiotics was prepared as needed.

Freezing medium: 90% FBS and 10% DMSO; storage at -20 °C.

Phosphate buffered saline (PBS) NaCl-8.0 g, KCl-0.2 g, KH_2PO_4-0.24 g, Na_2HPO_4. $2H_2O$-1.44 g dissolved in 1L distilled water; pH was adjusted to 7.4 and sterilized by autoclaving

Trypsin–EDTA: EDTA disodium salt-0.01g, D-glucose-0.1g, KCl-0.04g, NaCl-0.8g, $NaHCO_3$-0.058g, Trypsin-0.025g, pH was adjusted to 7.2 and volume made up to 100ml, sterilized by passing through 0.22µ sterile filter and stored at 4°C.

Transfection

Calcium Phosphate mediated transfection

2 M $CaCl_2$: 10.8 g $CaCl_2$.6H2O was dissolved in 20 ml distilled water, filter sterilized through 0.22 µ filter, 1.0 ml aliquots were made and stored at -20°C; 2X HEPES buffered saline (HBS): 280mM NaCl,10mM KCl, 1.5mM $Na_2HPO_4.2H_2O$, 12mM dextrose, 50mM HEPES. The pH was adjusted to 7.05 with 0.5N NaOH. The solution was filter sterilized through 0.22µ filter, 5 ml aliquots were made and stored at -20°C; 0.1X TE (pH 8): 1mM Tris.Cl (pH 8) and 0.1mM EDTA (pH 8) were sterilized by passing through 0.22µ filter and stored at 4^0C; DNA: Dissolved CsCl density gradient purified DNA in 0.1X TE (pH 8) at concentration of 40µg/ml. (~20µg DNA/10^6 cells); DMEM was prepared with 10% FBS and antibiotic; Cells in culture were maintained at appropriate confluency (~50-60 %).

Live cell imaging of transfected cells: DMEM without phenol Red, 1X PBS, 200mM glutamine

Cell lysis for Co-Immunoprecipitation

1X PBS, Cell lysis buffer: 50 mM Tris-HCl, pH 7.9, 50 mM NaCl, 1 mM phenylmethylsulfonyl fluoride, 0.5% NP-40 supplemented with the 10% Complete mini protease inhibitor cocktail (dissolved 1 tablet of complete mini in 1ml distilled water, stored at -20^{0}C)

Protein quantification: Bradford reagent, BSA 1mg/ml

Immunoprecipitation

3 mg of cell lysate; Protein A-agarose beads; Low salt buffer: 10mM HEPES (pH 7.9), 20µg/ml PMSF, 1mM DTT, 10mM KCl, 1.5mM $MgCl_2$; 1% bovine serum albumin; polyclonal rabbit anti FLAG antibody; Wash buffer:20 mM HEPES, 100mM NaCl, 0.1% NP40; SDS-PAGE sample buffer

SDS-PAGE

30% Acrlyamide solution: 29g Acrylamide and 1g Bis-acrylamide were dissolved in distilled water on a magnetic stirrer overnight (O/N) at room temperature. The volume was made up to 100 ml and filtered through 0.45 µm filter and stored in a dark bottle at 4^{o}C; 10% SDS solution in distilled water; 10 % (w/v) solution of ammonium per sulfate (APS) freshly prepared; Tetramethylethylenediamine (TEMED). 1 M Tris buffer (pH 6.8) and 1.5 M Tris buffer(pH 8.8); 1X and 6X sample loading buffer: 50mM Tris.Cl (pH 6.8), 10% glycerol, 2% SDS, 1% β-mercapto-ethanol (BME), 0.1 % bromophenol blue; electrophoresis buffer: 25mM Tris base, 250 mM Glycine (pH 8.3) and 0.1% SDS; pre-stained protein molecular weight marker.

Transfer of proteins on PVDF membrane: PVDF membrane, Whatman filter paper No. 1.5, methanol; high glycine transfer buffer: 0.1M Tris, 0.19M glycine, 20% methanol, 0.04% SDS

Western blotting

Tris buffered saline (TBS): 150/500 mM NaCl, 20 mM Tris (pH 7.4); 10X TBS: 200mM Tris.Cl (pH 7.6-8), 1.5M NaCl (pH 7.5); Tris buffered saline with Tween (TBS-T): 1X TBS + 0.1 % Tween 20; Blocking agent: 5% milk in 1X TBS; Primary antibodies and HRP conjugated secondary antibodies; Detection system: Chemi luminescent substrate (ECL+); X-ray films and exposure cassette.

Immunofluorescence

1X PBS, Methanol; Blocking solution: 20µl Normal Horse Serum in 1ml PBS, Mounting solution: To 90 mL glycerol, added 10 mL of 10X PBS that had been adjusted to pH 9 with 0.5 M Na_2CO_3. Dissolved *n*-propyl gallate, in this solution to 5% (w/v) using bath sonication. Stored at –80°C in 200-µL aliquots; BS3 solution (100X): dissolved bis (sulfosuccinimidyl) substrate to 10 mM in deionized water. Stored at -80^0C in 10µL aliquots. Ethylenediamine: 100 mM solution. Added 669 µl pure ethylenediamine to 90 mL deionized water. Added 2 mL of 6 M HCl to bring the pH to approximately 8.Then adjusted the pH to 7.5 with additional 6 M HCl. Adjusted to 100 mL with deionized water. Filter sterilized, and stored at 4^0C and protected from light.

2.2.4 Softwares: Snapgene 2.5, ImageJ, LSM browser, Bitplane-Imaris 7.7, Adobe Photoshop CS6, Microsoft office, Filemaker pro.

2.2.5 Methods

Designing cloning strategies: Molecular biology procedures were simulated and recorded using SnapGene software (GSL Biotech, Chicago, IL, USA)

Preparation of ultra-competent E. coli

Higher competency is very important to ensure high transformation efficiency that often helps cloning. For better cloning efficiency, EndoA$^-$ and RecA$^-$ genotype, *E.coli* strain DH5α was made ultra-competent for the transformation of recombinant/routine plasmid vectors.

1. E. coli DH5α cells were streaked on LB Agar plate and incubated overnight at 37^0C.
2. Single colony was inoculated in 250 ml SOB and incubated on shaker with 200 rpm speed at 18^oC until OD_{600} = 0.6.
3. Flask was kept on ice for 10 min. Culture was spun at 2500 x g (3500 rpm) in centrifuge for 10 min at 4^oC.
4. The cells were re-suspended gently in 80 ml of ice cold transformation buffer and kept on ice for 10 min.
5. The mixture was spun at 2500 x g (3500 rpm) centrifuge for 10 min at 4^oC.
6. The cells were gently re-suspended in 20 ml of ice cold transformation buffer. Kept on ice for 10 min.
7. DMSO was added to a final concentration of 7% i.e. 1.4 ml and mixed well and aliquots of 100ul were plunged in liquid nitrogen and Stored at -80^oC.

Plasmid DNA isolation

QIAGEN Miniprep method

The procedure is based on alkaline lysis of bacterial cells followed by adsorption of DNA onto silica column in the presence of high salt. Preparation is based on 3 basic

steps: 1. Preparation and clearing of a bacterial lysate, 2. Adsorption of DNA onto the QIAprep membrane, 3.Washing and elution of plasmid DNA.

1. 10ml bacterial culture was grown overnight in a flask at 37^{o}C with 180 rpm shaking for getting 100µl of plasmid DNA with concentrations around 400µg/µl.
2. The following protocol is for 1-5ml overnight grown bacterial culture. The amounts of solutions were scaled up or down in proportion to volume of culture used for plasmid isolation.
3. The cells were pelleted by spinning them at 13000 rpm for 1 min.
4. Pelleted bacterial cells were re-suspended in 250µl Buffer P1 and transferred to a microcentrifuge tube.
5. 250 µl buffer P2 was added and mixed thoroughly by inverting the tube 4–6 times.
6. 350 µl buffer N3 was added and mixed immediately and thoroughly by inverting the tube 4–6 times.
7. The mixture was centrifuged for 10 min at 13,000 rpm (~17,900 x *g*) in a table-top microcentrifuge.
8. The supernatant from step7 was applied to the QIAprep spin column by decanting or pipetting. The column was centrifuged for 30–60 s and flow-through discarded.
9. QIAprep spin column was washed by adding 0.75 ml buffer PE and centrifuged for 30–60 s.
10. The flow-through was discarded, and centrifuged at full speed for an additional 2 min to remove residual wash buffer.

11. The QIAprep column was placed in a clean 1.5 ml microcentrifuge tube. To elute DNA,50µl Buffer EB (10 mM Tris·Cl, pH 8.5) or water was added to the center of each QIAprep spin column, let stand for 2 min, and centrifuged for 1 min at 13000rpm. For better yield the EB buffer was pre-warmed at 55^{o}C.

TELT buffer method

This is a quick protocol for preparing plasmid DNA mainly for clone screening purpose. This protocol was used to identify positive clones after ligation and transformation by restriction digestion.

1. Bacterial culture was grown in 1.5ml microcentrifuge tube overnight at 37^{o}C.
2. Cells were spun at 14000 rpm to pellet down the cells at 4^{o}C for 1min.
3. Supernatant was removed and pellet was re-suspended in 150µl TELT buffer and vortexed well.
4. 5.7µl lysozyme was added from 50mg/ml stock solution and mixed well.
5. Vials were kept on ice for 1min
6. Vials were placed on boiling water bath for 1min.
7. Immediately the vials were placed on ice for 10min.
8. Centrifuged at 4^{o}C at 15000rpm for 10min. Supernatant was collected in fresh vial.
9. 330µl chilled absolute alcohol was added and incubated at -20^{o}C for 30min/-80^{o}C for 15min.
10. The mixture was spun at 15000 rpm at 4^{o}C for 10min.
11. 200µl chilled 70% ethanol was added for washing the DNA pellet and again centrifuged at 15000 rpm at 4^{o}C for 5min.
12. The pellet was air dried and re-suspended in 20µl TE buffer.

CsCl equilibrium density gradient centrifugation

It is very important to get high quality plasmid DNA for transfecting mammalian cells with high efficiency for downstream experiments. CsCl equilibrium density gradient centrifugation yields very pure plasmid DNA preparation which is completely free from salts, broken fragments. These broken fragments and phenol associated with DNA often reduce transfection efficiency. Under high centrifugal force, a solution of cesium chloride (CsCl) forms a shallow density gradient. DNA molecules placed in this gradient migrate to the point where they have the same density as the gradient (the neutral buoyancy or isopycnic point). The gradient is sufficient to separate types of DNA with slight differences in density due to differing [G+C] content, or physical form (*e.g.*, linear *versus* circular molecules).

1. 500 ml culture was spun at 5000 rpm for 10 minutes in a sorvall GS-3 at 4^0C. The supernatant was thrown and pellet was re-suspended in 18 ml solution I by vortexing.

2. After pellet is properly re-suspended (without clumps), 2 ml lysozyme solution was added to the tube and mixed.

3. 40 ml freshly prepared solution II was added to each tube and mixed by inverting slowly. The tubes were incubated at RT for 10 minutes.

4. 20 ml ice chilled solution III was added to the tubes, mixed by shaking and stored on ice for 10 minutes.

5. The tubes were spun at 5000 rpm for 15 minutes at 4^0C in sorvall SS-34. During this interval, TE buffer was prepared.

6. The supernatant was filtered into HS 50 tubes by passing through gauze (4 fold). 0.8 volume isopropanol was added to each tube. Reaction was incubated at RT for 10 minutes and then spun at 8000rpm for 15 minutes at RT in SS-34 sorvall rotor.

7. The pellet was washed with sterile 70 % alcohol, 5 ml/tube and then spun at 4^0C at 8000 rpm for 10 minutes.

8. The pellet was dissolved in TE 8.5 ml.

9. After pellet was dissolved properly, 8.5 grams CsCl was added to each tube. CsCl was dissolved properly and 0.25 ml of (10mg/ ml) ethidium bromide was added to it. It was mixed and spun at RT for 5 minutes at 8000 rpm.

10. This mixture was loaded in tubes, sealed and balanced. Ultra-centrifugation was done for 22 hours at 60, 000 rpm in ultracentrifuge.

11. After the run was over, the tube was pricked on top of the tube by 23 G needle and band of covalently closed circular DNA was pulled from tube by 18 G needle.

12. After pulling the band, it was released in 15 ml tube. Equal volume of water saturated butanol was added to it, vortexed and spun at 3000 rpm for 2 minutes.

13. Step 12 was carried out till pink color was completely gone and both layers were colorless. Step 12 was repeated one more time.

14. Now, 2 volume of sterile dH_2O and 6 volume of 100% alcohol were added to DNA solution (2ml DNA solution + 4ml dH_2O + 12ml 100 % ethanol) in new

T50.Mixture was incubated at 4^{o}C for 30 minutes to 1 hour then spun at 8000 rpm for 20 minutes at 4^{o}C.

15. 70% alcohol wash was given to the pellet and again spun 15 minutes at 4^{o}C at 8000 rpm.

16. Supernatant was thrown and tube was inverted on tissue paper. Pellet was completely dried till no alcohol smell is detected. DNA pellet is dissolved in ~500ul amount of H_2O.

Agarose gel electrophoresis

It is a routinely used method for the analysis and preparation of DNA molecules. The method uses naturally occurring polymer obtained from an Alga in order to achieve a semi solid gel conformation on which nucleic acids are separated based on their molecular weight and visualized by intercalating dyes like EtBr. Various size DNA fragments can be separated on agarose gels using different concentrations of agarose.

PCR fragments, DNA samples were analyzed on agarose gel made in 1X SB buffer. Ethidium bromide was used to visualize DNA fragments in gel. DNA solution was mixed with 6X agarose gel loading dye (so that final 1X concentration of dye is achieved). Agarose gels of varying concentration ranging from 0.5% to 2% were prepared depending on the size of DNA fragments that need to be separated. Standard 1Kb or 100bp ladders were run in parallel to understand the size of DNA fragments being analyzed. DNA bands were visualized using gel documentation system.

Polymerase chain reaction

PCR technique was developed by Karry Mullis which has proven really useful to all the molecular biologists. The technique provides specific amplification of the target

sequence with the help of two oligonucleotide primers that bind to opposite strand in a sequence specific manner. A thermostable DNA polymerase is then used for extension of the primers at 3' end. With help of this technique, primers can be designed to any specific gene of interest and this gene can be amplified from the template genome/plasmid/cDNA which can be further analyzed on agarose gel or cloned in the choice of vector for expression. Phusion high fidelity DNA polymerase was used for PCR amplifications because of its high speed and much lower error rate than other polymerases. This enzyme produces blunt ended amplicons. Atypical mixture of a PCR reaction includes following additives:

Components	**Final concentration**
H_2O	To make up volume (50µl)
5X buffer HF/GC (Depending on GC content)	1X
10mM dNTPs	200µM each
Forward primer	0.5µM
Reverse primer	0.5µM
Template DNA	50-100ng (plasmid DNA)
DNA polymerases	0.02 U/µl

Table 2.2: Contents of a PCR reaction

All the additions for PCR were done on ice. According to the need, additives like DMSO, $MgCl_2$ are added (if required) to achieve specific amplification. All components were mixed and centrifuged prior to use. It is important to add Phusion DNA Polymerase last in order to prevent any primer degradation caused by the 3′→

5´ exonuclease activity.After addition was done; the reaction was quickly transferred to a thermocycler preheated to the denaturation temperature (98°C).

The cycling instructions:

Cycle step	Temperature	Time	Cycles
Initial denaturation	98^{o}C	30s	1
Denaturation Annealing Extension	98^{o}C X^{o}C 72^{o}C	10s 30s 30s/Kb	30
Final extension	72^{o}C	8min	1

Table 2.3: Cycling conditions for PCR using Phusion DNA polymerase

The PCR product was then analyzed on agarose gels for checking amplicon size. Annealing temperatures required for Phusion tend to be higher than with other PCR polymerases. Typically, primers greater than 20 nucleotides in length were annealed for 30 seconds at 3°C above the Tm of the lower Tm primer (Lower Tm +3). If the primer length is less than 20 nucleotides, an annealing temperature equivalent to the lowest Tm among both primers was used. A temperature gradient was also be used to optimize the annealing temperature for each primer pair. Amount of template, annealing temperature, extension time was determined in every case by standardization to achieve maximum amplification of desired size with least non-specificity.

Quick change mutagenesis

To introduce point mutations or insertion or deletion of bases, quick change mutagenesis was carried out using high fidelity Pfu Turbo polymerase. Oligos were

designed as follows. 25 bases on either side of insertion/deletion/ mutation site were included for homology. Similar primer was designed for both top and bottom strands. The bases to be inserted were added or single base change was introduced between these flanking bases. Primer dilution was made by mixing 5µl of each forward and reverse primer (from 100µM stock) and 40µl ddH_2O (1:10 dilution). Template was prepared by diluting template plasmid with ddH_2O to get final concentration of 40ng/µl. The reaction was set up as follows:

Components	**Volume (µl)**
H_2O	41.5
10X buffer for Pfu Turbo	5
10mM dNTPs	1
Primer mix (1:10 dilution)	1
Template DNA (40ng/µl)	0.5
Pfu Turbo polymerases	1(20U)

Table 2.4: Contents of PCR reaction for site directed mutagenesis

Cycling conditions for quick change mutagenesis:

Cycle step	Temperature	Time	Cycles
Initial denaturation	95^oC	30s	1
Denaturation Annealing Extension	95^oC 55^oC 68^oC	30s 60s 2min/Kb	18
Final extension	68^oC	8min	1

Table 2.5: Cycling conditions for PCR for site directed mutagenesis by Pfu turbo polymerase

Restriction digestion

Restriction enzymes are the tools to cut template DNA at specific site in a sequence specific manner. This is the most important discovery in the history of molecular cloning. There are huge numbers of restriction enzymes identified till date. Each enzyme cuts at specific site after recognizing a specific sequence in the template DNA. To clone gene of interest in a suitable vector, restriction digestion cloning method was used. The components of preparative and analytical restriction digestion reaction were as follows:

Components	Preparative	Analytical
Template	2-3µg	100ng
H_2O	To make up volume to 50µl	To make up volume to 10µl
10X buffer	5µl	1µl
BSA	If required	If required
Enzyme	5-10U	2U

Table 2.6: Reaction mix for restriction digestion

All the components were added on ice and digestion reaction was carried out at 37^{o}C water bath for 4 hours to overnight for most enzymes. (Or at any other specific temperature as needed for enzyme in use) The digestion of DNA was analyzed on agarose gels.

Nucleotide removal

Enzyme contamination, salts or free nucleotides or <10mers generated from restriction digestion can interfere with subsequent downstream applications. While

doing successive digestion involving use of different buffers, a fast clean-up is often helpful instead of gel extraction. Such clean-up helps to get rid of enzymes, salts as well as free nucleotides or <10mers. The QIAquick system was used for fast clean-up of digestion reactions. QIAquick system combines the convenience of spin-column technology with the selective binding properties of a uniquely-designed silica-gel membrane. DNA was allowed to get adsorbed to the silica-membrane in the presence of high salt while contaminants pass through the column. Impurities were efficiently washed away, and the pure DNA was eluted with water.

1. 10 volumes of Buffer PN was added to 1 volume of the reaction sample and mixed. For DNA fragments ≥ 100 bp, only 5 volumes of buffer PN were added.

2. A QIA quick spin column was placed in a provided 2 ml collection tube.

3. To bind DNA to silica membrane, the sample was applied to the QIAquick column and centrifuged for 1 min at 6000 rpm.

4. The flow-through was discarded and QIAquick column was placed back into the same tube.

5. To wash QIAquick column, 750µl of buffer PE was added to column and centrifuged for 1 min at 6000 rpm. The flow-through was discarded completely. To ensure complete removal of ethanol, an additional 2 min centrifugation step at 13000 rpm was performed.

6. The QIAquick column was placed in a clean 1.5 ml micro-centrifuge tube. To elute DNA, 30-50µl of pre-warmed ($65^{o}C$) H_2O was added to the center of the

QIAquick membrane. The column was incubated for 2 min, and centrifuged at 13000rpm for 1min.

Purification of DNA fragments from agarose gel

Recovery of the restriction digested DNA fragments/ PCR products from agarose gel were done by using the GenElute Gel Extraction Kit (Sigma). DNA fragments of interest were extracted from slices of an agarose gel by solubilizing the gel. The gel solubilisation solution can dissolve an agarose slice from gels run in Sodium Borate Buffer. The extracted DNA fragments were then selectively adsorbed onto a silica membrane in the presence of the gel solubilisation solution. Contaminants were removed by a simple spin or vacuum wash. Finally, the bound DNA was eluted in Tris buffer. The isolated DNA was suitable for a variety of downstream applications, such as DNA sequencing, PCR, restriction digestion, cloning.

Precautions: Electrophoresis buffer, which has been used repeatedly, will reduce the DNA recovery efficiency hence freshly prepared agarose gel and fresh electrophoresis buffer were used for gel elution of DNA. Time for examination of ethidium bromide-stained gels with an UV transilluminator was minimized to avoid formation of Thymidine dimers. Preferably, a transilluminator equipped with a long-wavelength (302 nm) UV light source was used, as this will minimize the damaging effects of UV light on nucleic acids. For better yield of DNA or when eluting large linear DNA fragments (>3 Kb) the elution solution was preheated to 65 °C prior to use.

1. The DNA fragment of interest was excised from the agarose gel with a clean, sharp scalpel or razor blade. Excess agarose was trimmed away to minimize the amount of agarose**.**

2. The gel slice was weighed. 3 gel volumes of the Gel Solubilisation Solution were added to the gel slice. (For every 100 mg of agarose gel, added 300 ml of Gel Solubilisation Solution).

3. The gel mixture was incubated at 50-60°C for 10 minutes, or until the gel slice was completely dissolved with shaking at 1000rpm in thermo-mixer.

4. The binding column was prepared while the agarose was being solubilized. The GenElute binding column was placed into one of the provided 2 ml collection tubes.

5. 500 ml of the column preparation solution was added to each binding column and centrifuged for 1 minute. Flow through liquid was discarded.

6. Once the gel slice was completely dissolved, the colour of the mixture was checked. It should be yellow (If the colour of the mixture was red, added 10 ml of the 3 M Sodium Acetate Buffer, pH 5.2, and mixed. The colour should now be yellow. If not, added the 3 M Sodium Acetate Buffer, pH 5.2, in 10 mL increments until the mixture was yellow.

7. 1 gel volume of 100% isopropanol was added and mixed until solution was homogenous.

8. The solubilized gel solution mixture was then added to binding column and centrifuged for 1 minute at 6000rpm. The flow through liquid was discarded.

9. 700 ml of wash solution was added to the binding column and centrifuged for 1 minute at 6000rpm.

10. The binding column was removed from the collection tube and the flow-through liquid was discarded completely.

11. The binding column was placed back into the collection tube and centrifuged at 13000rpm again for 2 min without any additional wash solution to remove excess ethanol.

12. The binding column was transferred to a fresh collection tube and 50µl pre-warmed elution solution was added to the centre of the membrane and incubated for 2 min. The vial was centrifuged for 1 minute.

Blunting of DNA fragments

Because of unavailability of common cohesive end cutters in vector and insert fragments, the fragments need to be blunted to make ends ready for ligation. In this way, even if common cohesive ends are not available, vector and insert are cut with different cohesive cutters then blunted and ligated.

For blunting the DNA after cutting with an enzyme that leaves a 5' overhang, Klenow polymerase (*E coli* large subunit DNA polymerase) was used. Klenow polymerase has 5'→3' DNA polymerase and 3'→5' exonuclease activity. After the digestion, DNA was purified with nucleotide removal kit. For blunting, reaction mixture was prepared as follows: 1X Klenow buffer, 80µM of each dNTP, 1µl Klenow polymerase in total 50µl of DNA solution. The reaction was carried out by incubating at 25^{o}C for 30min. For blunting DNA after cutting with an enzyme that generates 3' overhangs, T4 DNA polymerase was used. The reaction conditions were as follows: 1X T4 DNA polymerase buffer, 100µM of each dNTP, 1X BSA, 1µl T4 DNA polymerase in total 50µl of DNA solution. Reaction was carried out at 11^{o}C for 20min.

Alkaline phosphatase treatment of vector DNA

Most common problem in efficient cloning is to avoid self-ligation of vector. This is usually avoided by removing 5'-phosphates from both the termini of digested vector using thermo-sensitive Alkaline Phosphatase that catalyzes the removal of 5'-phosphate groups from DNA, RNA, nucleotides, and proteins. Alkaline phosphatase is active in restriction digestion buffers. Hence after template digestion is complete, 1 µl alkaline phosphatase was added to same reaction and incubated at 37^0C for at least 2 hours.

Ligation

With help of T4 DNA ligase, sticky or blunt ended vector and insert fragments were ligated to generate desired clones. The typical ratio of vector: insert for a blunt/cohesive end ligation was set from 1:3 to 1:9 depending on sizes of the two components. Insert and vector fragments after various processes like digestion, blunting, alkaline phosphatase treatment were purified on agarose gel or by nucleotide removal method as needed. Before ligation, digested vector and insert fragments were checked on agarose gel for confirming proper digestion and concentrations. During ligation a phoshphodiester bond was formed between a 5'- phosphate and a 3'-hydroxyl of two DNA fragments. The reaction was catalyzed by the T4 DNA ligase. The reaction mix consisted of vector and insert at the required molar concentrations, 10X T4 DNA ligase buffer (final concentration of 1X), T4 DNA ligase-200U, nuclease free water to make up the volume to 10 µl; the reaction was incubated at 22°C for 2-4 hours. If required ligation reactions were incubated at 16^oC overnight.

Transformation

The process of introducing foreign DNA into bacterial cells is transformation. The cells were made susceptible (competent) to uptake DNA molecules by treatment with a solution of $CaCl_2$ and briefly warmed to generate pores in the bacterial cell wall for very short period of time. Surrounding DNA molecules in the solution were then taken up by competent cells.

1. Both ultra-competent cells and plasmid DNA vials were placed on ice; both were allowed to reach the ice temp.
2. 10ul of ligation mixture was added to 100µl competent cells. In case of plasmid DNA transformation, 100ng DNA was added to 100µl competent cells. The vial was gently tapped for mixing and placed back on ice.
3. The reaction was incubated on ice for 5-30 minutes on ice.
4. The reaction was then transferred to 42^oC water-bath for 45 seconds to give heat shock. Immediately, it was placed in ice for 5 minutes.
5. 200ul of ice cold SOC medium was added to reaction aseptically and was incubated at 37^oC with shaking at180 rpm for 60 min.
6. The cells were plated on appropriate antibiotic containing LB agar plate, incubated at 37^0C for overnight, and observed for colonies next day.

Screening of transformants

Many colonies were obtained after transforming the ligation mix. All these clones have to be screened for presence of specific insert. The transformants obtained by transformation of ligation mixture were screened for presence of desired insert by restriction digestion. Transformants were replica plated on antibiotic containing LB agar plates and also the same clones were inoculated in 1.5ml antibiotic containing

LB broth for miniprep by TELT buffer method. Vials were incubated at 37^0C overnight with 180 rpm shaking. Each clone was given a specific miniprep number for documentation. Following day, plasmids were isolated by small scale preparation method using TELT buffer. The plasmids along with vector control were then digested with restriction enzyme(s) to confirm presence of insert and digestions were analyzed by gel electrophoresis.

Freezing bacterial clones

In order to maintain the bacterial clones for future use, it is advised to store those in frozen condition. A glycerol stock kept at -80°C is the ideal way to store bacterial strains. Bacteria can be frozen using a solution of 50% glycerol. The process is simple and requires sterile cryo-vials, sterile 50% glycerol stock and overnight culture of the bacterial clone that needs to be frozen.

1. Single colony of bacterial clone was inoculated in LB Kana/ LB Amp. It was incubated overnight at 37^0C with 180 rpm shaking.
2. An entry was made in Filemaker database of the lab with all the details of the clone being frozen.
3. 0.55ml 50% sterile glycerol was added to 1.25ml overnight bacterial culture in a sterile cryo-vial.
4. A tough tag was stuck on top of cryo-vial and the freeze down number obtained from Filemaker database was written on it. The name of the strain and date was labeled on the freeze down vials.
5. Freeze stock was stored at specific location in bacterial freeze-down box in -80^oC.
6. Freeze stocks were always made in duplicates.

Reviving bacterial freeze downs

For reviving bacterial clones from freeze down, LB agar plate having specific antibiotic was pre-warmed at 37^{o}C. Frozen vial was taken out from -80^{o}C and was placed on ice. With the help of a sterile toothpick, chunk of material was picked from the freeze down vial and streaked on the pre-warmed plate. The plate was observed the following day for colonies after overnight incubation at 37^{o}C.

Mammalian cell culture:

Cell lines provide a continuous source of study material in laboratory conditions, with use of which, various biochemical, biophysical and cell biological processes can be studied. Cell lines are established from tissues in laboratory conditions. Normal cells usually divide only a finite number of times before losing their ability to proliferate, the event known as senescence. However, some cell lines become immortal through a process called transformation, which can occur spontaneously or chemically or virally induced. When a senescent cell line undergoes transformation and acquires the ability to proliferate indefinitely, it becomes a continuous cell line. Cell line maintenance requires a sterile atmosphere, nutrients through culture media and serum, optimum temperature (37°C), humidity and an optimum CO_2 level (~5%). All cultures were handled in appropriately certified bio-safety class II cabinets (Esco, Singapore) in sterile disposable plastic ware and cultured at 37°C in a humidified CO_2 incubator.

Reviving mammalian cell from frozen stocks

1. 10 ml pre-warmed respective media (For e.g. DMEM supplemented with 10% FBS and 1% Antibiotic) was added to 90 mm tissue culture petri plate.

2. Frozen vial was taken out from liquid nitrogen cylinder very carefully.

3. The vial containing cells was thawed in 37°C water bath for 2-3 min.
4. The entire content of the vial was pipetted out in 90mm tissue culture petri plate.
5. The plate was incubated in the CO_2 incubator.
6. Once cells were adhered to surface, they were washed with PBS and fresh media was added to the plate.

Routine maintenance of adherent mammalian cells

1. The media was removed with vacuum and the cells were washed with 1X PBS gently.
2. 1ml Trypsin EDTA was added in a T25 tissue culture flask and the flask was kept back in incubator for 4 minutes. (Trypsin concentration and incubation time will vary with different cell lines)
3. The plate was observed under microscope to make sure cells were completely detached (round in shape) from the surface of flask.
4. 5 ml of complete media was added to inactivate trypsin. The cells were detached from surface completely by pipetting gently.
5. The suspension was centrifuged at 500 rpm for 5 minutes in a T15 tube.
6. The supernatant was discarded; the cell pellet was re-suspended gently with 2-3 ml of complete media many times to make sure a single cell suspension was achieved.
7. The cells were counted with the help of Haemocytometer and seeded in required number in glass bottom plates (2ml fresh medium) for live cell

imaging or in 90mm plate (with 10ml fresh medium) for immuno-precipitation and also seeded in fresh 5ml complete media in T25 flask for maintenance.

8. The cells were routinely observed under microscope and passaged after every 2-3 days.

Freezing mammalian cells

1. Cells were grown in 90mm plates to sub-confluence. Over grown cells were not used for freezing purpose.
2. Cells were harvested by trypsinisation protocol and centrifuged at 500rpm for 5min to remove trypsin completely.
3. Cells were re-suspended in 3ml freezing media (90% FBS and 10% DMSO) by pipetting in and out to ensure single cell suspension formation.
4. Immediately, the re-suspended cells were aliquoted in 1ml aliquots into sterile cryo-vials.
5. The cryo-vials were placed in a cryo cooler with isopropyl alcohol that gives 1^{o}C/min cooling rate. This cooler was placed in -80^{o}C.
6. The next day, cryo-vials were taken out from cryo cooler and were immediately transferred to a cryo-box in liquid nitrogen.

Transfection using Calcium phosphate method [204]

The uptake of foreign DNA into the cells is facilitated by presenting nucleic acids as co-precipitates of calcium phosphate and DNA. This is a very cost effective method for routine transfections.

1. A day prior to transfection, freshly trypsinised cells were seeded in a 35mm glass bottom plate (for live cell imaging) or 90mm culture dish (for immuno-precipitation).

2. For transfection good quality plasmid DNA was prepared by cesium chloride density gradient method of plasmid purification. DNA was diluted in 0.1X TE buffer at the concentration of 40µg/ml.
3. Calcium phosphate-DNA precipitate was prepared as follows: For 35 mm plate, 200 µl of precipitate was added. First, 88µl of diluted DNA and 100µl 2X HBS was placed in a 1.5ml eppendorf. 12µl of 2M $CaCl_2$ was slowly added to the DNA-2X HBS mixture with gentle mixing over a period of 30s. For 90mm plate, 1ml of precipitate was added. It was prepared as follows: 440µl diluted DNA+ 500µl 2X HBS was placed in 15ml falcon tube. To this, 60µl 2M $CaCl_2$was added with gentle mixing over 30s.
4. The mixture was incubated at RT for 45 min. The above reaction mix after incubation was added drop wise to cells with gentle swirling of the plate and the cells were incubated overnight.
5. Next day, at least 16 hours post-transfection, fresh medium was added to the plate after washing the cells gently with PBS to remove residual precipitate of DNA and $CaPO_4$from the medium.
6. Expression of the gene was analyzed at different time points post transfection for live cell imaging, or cells were fixed for immunofluorescence 24 hours post transfection or harvested 24 hours post transfection for immuno-precipitation as per requirement of the experiment.

Live cell imaging of transfected cells

Localization of fluorescently tagged proteins can be studied accurately in live cell condition as fixation of cells using chemicals for immunofluorescence staining often leads to destruction of delicate intracellular structures. Localization of fluorescently tagged Sec12 and Sec 16 was analyzed by live cell imaging. For live cell imaging,

cells were seeded in 35mm glass bottom plates for transfection. Transfection of Sec12 and Sec16 was done using calcium phosphate method. Post 16 hours of transfection, cells were washed with PBS and DMEM media with glutamine supplementation without phenol red, was added to cells, which is a colorless medium suitable for fluorescence imaging. This plate was then directly placed on the microscope stage for live imaging at different time points (12 hour, 20 hour, 40 hour post transfection). While doing imaging, 37^0C and 5% CO_2 were maintained using a live cell chamber of microscope.

Immnunofluorescence [11]

Immunofluorescence is often used to study localization of a protein at its endogenous expression levels. Routine harsh fixation and washing steps tend to damage the delicate intracellular structures like ERES. A modified immunofluorescence method which makes use of fast dehydration using chilled organic solvent and rehydration in presence of a chemical cross-linker was used. Cross-linking stabilizes the subcellular structures during subsequent washing steps thus keeping cellular ultra-structures intact.

1. Secure Slip^{TM} coverslips were placed in 6 well plates and media was added to the wells. If a Secure SlipTM coverslip float, then they were pushed down with help of a sterile tip.
2. U2OS cells were seeded in such a way that cells are spread evenly without overcrowding. Cells were grown in normal growth conditions.
3. On the day of experiment, for each coverslip, a T50 tube was filled with methanol. The tubes were cooled to -20^{o}C.
4. Blocking solution was freshly prepared by adding 20µl NHS to 1ml 1X PBS and vortexed.

5. A humidified chamber was prepared for the incubations. A suitable chamber was created by placing a moist paper towel in a glass tray. This was covered with Saran wrap to avoid drying.
6. After 24 hours of seeding the cells, cover slip was taken out from media; excess media was soaked by inverting the coverslip on a paper towel and pressing gently on the bottom of the cover slip with forceps.
7. Within 30s of taking out the cover slip from 37^{o}C, cover slip was transferred to -20^{o}C pre-chilled methanol and cells were allowed to be fixed for 4 min in methanol.
8. Coverslip was taken out of methanol and excess methanol was allowed to evaporate by holding coverslip near air flow gratings.
9. Coverslips were placed on a clean paper towel in humidified chamber.
10. Diluted BS^3 cross-linker was prepared by adding a 10µl aliquot of 10 mM BS^3 to 990µL PBS. 10µl of diluted BS^3 was added into each well incubated for30 min at room temperature in a humidified chamber.
11. After 30min, the liquid was blotted from well by inverting the coverslip onto a paper towel. Each well was washed three times with a drop of PBS and PBS was removed as mentioned above. To quench any unreacted BS^3, 10 µL of ethylenediamine solution was added into each well and incubated for 15 min at room temperature.
12. To block nonspecific binding sites, a drop of blocking solution was added to each well and incubated for 20min at room temperature.
13. Primary antibodies (Sec12-Goat anti hPREB R and D Systems cat. #AF5557, Sec16- Rabbit polyclonal anti-KIAA0310 antibody from Bethyl Laboratories

cat. #BL2467) were diluted (1:50) in blocking solution. Solutions were spun at maximum speed to remove particulate matter.

14. 10µl of primary antibody solution was added to each well and incubated for 20 min at room temperature.
15. Coverslips were washed by dipping in coplin jar filled with 1X PBS 8-10 times, followed by similar dipping in 2ndcoplin jar. After this, wet coverslip was incubated for a minute and similar dipping process was followed for the 3rd time.
16. Secondary antibodies (Alexa Fluor 594 donkey anti-goat- A-11058, Alexa Fluor 488 chicken anti-rabbit IgG-A-21441) were also diluted (1:50) in blocking solution and spun at maximum speed to remove particulate matter.
17. 10µl of secondary antibody solution was added to each well and incubate for 15 min at room temperature. Washing was repeated in same way as performed for primary antibody.
18. The final drop of PBS was completely aspirated from each well. 5µl of mounting solution was added to each well. The coverslip was inverted onto a glass slide and sealed with clear nail polish.

Microscopy and image processing

Imaging for immunofluorescence and for live cell was done using Zeiss LSM 510 META. Imaging was done using 63X, 1.4NA oil immersion objective. Z sections were captured with 0.3µ-0.4µ interval. Single- or dual-color data sets were obtained using separate excitation and capture of red and green or CFP and YFP signals, with a pinhole of 1.0–1.2 AU. Live cells were imaged at 37^{0}C and 5% CO_2. Averaging was done wherever required. Laser power was kept minimum to avoid photo damage to

cells. Fluorescence micrographs were processed to remove background using ImageJ software. Micrographs were then assembled using Adobe Photoshop CS6.

Protein estimation

Protein estimation was done using Bradford's method.

BSA standards were prepared as follows

BSA concentration µg/ml	BSA µl (1mg/ml)	Distilled water µl
200	2	8
400	4	6
600	6	4
800	8	2
1000	10	0

Table 2.7: BSA dilutions for protein estimation

1. 1ml (1:4 diluted) Bradford reagent was added to each reaction.
2. Samples were incubated for 10 min at room temperature.
3. OD of samples was recorded at 595nm along with blank.
4. Standard curve was plotted
5. 5µl lysate was used for determination of protein concentration with reference to standards.

Cell lysis for co-immunoprecipitation

Co-immunoprecipitation was done to study if two proteins interact with each other in cells. Cells were lysed under non-denaturing conditions with mild detergent like NP40 to preserve protein- protein interactions during entire lysis procedure. Protease

inhibitor cocktail was included in lysis buffer and the procedure was carried out on ice to avoid degradation of proteins.

1. Cells were seeded in two 90mm plates and transfected using calcium phosphate method.
2. Cells were harvested for co-Immunoprecipitation 24 hours post transfection.
3. The medium was sucked off using vacuum from the culture plate. 1ml 1xPBS was added to plate and cells were scraped slowly with a cell scraper. Cells were collected in chilled microcentrifuge tubes. If required, additional 0.5ml PBS was added to collect more cells by scraping. Cells were kept on ice.
4. Suspension was spun at 4°C 3500 rpm for 5 min. PBS was decanted.
5. To one cell pellet from a 90mm plate, 1ml chilled lysis buffer was added. Mixture was pipetted several times gently avoiding foaming. Vials were kept on cell mixer for 6 hours in cold room. Mixture was then centrifuged at 15000rpm, 4^{o}C for 5min.
6. Supernatant was used for protein estimation, as input and for Immunoprecipitation.

Immunoprecipitation

Preparation of Protein Agarose beads:

Protein A is a cell wall component of *Staphylococcus aureus*. It consists of a single polypeptide chain shaped as a cylinder, which contains five antibody binding domains. These high affinity regions are specifically bound to the Fc region of immunoglobulins (IgGs). Protein A is temperature stable and it retains its native conformation even in the presence of denaturing agents. Because of its high affinity for Fc region, Protein A agarose was chosen for Co-IP experiment. Also milder

elution conditions for elution from protein A-agarose make it a suitable choice for preserving protein-protein interactions during elution.

1. Protein A-agarose beads slurry was mixed by gentle tapping. Once homogenized, 100µl slurry was pipetted using cut-tips in a fresh chilled microcentrifuge vial.
2. Slurry was washed 3 times by re-suspension in low salt buffer and gentle spinning at 500rpm at 4^0C. The supernatant was thrown after each wash. At the time of each wash, some supernatant was left in order to avoid loss of beads along with supernatant.
3. After 3rd wash, BSA was added to block the reactive sites on beads to reduce background. Volume was made up to 1.5ml with low salt buffer. Final concentration of BSA was made up to 1%. The vials were kept on rotator for 1 hour in cold room.
4. Beads were spun at 500rpm for 2min at 4^oC. Supernatant was removed gently by pipetting. To this, 1ml low salt buffer was added. Rabbit polyclonal anti FLAG F7425 was added to this (4µl per sample). Vials were kept on rotator for 1 hour in cold room achieving binding of antibody to protein A-agarose beads.
5. The mixture was spun at 500rpm at 4^oC for 2min. ~ 100µl supernatant was kept, rest was removed from beads. The beads were then ready for Immunoprecipitation.

Immunoprecipitation:

1. 20µl beads were added to 4 microcentrifuge vials to which lysate was added. Volume was made up to 1.5ml with low salt buffer. Contents were mixed by

inverting the vials gently. Vials were kept on rotator in cold room for 16 hours.

2. Next day, vials were taken out and kept on ice. Imminoprecipitates (IPs) were washed with wash buffer 3 times by spinning at 500rpm for 2min at 4^{o}C to remove supernatant.
3. After 3rd wash, supernatant was removed completely. Vials were spun again at 500rpm for 2min at 4^{o}C to remove left over wash buffer.
4. 50µl 1X SDS-PAGE loading dye was added to beads and vortexed briefly.
5. Inputs were thawed on ice and mixed with 6X SDS-PAGE loading dye.
6. Samples- inputs and IPs were boiled at 99^{0}C for 5min with 400rpm shaking. Samples were then centrifuged at 13000rpm for 5min at RT before loading.

SDS-PAGE [205]

Proteins are usually analyzed by separating them on by SDS-PAGE. SDS denatures the proteins giving uniform negative charge to proteins and separation is achieved on the basis of molecular weight of proteins. Depending upon requirement, polymerization of the acrylamide can be rigorously controlled to get uniform gels of desired pore size.

1. The resolving gel of 10% was made according to table 2.8.
2. The resolving gel was poured leaving space for the stacking gel. Water was gently poured over the resolving gel to avoid oxidation and the gel was allowed to solidify completely for ~20 min.
3. The stacking mix was made and poured over resolving gel after decanting the water layer and the comb was inserted.

Component	Volume for 20ml
H_2O	8ml
30% Acrylamide mix	6.6ml
1.5M Tris pH 8.8	5ml
10% SDS	200µl
10% Ammonium per sulphate	200µl
TEMED	8µl

Table 2.8 Reaction mixture of a resolving SDS PAGE gel

Component	Volume for 9ml
H_2O	6.3ml
30% Acrylamide mix	1.5ml
1M Tris pH 6.8	1.14ml
10% SDS	90µl
10% Ammonium per sulphate	90µl
TEMED	9µl

Table 2.9 Reaction mixture of a stacking SDS PAGE gel

1. The comb was removed after gel polymerization was complete, wells were cleaned with distilled water and then with running buffer. Gel was then placed in the tank and electrode buffer was poured to the appropriate level.
2. Protein samples were diluted in a sample buffer according to the amount of protein to be loaded on to the gel. Protein samples were boiled centrifuged and loaded on gel. Pre-stained protein molecular weight standard was loaded along with the test samples in defined order and the gel was run at constant voltage of ~180V.

Wet transfer of proteins on PVDF membrane

Wet transfer method is used to transfer proteins separated on SDS-PAGE onto PVDF membrane for further analysis by immunoblotting.

1. The resolving gel was removed from the electrophoresis assembly, rinsed gently in water to remove excess of SDS and immersed in transfer buffer for 10 min.
2. Membrane (PVDF) was activated by soaking for 1 min in methanol and immersed in transfer buffer and transfer was setup by placing the gel and membrane in between pieces of filter paper and fiber sheets in the transfer cassette and this sandwich was vertically immersed in the transfer apparatus, with the gel towards the negative electrode. Electroblotting at 300 mA was continued for 3 hrs at RT.
3. Membrane was removed from the sandwich and immersed immediately in TBST to avoid drying of the membrane.

Immunoblotting

Western blotting is an analytical technique which detects presence of native or denatured proteins which are first electro-transferred onto a membrane and are then detected using protein specific antibody.

1. The membrane was blocked in either 5% milk in TBS at RT 2-3 hr. Took out membrane from blocking. TBST was added to rinse membrane. The membrane was kept on rocker for 5 min. Washes were repeated 4 times.

2. The membrane was then incubated with appropriate concentration of primary antibody (diluted in5% milk/BSA in TBS), at RT for 2-3hrs or O/N at 4°C on a rocking platform.
3. After 5 washes in TBST, 5 min each, the membranes were incubated with a 1:3000 dilution (in 2.5% blocking milk) of horse radish peroxidase (HRP)-conjugated secondary antibody for 1hr at RT. After taking out from primary, 5 washes of TBST were given, 5 min each.
4. Signal was detected by enhanced chemiluminescence (ECL+), by incubating the blot with detection reagent for 5 min, followed by exposure to X-ray film and development.

2.3 Results

2.3.1 Constructs used in this study: CFP-Sec16b, pEGFP-C1-Sec12, pEGFP-C1-Sec16A (codons 1909–2332): were obtained from Glick lab. The maps of these constructs are as follows:

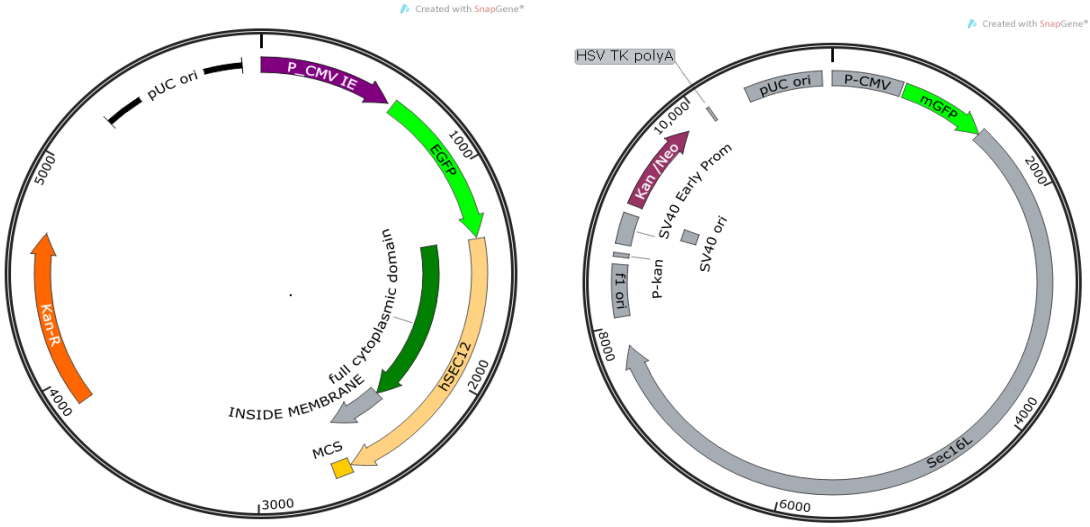

pEGFP–C1-hSec12 pEGFP-C1-c-term Sec16A

Fig 2.3: maps of constructs used

YFP-Sec12:

To check if Sec12 localizes at ERES in live cells, we decided to study localization of Sec12 along with CFP-Sec16b, well known marker of ERES. Sec12 ORF was cloned in pmYFP-C1 vector in which Sec12 was tagged with YFP at its N-terminus. Sec12 ORF was obtained by digesting the pEGFP-C1-hSec12 with BsrG1 and BamH1. 1.3Kb band released after digestion was gel purified. This was used as the insert. pmYFP-C1 vector was also digested with BsrG1 and BamH1. Vector was treated with alkaline phosphatase to prevent self-ligation. The free nucleotides and enzyme were removed from the reaction by nucleotide removal kit. The ligation of insert and vector was set up in 1:3 ratio at RT for 20 min. Ligation mixture was then

transformed and cells were plated on LB-Kana overnight. The clones were digested with Stu1 for identifying desired recombinant (Fig 2.4).

3X FLAG-Sec12:

To check if cytoplasmic domain of Sec12 interacts with Sec16, we pulled down cytoplasmic domain of Sec12 and checked if Sec16 associates with it in cells. For this purpose, we tagged cytoplasmic domain of Sec12 with FLAG epitope, antibody against which was used for immunoprecipitation from cytoplasm. To do this, cytoplasmic domain of Sec12 (amino acids 1-386) was amplified by PCR. pEGFP-C1-hSec12 construct was used as template and primers used were-hsec12-bglII-F and hsec12-Cyto-R.

1.17Kb amplicon was gel purified and was digested with BglII and HindIII and was then cloned in pCMV-3FLAG-1A vector downstream of 3X FLAG epitope. Ligation was set up for 20 min at 22^0C. The transformants were screened by digesting with Sac1 and correct clone was confirmed (Fig 2.5).

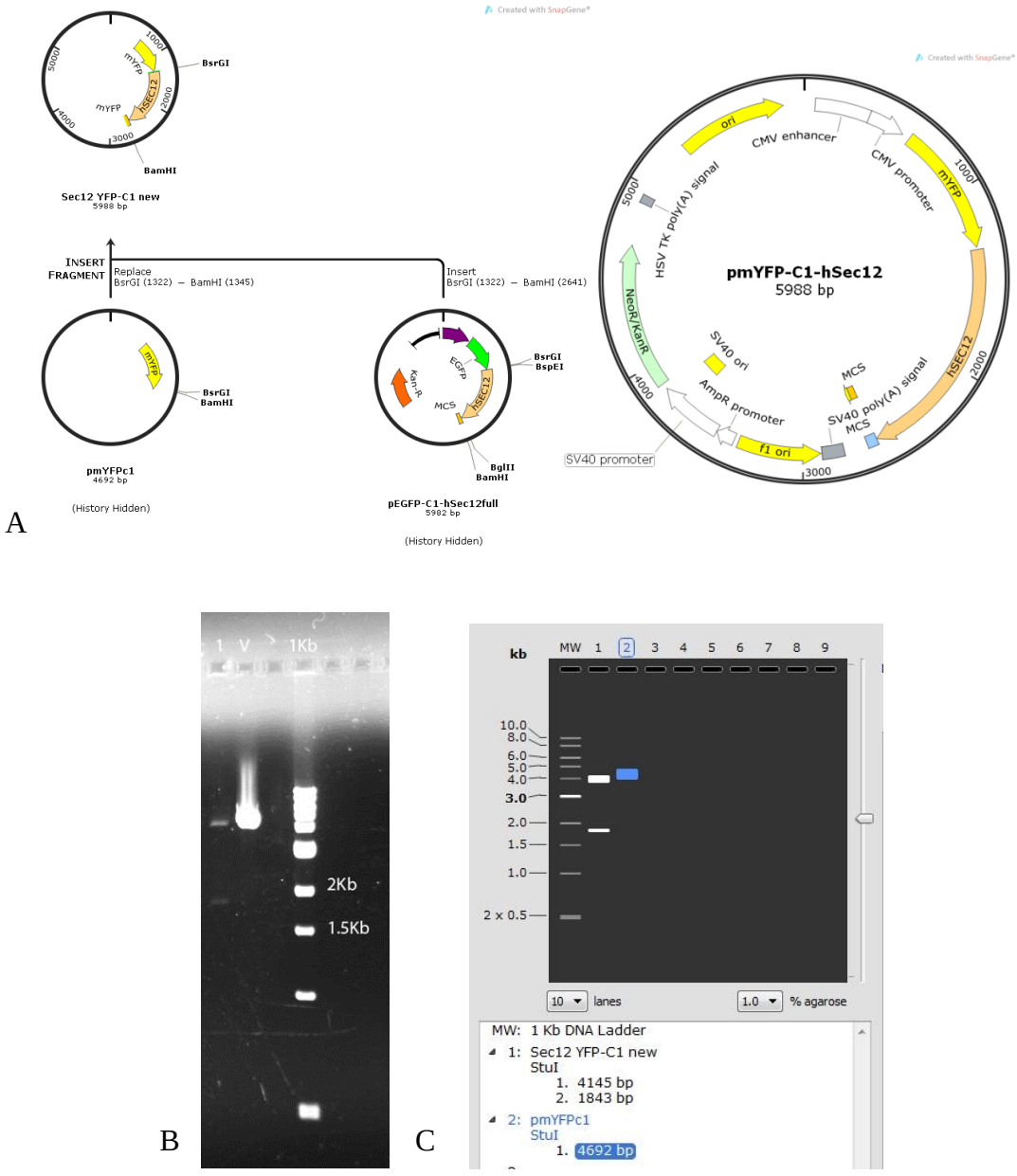

Fig 2.4: Diagnosis of pmYFP-C1-hSec12 clone A] Strategy of cloning hSec12 in pmYFP-C1 B] gel showing positive clone 1 and empty vector (V) after digestion with StuI along with 1Kb ladder, C] Simulation of diagnosis of clone and empty vector with StuI.

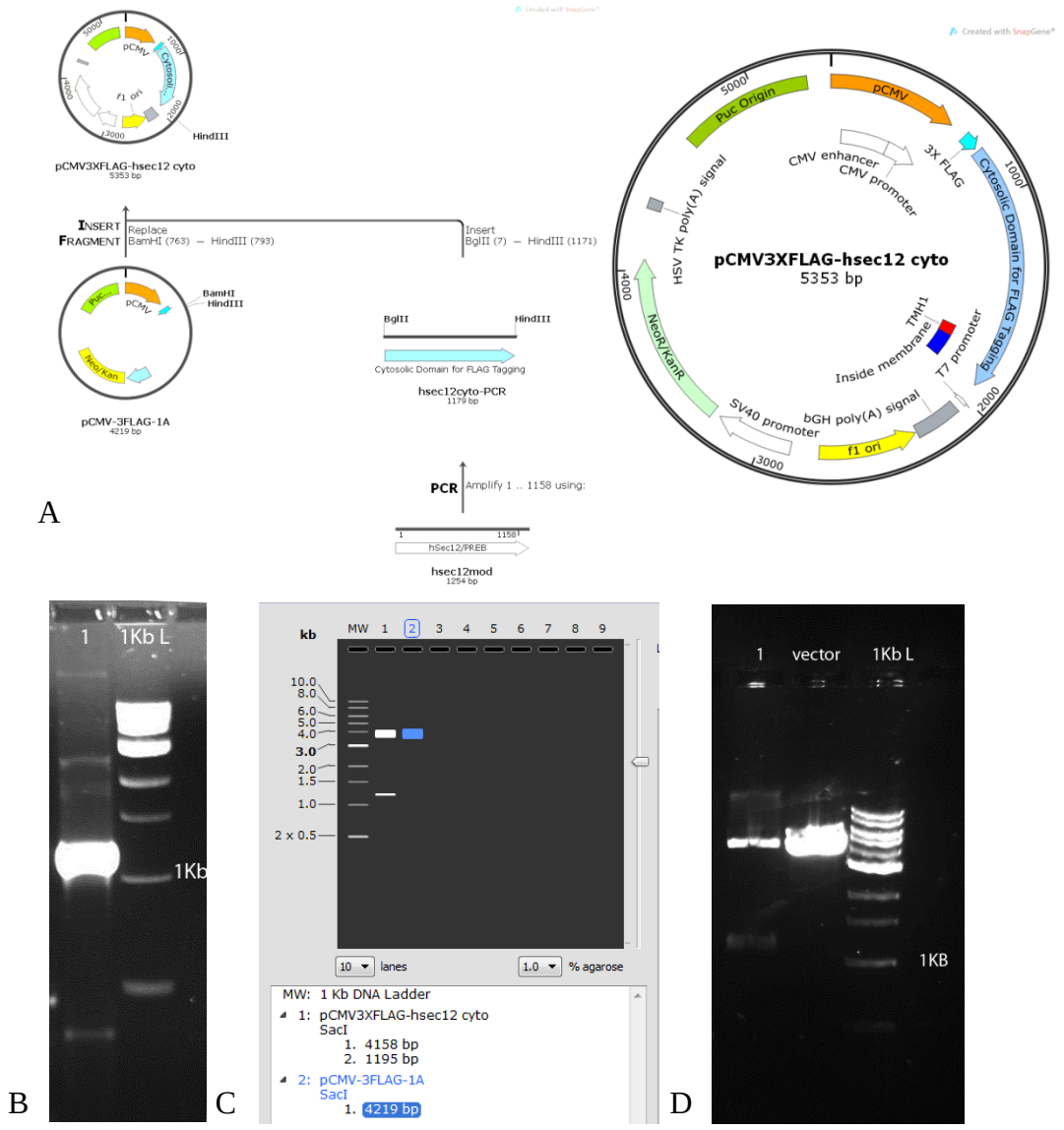

Fig 2.5: Cloning of pCMV 3X FLAG-hSec12cyto A] Strategy of cloning of pCMV-3X FLAG-hSec12 B] PCR amplification of hSec12 cytoplasmic domain (lane1) along with 1Kb ladder, C] Simulation of diagnosis of positive clone by SacI, D] Agarose gel showing diagnosis of positive clone with SacI diagnosis (lane1) and empty vector along with 1Kb ladder.

Sec12 deletion constructs:

We were interested to find out the exact region of Sec12 that is required for localization at ERES. The deletion constructs were designed and deletion fragments were cloned in pmGFP-C1. Various deletion fragments of Sec12 as depicted in fig 2.6 were amplified by PCR using pEGFP-C1-hSec12 as a template and cloned in pmGFP-C1 in BsrGI and HindIII. Positive clones were identified by digestion with appropriate restriction enzyme.

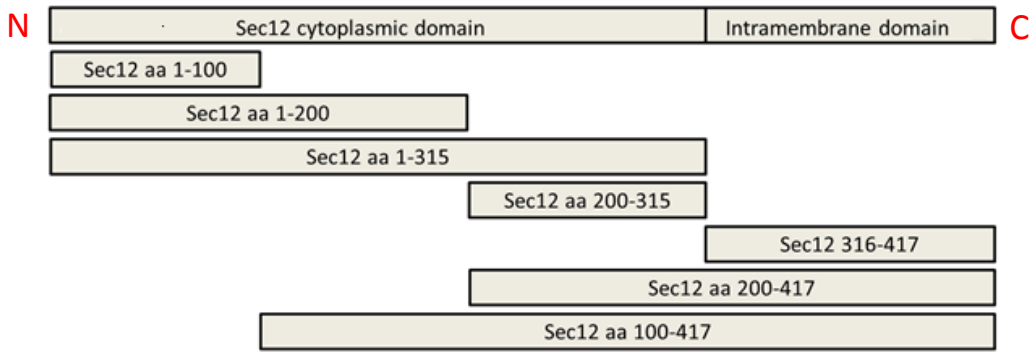

Fig 2.6: Schematic diagram showing various hSec12 deletion constructs used in this study

2.3.2 Fraction of endogenous Sec12 localizes at ERES along with general ER

Endogenous Sec12 localizes to general ER as well as punctate pattern similar to ERES:

According to previous reports, mammalian Sec12 was known to localize only to general ER although immunofluorescence data were ambiguous. But function of Sec12 is to activate Sar1 GTPase by exchanging its GDP with GTP at ERES and thus initiate COPII vesicle production. Hence we decided to revisit the localization of Sec12. We did immunofluorescence of endogenous Sec12 in U2OS cells. The

modified immunofluorescence method was used to protect delicate ERES structures in cells. This method uses quick fixation with chilled methanol and use of a chemical cross linker to cross link cellular proteins. This helps in preserving delicate cellular ultra-structures like ERES during vigorous washing steps. After doing immunofluorescence of endogenous Sec12, we found that Sec12 is present through-out ER as reported earlier but we also saw considerable fraction of Sec12 localized to punctate structures which are similar to ERES (Fig 2.7A).

Sec12 punctae co-localizes with Sec16 punctae at endogenous expression level:

To confirm if these punctate structures are ERES, we did co-immunofluorescence of Sec12 andSec16, well-known marker of ERES. U2OS cells were seeded. 24 hours post seeding, cells were fixed and processed for immunofluorescence against endogenous Sec12 and Sec16. The same modified immunofluorescence method was used. We found out that the majority of Sec12 punctae co-localize with Sec16A punctae (Fig 2.7B)

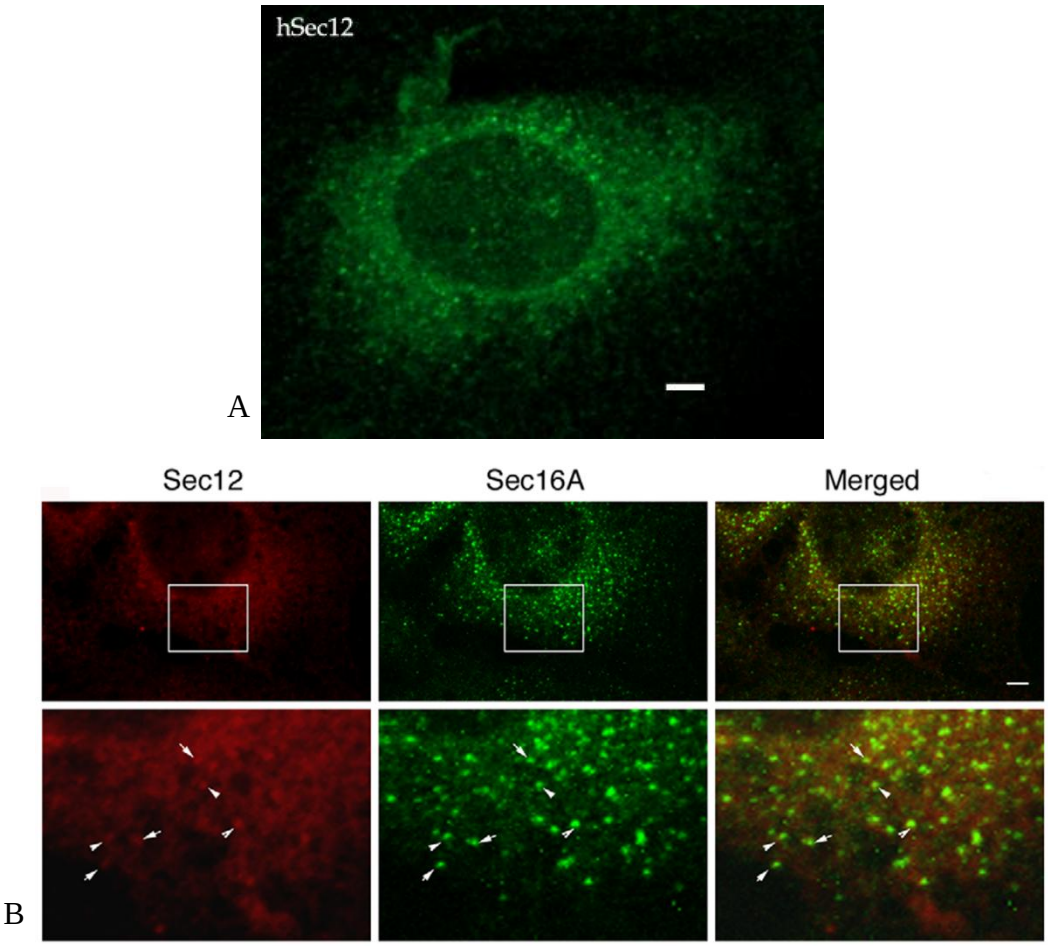

Fig 2.7: Localization of Sec12 at endogenous expression level A] U2OS cells were seeded on coverslips and after 24 hours subjected to immunofluorescence by method described earlier to study localization of endogenous Sec12 (with antibody against hPREB) and imaged by confocal microscopy. Scale bar, 5µm, B] U2OS cells were seeded on coverslips and processed for co-immunofluorescence by using antibodies against Sec12 and Sec16A. Scale bar, 2µm.

Sec12 localizes to punctate structures in live cell condition:

To check localization of Sec12 in live cell condition, we transfected mYFP-Sec12 in U2OS cells and did live cell imaging. mYFP-Sec12 was over-expressed from CMV promoter in U2OS cells. Live cell imaging was done 20 hours post transfection in confocal microscope. This data further confirmed that Sec12, along with forming web-like structure corresponding to general ER, also forms punctate structures (Fig 2.8A).

Sec12 co-localizes with Sec16b in live cell condition:

We did co-transfection of mYFP-Sec12 and mCFP-Sec16b in U2OS cells to check if Sec12 punctae seen in live cell condition correspond to ERES. Both Sec12 and Sec16 were expressed from CMV promoter. Live cell imaging data showed that most of the Sec12 punctae co-localize with Sec16b punctae (Fig 2.8B).

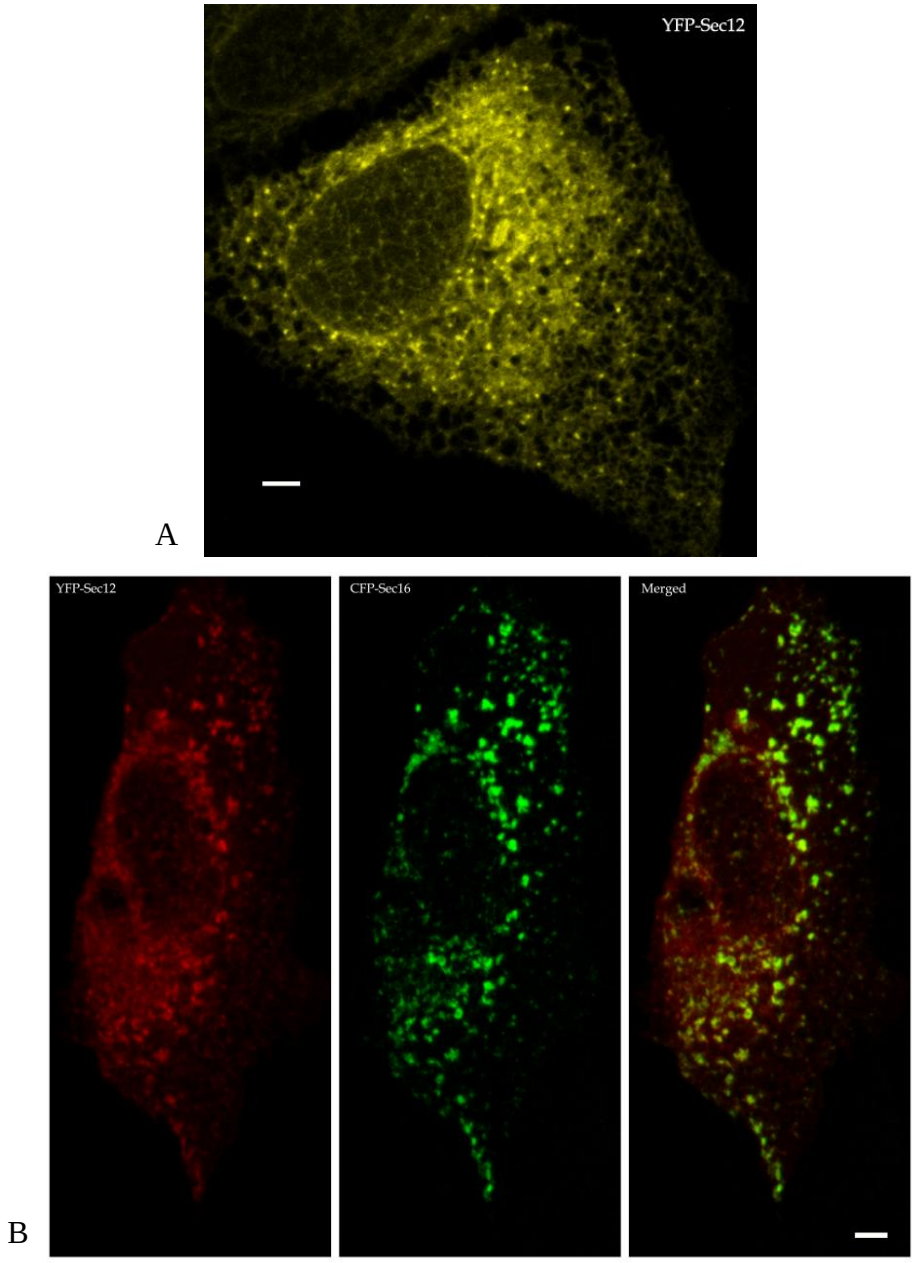

Fig 2.8: Localization of Sec12 in live U2OS cells by confocal microscopy. A] YFP-Sec12 transiently transfected in U2OS cells, live cell imaging was done 18 hours post transfection, B] Live cell imaging of YFP-Sec12 and CFP-Sec16 co-transfected in U2OS cells by transient transfection, Imaging was done 12 hours post transfection, Scale bar, 5µm.

2.3.3 Over-expression of GFP-Sec12 leads to formation of larger ERES

Sec12 over-expression leads to formation of larger Sec12 punctae:

mGFP-Sec12 was over-expressed in U2OS cells to study role of Sec12 on size of ERES. mGFP-Sec12 was over-expressed from CMV promoter. We found out from live cell imaging that over-expression of mGFP-Sec12 leads to formation of large Sec12 punctate structures. These punctae are similar to ERES with only difference being the larger size of these punctae compared to normal size distribution. Live cell imaging was done at different time points post transfection. We found out that at earlier time points post transfection, mGFP-Sec12 localizes to punctae corresponding to normal size distribution of ERES. As the level of mGFP-Sec12 increases in cells post transfection, the size of mGFP-Sec12 punctae goes on increasing. At around 30 hours post transfection, most cells showed very large size of mGFP-Sec12 punctae. When imaging was done at 40 hours post transfection, in most cells, mGFP-Sec12 was seen at general ER which is evident from web-like pattern seen from images (Fig 2.9A).

Enlarged Sec12 punctae correspond to enlarged ERES.

We co-transfected mYFP-Sec12and CFP-Sec16b to confirm that enlarged punctae seen after over-expressing Sec12 indeed represent enlarged ERES and not just aggregation of excess Sec12. After transfection, we did live cell imaging at early and late time points. At 20 hours post transfection Sec12 and Sec16b showed overlapping punctae representing ERES. These punctae had normal size distribution. At 40 hours post transfection, larger Sec12 punctae were observed which co-localized with Sec16b punctae. This confirmed that the larger punctae formed because of Sec12 over-expression indeed represent enlarged ERES (Fig 2.9B).

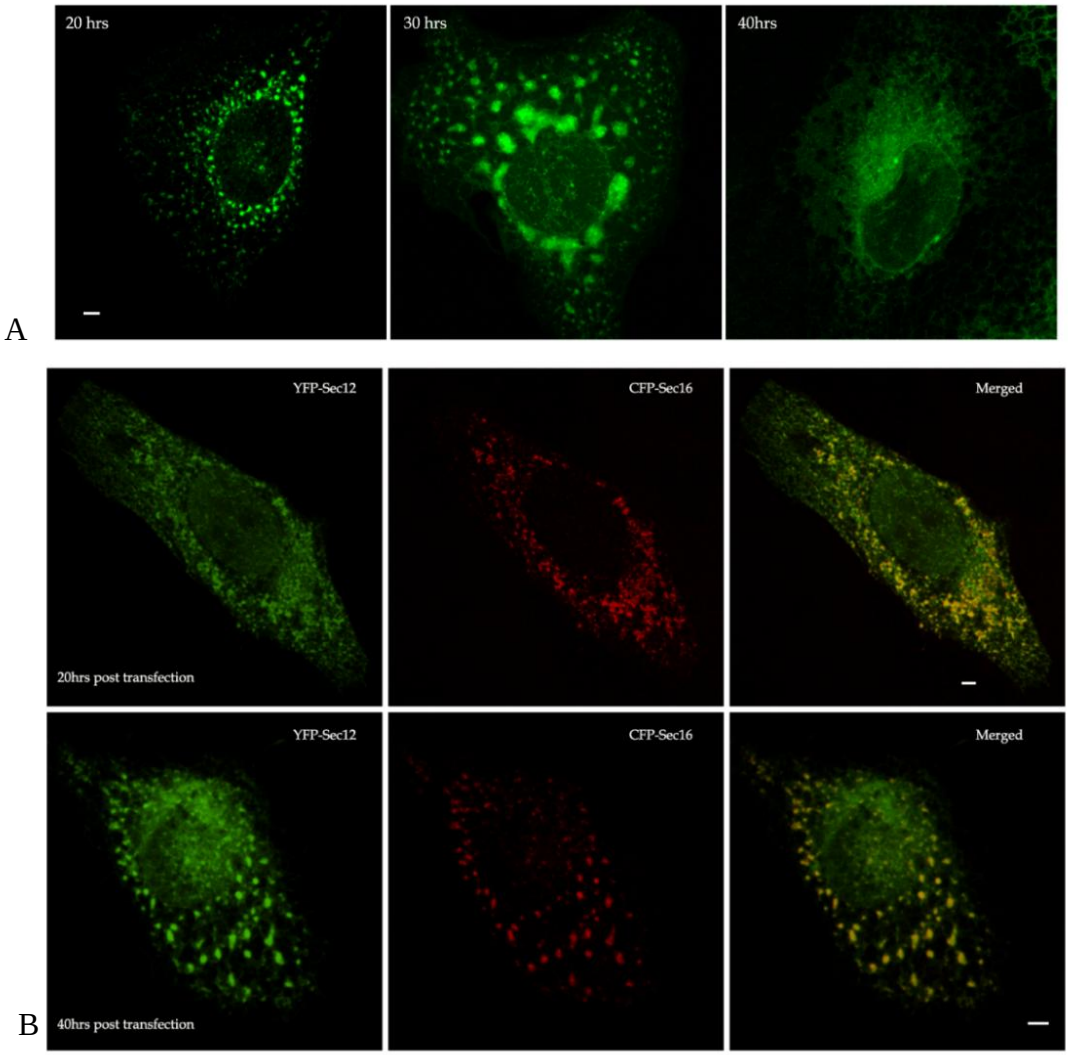

Fig 2.9: Over-expression of Sec12 leads to formation of larger ERES. A] GFP-Sec12 was transfected in U2OS cells and live cell imaging was done in confocal microscope at different time points post transfection, B] YFP-Sec12 and CFP-Sec16b were co-transfected in U2OS cells and live cell imaging was done in confocal microscope at different time points post transfection. Scale bar, 5µm.

2.3.4 Sec12 cytoplasmic domain interacts with C-terminal domain of Sec16

As we saw from live cell imaging that Sec12 initially localizes at punctate structures which eventually become larger and after certain level, it falls back to general ER. When Sec12 and Sec16 both were equally over-expressed, Sec12 localized to large punctate structures without falling back to general ER even at later time points post transfection. Hence it is quite possible that Sec12 is held at ERES with help of a binding partner, preferably by Sec16. To verify this, cytosolic domain of Sec12 (amino acids 1-386) was tagged with FLAG and C-terminal conserved domain of Sec16A (residues 1909–2332) was fused with mGFP by cloning in pmGFP-C1 vector. Sec12 FLAG and Sec16 GFP along with controls were transfected in HeLa cells by calcium phosphate method. For immunoprecipitation, rabbit anti-FLAG antibody was coated on Protein-Aagarose beads. 10% inputs and IP samples were loaded on 10% SDS-PAGE to resolve. Western blotting was performed using anti FLAG monoclonal antibody as well as with anti-GFP to check if Sec 12 and Sec16 are interacting. This data showed that Sec12 cytosolic domain does interact with Sec16 which is well known ERES marker (Fig 2.10).

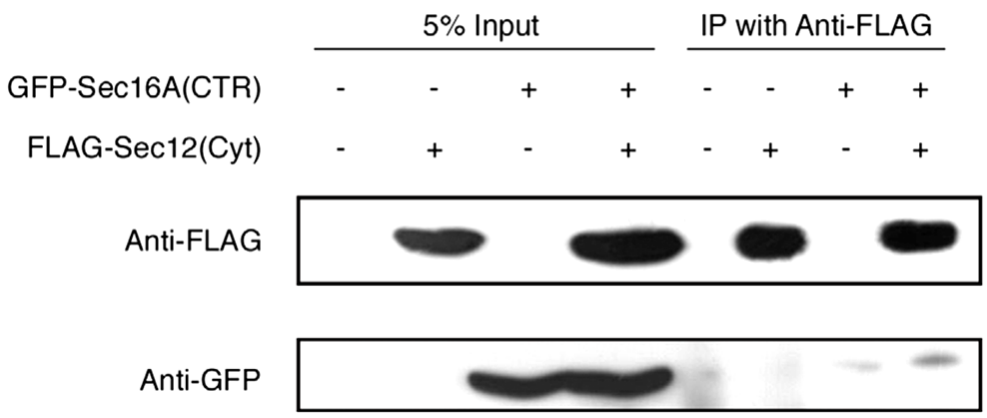

Fig 2.10: Sec12 cytoplasmic domain interacts with C-term domain of Sec16A. HeLa cells were transfected with indicated plasmids encoding either mGFP fused to a C-terminal region (CTR) of human Sec16A (residues 1909–2332), or an N-terminally triple-FLAG-tagged cytosolic domain (Cyt) of human Sec12 (residues 1–386). At 24 h post-transfection, the cells were lysed and the lysate was subjected to immunoprecipitation (IP) with rabbit anti-FLAG antibody. The immunoprecipitated material and 5% of the lysate (5% Input) was subjected to SDS-PAGE followed by immunoblotting with either monoclonal anti-FLAG or anti-GFP antibody.

2.3.5 Sec12 deletion constructs study to identify the domain required for ERES localization:

To identify the exact region in Sec12 that is required for localization at ERES, we made various deletion constructs by cloning the deleted fragments in pmGFP-C1 vector. These constructs were transfected in U2OS cells along with full length Sec12 tagged with GFP. Live cell imaging was done in confocal microscope. The deletion constructs included different fragment lengths of only cytoplasmic domain of Sec12 which lacked intra-membrane domain completely. Other deletion constructs contained only intra-membrane region as well as intra-membrane region along with part of cytoplasmic region. We noticed that only intra-membrane region alone was sufficient for punctate localization. But constructs expressing even full length cytosolic domain but lacking intra-membrane domain could not localize punctate pattern. This study showed that intra-membrane region of Sec12 is important for its punctate localization (Fig 2.11).

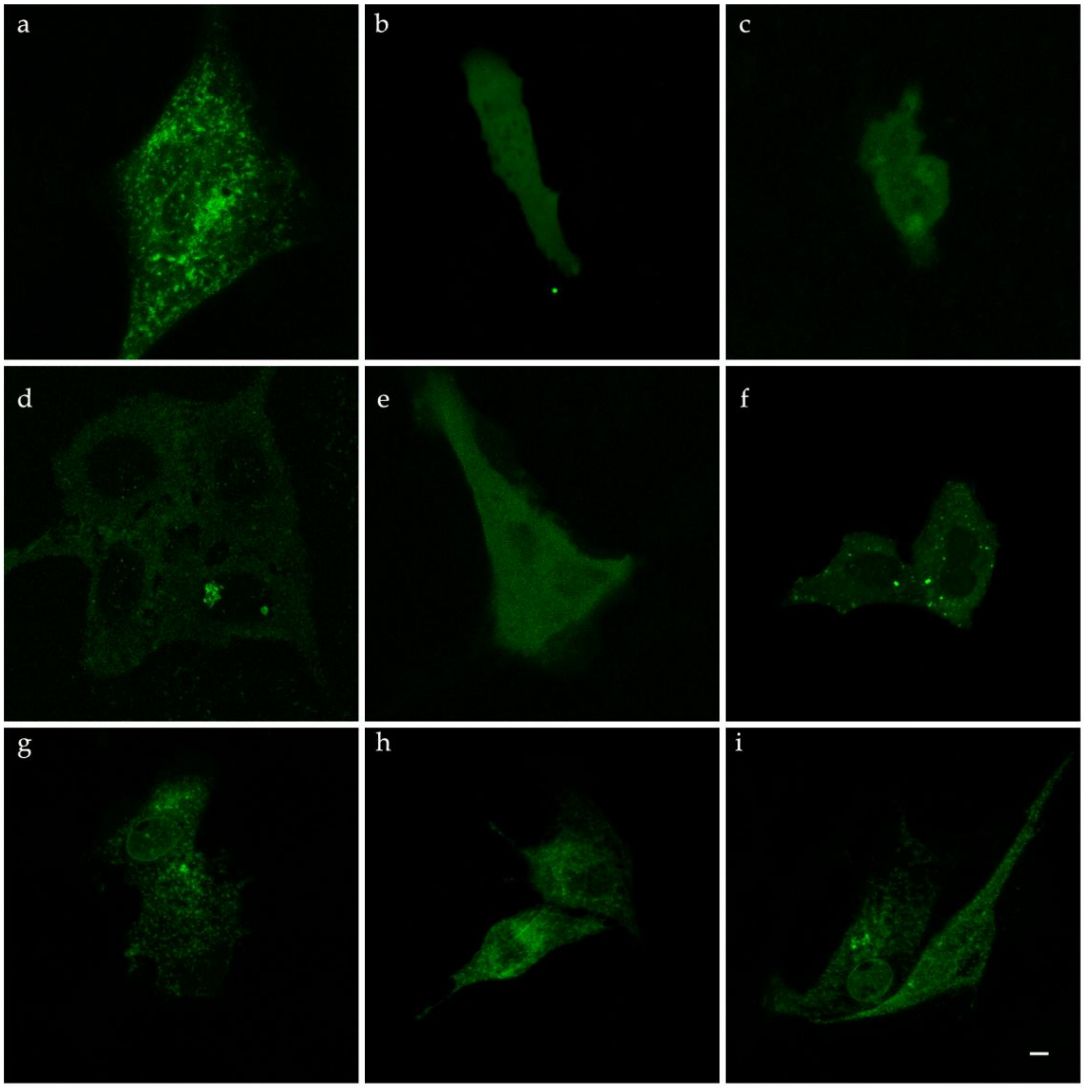

Fig 2.11: Localization of Sec12 deletion constructs: Different deletion fragments of Sec12 were cloned in pmGFP-C1 vector and transfected in U2OS cells. Live cell imaging was done post 16-18 hours of transfection. a) Full length Sec12, b) Sec12 amino acids 1-100, c) Sec12 amino acids 1-200, d) Sec12 amino acids 200-300, e) and f) Sec12 amino acids 1-300, g) Sec12 intra-membrane domain only, h) Sec12 amino acids 200-417, i) Sec12 amino acids 100-417. Scale bar, 5µm.

2.4 Discussion:

The present study was aimed at understanding role of Sec12 in size control mechanism of ERES. We also aimed to find out if Sec12 interacts with ERES scaffold protein Sec16A. We have shown that a fraction of Sec12 molecules are concentrated at ERES. Our results show that over expression of Sec12 results in enlargement of ERES and after certain level, Sec12 falls back to general ER. Thus our results indicate that Sec12 localization at ERES is saturable and may require a binding partner. We have also shown that cytoplasmic domain of Sec12 (amino acids 1-386) interact with C-terminal region of Sec16 (residues 1909- 2332). Thus Sec16 is the binding partner of Sec12 at ERES.

It is very well known that Sec12 acts as a GEF for GTPase Sar1. Sar1 activation further triggers formation of COPII vesicles. All the components required for COPII vesicle formation are concentrated at ERES. But previously it was shown that although Sec12 functions at ERES to activate Sar1, it is present through-out ER rather than being concentrated at ERES. We reexamined the localization of Sec12 by two approaches. We studied localization of Sec12 by fixing the cells and detecting endogenous Sec12 and we also checked localization of Sec12 in live cell condition by over-expressing GFP-Sec12 in U2OS cells by confocal microscopy. In both approaches we found out that although majority of Sec12 does localize through-out ER as reported earlier, a considerable amount of Sec12 pool also localizes to ERES. This was clearly seen by small Sec12 punctae seen in immunofluorescence study. It was also confirmed by co-immunofluorescence with Sec16 that Sec12 punctae indeed represent ERES. The same was also confirmed further by live cell imaging of YFP-Sec12 and CFP-Sec16. In support of this data, a recent paper from Saito et al also found concentrated Sec12 at ERES in mammalian cells [206].

It is known from previous literature that defects in budding of COPII vesicles resulted in larger size of ERES in *S. cerevisiae* [71]. We observed that size of ERES becomes enlarged in the cells that showed very high expression of GFP-Sec12. As time progresses after transfection of GFP-Sec12, level of GFP-Sec12 gradually increases in cells and depending on the level of expression, GFP-Sec12 localization changes. In cells having lower levels of GFP-Sec12, GFP-Sec12 localizes to punctae that are similar to normal size distribution of ERES. The cells which have high expression show the enlarged size of Sec12 punctae. The enlarged YFP-Sec12 structures co-localized with CFP-Sec16 suggesting that upon Sec12 over expression, size of ERES increases. In cells having very high expression of Sec12 alone, excess of Sec12 cannot be held at ERES and it falls back to general ER. Sec12 might require a binding partner which would hold excess of Sec12 at ERES. Since Sec16 is involved in organization of ERES and budding of COPII vesicles in other species as well as in mammalian cells, most likely Sec16 could be this binding partner [65], [105], [62]. This hypothesis was actually true because when we over-expressed equal amount of Sec16 along with Sec12, excess of Sec12 was held at ERES which are larger in size without falling back to general ER. Similar results were also obtained for *P. pastoris* Sec12 and Sec16 overexpression leading to formation of exaggerated ERES [207]. This observation led to a question whether Sec12 physically interacts with Sec16?

Co-immunoprecipitation showed that indeed cytoplasmic domain of Sec12 interacts with C-terminal region of Sec16A. This interaction is also a conserved phenomenon as similar results were also seen in *Pichia pastoris* [207]. The immunoprecipitation of 3X FLAG-Sec12 from cells resulted in comparatively lesser amount of bound Sec16. This result could be explained by closely looking at

immunofluorescence and live cell imaging of GFP-Sec12. We have seen from these studies that it is only fraction of total YFP-Sec12 that localizes to ERES.

Studying localization of GFP tagged Sec12 deletion constructs showed that intra-membrane domain of Sec12 alone is sufficient for giving punctate localization pattern similar to that of full length Sec12 cytoplasmic domain.

This study opens several questions which need to be addressed in future. The most important question that further needs to be answered is whether increase in the size of ERES is a result of blocking ER to Golgi transport. Previous studies show that the ERES collapse in S. cerevisiae which is result of limited COPII budding in Sec12-4 mutant cells [71]. Also, over expression studies of Sec12 in S. cerevisiae & in plant cells have reported the ER export block [208-210]. Another fact that needs to be studied further is about the functional significance of conserved Sec12 and Sec16 interaction at ERES. It will also be interesting to know if this interaction precedes formation of ERES and/or budding of COPII vesicles. Sec12 acts as GEF for Sar1 GTPase switch at ERES. It can also play a role in regulating the kinetics of COPII vesicle budding by controlling activation of Sar1; thus regulating the size of ERES. Systematic biochemical study and super-resolution microscopy may aid in further understanding the answers to these questions.

Chapter 3

Understanding Size Control Mechanism of Golgi apparatus

3.1 Introduction:

Any eukaryotic cell in normal condition is able to sense and maintain its fundamental features like number, polarity, size and shape of intracellular organelles in a constant manner [17]. The current project was designed to study the process that controls and maintains the size and shape of an intracellular organelle, the Golgi apparatus. The Golgi apparatus is essential for protein sorting and transport. Secretory products move through the stack from the 'cis' cisternae (fig 3.1) which receives cargo from the endoplasmic reticulum (ER) to the 'trans' cisternae on the opposite side. Golgi-localized proteins localize to the cis, medial or trans sub compartments where they carry out various post-translational modifications on the cargo proteins.

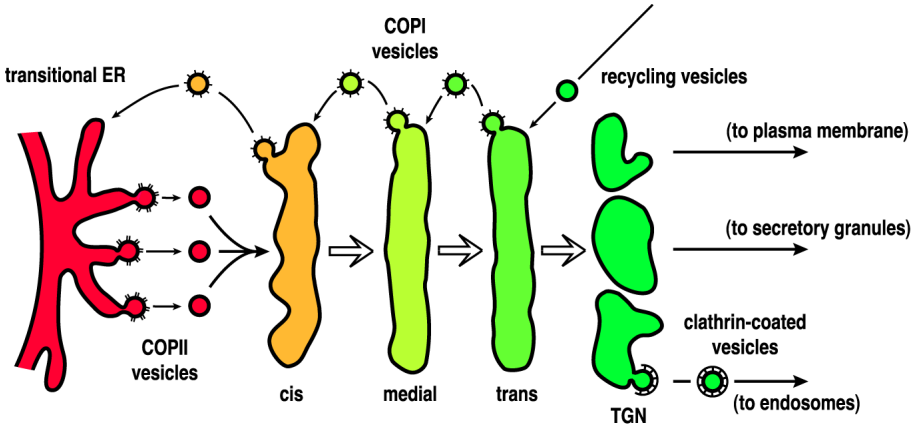

Fig 3.1: Secretory Pathway

Golgi shape and size remains mostly constant for a species but they change depending on the functional requirement. But the Golgi apparatus has different number, size, and shape of cisternae in different species. In budding yeast *Pichia pastoris* Golgi has 3-5 number of cisternae (Fig 3.2, left, green arrow) while in the protist Euglena, the number is twenty-seven (Fig 3.2, right). However even within a same species, the size and shape of Golgi apparatus changes during different differentiation stages or pathological conditions. For example during hormonal

changes at parturition, there is a rapid expansion of the organelles in the mammary epithelial cells. The endoplasmic reticulum increases from 15 to 25% of total cell volume; the Golgi complex increases from 1–3% to 5–15% of the total cell volume and the total number of cisternae in the Golgi stack increases more than 2-fold [164, 165]. Enlargement of Golgi complex has been reported during viral infections. It is known that the size of Golgi is altered in case of some cancers and some neurological disorders [5]. Hence it is very important to understand first how the cells maintain the size of Golgi apparatus in normal condition?

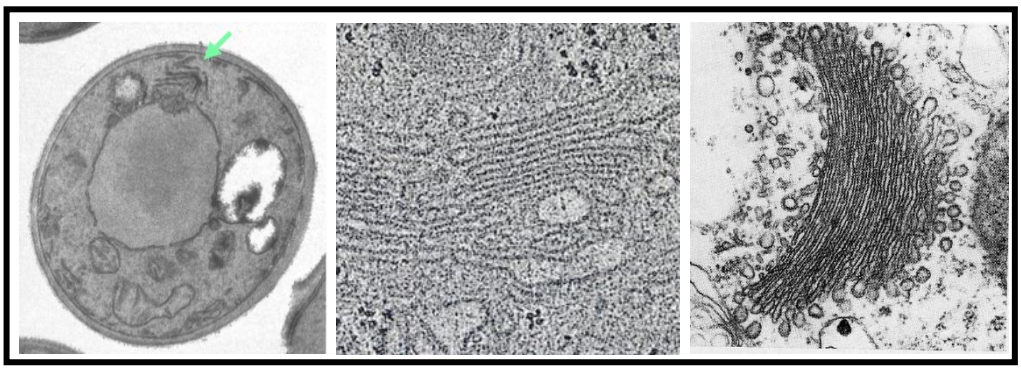

Fig 3.2: Variation of Golgi structure (left to right: Golgi apparatus from *Pichia pastoris*, normal rat kidney, Euglena)

The size of the Golgi apparatus is depends on the balanced flux of material through the compartment. Inhibition of ER to Golgi transport results in the disintegration of the Golgi apparatus. Similarly, inhibition of membrane budding from the trans-Golgi network results in the enlargement of the TGN and a reduction in the size of the Golgi apparatus [173].

Homotypic fusions of pre-Golgi elements lead to the formation of new Golgi cisternae. These new cisternae in turn mature into medial and late Golgi cisternae. We propose that homotypic membrane fusions of pre-Golgi elements play a role in regulating the size of Golgi apparatus.

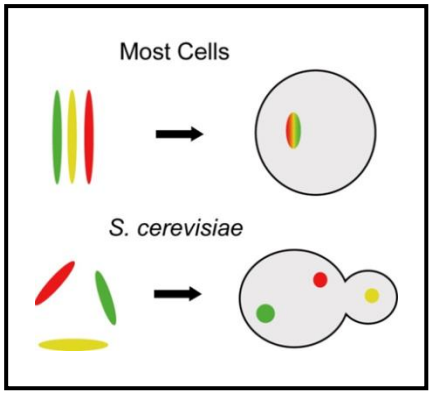

Fig 3.3: Unstacked Golgi cisternae in *S. cerevisiae*

To understand size control mechanism of Golgi apparatus, we have used *Saccharomyces cerevisiae* as an assay system. The main reason to use this as assay system is that the cells of *S. cerevisiae* have un-stacked Golgi cisternae unlike most other organisms (Fig 3.3). Hence it is possible to follow individual cisterna with the help of conventional diffraction limited light microscopy methods. To study the Golgi size control mechanism we used *S. cerevisiae* cells that have endogenous Sec7 replaced with Sec7-3xGFP. Sec7 proteins label the late Golgi cisternae. We started with a random approach of genome wide mutation using EMS mutagenesis to identify Golgi size mutants. While studying Golgi inheritance, Rosaneese et al identified a mutant having larger Golgi cisterna compared to wild type [201]. We started our Golgi size study using this mutant. After genomic library complementation we found out that NMT1 gene was mutated in this Golgi size mutant. NMT1 is a myristoyating enzyme which also myristoylates Arf1.

Arf1 was previously reported to be important for maintenance of Golgi structure [32]. Arf1p is a small guanine nucleotide-binding protein. The small GTPase ARF1 is involved in the recruitment of coat protein complexes that polymerize on endomembrane to form transport vesicles [211]. Because coat proteins can only bind

to the active GTPase, Arf1 is a key regulator of vesicle coating and uncoating. Indeed, activation of Arf1 is a prerequisite for coat recruitment. ArfI, when bound to GTP, forms a dimer on the membrane [212]. Arf1-GTP induces positive membrane curvature. Activated Arf1 is always membrane associated because, in this conformation, its myristoylated N-terminal amphipathic helix is exposed, ensuring membrane anchorage. Myristoylation of Arf1 is important for its recruitment into membrane. Although we started with a random approach, our results too pointed towards importance of Arf1 in regulation of Golgi size. Deletion of Arf1 to test role of Arf1 in size regulation of Golgi apparatus suggested further enhanced size of Golgi cisternae compared to nmt1 mutant. In present study, contribution of Nmt1 and Arf1 was studied in context of Golgi size regulation.

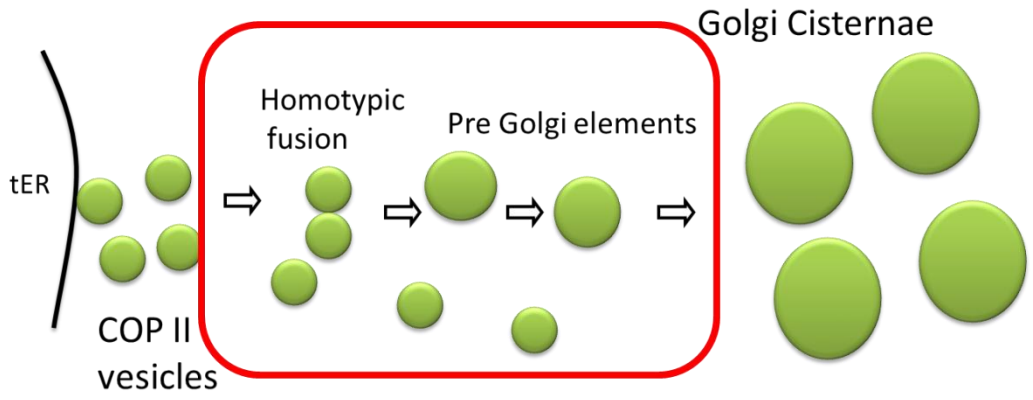

Fig 3.4: Formation of new Golgi cisternae by homotypic fusions of pre-Golgi elements

The current project aims at finding out contribution of homotypic membrane fusions in Golgi size control. It is very well known that the homotypic fusions of vesicles coming out from ERES lead to formation of new Golgi cisternae (Fig 3.4). So we did a screening to find out correct marker protein which represents exact stage of homotypic fusions. We speculated that in wild type cells, it will not be possible to visualize homotypic fusions as the size of such ER derived vesicles is beyond

detection capacity of a regular light microscope. Using Arf1 deletion background, we were able to change the system in such a way that resulted in increased average size of the Golgi cisternae. We expected that the homotypic fusions will continue until this new threshold size is reached. Because of this, the entire phenomenon of homotypic fusions was brought in the limits of diffraction limit of regular light microscope. Using appropriate marker protein and high speed confocal microscopy it may be possible to capture the homotypic membrane fusions in real time.

3.2 Materials and methods:

Materials and methods for bacterial and molecular biology work were same as given in chapter 2. Materials and methods used for yeast culture are discussed here.

3.2.1 Source of reagents:

1] Yeast strain: *Saccharomyces cerevisiae* strain JK9-3d

Genotype: leu2-3,112 ura3-52 rme1 trp1 his4 [8]

2] Yeast cell culture media:YPD ready mix powder (HiMedia), synthetic complete media powder SD (HiMedia), ammonium sulphate (SDfine), Yeast nitrogen base (YNB) (HiMedia), glucose (Sigma Aldrich), complete supplementary mixture (CSM) (HiMedia), CSM without URA/ TRP/ LEU (HiMedia), Agar (Difco laboratories), 5-Fluorooratic acid (5FOA) (US Biological #F5050), G418 (Sigma Aldrich), glycerol (SRL), Sorbitol (Sigma Aldrich), 2-propanol, Na_2EDTA (Sigma Aldrich)

3] Plastic ware and glass ware: round bottom pre-culture tubes (BD Falcon/Genetix), petri plates (Tarsons/Laxbro), Glass bottom plates with cover glass no 1.5 (Cell E and G Cat no.# GBD00002-200), cryo-vials (Tarsons), plastic baffled flasks (Nalgene), glass baffled flask (Allied scientific), 50ml and 15ml plastic centrifuge tubes (Greiner/ Tarsons/Nunc)

4] Others: toothpicks, glass slides and cover slips (Rohem India), transparent nail polish, glass beads (Sigma Aldrich)/ spreader for spreading (Genetix)

5] Yeast transformation: Autoclaved distilled water, Lithium acetate (Sigma Aldrich # L4158), Poly ethylene glycol 3350 (Sigma #P-3640), single stranded DNA (Sigma Aldrich #D1626)

6] Genomic DNA isolation from yeast: distilled water (autoclaved), Triton X-100, NaCl, EDTA (Sigma Aldrich), SDS(Sigma Aldrich), Tris-Cl, glass beads (Sigma Aldrich #G8772), Tris saturated phenol (Sigma Aldrich), chloroform, TE buffer, DNase free Rnase A (Fermentas), Ammonium acetate (Fisher scientific), absolute ethanol (Merck), 70% ethanol.

7] Live cell imaging: Concanavalin A (Sigma Aldrich), distilled water, Colin cleaner.

3.2.2 Instruments: Table top centrifuge (eppendorf Centrifuge 5418), Refrigerated centrifuge (Eppendorf Centrifuge 5430R), Bacto hood (Micro-filt), shaker incubator with refrigeration, 30^0C water-bath with refrigeration, Weighing balance (AND), pH meter (Eutech), Magnetic stirrer (Spinot), Autoclave, Vortex mixer (Genei),-80^0C refrigerator (Sanyo), -20^0C refrigerator (Sanyo), 4^0C refrigerator (Godrej), 42^0C water-bath (Trishul Equipments), inverted microscope (Nikon),Spectrophotometer (Shimadzu),Thermo mixer comfort (eppendorf), Confocal microscope- Zeiss LSM 510 Meta andLSM 780.

3.2.3 Softwares: Snapgene 2.5, Lasargene DNAStar, ImageJ, LSM browser, Bitplane-Imaris 7.7, Adobe Photoshop CS6, Microsoft office, Filemaker pro, Quick time player, GraphPad Prism 5

3.2.4 Maps of commercial vectors used: Ycp50 [213]and Ycplac33, Yeplac195,Yiplac204, Yiplac211[214].

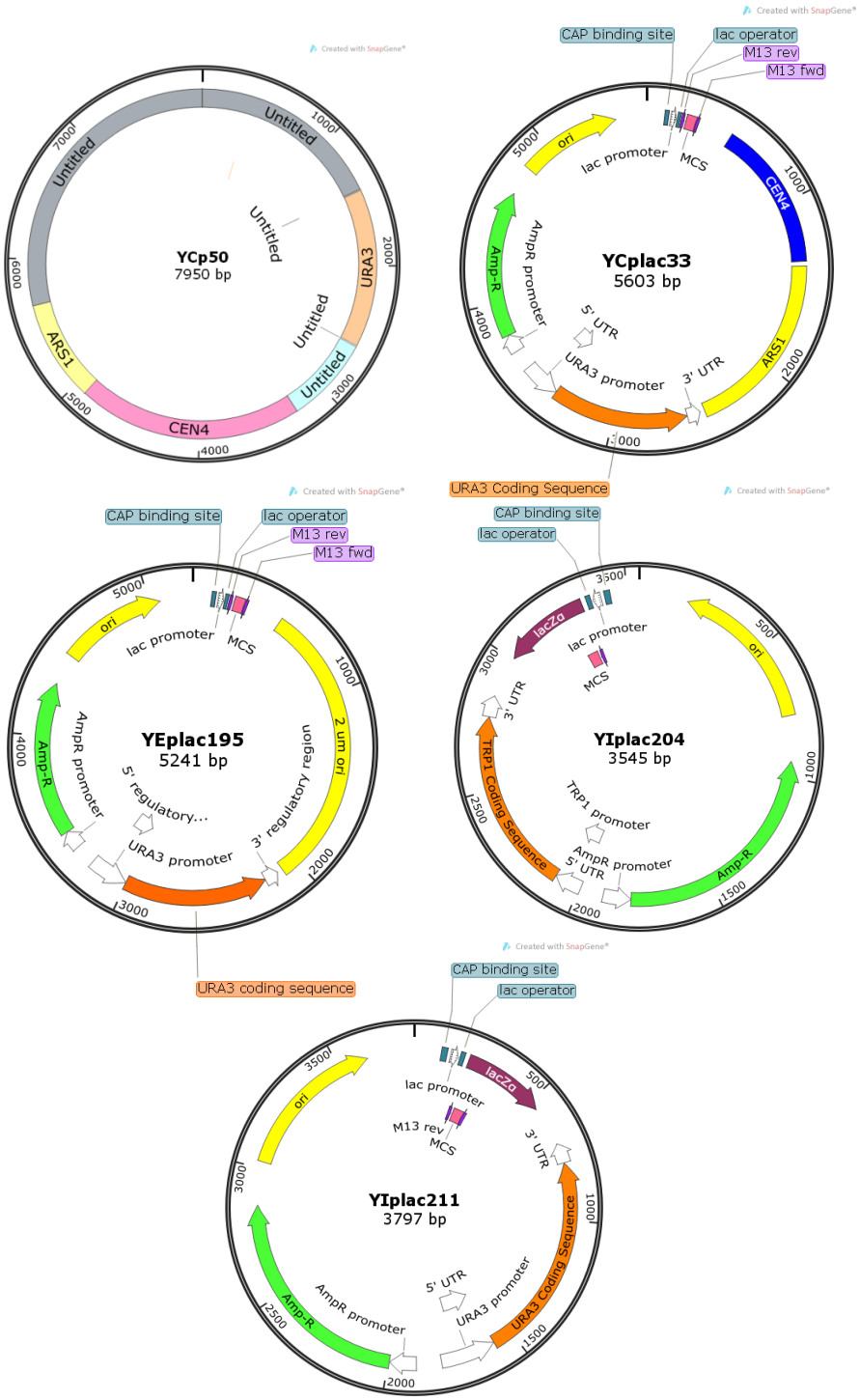

Fig 3.5: Maps of commercial yeast expression vectors

3.2.5 Materials:

Media recipe: Media were prepared as indicated on the bottles; by dissolving powder in distilled water and autoclaved for sterilization. Drop out media were prepared for selection of clones after transformation. These were prepared by adding yeast nitrogen base, glucose, CSM without a particular amino acid for selection, in a proportion as indicated on media bottles. They were sterilized by autoclaving.

5-FOA plates for popping out URA based plasmid:

Yeast cells expressing $URA3^{+}$ are unable to grow on media containing 5-Fluoro-orotic acid (5FOA) (a pyrimidine analog) but mutant yeast strains containing $ura3^{-}$ mutants grow normally [215]. This gives advantage of selecting yeast cells which lack wild type URA3 allele. By this method, it is possible to take out the URA3 expressing plasmid out of cells.

Preparation of FOA plates: Contents for making 250ml SD media were mixed in 125ml distilled water; 250mg of 5-FOA powder was added to this mixture and sterilized by filtering through 0.22µ filter. The bottle containing 5 FOA was wrapped with aluminum foil as FOA is light sensitive. In 125ml distilled water, 5g agar was added and this was autoclaved. Later this autoclaved agar solution and sterilized medium with 5-FOA were mixed well and poured in plates. Final concentration of 5FOA was 1mg/ml.

G418 solution: G418 powder was dissolved in distilled water to concentration of 50mg/ml. This was sterilized by passing through 0.22µ filter and stored at -20°C. Final concentration in the media was around 200µg/ml. Based on requirements; different concentrations in the range of 200-400µg/ml were tried.

Glycerol solution for freezing yeasts: 15% glycerol was prepared in distilled water and was sterilized by autoclaving.

Concanavalin A solution: Concanavalin A was dissolved in distilled water to the concentration of 2mg/ml and100µl aliquots were made and stored at -20°C.

1M Lithium acetate: 10.2 g of lithium acetate dehydrate was dissolved in 100 ml sterile

Distilled H_2O and sterilized by filtration through 0.22 µ filter. Solution was stored at room temperature.

50% Polyethylene glycol: 50g of PEG 3350 was weighed and added in a 150-ml beaker. Distilled H_2O was added slowly to this beaker. Mixture was stirred with a magnetic stirrer until the PEG dissolved completely. The volume was adjusted to 100 ml with distilled H_2O. The solution was filter sterilized through 0.22µ filter and stored in a tightly capped bottle at room temperature.

Breaking buffer for genomic DNA isolation:

Components	Stock	For 200 ul
2 % (v/v) Triton X-100	Triton X-100	4 µl
1% (v/v) SDS	10% (v/v) SDS	20 µl
100 mMNaCl	5M NaCl	5 µl
10 mM Tris-Cl, pH 8.0.	1M Tris-Cl	2 µl
1 mM EDTA, pH 8.0	0.5M EDTA	0.4 µl
Distilled H20(sterile)		168.6 µl

Table 3.1 Breaking buffer for yeast genomic DNA isolation

3.2.6 Methods:

Retrieving strains from the yeast collection:

The appropriate vial number was identified from Filemaker database of lab yeast freeze downs. The same vial was identified in the standard -80°C collection boxes. The vial was always placed on ice once taken out from -80°C freezer. Using a sterile toothpick, a small amount of the frozen cell paste was scraped off and streaked on YPD plate or selection media containing plate in case of strains containing episomal plasmids. The vial was returned to -80°C as soon as possible. Precaution was taken to avoid thawing of contents of the vial.

Yeast cell culture:

All the yeast strains were revived from freeze down as mentioned above. Wild type cells were incubated at 30°C while the thermo-sensitive mutants were incubated at 25°C for 48 hrs. Once the colonies appeared, pre-cultures of 5-6 ml were started in YPD or selection medium from a single colony a day before experiment in a round bottom pre-culture tube and grown overnight to get a saturated culture. On the day of experiment, OD_{600} of this pre-culture was measured. From this pre-culture, a log phase culture was started in baffled flask. The formula used for calculating required inoculum is as follows:

$$\mathbf{Required\ OD} * \mathbf{total\ volume(ml)/OD\ preculture} * \mathbf{2^n}$$

Here, n is number of generations.

Yeast cultures were always grown in rich glucose medium (YPD) or minimal medium (SD) or selection medium when required[216], with shaking at 200rpm in baffled flasks. Wild-type strains were grown at 30°C unless otherwise indicated.

Thermo-sensitive mutants were grown at 25°C, and were shifted to 37°C for 30 minutes before analysis.

Yeast Plasmid Recovery: The protocol for yeast plasmid recovery was adapted from Berger and Kimmel's Guide to Molecular cloning techniques [217].

1. 10ml culture of cells was grown to saturation.

2. Cells were harvested by centrifugation at 3000rpm for 3 min and washed in 0.6ml of 0.9M Sorbitol, 0.1M Na_2EDTA(pH 7.5).

3. Cells were re-suspended in 0.4ml of 0.9M Sorbitol, 0.1M Na_2EDTA (pH 7.5), 14mM 2-mercaptoethano (=1:1000). 20µl of lyticase was added. Cells were incubated at 37^{o}C for 20-30min. Spheroplast formation was monitored by diluting 1% SDS and measuring OD_{600}.

4. Spheroplasts were centrifuged and re-suspended gently in 0.45ml of 50mM Tris-Cl (pH 8), 50mM Na_2EDTA. 50 µl of 2% SDS was added and mixed. Vials were incubated at 65^{o}C for 30min.

5. 80 µl 5M KAc was added and vials were put on ice for at least 60min.

6. Vials were centrifuged at 13000rpm for 15min. Supernatant was transferred to fresh tube.

7. DNA was precipitated by adding 1ml ethanol at room temperature andmixed. Tubes were centrifuged briefly at 13000rpm for 5min. The pellet was rinsed with cold 70% ethanol and air dried.

8. The pellet was re-suspended in 0.5ml TE. Insoluble material was centrifuged for 15min at 13000rpm. The supernatant was transferred to fresh tube. 25 µl of RNase (1mg/ml) was added and incubated at 37^{o}C for 30min.

9. Equal volume of 2-propanol was added, mixed gently and spun for 10min at 13000 rpm.

10. Supernatant was discarded; pellet was rinsed with cold 70% ethanol, air dried andre-suspended in 50µl of TE.

Yeast transformation: High Efficiency Yeast Transformation with LiAc [218] was used for transforming integrating, centromeric, episomal plasmids as well as PCR products in yeast cells.

1. Cells were grown as discussed earlier with good aeration in 50mI YPD media to an OD_{600} of 0.5 -1.0. This procedure supplied enough cells for 10 transformations.

2. A fresh 0.1 M LiAc solution was prepared by diluting 0.5 ml of the 1.0 M stock solution with 4.5ml sterile distilled H_2O. A fresh solution of PEG/LiAc was prepared by mixing 0.5 ml of the 1 M LiAc stock solution, 0.5 ml sterile distilled H_2O, and 4.0 ml of the sterile 50% PEG stock solution. This was pipetted well to get uniform mixture.

3. The cells were spun for 3 min at 3000 rpm at room temperature in a table top centrifuge. The pellet was re-suspended in 20 ml sterile distilled H_2O. Cell suspension was spun again, and re-suspended in 0.5 ml 0.1M LiAc. The cells were then transferred to a sterile microcentrifuge tube.

4. The cell suspension was incubated for 15 min at 30ºC in a water bath.

5. Meanwhile, an aliquot of single-stranded carrier DNA was boiled at 99ºC for 10min in thermo-mixer, and then immediately cooled by placing vial on ice.

6. For each transformation, 5 µl boiled carrier DNA and approximately 100ng transforming DNA (in 5 µl or less) was added to a sterile microcentrifuge tube at room temperature. For each transformation, negative control and a positive control were included.

7. The cell suspension was vortexed briefly, 50 µl cells were added to each transformation tube, cells and DNA mixture was vortexed briefly.

8. To each tube, 300 µl PEG/LiAc was added and mixed by repeated gentle pipetting with a 1ml pipette. Pipetting was continued until a uniform mixing was achieved.

9. The tubes were incubated for 30 min at 30ºC.

10. Heat shock was given to the cells for 15 min at 42ºC. In case of temperature sensitive cells, heat shock was avoided and incubation was continued at 30ºC for total of 45min.

11. After incubation was over, cells were spun for 10 sec in a microcentrifuge at top speed to pellet cell from solution.

12. The PEG/LiAc supernatant was removed and cells were re-suspended gently in 200µl sterile distilled H_2O. 200 µl of cells were spread onto a selective plate. The plates were incubated at appropriate temperature until colonies appeared.

Replica plating for screening transformants:

Once colonies appeared on transformation plates, replica plating was done for further use like screening under microscope for fluorescence or inoculating for genomic DNA isolation. Around 20-30 transformants were replica plated on selection media by making a grid on them. Plates were again incubated at appropriate temperature. In case of less efficient transformations (for eg G418 resistant colonies), 50-100 colonies were replica plated.

Genomic DNA isolation:

1. Cells were grown in 5-6 ml media culture overnight by inoculating single colony. The entire culture was spun for 5min, 3000 rpm at room temperature. Supernatant was removed and pellet was re-suspended in 0.5 ml MQ. The suspension was transferred to micro centrifuge tube and spun at room temperature again. Supernatant was carefully removed.

2. Pellet was vortexed. 200µl of freshly prepared breaking buffer was added to this pellet and mixed well by tapping.

3. 0.3 g (200 µl in vol.) glass beads were added to this and 200 µl phenol (cold)/chloroform was added to this.

4. The mixture was vortexed at highest speed for 3min to achieve cell lysis. 200 µl T.E buffer was added andvortexed briefly.

5. The solution was centrifuged for 5 min, at highest speed at room temperature.

6. Aqueous layer was transferred to fresh tube and 1ml 100% ethanol (ice cold) was added to this andmixed by inverting. The tubes were incubated at -20ºC for 20 min to 1 hour for nucleic acid precipitation.

7. The tubes were then centrifuged for 3 min at high speed at room temperature. The supernatant was removed and pellet was re-suspended in 0.4 ml 1X T.E. Buffer.

8. 3µl of l0 mg/ml DNase-free RNase A was added to this, mixed and incubated for 5 min at 37^{o}C. After incubation was over, 10 µl of 4M Ammonium acetate and 1ml of 100% ethanol were added and mixed by inversion. Again vials were incubated at -20ºC for 30min.

9. Tubes were centrifuged at room temperature for 10-15 min at 13000rpm. Supernatant was discarded and pellet was air dried

10. DNA pellet was re-suspended in 100µl TE buffer and stored in -20ºC.

Checking fluorescence signal in upright microscope for screening:

The colonies which were to be screened were re-suspended in 20µl of SD media. Glass slides and coverslips were cleaned with Colin and air-dried. 5µl of cell suspension was placed on slide and cleaned coverslip was dropped from the top on this suspension. Slide was inverted on a piece of tissue paper and gently pressed by forcing at both ends to wipe excess suspension on tissue paper. The coverslips were sealed with transparent nail polish. Once nail polish was dried, a drop of immersion oil was placed on the coverslip and slide was placed on microscope stage for viewing. Cells were focused in bright field and then fluorescence was checked by selecting appropriate filter.

Chromosomal gene replacements:

Gene replacement was performed by using URA based integrative plasmid and the pop-in/pop-out method [219]. For integration of 3' tagging plasmid, the plasmid was linearized at a unique site within the 3' fragment of the gene. The unique site was at least 100-150 bp from the stop codon, and the same distance from the beginning of the 3' fragment. Thus, linearization created a fragment that has homology at both ends to the site of integration. For eg., to tag Sec13 with GFP at its C-terminus, such construct has to be first made.

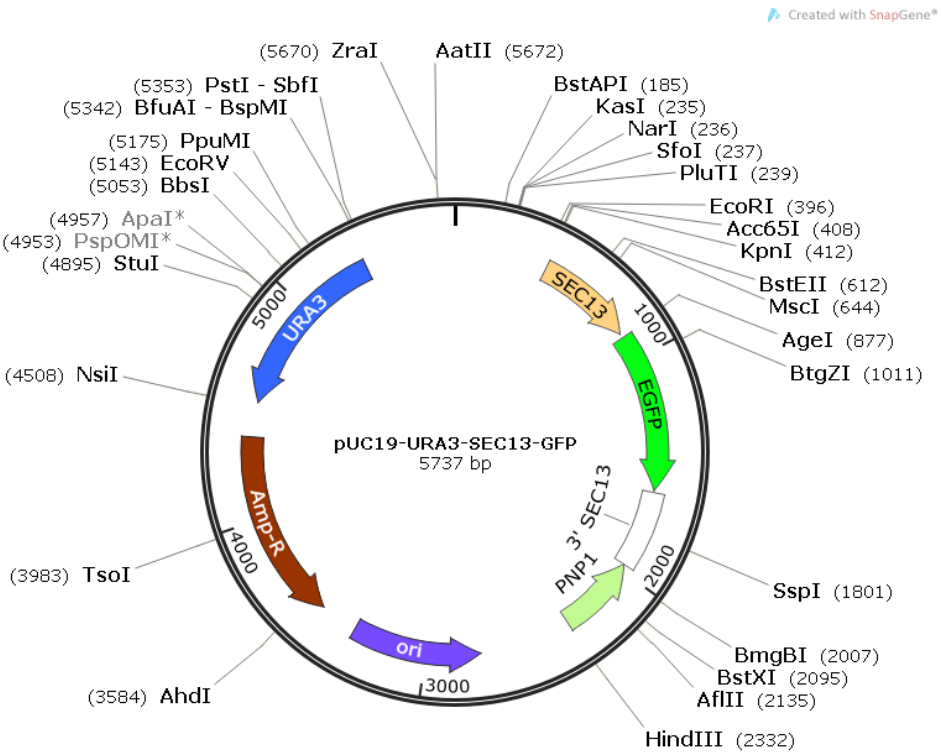

Fig 3.6: Sec13 GFP integrative plasmid

Cut this plasmid at BstEII for linearizing at Sec13.

After linearizing, plasmid will look like this:

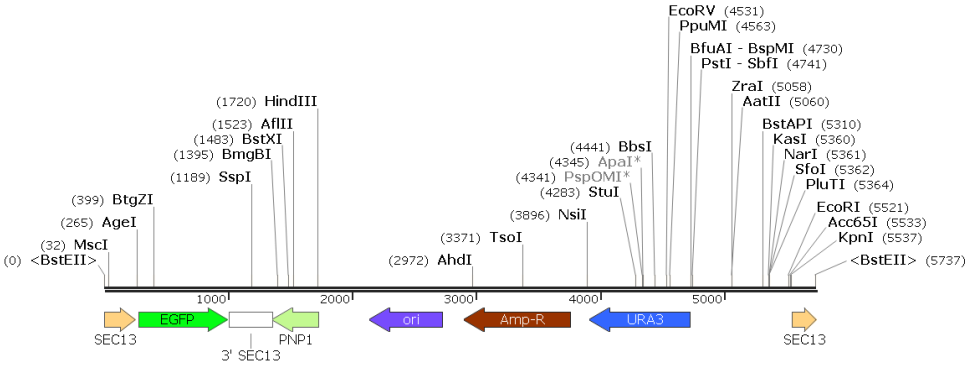

Fig 3.7: Linearized pUC19-URA3-Sec13-GFP

The linearized fragment was transformed in the cells. Once the colonies appeared, they were called pop-in. Such strain had a genomic locus as follows:

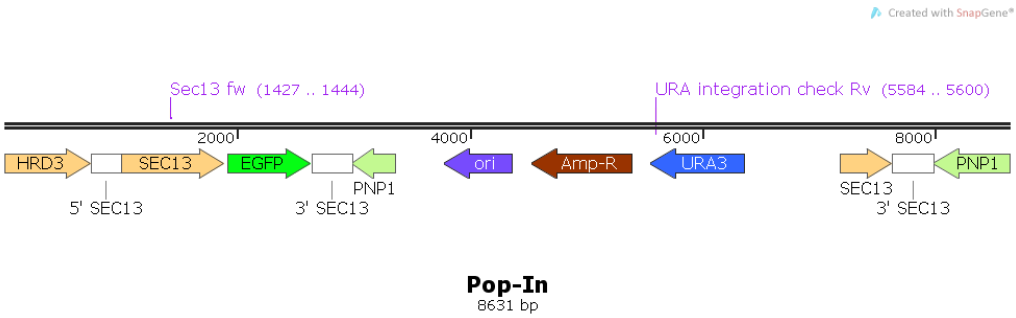

Fig 3.8: Sec13 locus after integration at BstEII in C-terminus of Sec13 (Pop-in)

There was a single complete copy of SEC13-GFP, including both the promoter and terminator regions in a pop in strain. Downstream, after the Amp-R and URA3 genes, is a non-functional 3' fragment of untagged SEC13.Thus, the pop-in strain already carried a gene replacement. But this strain can be genetically unstable because of the duplicated sequences. Such integration at desired locus has to be confirmed by PCR using primers like Sec13 fw and URA integration check Rv as shown in figure. Forward primmer has to be located before the unique restriction site so that the positive PCR will ensure integration at correct genomic locus. Positive clone for correct integration as checked by PCR from pop-in strain was plated on 5-FOA plates for obtaining a pop out clone. After popping out, the genomic locus will look like as follows:

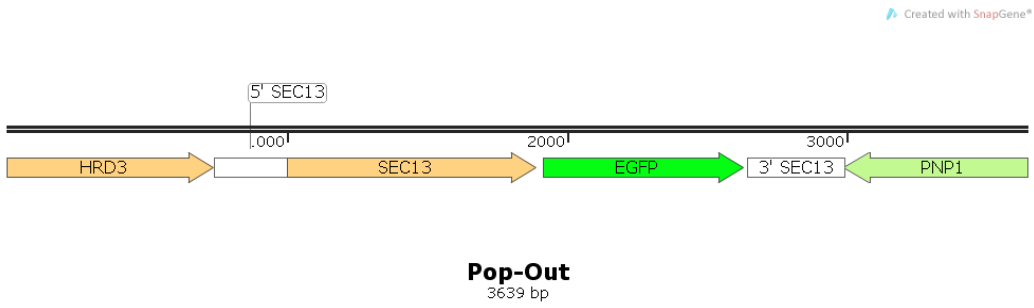

Fig 3.9: Sec13 locus after popping out URA3 plasmid by plating on 5-FOA containing media

Recombination occurs in the 3' region downstream of the stop codon, looping out URA3 and the rest of the plasmid sequence. As a result, the genomic locus now has a clean replacement of SEC13 with SEC13-GFP. To ensure recombination at 3' downstream region, it's important to take large 3' downstream region while cloning the gene fragment. In similar way, this strategy can be used for N-terminal tagging. In this case, entire 5' upstream region has to be cloned along with complete ORF of the gene. Unique restriction site has to be located within 5' upstream region for achieving recombination at 5' upstream region. In case of 5' tagging by pop-in pop out, it's very important to pop out the plasmid, as a full length duplicate gene copy might express and result in toxicity.

Preparing live cell chambers for imaging yeast cells:

A 200µl aliquot of Concanavalin-A was removed from -20°C freezer and thawed. A new confocal glass bottom dish surface was cleaned properly with Colin and an entire aliquot of Con-A was placed onto glass surface. The glass surface was treated with Con-A for 30 min at room temperature. The Con-A solution was then removed and rinsed with distilled water. Using vacuum it was air dried completely. Log phase yeast culture with OD_{600} 0.5-0.7 was added to Con-A coated glass surface and incubated at room temperature for 12 min. The culture was removed and washed gently with SD media twice. Later 200µl of SD media was added for imaging.

Live cell imaging of yeast cells for volume measurement:

All the images of different Golgi size mutants for measuring Golgi cisternal volume and diameter were taken in Zeiss LSM 510 confocal microscope. Cells were imaged at 23-25^{o}C. The cells were focused in bright field first. Images were taken by using 63X, 1.4 NA objective. Optical zoom was kept 3 to get pixel size of 90nm. Single- or

dual-color data sets were obtained using separate excitation and capture of red and green signals, with a pinhole of 1 AU and with line averaging of 4 to improve the signal-to-noise ratio. Multiline Argon and 543nm lasers were used for imaging GFP and DsRed respectively. Signals were recorded by using default PMT detectors. Along with fluorescence, DIC image was also captured. Optical sections were 0.38µm apart, and, 15–20 optical sections were collected to span an entire cell. A ROI (region of interest) was drawn around a mother cell and selectively only that ROI was imaged. To limit photo-damage, laser illumination was minimized and confocal scans were carried out as quickly as possible. To get faster scans, piezo stage was used. For each strain 20 images were obtained in one experiment and each experiment was done in triplicates giving total of 60 images from 3 independent experiments for volume measurement.

Measurement of cisternal volume:

3D volume of the Golgi cisterna was calculated using Bitplane Imaris software. Images acquired in confocal microscope were directly opened in Imaris. Image was viewed in 'Surpass' mode. The ROI from 512*512 image was cropped using 'Crop 3D' tool. Volume of the Golgi surface was filled using 'surface fill' option. The desired channel was selected. As the size of cisterna is around 500nm, a threshold was set to 500nm. Threshold for smoothing was kept 70nm as that was the pixel size in the acquired image. Surface filling was done around fluorescent signal in the image by dragging the control line so as to exactly cover the fluorescent surface. To check appropriate surface filling, 3D volume was rotated and examined from different directions. Once the filling was complete, statistics was exported as an excel file. Values of cisternal volume for one set of experiment were compiled and average was calculated. 3 average values from 3 different experiments for each strain were

plotted in Graph Pad Prism 5 to obtain a graph from volume measurement data from all strains. Student's t test was used to calculate statistical significance wherever desired.

Measurement of cisternal diameter:

LSM image from confocal microscope was directly opened in Bitplane Imaris. The image was observed in 'Slice' which enabled viewing of 3D image section wise in Z direction. A cisterna was identified and it was observed through all z sections. A section which shows the largest diameter of this cisterna was identified. In this section, a line was drawn from one end to opposite end to measure maximum diameter of the identified cisterna. This gave the distance in µm. The value was noted down in excel file. In such a way, diameter was measured randomly for 4 cisternae per image. Total 40 diameter values were taken into account for calculating average diameter. These values were plotted in Graph Pad Prism5 for each strain and graph was plotted which gave the average diameter for each strain in µm.

Correlative fluorescence microscopy and electron tomography:

Wild-type or arf1Δ strains carried a Sec7-3x mEGFP gene replacement plus an integrating vector that drove mild (~3X) overexpression of Sec7-3xmEGFP [6]. A 100 ml culture was grown in SD medium at 30°C to mid-log phase with shaking. Cells were then subjected to high-pressure freezing, freeze substitution, and embedded in plastic as described previously [220], except that glutaraldehyde was omitted during freeze substitution and the resin was Lowicryl K4M.Embedded samples were trimmed and cut with a Leica EM UC6ultramicrotome to produce, 300 nm sections, which were placed on 200mesh London Finder Formvar/carbon-coated copper grids (Electron Microscopy Sciences, Hatfield, PA, USA). To provide fiducial

markers for both light and electron microscopy, 15nm colloidal gold was applied to both sides of the grid as described previously [220]. For light microscopy, a grid was placed on a glass slide with the resin side facing up, and a 22 X 22 mm number 1.5 glass coverslip with a 10-ml drop of 500 mMNa+ HEPES, pH 7.5 was inverted onto the grid. After capture of fluorescence and differential interference contrast micrographs on a Zeiss Axioplan 2 with a 1.4 NA objective, the grid was retrieved and blotted dry. For embedded wild-type cells, the samples were post-stained for 8 minutes with 2% uranyl acetate in 70% methanol, rinsed with water followed by 5 minutes rinse with Reynold's lead citrate. Cells that showed promising morphologies and fluorescence patterns were analyzed by electron tomography as described previously [220]. Golgi membrane contours were traced in the tomograms, and the structures were modeled.

Live cell imaging of yeast cells for calculating maturation parameters:

4D data sets for calculating maturation parameters were captured using LSM780. Multiline Argon and DPSS 561nm lasers were used for imaging GFP and DsRed respectively. Gallium arsenide phosphide detector was used to acquire DsRed signal where as normal PMT of LSM780 was used to acquire GFP signal. All the imaging parameters were kept same as used for capturing images for volume and size measurement except, optical zoom which was kept 4 to get pixel size of 70nm. Also the line averaging was reduced to 2 to improve the speed of movie capture. 4D data were obtained without keeping any time interval between 2 consecutive stacks. But it took around 4-5 seconds to complete one volume with two colors for ROI. So the effective interval between two stacks was 4-5seconds. 5-6 minute movies were captured for each strain using mentioned parameters.

Processing 4D data sets in ImageJ:

Raw LSM movie files were opened in ImageJ. To remove shot noise, individual optical sections were processed with a custom plugin that implemented a 3D version of a 3X3 hybrid median filter [10]. The processed optical sections were corrected for exponential photo-bleaching using EMBL tools for bleach correction plug-in in ImageJ. Such image sequence was then imported in Imaris for further analysis.

Calculating maturation parameters:

A. Persistence time of cisterna: For this calculation, 20 random early and late cisternae were selected from 10 movies and were followed. For calculating persistence time of early cisternae (sGFP-VRG4), 20 random green cisternae were selected from 10 movies. The time (in seconds) taken by completely newly forming green cisterna to mature into a red colored late (Sec7-6X DsRed) cisterna was measured. For calculation of persistence time of late cisternae (Sec7-6XDsRed), time (in seconds) taken by late cisternae from their appearance till their disappearance was measured. This data points were plotted in GraphPad Prism5 and average value was compared between WT and arf1Δ cells.
B. Maturation frequency: The maturation frequency was calculated from 10 different 4D data sets. The number of green cisternae (sGFP-VRG4) getting converted to red cisternae (Sec7 6X DsRed) per minute was calculated. This was calculated for three successive minutes in each of 10 movies. This generated 30 data points for WT and arf1Δ cells. These values were plotted in

GraphPad Prism5 to get average maturation events/min. Maturation frequency was then compared between WT and arf1Δ.

C. Fusion frequency: The fusion frequencies were calculated from 10 4D data sets. For fusion frequency calculation, number of fusion events was counted for early (Vrg4) andlate (Sec7) cisternae in wild type and arf1Δ strain by following the cisternae for two minutes. This gave fusion events/2 min. We divided these values by 2 to get fusion events / min. All these values were plotted in GraphPad Prism5 to get average fusion frequencies. Then fusion frequencies of early and late Golgi cisternae in WT and arf1Δ cells were compared.

D. Number of cisterna**:** To calculate the average number of early and late Golgi cisternae per cell, 10 cells were examined for each strain, and the number of green and red cisternae was counted for 10 consecutive frames in 4D data set, to obtain average cisternal number/cell. The cisternae that didn't persist for minimum 2 frames were not considered. These 10 average values from each of the 10 cells were plotted in GraphPad Prism5 to compare between WT and arf1Δ cells.

Statistical analysis: For volume and diameter calculation, each experiment was done in triplicate. Average value of volume/ diameter was calculated for each experiment and these were plotted in GraphPadPrism5 to generate graph. To find out if the means differ significantly, student's t test (unpaired, two tailed) was used. To compare maturation parameters again, student's t (unpaired, two tailed) test was used.

Generating fluorescent image panels:

The images were processed in ImageJ as explained earlier and were saved as '.tiff' images. They were opened in Photoshop CS6. For all images, resolution was changed to 300dpi. Image size was kept 512*512. Now image mode was changed to RGB. On requirement, brightness was adjusted uniformly. Required area from green channel was copied and pasted on red channel image or vice versa. New layer was screened in order to show both green and red signal. Scale bar obtained from LSM browser/ ImageJ was also placed as a new layer on this merged image and a new scale bar was then drawn over scale bar from previous layer using line tool. Images were saved as .PSD/.tiff files for further use.

Freezing down yeast strains:

1) Yeast cells were grown in pre-culture tube overnight until culture was saturated. 400µl cell suspension from saturated pre-culture was plated on 2 YPD plates or plates of selection medium. Plates were incubated at the appropriate temperature until lawn growth appeared.

2) For each strain, two cryo-vials were prepared by placing 1.5ml sterile 15% Glycerol in each vial. A location number for freeze down of the strain was obtained by making new entry in Filemaker yeast database of lab. Each vial was labeled with this location number on the top. The details of the strain were written on the side of cryo-vial.

3) Using a small sterilized tip, about a third of the lawn (YPD plates) or an entire lawn (selective plates) was scraped off and re-suspend in one of the vials. Procedure was repeated for the second vial.

4) The vials were placed in respective yeast freeze down box in the -80^{o}C freezer. One vial was placed in standard collection, and an identical vial was kept in the back up collection.

5) Complete information about the strain was entered in the Filemaker yeast database of the lab.

3.3 Results:

3.3.1 Characterization of Golgi size mutant

3.3.1.1 Creating an assay system for studying Golgi size in *Saccharomyces cerevisiae*

To visualize Golgi cisternae in light microscope, it is important to label Golgi resident protein with a fluorescent tag. Trans Golgi resident Sec7 protein was chosen as a marker to label Golgi cisternae. Sec7-3X GFP construct was obtained from Glick lab [6]

To get integration at genomic Sec7 locus, plasmid was linearized at Spe1 in Sec7 C-terminus region and transformed in wild type and Golgi size mutant strain. Transformants were selected on SD-URA$^-$ plates. Clean replacement of genomic Sec7 with Sec7-3X GFP was carried out by pop-in-pop-out method as described in methods section [219].

To label cell membrane, Ras2, a plasma membrane localized protein was tagged at N-terminus with mCherry fluorescent tag [221, 222] as follows. A fragment encoding mCherry–Ras2 was expressed from the TPI1 promoter for strong constitutive expression (Prasanna Iyer, Bhattacharyya lab, Thesis work).This construct was linearized with EcoRV for integration at the TRP1 locus and transformed. The transformants were selected on SD-TRP$^-$ plates. The representative picture of assay system is shown in fig 3.11. The green spots represent Golgi cisternae and the cell membrane is marked by red color.

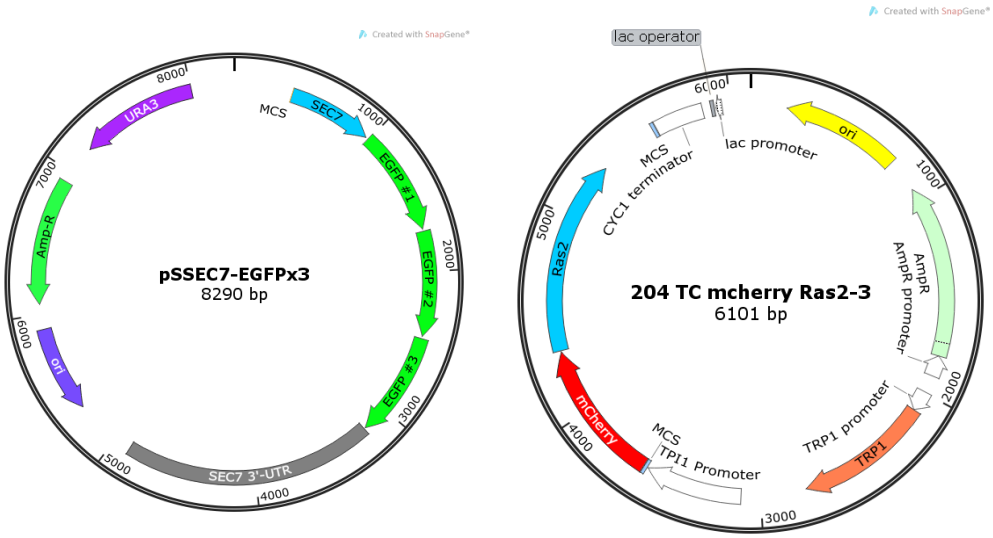

Fig 3.10: Maps of clones used to label Golgi cisternae and plasma membrane Sec7 is tagged by 3 tandem copies of mGFP at its C-terminus to label Golgi cisternae with GFP. Membrane localized Ras2 is tagged at its N-terminus with mCherry to label cell membrane in red color. mCherry-Ras2 is expressed from TPI promoter as a second copy.

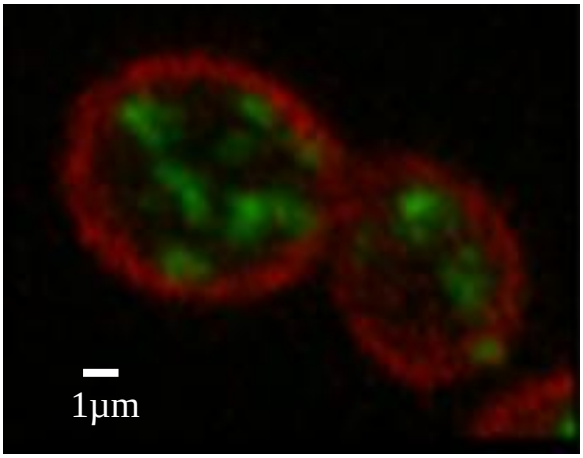

Fig3.11: **Assay system for Golgi size control study**: Golgi cisternae are labeled with Sec7-3X GFP by replacing genomic Sec7 with Sec7 3X GFP and cell membrane labeled with mCherry-Ras2 which is expressed as second copy from TRP locus under TPI promoter.

3.3.1.2 Golgi size mutant showed larger size of Golgi cisternae compared to the wild type cells

To study Golgi size, we started with a temperature sensitive (Ts) Golgi size mutant that showed larger size of Golgi cisternae compared to the wild type cells. This temperature sensitive Golgi size mutant was a kind gift from Dr. Glick [201]. The study was to find out Golgi inheritance mutants through EMS mutagenesis approach. But one class of mutants showed increased size of Golgi cisternae instead of inheritance defects. So this mutant was not further characterized in that study. We were particularly interested in the Ts mutant as it showed alteration in the size of Golgi cisternae. As seen from fig 3.12 A, Golgi size mutant failed to grow at 37^{o}C. The wild type and mutant cells were then imaged in confocal microscope to measure Golgi volume and diameter. Imaging and quantification was performed as described in methods section and graphs were plotted. As seen from fig 3.12 B and C, the mutant showed considerably larger and fewer Golgi cisternae than wild type cells. Increase in volume and diameter in the mutant is statistically significant ($P \leq 0.001$) (Fig 3.12 D, E).

3.3.1.3 Two overlapping clones from wild type genomic library which could rescue temperature sensitive and large Golgi phenotype of Golgi size mutant shared ORF of NMT1 gene.

In order to find out the mutation responsible for larger Golgi cisternae, we did wild type genomics library complementation. The wild type genomic library was transformed in Golgi size mutant and cells were plated at 37^{o}C. As the original mutant was temperature sensitive; it failed to grow at 37^{o}C. We identified the cells that were able to grow at 37^{o}C after transforming wild type genomic library.

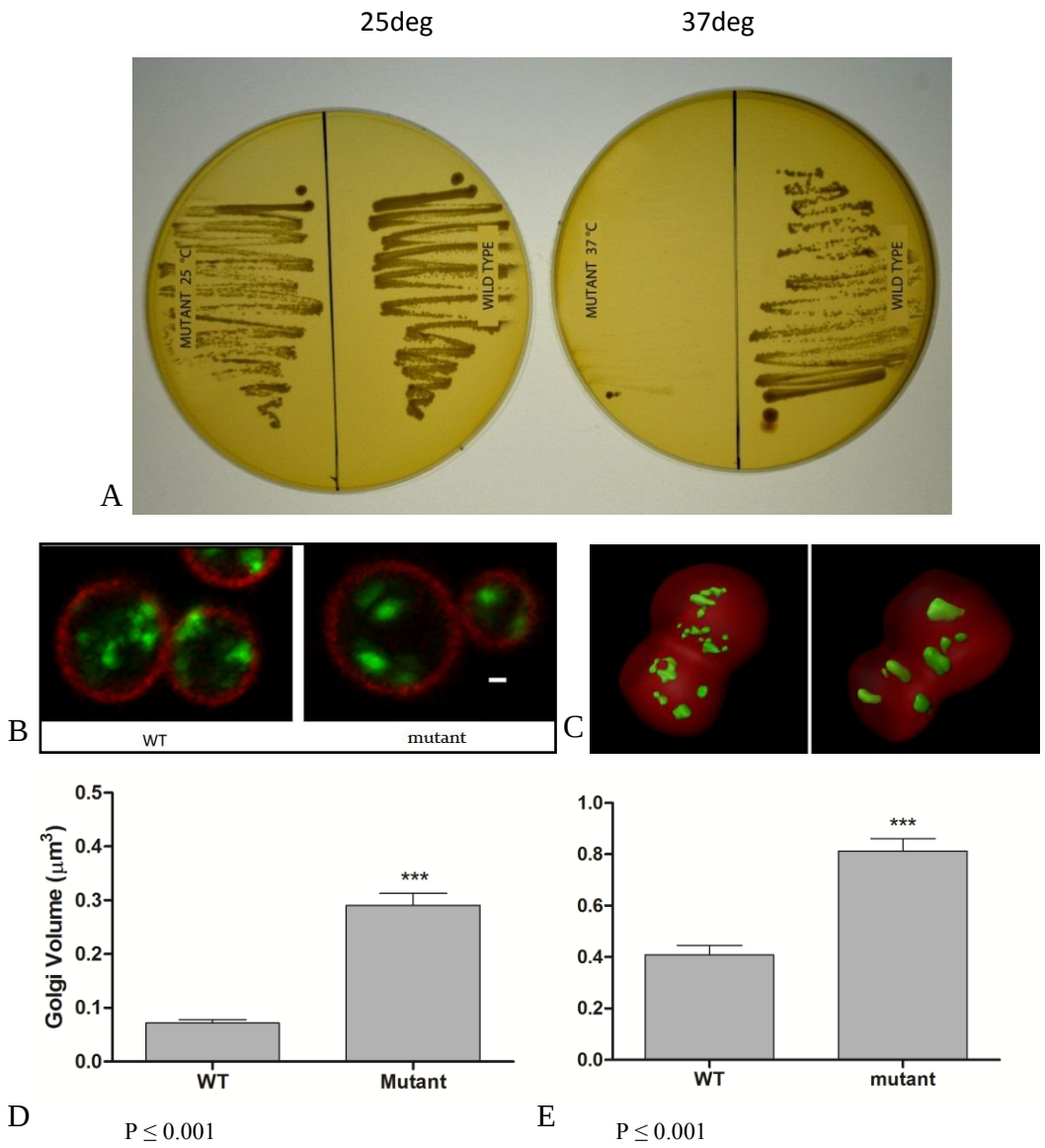

Fig 3.12: Ts Golgi size mutant shows larger Golgi cisternae A] Temperature sensitive phenotype of Golgi size mutant: The wild type and mutant cells were grown at 25 and 37^{o}C. The wild type cells grew well at 37^{o}C but the mutant cells failed to grow at 37^{o}C. B] Mutant with large Golgi phenotype: image on the left is wild type cells showing normal size of Golgi cisternae whereas the image on the right hand side is image of the Golgi size mutant which showed larger Golgi cisternae compared to wild type Golgi cisternae. Scale bar represents 1μm. C] 3D reconstruction of the same images for volume calculation. D] Comparison of Golgi volume (N=60) E] Comparison of Golgi cisternal diameter (N=40) in wild type and Golgi size mutant.

The plasmid DNA was isolated from such cells and cloned portion was sequenced by using vector specific primers which flanked the cloned fragment (YCp50-S1 and YCp50-AS1).

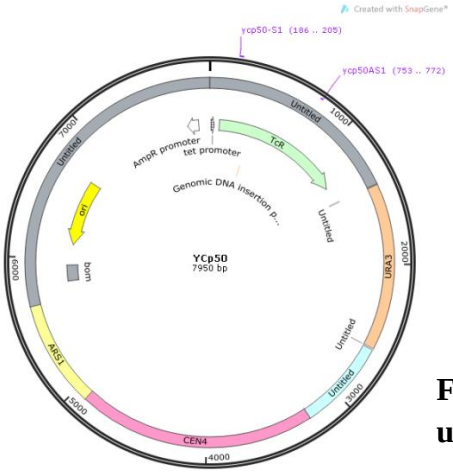

Fig 3.13 Map of YCp50 with the primers used for sequencing

BLASTN was performed against genome of *S. cerevisiae* by NCBI BLASTN tool. Fig 3.14A shows the region of genomic DNA identified for two different clones after performing BLASTN. As can be seen from the fig 3.14A, both clones shared only one complete ORF that coded for a gene NMT1 (N-Myristoyl transferase 1). The mutant cells having these plasmids from wild type genomic library could grow at 37^{o}C (Fig 3.14B) and also showed reduced Golgi cisternae size (Fig 3.14C).

3.3.1.4 Wild type NMT1 can rescue temperature sensitive and large Golgi phenotype of the Golgi size mutant.

In order to confirm if only NMT1 gene function was compromised in Golgi size mutant that gave rise to large Golgi phenotype, wild type NMT1 gene was cloned in CEN plasmid and transformed in Golgi size mutant.

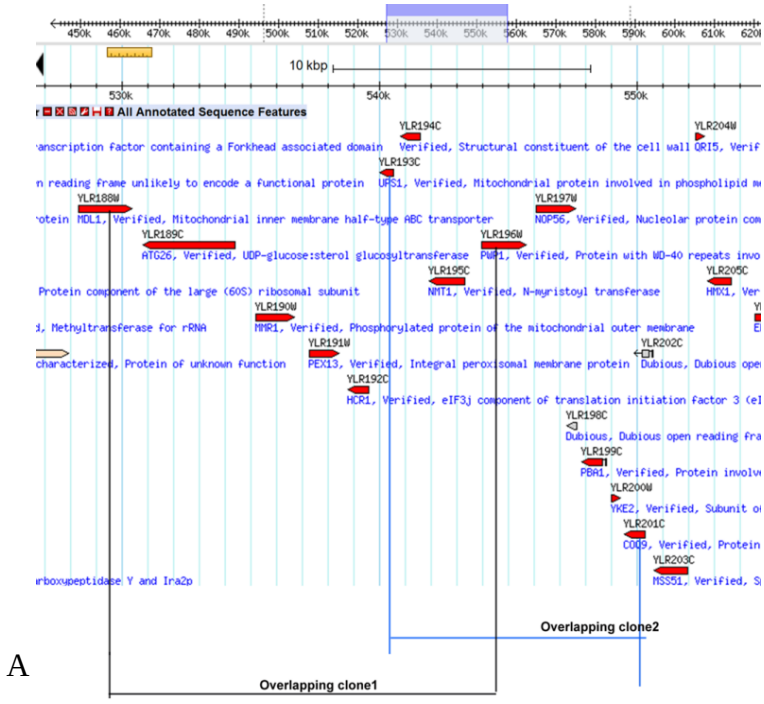

A

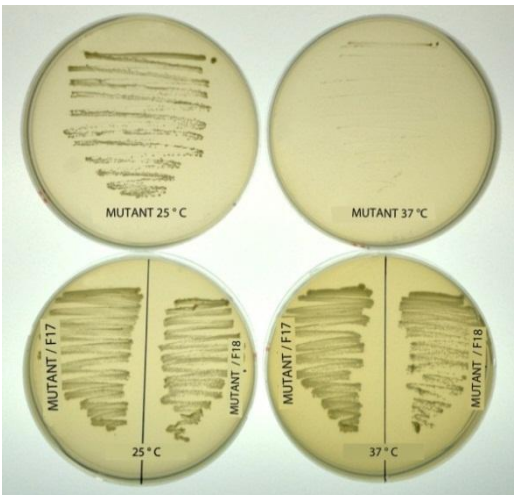

B

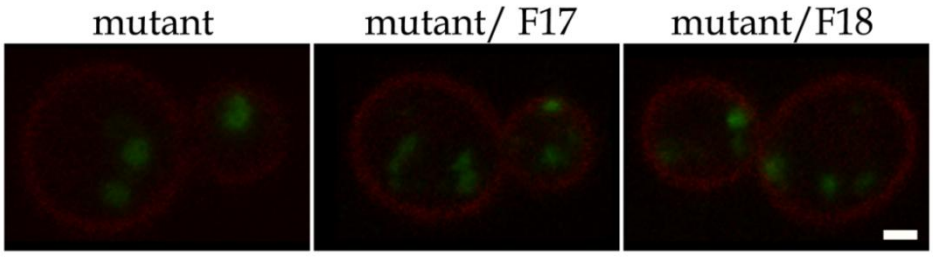

C

Fig 3.14: Rescue of Ts and large Golgi phenotype by wild type genomic library clones A] Result of BLAST performed from sequencing data from clones of wild type genomic library which complemented Ts phenotype. The sequence was BLAST against *S. cerevisiae* genome. Both clones share a complete ORF that belongs to N-Myristoyl transferase. B] Purified clones that rescued Ts phenotype were transformed in Golgi size mutant cells and plated at 25 and 37^0C. C] Cells of Golgi size mutant

after transforming clones from wild type library that rescued Ts phenotype were grown to log phase and imaged in confocal microscope to check effect on Golgi size. Scale bar represents 1µm.

Cloning wild type NMT1 in CEN plasmid:

Wild-type NMT1 gene with its 5' and 3' UTR regions was amplified and sub cloned as HindIII–KpnI fragment into YCplac33. Wild-type NMT1 gene with its 5' and 3' UTR regions was amplified using primers NMT1 prom1For and NMT1-Term1-R. The expected amplicon size was 2.07Kb (Fig 3.15B). Both the PCR product and YCplac33 vector were digested with HindIII and KpnIand subsequently ligated with T4 DNA ligase. The positive clone was selected by diagnosis with BamHI andSphI which gave expected release of 788bp (Fig 3.15 C and D).

Transformation of wild type NMT1 in Golgi size mutant led to rescue of temperature sensitive as well as large Golgi phenotype:

Once the wild type NMT1 gene was cloned in a CEN plasmid, this plasmid was transformed in Golgi size mutant by high efficiency yeast transformation method [218]. The plasmid had URA3 as an auxotrophic marker for selection. The colonies got after transformation on SD-URA$^-$ plates were screened for Ts and Golgi phenotype. Ts phenotype was checked by streaking wild type, mutant and mutant with wt NMT1 cells on YPD plates and incubating them at 25 and 37^{o}C. The growth at 37^{o}C particularly was checked. As seen in fig 3.16 B, the mutant cells were now able to grow at 37^{o}C after transforming wild type NMT1. Effect on large Golgi phenotype was studied by growing wild type, mutant and mutant with wt NMT1 cells to log phase and imaging in confocal microscope.

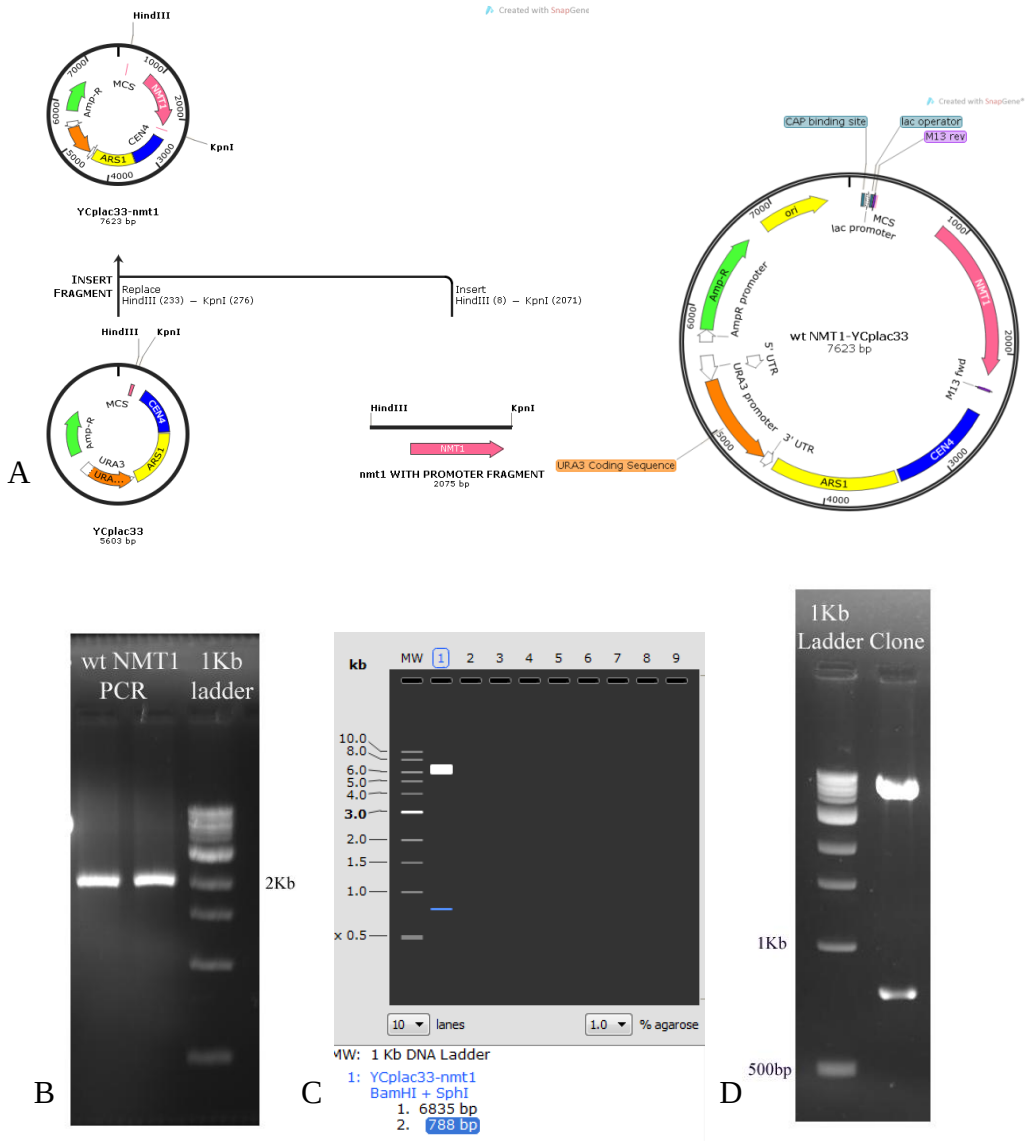

Fig 3.15 Cloning wild type NMT1 gene: A] Cloning strategy for wt NMT1-YCplac33 B] PCR of NMT1 ORF along with 5' and 3' UTRs gave 2Kb amplicon as expected. C] Simulation of agarose gel: diagnosis of positive clones by BamHI and SphI. D] Diagnosis of clone with BamHI and SphI showed expected release of 788bp.

The large Golgi phenotype of the Golgi size mutant was rescued after transformation of wild type NMT1 (Fig 3.16 A). The mutants with wild type NMT1 expressing plasmids were then plated on 5-FOA plates to cure the wild type NMT1 expressing plasmid from cells. After plasmid was cured by negative selection on 5-FOA plates, cells were rechecked for Ts and Golgi size. The quantification of volume and diameter of these cells after curing wild type NMT1 were similar to original mutant suggesting that the rescue of Tsand large Golgi phenotype was specifically due to wild type NMT1. To plot statistical significance, 3 independent imaging experiments were carried out and graphs for volume and diameter comparison were plotted as described in methods section. The rescue of large Golgi phenotype after wild type NMT1 transformation was further proved by volume and diameter calculation (Fig 3.16 C, D).

3.3.1.5 Sequencing of mutant NMT1 gene from Golgi size mutant revealed presence of T400I mutation in NMT1 ORF

The mutant NMT1 gene from Golgi size mutant was cloned in similar way as wild type NMT1. Mutant NMT1 ORF was amplified from genomic DNA of mutant and sub cloned in HindIII and KpnI in YCplac33. The diagnosis was performed with MluI and BamHI and expected release of 1.37 Kb band was obtained (Fig 3.17 B, C). This plasmid was then sequenced for entire NMT1 ORF. The sequencing data was compared with wild type NMT1 sequence by using Lasargene DNAStar software. Sequencing data (Fig 3.17 D) showed a single point mutation in NMT1 ORF at Threonine 400 position which was changed to Isoleucine (T400I).

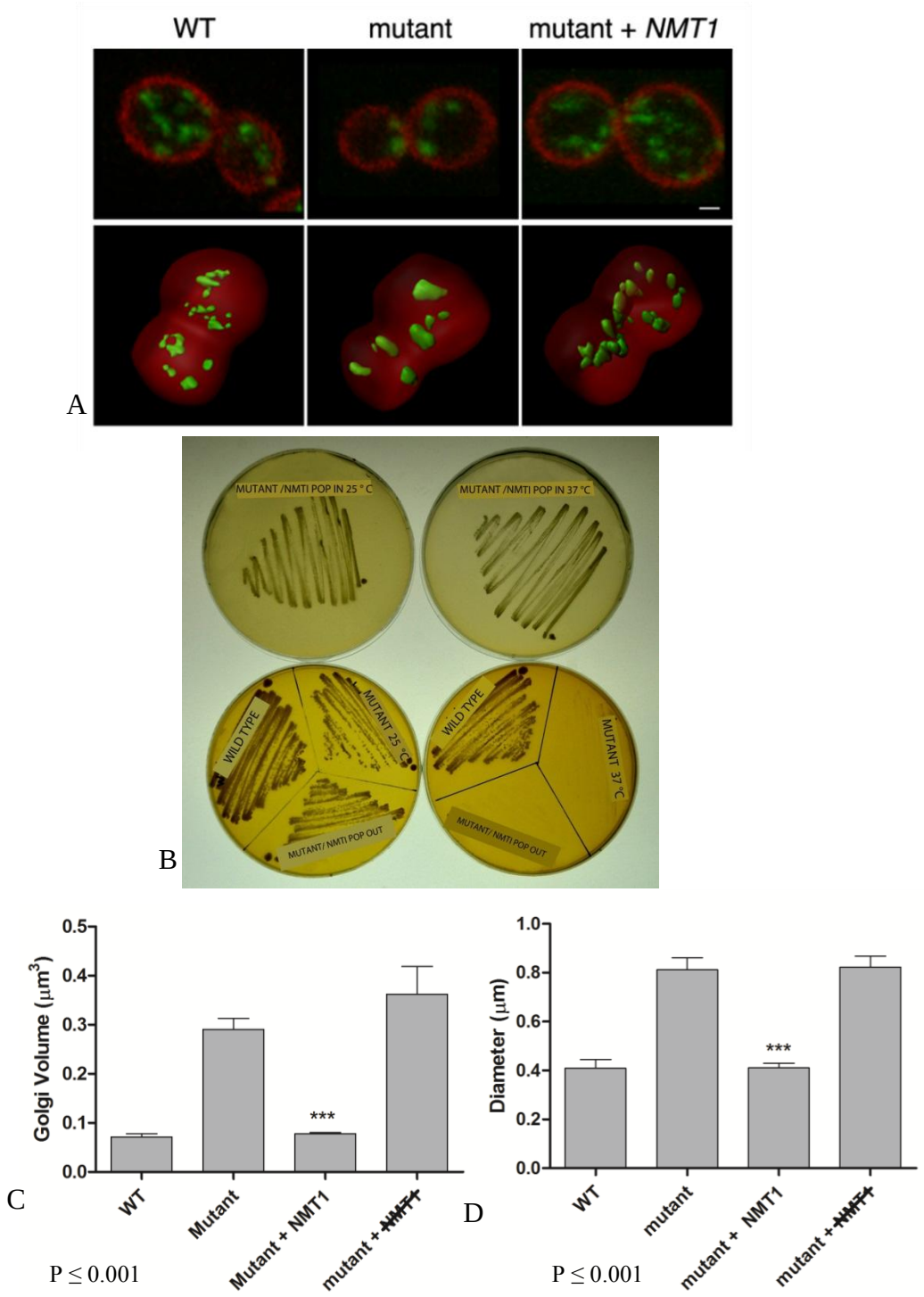

Fig 3.16 Functional complementation of Golgi size mutant by wild type NMT1: A] Large Golgi phenotype in Golgi size mutant is rescued upon transforming wild type NMT1 gene. The upper panel indicates confocal images of wild type, mutant and mutant after transforming wild type NMT1. Scale bar represents 1μm. The lower panel indicates 3D reconstruction of same images for calculating volume. B] Ts Golgi size mutant can grow at 37^{o}C after transforming wt NMT1. C] Quantification of Golgi volume (N=60) D] Quantification of Golgi cisternal diameter (N=40) after complementation by wild type NMT1.

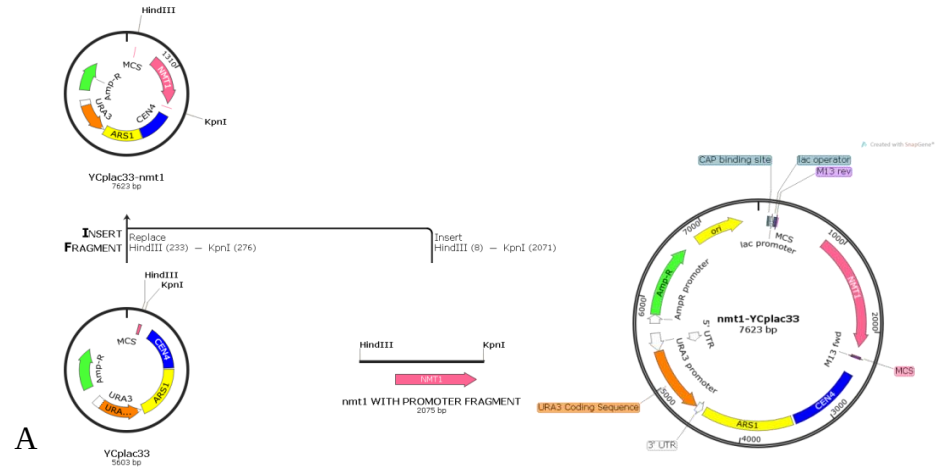

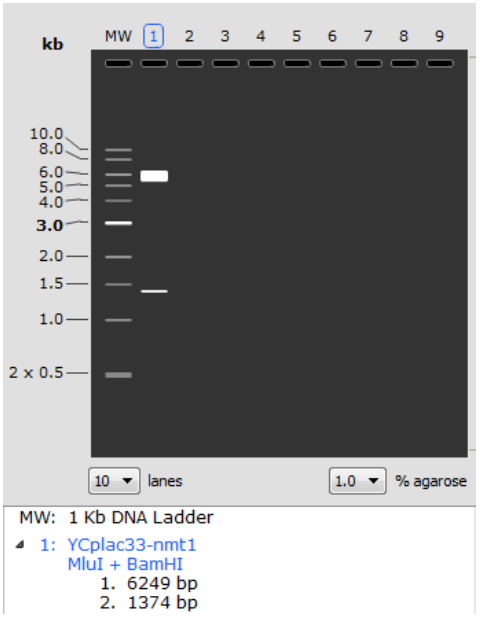

B

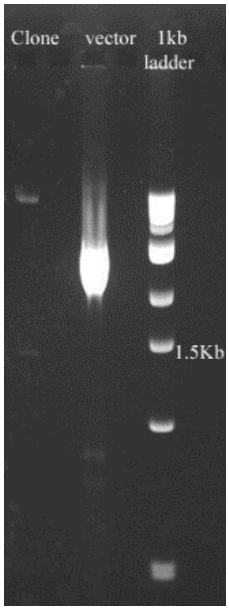

C

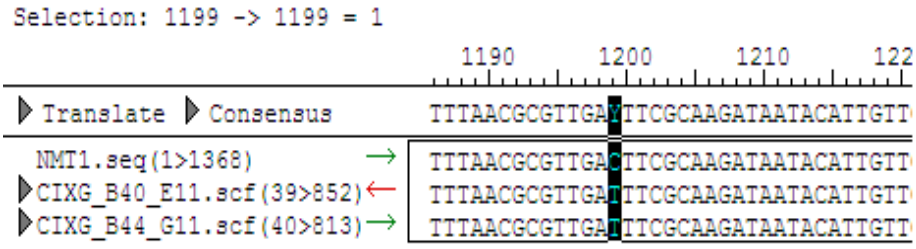

D

Fig 3.17 Mutant NMT1 cloning and sequencing: A] Strategy for cloning nmt1 ORF in YCplac33 B] The simulation of diagnosis of positive clones for nmt1 ORF in YCplac33. C] Correct diagnosis digestion by positive clone after digestion with MluIand BamHI. D] Mutant nmt1 sequenced. Sequence was compared with wt NMT1 sequence. Comparison of sequencing data showed mutation T400I in the NMT1 ORF from Golgi size mutant.

3.3.1.6 Correction of T400I mutation can rescue Ts and large Golgi phenotype.

With the knowledge of position of point mutation, we decided to cross check if this single point mutation causes large Golgi phenotype. NMT1 ORF (amino acids 64-456) was first cloned in yeast integrative plasmid YIplac211 by amplifying DNA fragment encoding from Threonine 63 to stop codon (1.3Kb) (Fig 3.18 B). This was sub cloned in YIplac211 (destroyed for EcoRI site by digesting with EcoRI then filling in 5' overhangs and blunt end ligation) in HindIII and KpnI (Fig 3.18 C and D).

The T400I mutation was then repaired in the cloned NMT1 ORF by quick change mutagenesis using NMT1- YIplac211 as template (see appendix). This T400I corrected NMT1 plasmid was linearized at EcoRI to get integration at genomic NMT1 locus in Golgi size mutant. The linearized plasmid was transformed. Transformants were selected on SD-URA$^-$ plates as YIplac211 has URA3 as an auxotrophic selection marker. The pop-in clones were popped out as explained in methods section to get clean gene replacement. The NMT1 ORF in transformants was sequenced to confirm reversion of T400I mutation in the genome of Golgi size mutant (Fig 3.18 E). When mutation T400I was corrected, both temperature sensitive phenotypes as well as large Golgi phenotypes were reverted (Fig 3.18 F and G). The rescue of large Golgi size was also confirmed by quantification of volume and diameter of Golgi cisternae (Fig 3.18 H). This suggested that mutation T400I is sufficient to cause larger Golgi spots phenotype.

A

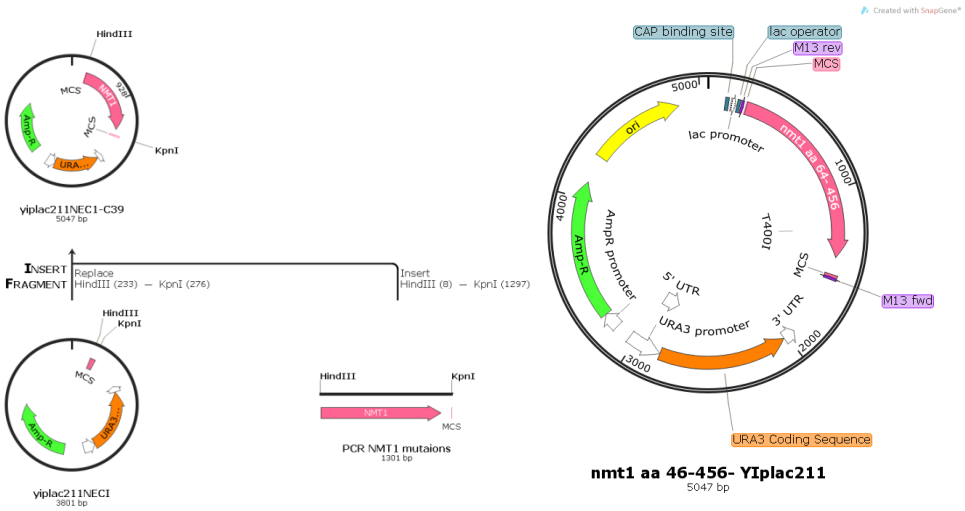
HindIII
MCS
NMT1
Amp-R
MCS
URA...
KpnI
yiplac211NEC1-C39
5047 bp
INSERT FRAGMENT
Replace
HindIII (233) — KpnI (276)
Insert
HindIII (8) — KpnI (1297)
HindIII
KpnI
MCS
Amp-R
URA3...
yiplac211NECI
3801 bp
HindIII
KpnI
NMT1
MCS
PCR NMT1 mutaions
1301 bp
CAP binding site
lac operator
M13 rev
MCS
5000
ori
lac promoter
nmt1 aa 64-456
1000
4000
Amp-R
Amp-R promoter
T400I
MCS
M13 fwd
5' UTR
URA3 promoter
3' UTR
3000
2000
URA3 Coding Sequence
nmt1 aa 46-456- YIplac211
5047 bp

B

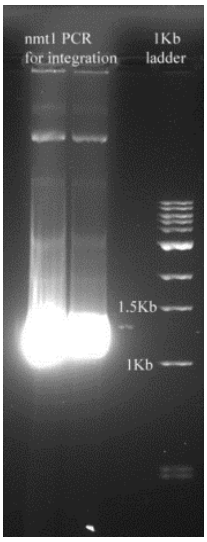
nmt1 PCR for integration
1Kb ladder
1.5Kb
1Kb

C

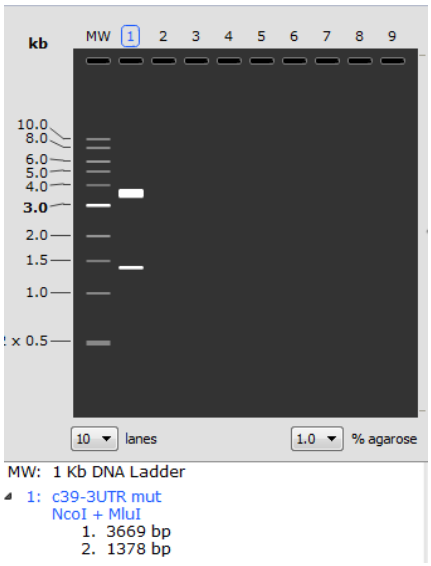
kb
MW 1 2 3 4 5 6 7 8 9
10.0
8.0
6.0
5.0
4.0
3.0
2.0
1.5
1.0
x 0.5
10 lanes
1.0 % agarose
MW: 1 Kb DNA Ladder
1: c39-3UTR mut
NcoI + MluI
1. 3669 bp
2. 1378 bp

D

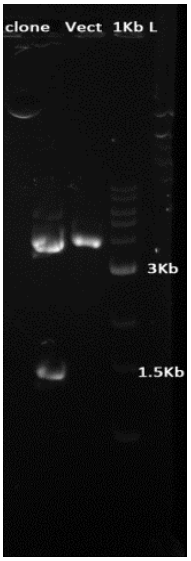
clone Vect 1Kb L
3Kb
1.5Kb

E

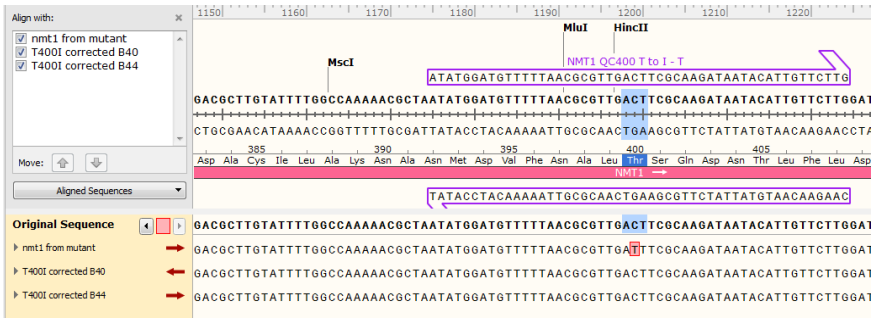
Align with:
nmt1 from mutant
T400I corrected B40
T400I corrected B44
Move:
Aligned Sequences
Original Sequence
nmt1 from mutant
T400I corrected B40
T400I corrected B44
MluI
HincII
MscI
NMT1 QC400 T to I - T
ATATGGATGTTTTTAACGCGTTGACTTCGCAAGATAATACATTGTTCTTG
GACGCTTGTATTTTGGCCAAAAACGCTAATATGGATGTTTTTAACGCGTTGACTTCGCAAGATAATACATTGTTCTTGGAT
CTGCGAACATAAAACCGGTTTTTGCGATTATACCTACAAAAATTGCGCAACTGAAGCGTTCTATTATGTAACAAGAACCTA
Asp Ala Cys Ile Leu Ala Lys Asn Ala Asn Met Asp Val Phe Asn Ala Leu Thr Ser Gln Asp Asn Thr Leu Phe Leu Asp
NMT1
TATACCTACAAAAATTGCGCAACTGAAGCGTTCTATTATGTAACAAGAAC
GACGCTTGTATTTTGGCCAAAAACGCTAATATGGATGTTTTTAACGCGTTGACTTCGCAAGATAATACATTGTTCTTGGAT
GACGCTTGTATTTTGGCCAAAAACGCTAATATGGATGTTTTTAACGCGTTGATTCGCAAGATAATACATTGTTCTTGGAT
GACGCTTGTATTTTGGCCAAAAACGCTAATATGGATGTTTTTAACGCGTTGACTTCGCAAGATAATACATTGTTCTTGGAT
GACGCTTGTATTTTGGCCAAAAACGCTAATATGGATGTTTTTAACGCGTTGACTTCGCAAGATAATACATTGTTCTTGGAT

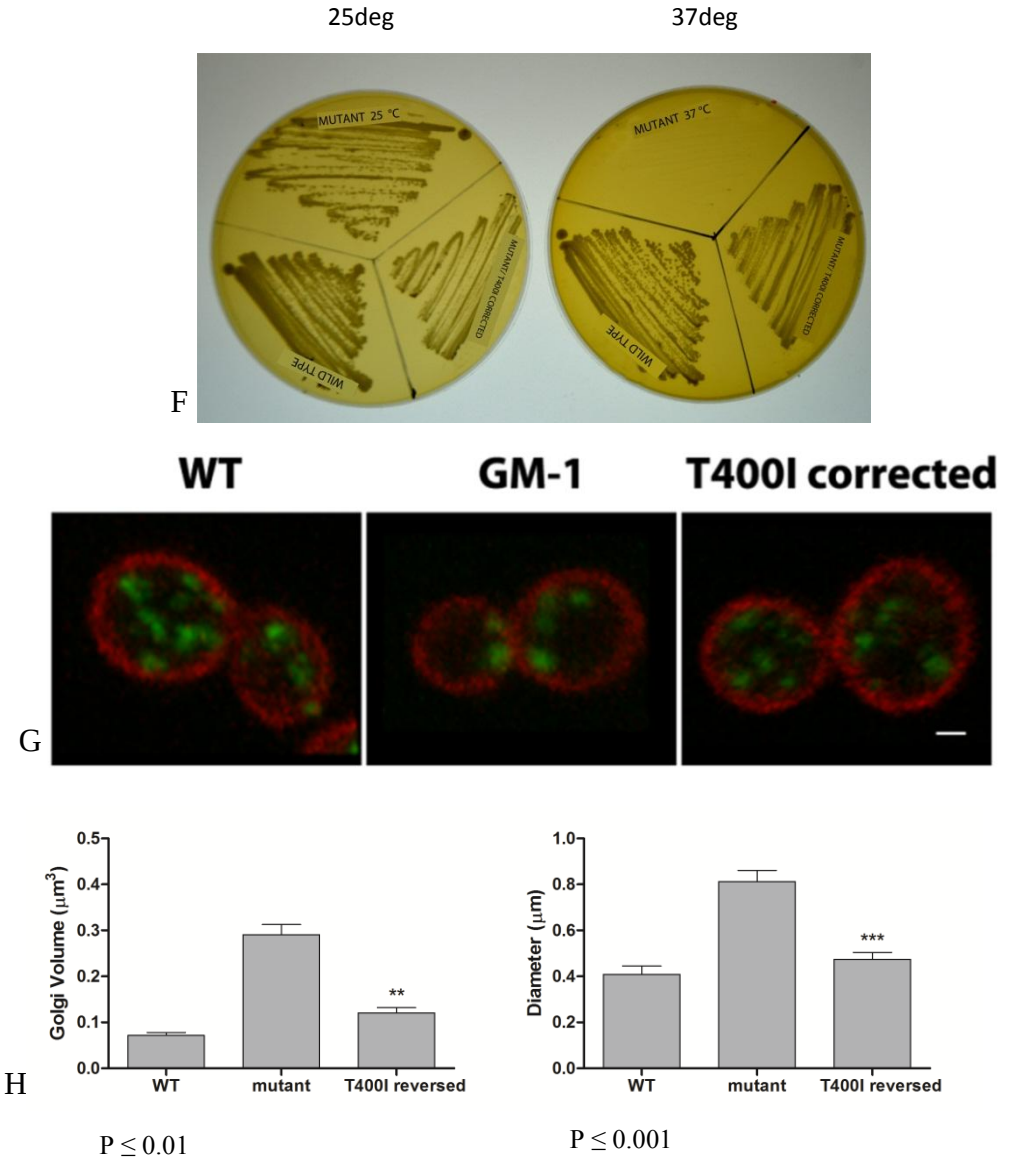

Fig 3.18 Reversion of T400I mutation leads to rescue Ts as well as large Golgi phenotype. A] Strategy of cloning nmt1 in YIplac211 B] PCR of NMT1 ORF (aa 64-456) from Golgi size mutant gave expected amplicon size of 1.3Kb. C andD] Diagnosis of NMT1-YIplac211 clone for selecting positive clone with MluI and NcoI. Positive clone gave expected release of 1.37Kb after digestion. E] Sequencing of NMT1 ORF to check status of T400I mutation. Wild type NMT1, sequence of NMT1 ORF from mutant and data for 2 independent sequencing reactions for T400I corrected mutant strain are aligned for comparison. F] T400I corrected cells were streaked on YPD plates and incubated at 25 and 37^{o}C. G] Confocal imaging of cells with T400I mutation corrected. Scale bar represents 1μm. H] Quantification of Golgi cisternal volume (N=60) and diameter (N=40) in T400I corrected strain.

3.3.2 Role of ARF1 in size control mechanism of Golgi apparatus in *S. cerevisiae*

NMT1 (N Myristoyl transferase 1) is an enzyme which catalyzes transfer of myristic acid to N-terminal Glycine residue of substrate proteins [180]. One of the substrate of NMT1 is Golgi associated GTPase ARF1. ARF1 is a GTPase of the Ras superfamily that is involved in regulation of coated vesicle formation in intracellular trafficking at the Golgi. ARF1 is a GTPase that recruits multiple effectors, including the COPI coatomer and clathrin adaptors [186, 223]. Because Arf activity depends on N-terminal myristoylation, we suspected that the enlarged Golgi cisternae in the mutant strain were due to reduced myristoylation of Arf because of mutant nmt1 function. ARF1 was also previously reported to be involved in maintenance of Golgi structure [32]. We decided to further study role of ARF1 in Golgi size regulation.

3.3.2.1 Over expression of wild type ARF1 in Golgi size mutant rescued Ts as well as large Golgi phenotype

NMT1 is a myristoylating enzyme. In Golgi size mutant, NMT1 was mutated at T400I position. Whenever an enzyme is mutated, most likely its activity is compromised. But the enzyme can still carry out the reaction at lesser efficiency depending on the effects caused by mutation. In such cases, if substrate, co-factors or enzyme concentration is increased, the reaction can be driven towards product formation.

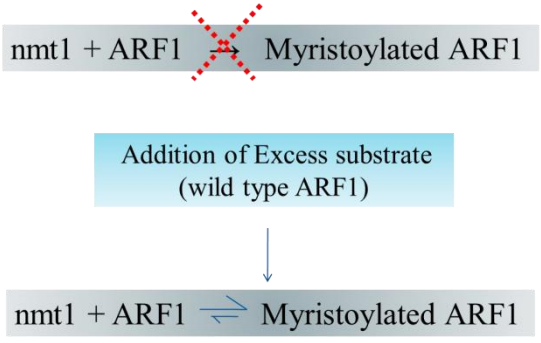

Based on this, an experiment was designed to over express wild type ARF1 in Golgi size mutant and to see if the Ts and large Golgi phenotype is rescued or not. ARF1 ORF along with its 5' and 3' UTR (1.8Kb) was amplified using primers D23 and D24. The amplicon of expected size (Fig 3.19 B) was purified from agarose gel andsub-cloned in EcoRI and HindIII in yeast episomal plasmid YEplac195.The diagnosis of the clones was done by HindIII and XbaI. Positive clone showed a release of 800bp (Fig 3.19 C and D). This clone was then transformed in Golgi size mutant and transformants were selected on SD-URA$^-$ plates as YEplac195 had URA3 as an auxotrophic selection marker. Golgi size mutant cells were able to grow at 37^oC after over expressing wild type ARF1 as can be verified from Fig 3.19 E. To study effect of ARF1 over expression on Golgi size, confocal imaging was performed. Confocal imaging data and quantification of Golgi cisternal volume and diameter both showed that over expression of wild type ARF1 could rescue large Golgi phenotype (Fig 3.19 F, G and H). Decrease in Golgi size after wild type ARF1 over expression is statistically significant. To further support that this rescue was specifically due to presence of ARF1 over expression plasmid in Golgi size mutant, the plasmid was cured from cells by plating on 5-FOA. The loss of ARF1 over expressing plasmid led to increased Golgi size in the mutant cells as before.

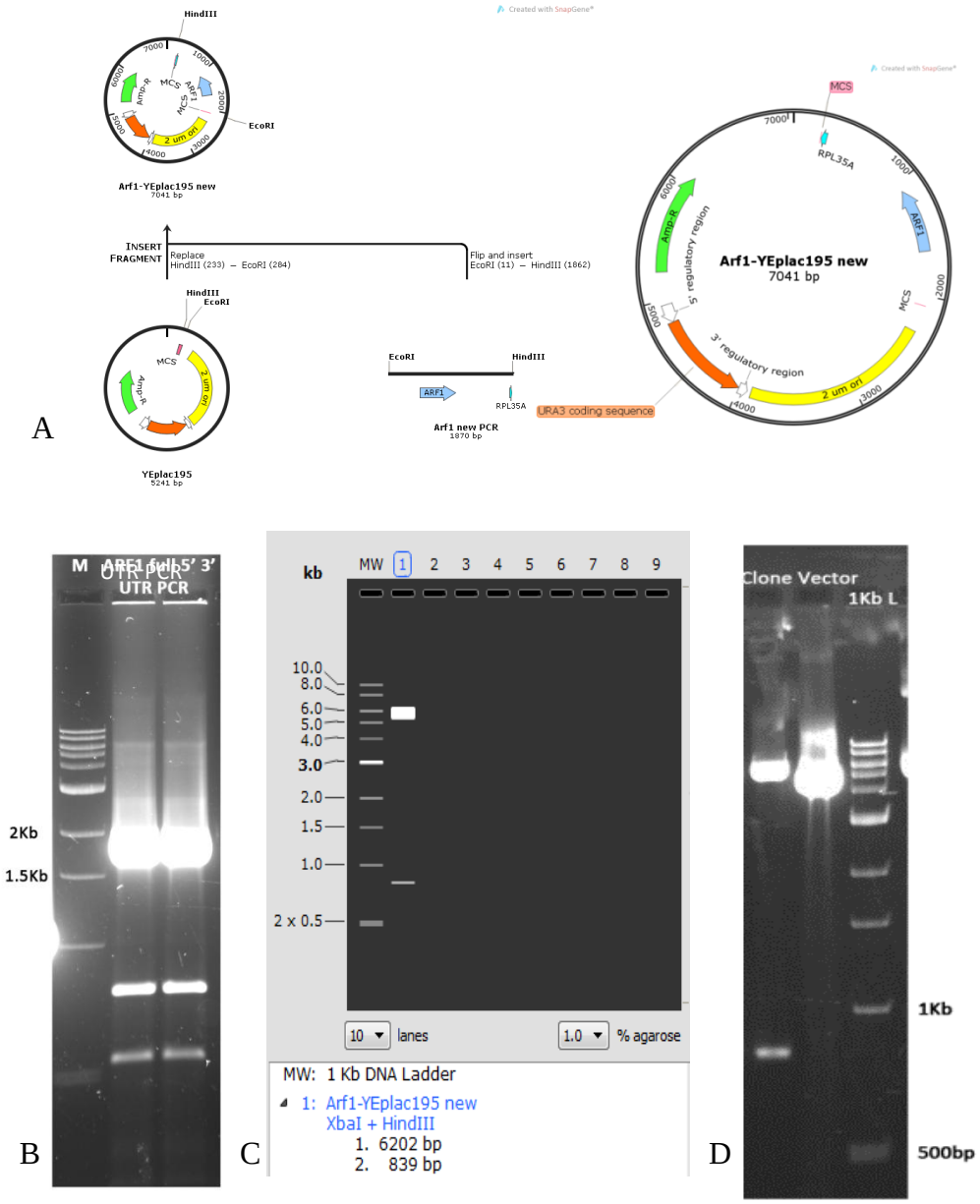

Fig 3.19 ARF1 over expression can rescue Ts and large Golgi phenotype: A] Strategy for cloning wt ARF1 in YEplac195 B] PCR of ARF1 ORF along with 5' and 3' UTR gave expected amplicon of size 1.8KB. C] Simulation of diagnosis of positive clones of ARF1-YEplac195.D] Clones were digested with HindIII and XbaI for diagnosis of positive clone and visualized on agarose gel.

E

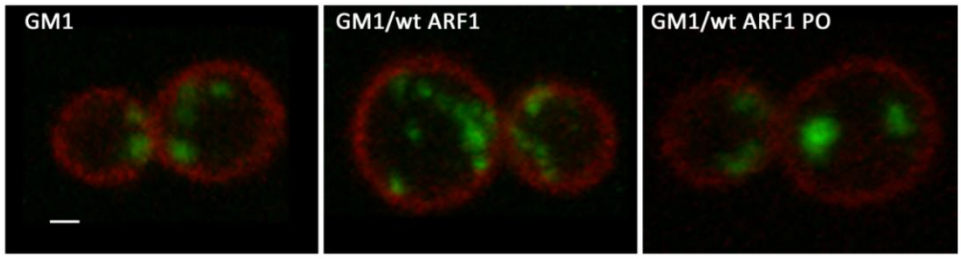

F

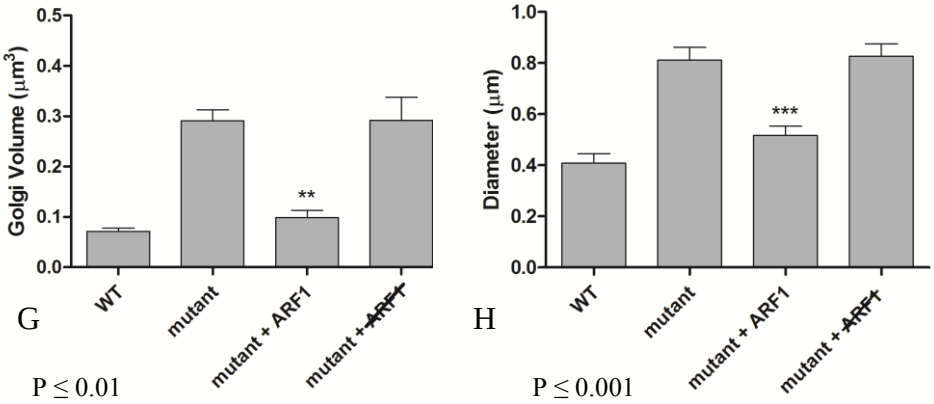

G

P ≤ 0.01

H

P ≤ 0.001

Fig 3.19 ARF1 over expression can rescue Ts and large Golgi phenotype: E] Golgi size mutant cells after transforming wild type ARF1-YEplac195 were plated at 25 and 37^{o}C to check effect on Ts phenotype. F] Confocal imaging of Golgi size mutant before and after transforming plasmid over expressing wild type ARF1. Scale bar represents 1µm. G] Quantification of Golgi cisternal volume from confocal images (N=60). H] Quantification of Golgi cisternal diameter (N=40)

3.3.2.2 arf1 Δ results into enhanced large Golgi phenotype

Since it was observed that over expression of ARF1 rescued Ts as well as large Golgi phenotype, the next experiment that could be done to examine direct role of ARF1 in Golgi size control mechanism was to study effect of deletion of ARF1 from wild type cells. PCR products consisting of a marker cassette with short flanking homology regions to the target locus (SFH-PCR) are used for directed gene alterations in *S.cerevisiae*. This technique has been termed PCR-targeting [224].Transforming DNA was generated in a PCR reaction using Kanamycin resistance cassette as template and two 60-70 bp oligonucleotides primers. The oligonucleotide primers used had the following features: From 5' to 3', primer 1 (primer 2) had 45 bases homologous to the 5'-site (or 3'-site) of the *S. cerevisiae* genomic ARF1 locus followed by18-19 bases of sequence derived from the 5'-region (3'-region) of the Kanamycin resistance cassette (KanMX) from vector. A schematic is shown in Fig 3.20 A to explain strategy of PCR based gene deletion method. The resulting PCR-product (1.5Kb) thus contained the KanMX module flanked by 45 bp of DNA homologous to the genomic ARF1 5’ and 3’ UTRs. The 1.5 Kb PCR products was cut and purified from agarose gel (Fig 3.20 B). The PCR product was transformed in wild type cells. In this procedure target ARF1 got replaced by gene for kanamycin resistance. Potential deletion mutants were selected on G418 containing media (250µg/ml). These cells were checked for Golgi phenotype. arf1 Δ cells contained a small number of late Golgi cisternae (Sec7 3X GFP) that were often abnormally large in size. The cells showed very large Golgi cisternae and number of cisternae was drastically reduced as compared to wild type (only 2-3 cisternae per cell) as seen from Fig 3.20 C. Average volume as well as diameter of each cisterna was much higher as compared to the wild type (Fig 3.20 D).

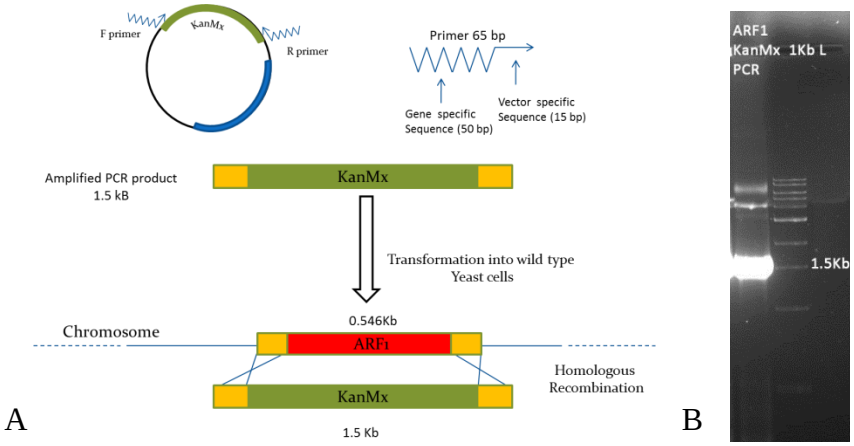

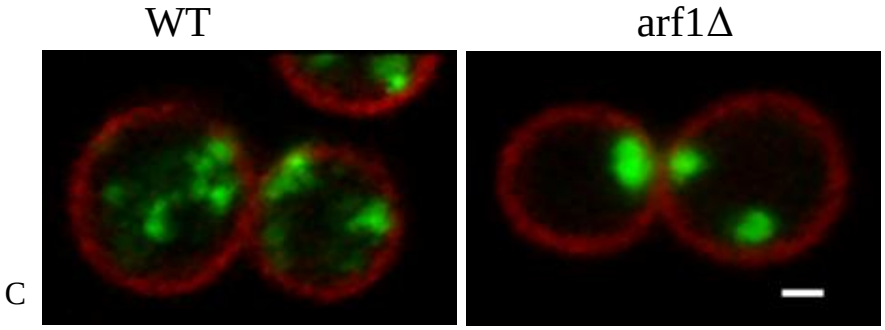

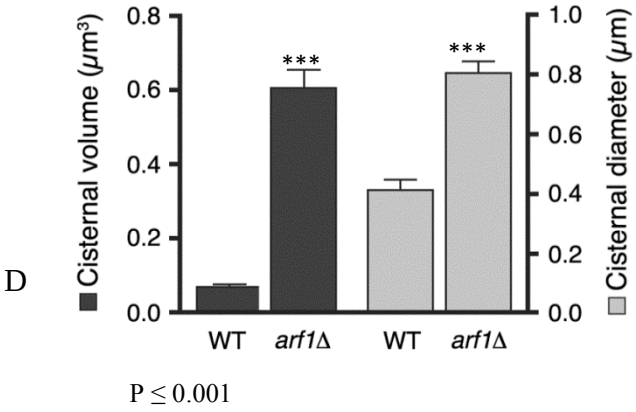

$P \leq 0.001$

Fig 3.20 arf1Δ results in enhanced large Golgi phenotype. A] Strategy for homologous recombination and amplification of KanMX cassette having flanking sequences of 5' and 3' UTRs of ARF1. B] Using pJKanMX as template, the KanMX module was amplified by PCR and expected amplicon size of 1.5Kb was obtained. C] Confocal imaging of wild type and arf1Δ cells. Scale bar represents 1µm. D] Quantification of Golgi cisternal volume (N=60) and Golgi cisternal diameter (N=40)

3.3.2.3 arf1Δ results into more fenestrated and tubulated late Golgi cisternae

Fluorescence microscopy could not reveal whether the late Golgi structures in arf1Δ cells were large individual cisternae or clusters of smaller cisternae. To address this question, we combined fluorescence microscopy with electron tomography [225]. For wild-type cells; we labeled late Golgi cisternae with Sec7-GFP, and prepared ~300-nm sections from plastic-embedded samples. The labeled cisternae were visible by fluorescence microscopy (Fig 3.21). The same structures were then analyzed by electron tomography. This method examines a single thick section, so only part of each cisterna was visible, but the results indicated that wild-type late Golgi cisternae were curved and perforated disks (Fig 3.21 top panel). The same method was applied to arf1Δ cells. Partial reconstructions indicated that mutant late Golgi cisternae were large fenestrated hollow structures (Fig 3.21 bottom panel), presumably identical to the fenestrated compartments previously visualized in arf1Δ cells by thin-section electron microscopy [32]. We concluded that deletion of ARF1 generates abnormally large and fenestrated late Golgi cisternae.

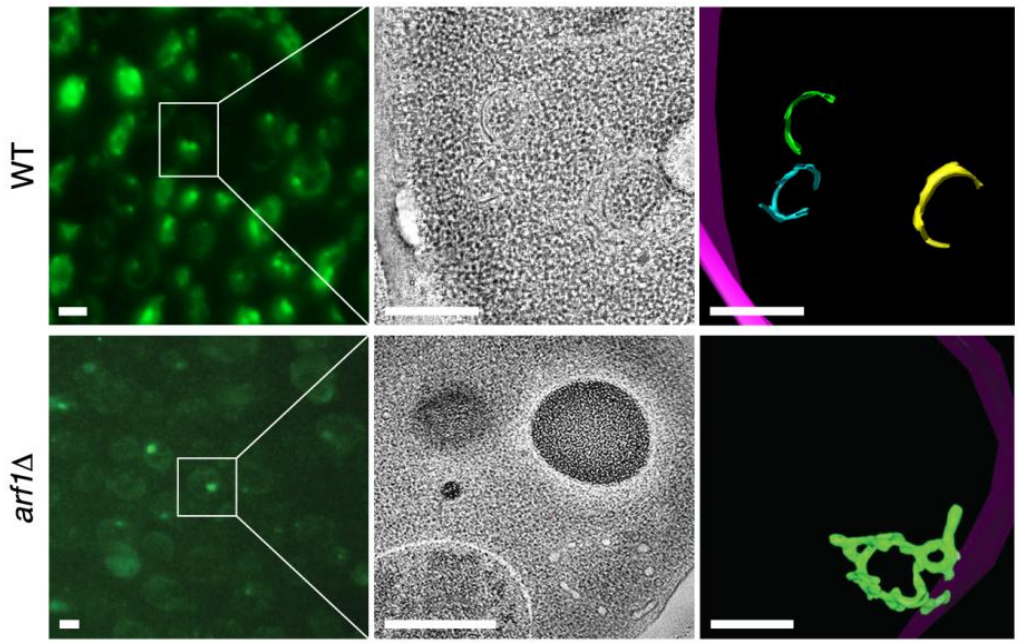

Fig 3.21: arf1Δ results in very large and fenestrated late Golgi cisternae. Wild-type or arf1Δ cells expressing Sec7- 3x GFP were rapidly frozen, then freeze substituted and embedded in plastic. Left: thick sections were imaged by fluorescence microscopy to identify late Golgi cisternae. Scale bars: 2µm. Middle: the same sections were analyzed by electron tomography to visualize membranes in tomographic slices. Scale bars: 0.5µm. Right: membrane contours were traced to model Golgi cisternae (green, blue, yellow) and the plasma membrane (purple). Scale bars: 0.5µm.

3.3.2.4 arf1Δ results in moderate increase in the size of early Golgi cisternae

So far effect of arf1Δ was checked on late Golgi cisternae. It was also interesting to find out if arf1Δ exerts similar effects on size of early Golgi cisternae or not. To check this, early Golgi cisternae were labeled with GFP-Vrg4 [6]. Cells expressing GFP-Vrg4 were imaged by confocal microscopy and quantification of volume and diameter of early Golgi cisternae was done. As can be seen from Fig 3.22 A, the size of early Golgi cisternae was increased in arf1Δ cells and number of early cisternae was also reduced compared to wild type cells. Wild-type cells contained an average of nine early Golgi cisternae. arf1Δ strain contained early Golgi cisternae that were slightly enlarged and their average number was reduced to five. But this effect was less pronounced compared to the effect on late Golgi cisternae. The volume and diameter were also quantified. (Fig 3.22 B and C)

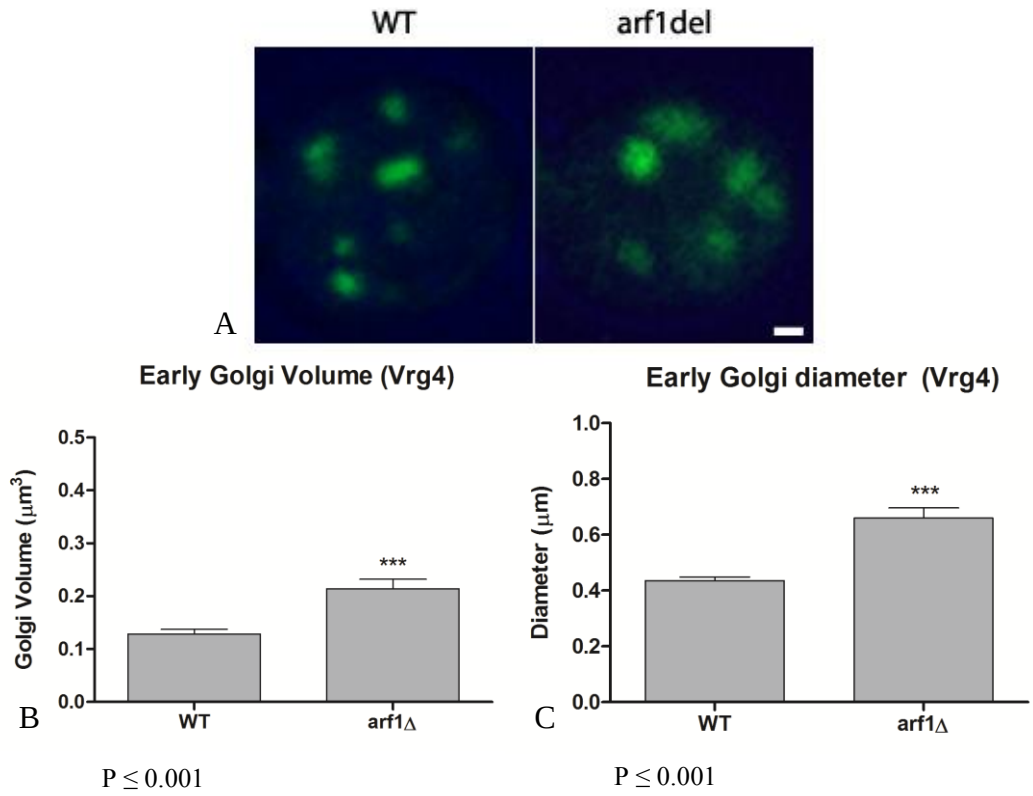

Fig 3.22 arf1Δ results in moderate increase in size of early Golgi cisternae. A] Early Golgi cisternae were labeled with GFP-Vrg4 in wild type and arf1Δ cells and imaged by confocal microscopy. Scale bar represents 1μm. B] Early cisternae volume was quantified by 3D reconstruction (N=17) C] Early cisternal diameter was quantified (N=10)

3.3.2.5 Effect of ARF1 G2A mutation on Golgi cisternal size

ARF1 gets myristoylated at Glycine 2 position. This modification helps ARF1 for membrane anchorage and is important for ARF1 function [226]. In our study we have seen that mutation in myristoylating enzyme causes increase in Golgi cisternae size. To further confirm the importance of ARF1 myristoylation on Golgi cisternal size, we designed an experiment to mutate the Glycine2 residue where the myristoylation takes place on Arf1p and check the effect on Golgi size. Using ARF1-YEplac195 clone as a template, mutagenesis was performed to replace Glycine 2 by Alanine. Positive clone was confirmed by sequencing (Fig 3.23 A). This ARF1 G2A-YEplac195 plasmid and wild type ARF1-YEplac195 were then transformed in arf1Δ cells. Transformants were selected on SD-URA- plates. arf1Δ, arf1Δ/wild type ARF1 and arf1Δ/ ARF1 G2A cells were imaged using confocal microscope and Golgi cisternal volume was quantified (Fig 3.23 B and C). After over expressing wild type ARF1 in arf1Δ cells Golgi cisternal volume was reduced to normal level but when ARF1 G2A mutant was over expressed in arf1 null background, large Golgi phenotype shown by reduced ARF1 could not be reversed. The difference between mean average volumes was not significant for arf1Δ and arf1Δ/ARF1 G2A cells but it was significant for arf1Δ and arf1Δ/ wt ARF1 cells. This clearly suggested the importance of ARF1 Glycine 2 myristoylation in Golgi cisternal size regulation.

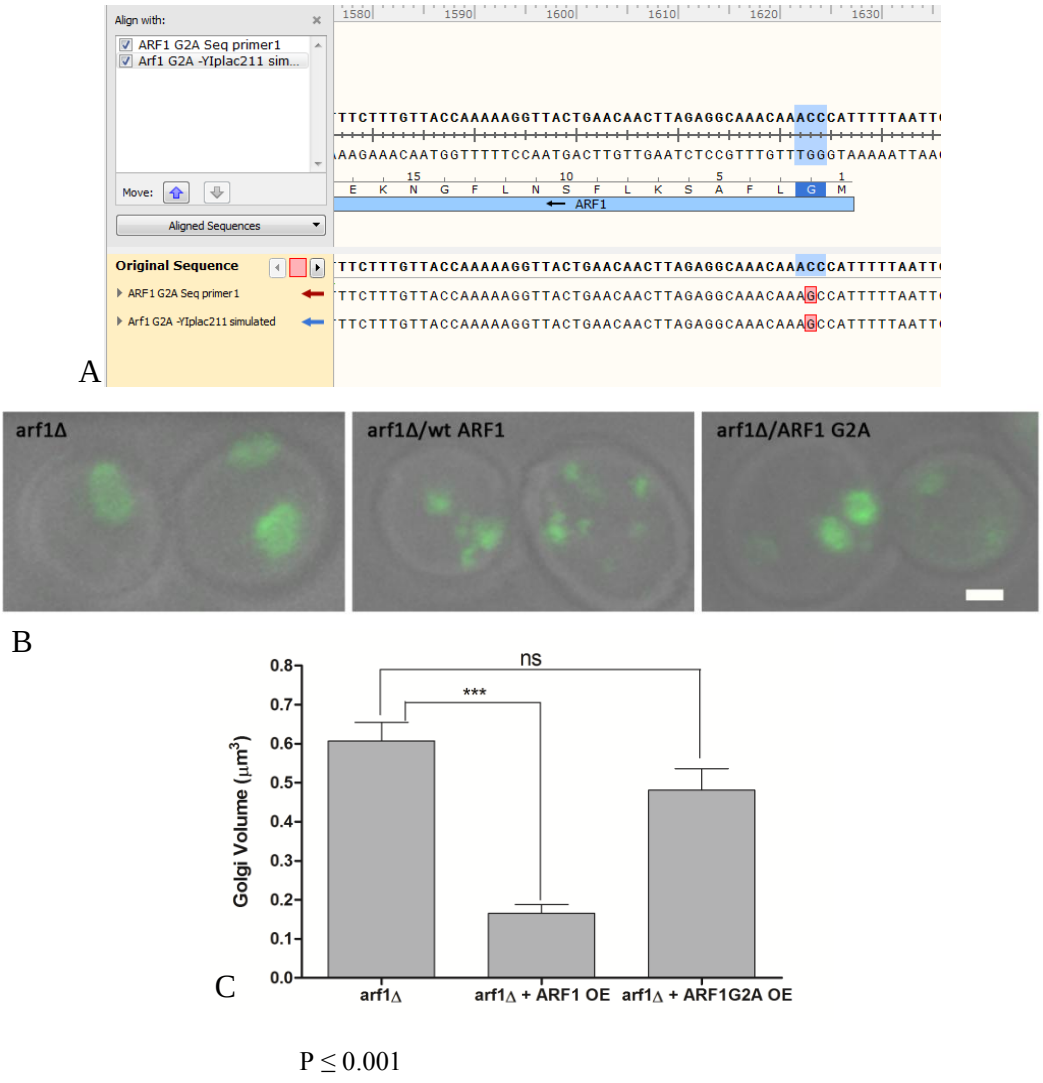

Fig 3.23 Myristoylation of ARF1 at Glycine 2 is important for Golgi size regulation. A] Mutagenesis was done at ARF1 Glycine 2 to replace it with alanine. The clone was sequenced for G2A mutation. B] Confocal imaging of arfΔ/ARF1 G2A cells along with arf1Δ and arf1Δ/wt ARF1 cells. Scale bar represents 1μm. C] Quantification of Golgi cisternal volume (N=70).

3.3.3 Visualizing the homotypic membrane fusions in real time in altered arf1 function background and their effect on Golgi size regulation

Secretory vesicles emerge from a specific ER exit sites. These vesicles are coated with COPII coat proteins. After emerging from ER these vesicles fuse to each other by homotypic membrane fusion and form new Golgi cisterna [227, 228].

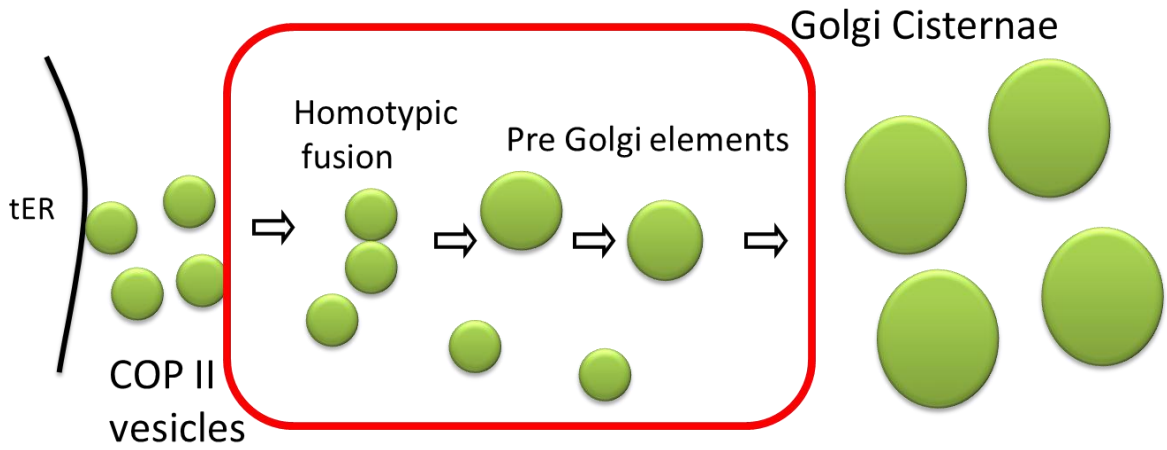

Homotypic fusion of vesicles is difficult to visualize in normal conditions because of limit of resolution of conventional light microscopes. Usually it is not possible to visualize COPII vesicle fusions in light microscope since they are only 40-50 nm structures and they are very dynamic. But as we have seen in arf1Δ background, size of Golgi cisternae increase considerably, it might be able to capture homotypic fusions as the fusions will continue until new threshold of size is reached. To visualize homotypic fusions, GFP fusions of some of the proteins that mark different stages of ER-Golgi transport pathway were created. BET1, EMP47, OCH1, RER1, GEA1, GEA2, VRG4 were the chosen candidates [6, 100, 229-232].

3.3.3.1 Creating GFP fusions of various maker proteins to visualize homotypic fusions

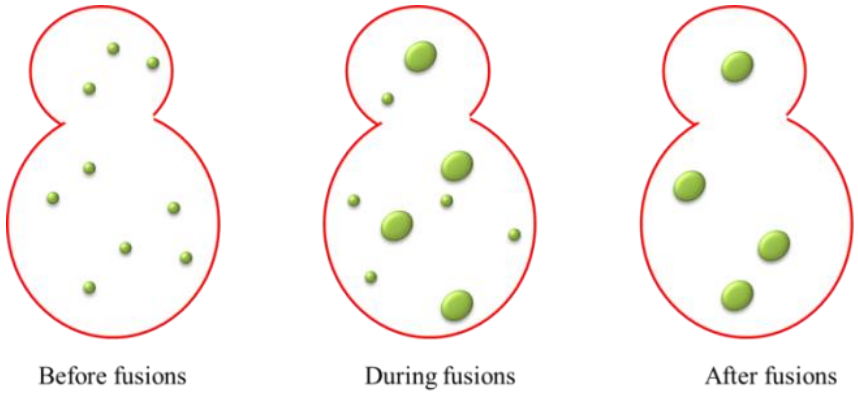

Fig 3.24 Strategy to identify correct marker protein representing stage of homotypic membrane fusions

As shown in figure below, a correct marker which represents exact stage of homotypic fusions would show mixture of smaller and larger Golgi cisternae in arf1Δ background. The following list in table 3.2 shows various marker-GFP fusions cloned in order to find correct marker for visualizing homotypic fusions.

Cloning strategy: Basic cloning strategy was similar for making all marker-GFP fusions.

1. Amplification of the ORF of marker
2. Cloning in YIplac211 vector
3. Creating BamHI-NotI cassette by site directed mutagenesis
4. Cloning different versions of GFPs in BamHI-NotI

These GFP fusions were transformed in wild type as well as in ARF1 deletion background to replace endogenous copy. Almost all markers chosen are known to localize to pre-Golgi elements or cis Golgi cisternae. These vesicles are very dynamic and it is difficult to get robust localization like other medial or trans Golgi markers routinely used. Different variants of GFP were used to optimize visualization of these

proteins under confocal microscope. We have also tried N-terminal and/ C-terminal GFP fusions of these proteins to get better expression of these marker proteins.

Protein name	Type of GFP	Type of fusion
BET	msGFP	C-term fusion
EMP47	msGFP	C-term fusion
EMP47	Linker- msGFP	N-term fusion
EMP47	mGFP	N-term fusion
OCH1	Linker- msGFP	C-term fusion
OCH1	mGFP	C-term fusion
OCH1	3X mGFP	C-term fusion
RER1	Linker- msGFP	C-term fusion
RER1	Linker- msGFP	N-term fusion
RER1	mGFP	N-term fusion
RER1	3X mGFP	N-term fusion
GEA1	3X mGFP	C-term fusion
GEA2	3X mGFP	C-term fusion
VRG4	msGFP	N-term fusion

Table 3.2 List of markers tested for visualizing homotypic fusion

Most of the marker-GFP fusions showed punctate localization in stationary phase under wide field microscope after using very high exposure time. These conditions were not suitable for taking long 4D data sets for visualization of homotypic fusions. When observed in log phase under confocal microscope LSM510 or LSM780, none of these markers like BET1, OCH1, EMP47, RER1 showed any robust localization to punctate structures. Those which did localize to puntate

structures, their fluorescence signal were very poor to be visualized by available confocal microscopes.

3.3.3.2 Homotypic fusions were visualized by using Vrg4 as a marker.

Out of all the markers tested, only two markers, namely Vrg4 and Gea2 showed robust punctate localization in log phase culture which was detectable under LSM780 and signal for the same sustained for 5-10 minutes which was sufficient time for taking 4D movies.

A strain was created by transforming YIplac211-sGFP-Vrg4 as early Golgi marker and Sec7 6X DsRed as late Golgi marker [6]. Vrg4 is a Golgi GDP-mannose transporter that regulates Golgi function and glycosylation in Golgi. Vrg4 showed very bright and stable green punctate structures in WT and arf1 deletion background. sGFP-Vrg4 was transformed to replace genomic copy of Vrg4 by pop-in pop-out method. Sec7 6X DsRed was expressed as second copy from TRP locus under TPI promoter to drive strong over expression. This strain showed very clear fusion events of two small green Vrg4 puncta forming a larger puncta in Arf1 background. This larger puncta formed after fusion also matured to trans cisterna as can be visualized by acquisition of Sec7 Ds-red marker by same cisterna (Fig 3.25).

To understand detailed mechanism of why arf1Δ cells showed increase size of Golgi cisternae, parameters like number of early and late cisterna, maturation frequencies, persistence time of early and late cisternae as well as fusion frequency were measured from these 4D data sets.

3.3.3.3 arf1Δ cells show reduction in number of early and late cisternae

We counted early and late Golgi cisternae by using Vrg4-Sec7 strain. Wild-type cells contained an average of 9 early Golgi cisternae and 7 late Golgi cisternae (Fig. 3.26). In the arf1Δ strain, average number of early Golgi cisternae was reduced to five. For

the late Golgi, the reduction in the arf1 Δ strain was more pronounced, with an average of only two cisternae per cell (Fig. 3.27). Thus, as the Golgi matures, the arf1 Δ mutation progressively reduces the number of cisternae.

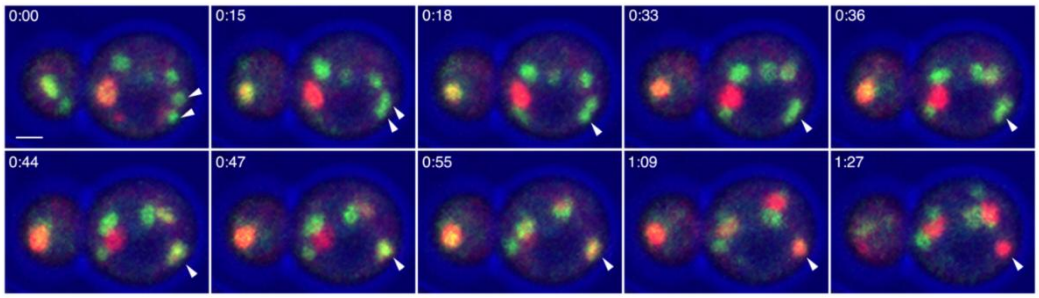

Fig 3.25 Homotypic fusion visualized with Vrg4 marker. The cells were grown to log phase at 30^{o}C and 4D data sets were obtained as described in methods section. Frames from a 4D movie illustrate a homotypic fusion event in an arf1Δ cell. The arrow heads mark two GFP‑Vrg4-labeled early Golgi cisternae that fused before maturing into a Sec7‑DsRed-labeled late Golgi cisterna. Time is shown in minutes: seconds. Scale bar: 1µm.

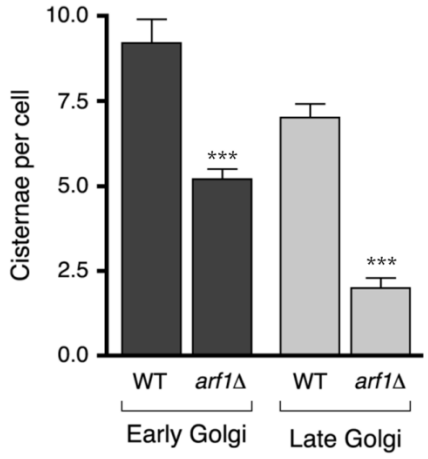

$P \leq 0.001$

Fig 3.26 arf1Δ cells have reduced number of early and late Golgi cisternae compared to wild type cells. The average numbers of early Golgi cisternae, marked with GFP–Vrg4, or late Golgi cisternae, marked with Sec7–DsRed, in wild-type and arf1Δ strains. Cisternae number was calculated 4D datasets. Error bars indicate s.e.m.

3.3.3.4 Design of quantitative framework to explain the effects of arf1Δ

A schematic diagram in Fig 3.27 illustrates the formation, maturation and fission as a continuous process in a cell. The effects of the arf1Δ mutation on Golgi cisternal number might be due to altered maturation kinetics. To test this idea, we devised a simple quantitative framework to understand effects of arf1 deletion on Golgi size. The parameters for calculation were as follows:

E = average number of early Golgi cisternae per cell, *L* = average number of late Golgi cisternae per cell, *m* = average maturation frequency, *m* can be defined as the number of early-to-late Golgi transitions per minute, i.e., the frequency at which early Golgi cisternae disappear and late Golgi cisternae appear. *pE*= average persistence time of early Golgi cisternae, *pL*= average persistence time of late Golgi cisternae.

Because the average numbers of early and late Golgi cisternae are constant at steady-state, *m* also refers to the frequencies at which early Golgi cisternae appear and late Golgi cisternae disappear. The average number of early or late Golgi cisternae should be equal to the frequency of appearance multiplied by the persistence time. Thus:

$E = m \times pE$ *and* $L = m \times pL$.

Combining these equations yields: $E / L = pE / pL$

The implications are that changes in maturation frequency or persistence time could alter the number of cisternae, and that a selective change in one of the persistence times could alter the ratio of early to late Golgi cisternae. This model was tested by measuring maturation parameters for wild-type and arf1Δ strains.

3.3.3.5 The arf1Δ mutation slows maturation of the early Golgi cisternae

Calculation of maturation parameters like maturation frequency and persistence time was performed with 4D data sets of strain expressing msGFP-Vrg4and Sec7-DsRed. To measure the maturation frequency m, we counted the number of early-to-late Golgi transitions per minute. Precisely, we counted events in which green cisternae turned red per min (Fig 3.28). The maturation frequency m was 2.5-fold greater in wild type cells than in arf1Δ cells (Table 3.3 and fig 3.29A).

To measure the persistence times of early (pE) and late (pL) cisterna, we identified cisternae that acquired GFP–Vrg4 or Sec7–DsRed markers and measured the time for which green or red fluorescence persisted for such cisternae. Our analysis revealed a striking effect: the arf1Δ mutation selectively increased the early Golgi persistence time pE. The pE /pL ratio was 1 in wild-type cells but, 2 in arf1Δ cells (Table 3.3 and Fig 3.29 B). This finding could explain why the number of early Golgi cisternae, E was almost similar to the number of late Golgi cisternae L, in wild-type cells, whereas E was about twice as large as L in arf1Δ cells (Fig 3.26).We infer that the entire early Golgi maturation process is slowed in arf1Δ cells, with early Golgi cisternae persisting longer and maturing less frequently than in wild-type cells.

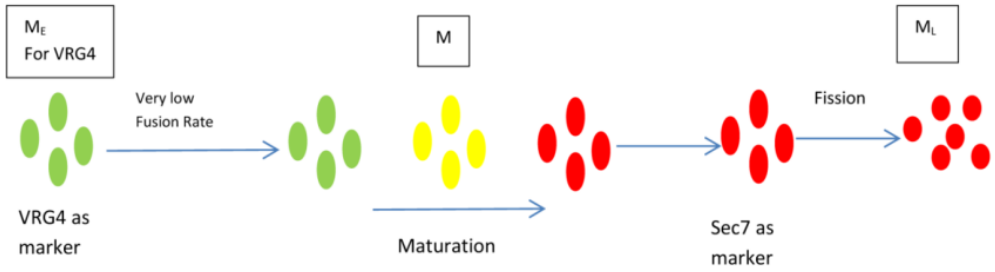

Fig 3.27 Schematic to understand the Golgi cisternae formation, maturation and fission

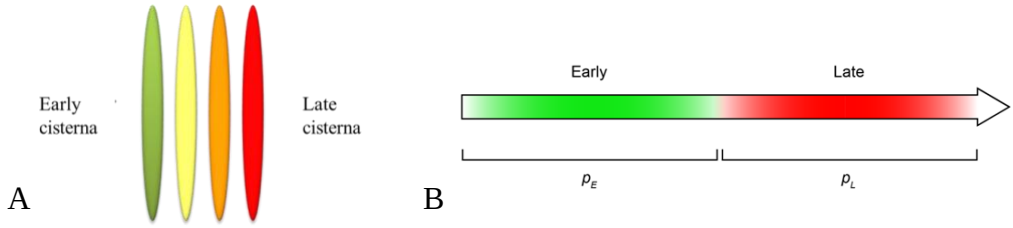

Fig 3.28 Schematic for understanding calculation of maturation frequency (A) and persistence time (B)

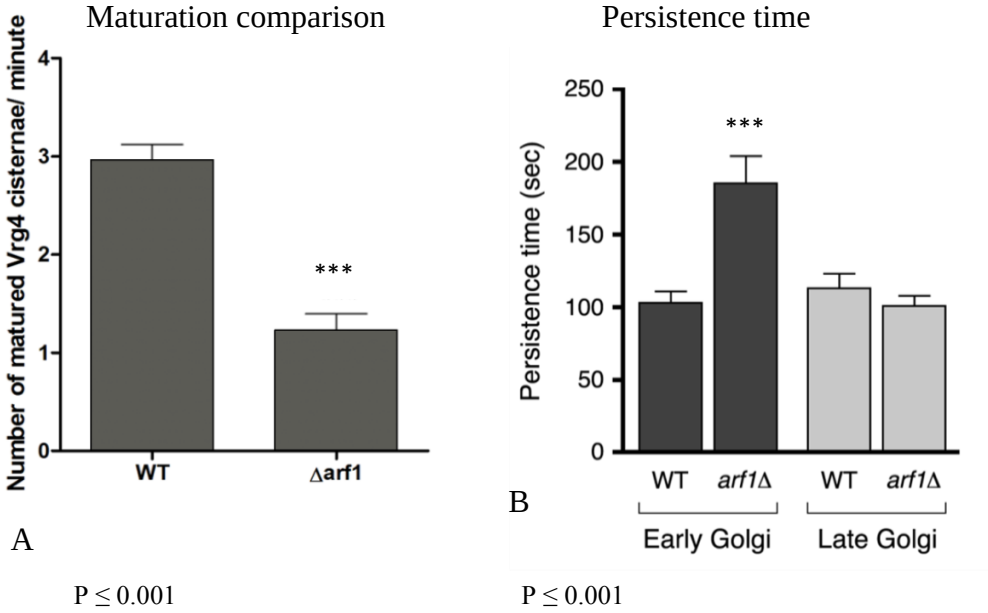

Fig 3.29 Maturation of early Golgi cisternae is slowed down in arf1Δ cells A] The average frequency of early-to-late Golgi transitions as indicated by loss of GFP–Vrg4 and acquisition of Sec7–DsRed in wild-type and arf1Δ strains. Error bars indicate s.e.m. (B) The average persistence time of the early Golgi marker GFP–Vrg4 and the late Golgi marker Sec7–DsRed in wild type and arf1Δ strains. Error bars indicate s.e.m.

3.3.3.6 Golgi cisternae undergo homotypic fusion

Table 3.3 shows a comparison of the measured values E, L and the corresponding predicted values m *x* pE and m *x* pL. The number of late Golgi cisternae, L, agrees reasonably well with the predicted value m *x* pL for both wild-type and arf1Δ strains. However, the number of early Golgi cisternae, E, is higher than the predicted value m *x* pE for both strains. To explore this discrepancy, we re-evaluated the rationale for using m *x* pE as an estimate of E. Because the spatial and temporal resolution of the 4D movies was insufficient for counting early Golgi formation events directly, we assumed that the frequency of early Golgi formation events matched the frequency of early-to-late Golgi conversion events. This assumption would be incorrect if early Golgi cisternae undergo homotypic fusion. Such homotypic fusion events took place, as illustrated in Fig. 3.26. So we further quantified such fusion events in wild type and arf1Δ cells from 4D data sets using Vrg4 as a marker. A typical wild-type or arf1Δ cell exhibited about one early Golgi homotypic fusion event per minute (3.30). As a consequence of homotypic fusion, the frequency of early Golgi formation events is higher than the maturation frequency m, so m *x* pE was an underestimate of the number of early Golgi cisternae.

	E	***L***	***m*** **(min^{-1})**	p_E **(sec)**	p_L **(sec)**	$m \times p_E$	$m \times p_L$
WT	**9.2 ± 0.7**	**7.0 ± 0.4**	**3.0 ± 0.2**	**103 ± 8**	**113 ± 10**	**5.2**	**5.7**
arf1Δ	**5.2 ± 0.3**	**2.0 ± 0.3**	**1.2 ± 0.2**	**185 ± 19**	**101 ± 7**	**3.7**	**2.0**

Table3.3 Comparison of expected and experimental maturation parameters

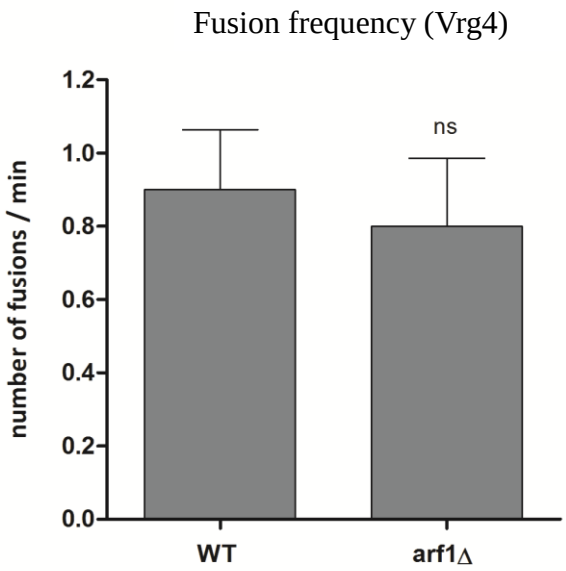

Fig 3.30 Quantification of homotypic fusion events: The average number of homotypic fusion events per minute for early Golgi cisternae in wild-type and arf1Δ strains.

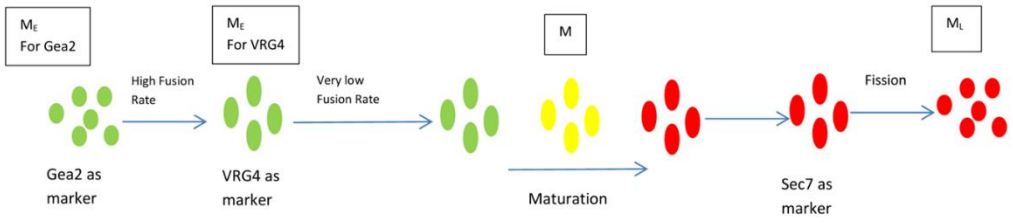

Fig 3.31: Revised schematic to understand Golgi cisternae formation using an early localizing marker Gea2

3.3.3.7 Visualizing homotypic fusion events using Gea2 as early Golgi marker

Our 4D data using Vrg4 as early Golgi marker did not provide enough resolution to measure the frequency of early Golgi formation events, so the contribution of homotypic fusion is hard to assess. We speculate that the slowed maturation in *arf1*Δ cells prolongs the time that early Golgi cisternae remain fusion-prone, thereby increasing the number of homotypic fusion events. This eventually leads to formation of larger early Golgi cisternae and decreasing the number of early Golgi cisternae. Such an effect may be most pronounced at a stage before the cisternae acquire Vrg4. This idea could be tested by visualizing early intermediates in cisternal formation. A schematic to understand this is shown in Fig 3.31.

Gea2 is nucleotide exchange factor for Arf1 GTPase. Gea2 is required for vesicle budding and protein transport from the Golgi to the endoplasmic reticulum [232]. Another strain having Gea2-3x mGFP as early Golgi marker was created. C-terminal region of GEA2 ORF was amplified using primers GEA2 Pst1 fw and GEA2 EcoR1 Rv. A PCR product of 2.1 Kb was obtained (Fig 3.32B). This was digested with PstI and EcoRI and cloned in yeast integrative plasmid YIplac211. BamHI-NotI cassette was introduced at stop codon of GEA2 ORF by site directed mutagenesis. 3X mGFP from pmEGFP-13 was then cloned in BamHI and NotI cassette at C-termini of Gea2 ORF. The positive clone was selected by digestion with BamHI and NotI to get insert release of 2.1Kb (Fig 3.32 C). Thus, Gea2 was labeled with 3 tandem copies of mGFP at its C-terminus. This Gea2-3X mGFP fusion construct was linearized with BspEI in C-terminal region of Gea2 to get replacement at genomic Gea2 locus. Thus genomic Gea2 was replaced with Gea2 3X mGFP by pop-in pop-out method.

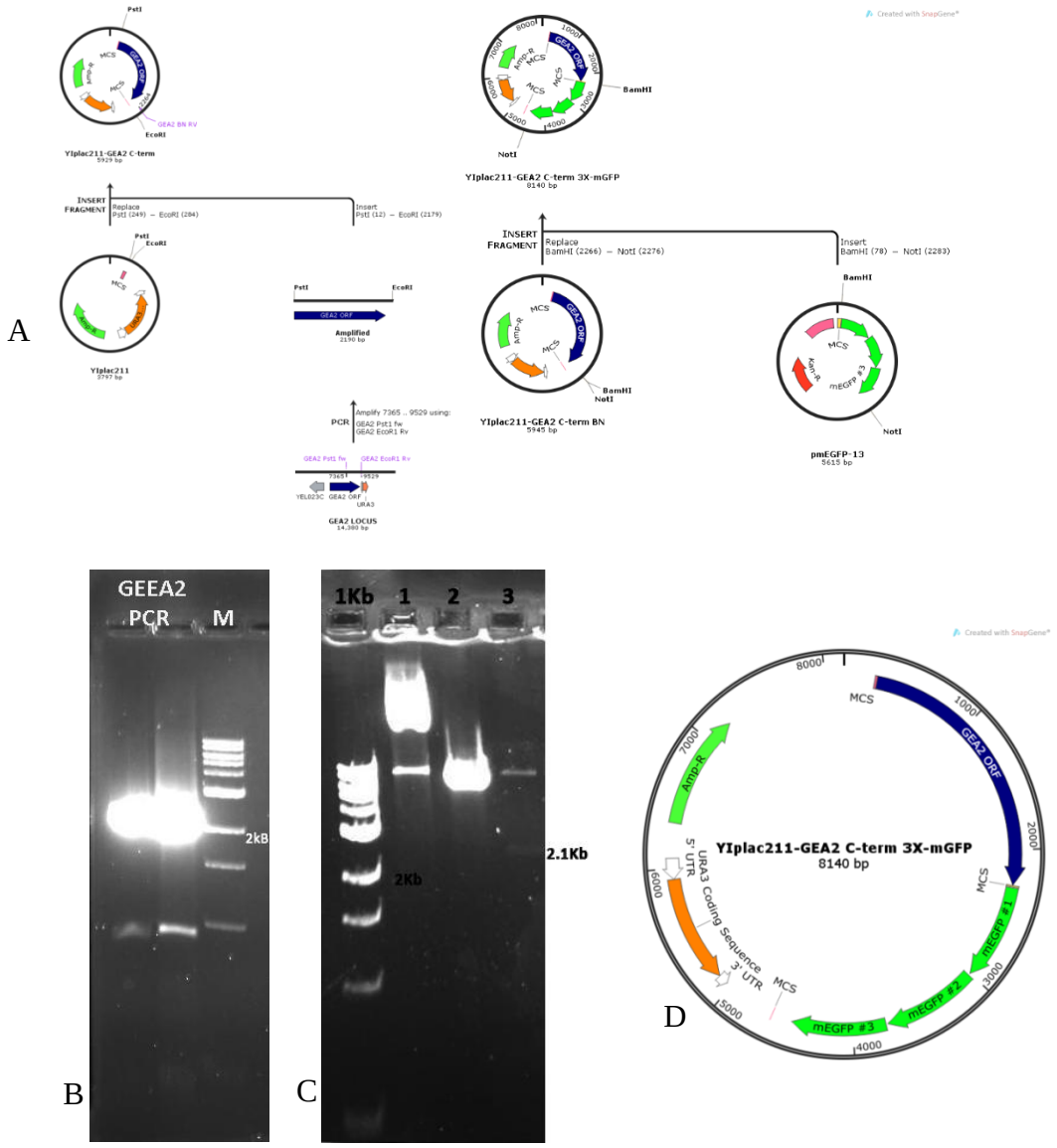

Fig 3.32: Cloning of Gea2-3X mGFP A] Cloning strategy for Gea2-3X mGFP-YIplac211. B] GEA2 C-terminal 2.1Kb region was amplified by PCR and purified from agarose gel for further cloning. C] Diagnosis of final clone Gea2-3X mGFP-YIplac211 by digestion with BamHI and Not1 (Lane3) showed expected insert release of 2.1Kb. D] Map of Gea2-3x mGFP-YIplac211.

Localization of Gea2 is a matter of debate. There are many reports suggesting localization of Gea2 at early Golgi. But there are also few reports which indicate that Gea2 segregates with another trans Golgi markers during fractionation making use of Gea2 as early Golgi marker questionable. We have addressed this issue by checking co-localization of Gea2 with well-known early Golgi marker Vrg4.

A dual color strain was created in which one early Golgi marker Vrg4 was labeled with msGFP and Gea2 was labeled with 6X DsRed. Gea2 6X DsRed was constructed in similar way as Gea2 3X mGFP but in the last step, 6X DsRed was inserted in BamHI-NotI cassette instead of 3X mGFP. Both these fusion proteins were used to replace respective endogenous copies with labeled copies.

We saw that most of the Gea2 labeled punctae do co-localize with Vrg4 punctae (Fig 3.33A). To further check if there are more number of homotypic fusions detectable using Gea2 as early Golgi marker as we speculated, we obtained 4D datasets using Gea2 3X GFP strain. The homotypic fusion events were quantified from these datasets. When we used Gea2 as marker to label early Golgi cisternae, we saw clearly more homotypic fusion events in arf1Δ background compared to wild type cells. The fusion events can be observed from (Fig 3.33B) which shows selected frames from Gea2 4D data sets. Homotypic fusions were also quantified in wild type and arf1Δ background (Fig 3.33C).

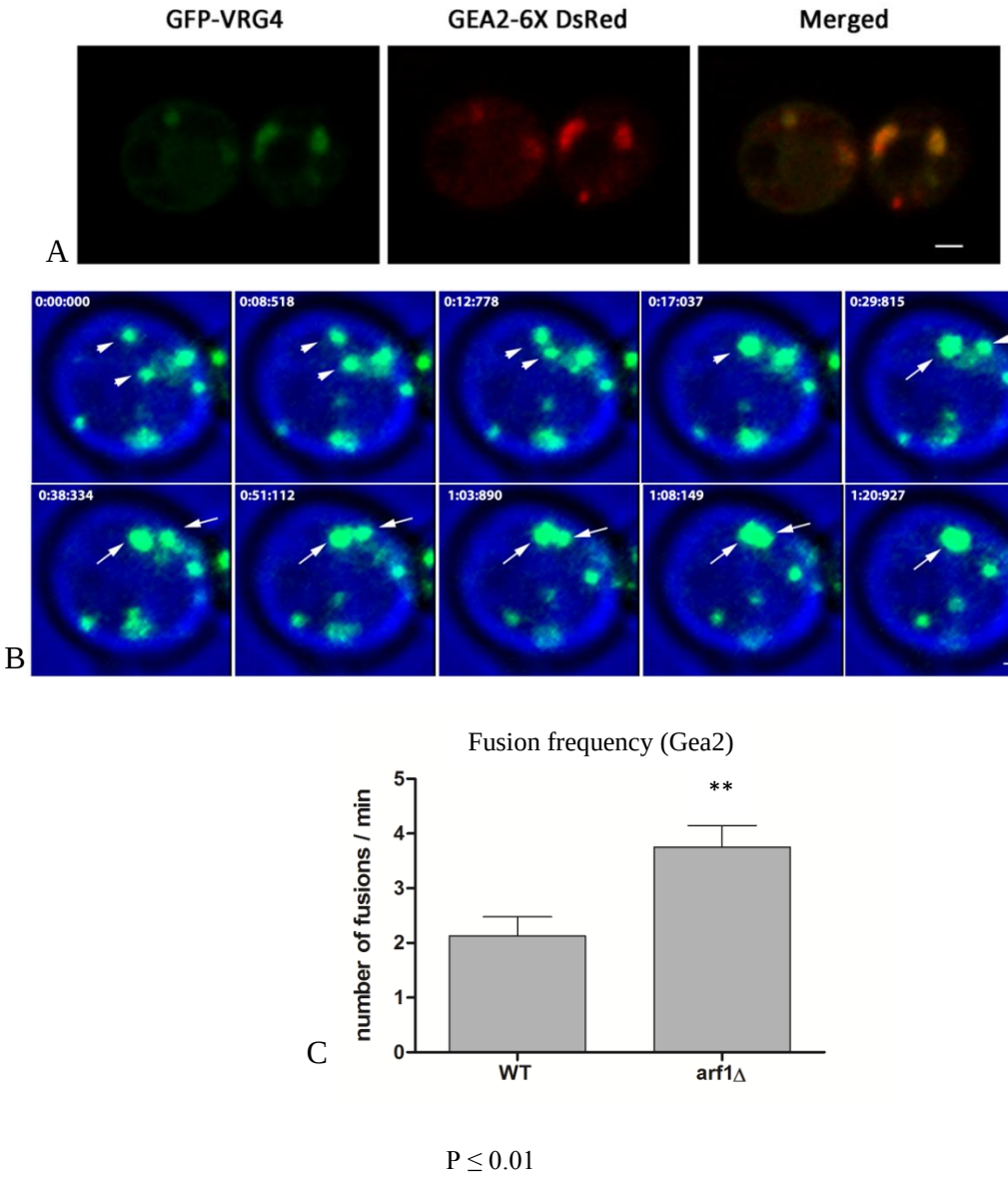

Fig 3.33 Homotypic fusions detected using Gea2 as early Golgi marker. A] Cells expressing Gea2 6X DsRed and GFP-Vrg4 were imaged by confocal microscope. Scale bar represents 1µm. B] The frames of a 4D data set showing homotypic fusions in arf1Δ cells using Gea2 as early marker. The arrowheads indicate two spots fusing with each other forming a new larger spot, this further fuse with another spot as indicated by arrows to form even larger spot. Time is shown in minutes:seconds. Scale bar represents 1µm. C] Quantification of homotypic fusion events in wild type and arf1Δ cells using Gea2 as an early marker. Error bars indicate s.e.m

3.4 Discussion

Organelle size control is a fundamental yet unanswered question in eukaryotic cell biology. As mentioned earlier, many diseases show altered organelle size and morphology [30-35]. Golgi apparatus is an organelle which performs glycosylation and other modifications of newly synthesized proteins and lipids coming out from ER. Once modified, Golgi apparatus also sorts the proteins and lipids into different types of carrier vesicles which are then delivered to various intracellular organelles, plasma membrane or secreted outside the cell. Alterations in Golgi apparatus are reported for several cancers like colorectal, breast cancers and neurological disorders like Parkinsons's disease, Alzeimer's disease. Golgi size probably changes to suit the cellular secretion needs. Hence it is very interesting to study how Golgi size change is achieved in a regulated manner in normal condition and how does this regulation goes wrong in case of diseases.

The present project was designed to understand how Golgi apparatus regulates its own size in normal physiological condition. In most cells Golgi cisternae are stacked together. Hence it is very difficult to resolve between two adjacently placed cisternae and accurately measure their size. To carry out precise measurements of Golgi cisternal size, we chose an assay system which has unstacked Golgi cisternae where it is possible to resolve different cisternae- budding yeast *S. cerevisiae*. The study carried out systematic characterization of a temperature sensitive Golgi size mutant obtained from a random mutagenesis study. This characterization procedure yielded important role of two proteins namely N-Myristoyl transferase-1 (NMT1) and ADP ribosylation factor-1 (ARF1). Further, the detailed understanding of Golgi maturation parameters in wild type as well as arf1Δ cells with help of 4D live cell imaging explained why the cells having deletion of Arf1 show enlarged early and late

Golgi cisternae which are also drastically reduced in number compared to wild type cells.

Characterization of temperature sensitive Golgi size mutant:

The study was initiated with a mutant generated by EMS mutagenesis study carried out to find out Golgi inheritance [201]. While studying Golgi inheritance mutants, one class of mutant was identified showing large Golgi phenotype. This class of mutants was not characterized further. This mutant was of particular interest to us because of abnormal Golgi size phenotype. This Ts mutant showed larger Golgi cisternae compared to the wild type Golgi cisternae. Wild type genomic library complementation led to identification of mutant nmt1 gene in the Golgi size mutant. When sequenced, nmt1 gene from Golgi size mutant showed T400I mutation. When wild type NMT1 was cloned under its own promoter and expressed in a CEN plasmid in the Golgi size mutant, this could rescue the temperature sensitive as well as large Golgi phenotype. In addition, when single base pair mutation T400I was repaired in the genome of the mutant cells, the temperature sensitive as well as large Golgi phenotype could be rescued. These experiments led to conclusion that mutation T400I in NMT1 gene in Golgi size mutant was responsible for enlarged Golgi size phenotype.

The known function of NMT1 is to myristoylate substrate proteins allowing them to associate with target membranes. Altered Golgi phenotype seen in Golgi size mutant could be due to altered myristoylation of some of the substrates of NMT1. One of the important Golgi associated substrate of Nmt1p is Arf1p [185]. Myristoylation is a crucial step for anchorage of Arf1 proteins to Golgi membranes

which in turn makes them functional at Golgi. Could the large Golgi phenotype in Golgi size mutant be possibly because of altered myristoylation of Arf1?

A study in *Arabidopsis thaliana* showed that Nmt1 gene is important for the postembryonic development stages. In *Arabidopsis thaliana*, nmt1 mutant led to defective Golgi traffic and integrity by predominantly affecting the Golgi membrane/cytosol partitioning of ADP-ribosylation factor proteins. The loss of activity of mutant nmt1 enzyme was ascribed to reduced binding affinity for both myristoyl-CoA and peptide substrates [233]. NMT1 indeed can play a role in Golgi size control by changing myristoylation status of Golgi associated Arfs.

To verify this possibility in our case, we overexpressed wt Arf1 in Golgi size mutant having compromised myristoylation activity. Whenever an enzyme is mutated, most likely its activity is reduced because of mutation. In such cases, providing excess of substrate can help to restore the function in mutant system by generating enough processed substrate to carry out its function at desired level. Overexpression of wt Arf1 in Golgi size mutant resulted in rescue of large Golgi phenotype.

Importance of Arf1 myristoylation was also checked in another way where we mutated the Glycine2 in Arf1p which is the site of myristoylation on Arf1 proteins. ARF1 G2A substitution will compromise myristoylation of Arf1p. This experiment was performed in arf1 null background. arf1Δ cells show much enlarged Golgi cisternae. We overexpressed the wt and G2A Arf1 mutant in arf1Δ cells. wt ARF1 over expression was able to rescue the large Golgi phenotype but G2A arf1 mutant was unable to rescue large Golgi phenotype. This confirmed that Nmt1p exerts the large Golgi phenotype through regulating myristoylation of Arf1 in Golgi size mutant.

Arf1 is an important Golgi associated GTPase. This protein plays role in recruitment of various coat protein complexes like COPI, AP/Clathrin coat proteins to Golgi membranes [124]. Thus Arf1 acts as an important regulator of vesicle budding from Golgi membranes.

Arf1 mutants have shown defects in the transport of secretory cargo. Arf1 has been previously implicated in the maintenance of yeast Golgi and endosome structure by Gaynor et al in1998 [32]. The study also reported that hollow, large ring like Golgi cisternae are seen in arf1Δ cells. Although we started with a random approach, our results too pointed towards importance of Arfs in regulation of Golgi size.

Effects of arf1Δ on Golgi size and Golgi cisternal morphology:

To further investigate in detail the role of Arf1 in Golgi size control in more quantitative manner, we deleted ARF1 from wild type genomic background. Live cell imaging of fluorescently labeled Golgi cisternae and quantification of their volume and diameter clearly showed a huge difference in the size of Golgi cisternae in arf1Δ cells compared to wild type Golgi cisternae. To be more specific, the size of Golgi cisternae was further enlarged as compared to size of Golgi cisternae in nmt1 T400I mutants. The volume of late cisternae in arf1Δ was 3 times as compared to wild type and the diameter twice as compared to wild type Golgi cisternal diameter. Arf1Δ cells showed marked reduction in number of early and late Golgi cisternae. The effect of reduced number of cisternae was more pronounced for late cisternae. arf1Δ not only resulted in alteration of size of late Golgi cisternae but also size of some of the early Golgi cisternae was increased. Thus our results corroborate the data from Gaynor et al about enlarged Golgi cisternae in arf1Δ cells with precise quantification by measurement of volume and diameter of Golgi cisternae.

The possibility that the large Golgi cisternae as observed from confocal fluorescence imaging can be just an aggregation of various small cisternae could not be ruled out because of limit of resolution of conventional light microscope. Hence we needed to see these enlarged Golgi cisternae in higher resolution. To do this, we used correlative light electron microscopy where it is possible to identify a cisterna by its fluorescence and then observe its detailed high resolution structure under electron microscope from which 3D electron tomographs are constructed. The data from CLEM showed that wild type Golgi cisternae are curved disc shaped structures but cisternae from arf1Δ cells are much fenestrated and tubulated structures. Thus the enlarged structures seen in fluorescence microscopy are actually hollow ring shaped cisternae which have fenestrated and tubulated membranes. Gaynor et al observed similar reticulated Golgi membranes in arf1Δ cells but 3D tomographs of such fenestrated structure are reported for the first time in this study which gives detailed 3D structure of Golgi cisternae in arf1Δ background [32].

These gross changes in Golgi structure could be because of lipid modifying functions of Arf1p. Arf1 activates the phospholipase D. Activity of Phospholipase D is needed for formation of COPI vesicles. Recruitment of Arf1 to Golgi membranes is also required for COPI vesicle formation. However, ARF seems to be dispensable for coatomer recruitment in vitro if membranes are pre-treated with Phospholipase D [234]. These observations point towards primary role of Arf1 in lipid modifications. Another study in BY-2 cells shows if Arf1 is dissociated from Golgi by treatment of 1-butanol, Golgi cisternal length is increased. This could be because of continuous flow of membrane in absence of retrograde COPI vesicle transport caused by dissociation of Arf1. Hollow, ring like structures seen in arf1Δ cells in budding yeast could be generated by fusion of two ends of such single elongated cisterna.

Effects of arf1Δ on Golgi cisternal maturation kinetics:

In order to understand the reason behind reduced number of early and late Golgi cisternae and their increased size, we did live cell imaging and acquired 4D datasets to analyze kinetic parameters of arf1Δ and wild type Golgi cisternae. We found out that in arf1Δ cells, the persistence time (the time for which a cisterna is present in the system as seen by a fluorescence of tagged resident protein) of early cisternae is typically increased twice as compared to wild type cisternae, without affecting persistence time of late cisternae.

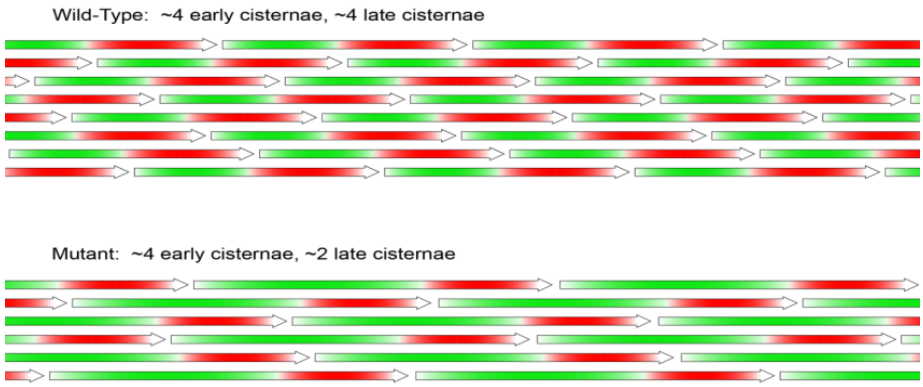

Fig 3.34 Schematic diagram explaining effects of higher persistence time of early cisternae compared to persistence time of late cisternae.

This means at any time point, there would be more early Golgi cisternae than late Golgi cisternae in arf1Δ cells; which is the exact case we have seen in our data. Another kinetic parameter we measured was maturation frequency (number of early to late cisterna transition/min). We found out in arf1Δ cells, maturation frequency was one third of the wild type maturation frequency. This explains the delay in secretion observed by Gaynor et al in arf1Δ cells. Another possibility is that arf1Δ also up regulates the UPR pathway and in turn alters phospholipid biosynthesis [14, 15].

Although it is well known that rate of membrane influx and efflux causes the change in the size of a self-assembling compartment like Golgi apparatus in mammalian system [173, 235], our study proved that the kinetic parameters of the conversion of one compartment into other can also alter copy number and size of organelle. This phenomenon can be clearly studied in *S. cerevisiae* as the cisternae are well-separated from each other making observations easier. Hence how often a Golgi compartment forms, sustains also influences its copy number. We suspect that in our case, total amount of membrane must be constant as we observed if the number of Golgi cisternae is less, they are often enlarged in size and vice versa. This also indicates possibility of fusions of the compartments leading to fewer and larger cisternae.

Contribution of homotypic membrane fusions in size control of Golgi apparatus:

To understand Golgi cisternal maturation and size change brought about by arf1Δ in more quantitative manner, we designed a simple mathematical equation assuming rate of formation of early Golgi cisternae is equal to rate of early to late cisternal maturation and is also equal to rate of dissipation of late cisternae. But in reality, homotypic fusions do take place that lead to formation of new early cisternae. In such case, rate of formation of new early cisternae will be much higher compared to early to late maturation rate. Also, rate of dissipation of late cisterna would probably larger than maturation rate. So this simple linear equation has to be further modified taking these differential rates into account.

As is clearly seen from the 4D datasets using Vrg4 as an early cisternal marker, homotypic fusions indeed take place leading to formation of larger cisternae. Arf1 deletion leads to higher rate of homotypic fusions compared to wild type. As

observed from Vrg4 as well as Gea2 fusion frequency, rate of homotypic fusions increases as we go temporally away from maturation step that is early to late conversion. That's why homotypic fusion frequency of Gea2 is higher compared to homotypic fusion frequency of Vrg4 as Gea2 occupies earlier compartments compared to Vrg4. This explains why there is more number of small sized Gea2 labeled structures compared to number of small sized Vrg4 labeled structures in arf1 deletion. These fusion events could be visualized clearly only because arf1Δ increases the overall threshold of size of cisternae and that the markers used Vrg4 and Gea2 localize to Golgi compartments which represent true stage of homotypic fusions.

Homotypic fusions of pre Golgi elements lead to formation of new early Golgi cisternae. arf1 deletion causes increase in the frequency of homotypic fusions. The mechanism behind increased homotypic fusion frequency needs to be determined further. Another effect arf1 deletion causes is increase in the persistence time of early cisternae. This in turn allows more time for cisternae to undergo homotypic fusions. Both these reasons explain the increased size and reduced number of early cisternae in arf1 deletion. These cisternae also undergo maturation forming late cisternae which are also in turn larger in size. As discussed earlier further reduction of late cisternae number is because slow maturation of early cisternae and unchanged persistence time of late cisternae in arf1 deletion.

This study opens several questions that can be solved further. Very important question is to understand the mechanism of how exactly Arf1 controls Golgi maturation kinetics. One reason can be compromised COPI recruitment in absence of Arf1 as COPI mutants also show slowed maturation at restrictive temperature [7]. In the background of compromised of COPI retrograde transport, Golgi associated enzymes will not be localized to target cisternae efficiently leading to inefficient and

hence slowed maturation. Another important question is understanding how arf1 absence causes fenestrated and tubulated Golgi cisternae. Such modified structure may also lead to improper localization of some of the Golgi associated enzymes. Most likely this structural modification of Golgi cisternae is because of perturbed lipid metabolism in arf1 deletion. The quantitative framework can also be modified further taking into account differential rate of formation and dissipation of early and late Golgi cisternae respectively.

Another interesting point is to study is contribution of other Golgi associated GTPases of Rab, Arl family in size control mechanism of Golgi cisternae. Although studies of Arf1 clearly show that it is a master regulator of Golgi cisternal kinetics as well as structural integrity of Golgi and endosomes, other GTPases may also contribute by acting in earlier or later stages in the pathway giving more insights about Golgi structure, function and its size control mechanism.

Chapter 4

Summary and conclusions

Chapter 2: Role of Sec12 in size control mechanism of Endoplasmic Reticulum exit sites

This study for the first time established the fact that a fraction of Sec12 does localize at ERES and that over expression of Sec12 also causes enlarged ERES. This also gave information on possible binding partner of Sec12 at ERES and the region of Sec12 important for its localization at ERES.

- Sec12 localizes to ER exit sites as well as general ER in mammalian cells in fixed cells as well as live cell condition.
- Fraction of Sec12 that localizes to ER exit sites colocalizes with ERES marker Sec16.
- Sec12 over expression leads to enlarged Sec12-GFP spots.
- Larger punctae formed by over expression of Sec12 colocalize in live cell condition with Sec16, a *bona fide* ERES marker.
- ER exit site localization of Sec12 requires a saturable binding partner and Sec16 is the binding partner of Sec12 at ER exit sites.
- Intra-membrane domain of Sec12 alone is sufficient for giving punctate as well as web like localization pattern similar to full length cytoplasmic domain.

Chapter 3: Understanding Size Control Mechanism of Golgi apparatus

This section describes characterization of a Golgi size mutant. This characterization uncovered role of two proteins namely Nmt1 and Arf1 in the context of Golgi size regulation. This section also describes in detail the effects of arf1 deletion on structure of enlarged Golgi cisternae and Golgi cisternal maturation kinetics; finally it describes clear visualization of homotypic fusion events for the first time leading to formation of new early cisterna which further also matures into a late

cisterna. Also, this section highlights homotypic fusions of Golgi cisternae in relation to the size control mechanism of Golgi cisternae in *S. cerevisiae*.

- Ts Golgi size mutant showed larger Golgi cisternae than wild type.
- This mutant could be functionally complimented with wild type NMT1 and T400I mutation in NMT1 is responsible for mutant phenotype.
- NMT1 exerts effects on Golgi size via Arf1 as seen from wild type Arf1 over expression and Arf1 G2A mutation study.
- Deletion of Arf1 produces drastically enlarged and fenestrated Golgi cisternae.
- Homotypic fusions were visualized by using Vrg4 as well as Gea2 marker in arf1 deletion background.
- Arf1 deletion causes ~2X increase in persistence time of early Golgi structures; whereas persistence time of late Golgi structures is not changed.
- Arf1 deletion results in increased homotypic fusions of early Golgi cisternae and reduced early to late transition events by ~2.5X compared to wild type.
- Kinetics of cisternal maturation of Golgi complex plays important role in regulation of its size.

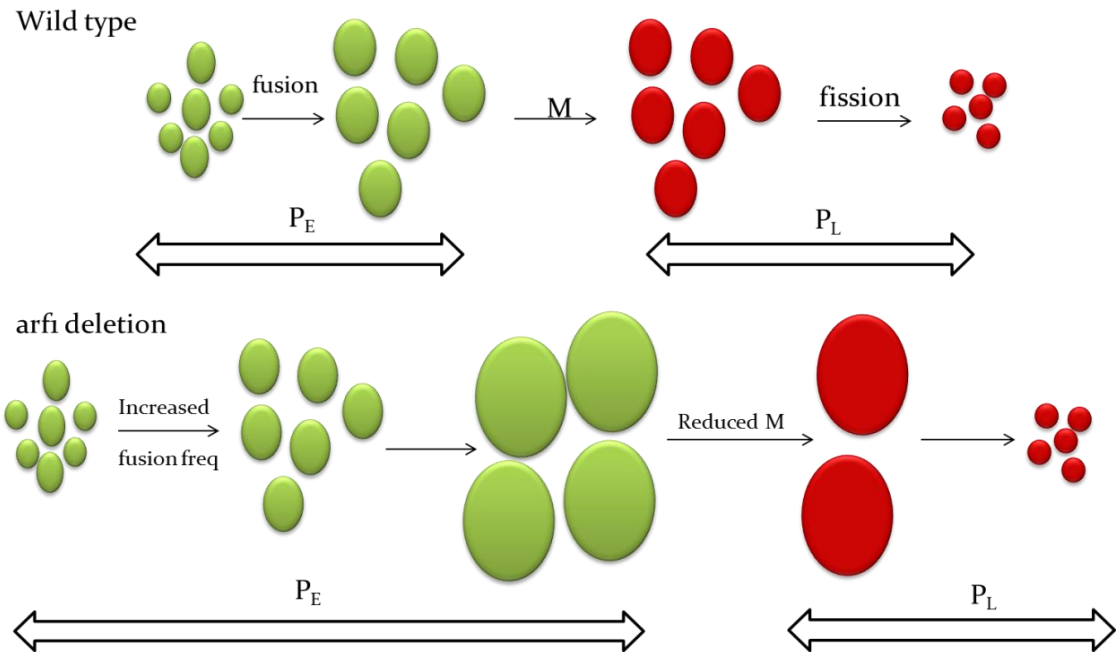

Fig 4.1 Model explaining effects of arf1 deletion on size and number of Golgi cisternae

In short, effects of arf1 deletion can be explained with this cartoon. In arf1 deletion, because of increased fusion frequency and increase persistence time of early cisternae, more fusions of early cisternae take place for a longer time resulting in reduced number and larger size of early Golgi cisternae. Eventually these larger early cisternae mature into late cisternae but with reduced maturation frequency leading to further reduction of number of late cisternae.

References

References:

1. Bevis, B.J., et al., *De novo formation of transitional ER sites and Golgi structures in Pichia pastoris.* Nature Cell Biology, 2002. **4**(10): p. 750-6.
2. Chan, Y.H. and W.F. Marshall, *Scaling properties of cell and organelle size.* Organogenesis, 2010. **6**(2): p. 88-96.
3. Wang, Y.J., et al., *Phosphatidylinositol 4 phosphate regulates targeting of clathrin adaptor AP-1 complexes to the Golgi.* Cell, 2003. **114**(3): p. 299-310.
4. Baloyannis, S.J., et al., *The acoustic cortex in frontotemporal dementia: a Golgi and electron microscope study.* Acta Otolaryngol, 2011. **131**(4): p. 359-61.
5. Kellokumpu, S., R. Sormunen, and I. Kellokumpu, *Abnormal glycosylation and altered Golgi structure in colorectal cancer: dependence on intra-Golgi pH.* FEBS Lett, 2002. **516**(1-3): p. 217-24.
6. Losev, E., et al., *Golgi maturation visualized in living yeast.* Nature, 2006. **441**(7096): p. 1002-6.
7. Matsuura-Tokita, K., et al., *Live imaging of yeast Golgi cisternal maturation.* Nature, 2006. **441**(7096): p. 1007-10.
8. Kunz, J., et al., *Target of rapamycin in yeast, TOR2, is an essential phosphatidylinositol kinase homolog required for G1 progression.* Cell, 1993. **73**(3): p. 585-96.
9. Bevis, B.J., et al., *De novo formation of transitional ER sites and Golgi structures in Pichia pastoris.* Nat Cell Biol, 2002. **4**(10): p. 750-6.
10. Hammond, A.T. and B.S. Glick, *Raising the speed limits for 4D fluorescence microscopy.* Traffic, 2000. **1**(12): p. 935-40.
11. Bhattacharyya, D., A.T. Hammond, and B.S. Glick, *High-quality immunofluorescence of cultured cells.* Methods Mol Biol, 2010. **619**: p. 403-10.
12. Rossanese, O.W., et al., *A role for actin, Cdc1p, and Myo2p in the inheritance of late Golgi elements in Saccharomyces cerevisiae.* J Cell Biol, 2001. **153**(1): p. 47-62.
13. Gaynor, E.C., et al., *ARF is required for maintenance of yeast Golgi and endosome structure and function.* Mol Biol Cell, 1998. **9**(3): p. 653-70.
14. Jonikas, M.C., et al., *Comprehensive characterization of genes required for protein folding in the endoplasmic reticulum.* Science, 2009. **323**(5922): p. 1693-7.
15. Travers, K.J., et al., *Functional and genomic analyses reveal an essential coordination between the unfolded protein response and ER-associated degradation.* Cell, 2000. **101**(3): p. 249-58.
16. Peyroche, A., et al., *The ARF exchange factors Gea1p and Gea2p regulate Golgi structure and function in yeast.* J Cell Sci, 2001. **114**(Pt 12): p. 2241-53.
17. Marshall, W., *Size control in dynamic organelles.* Trends Cell Biol, 2002. **12**(9): p. 414-9.
18. Marshall, W.F., *Organelle size control systems: from cell geometry to organelle-directed medicine.* Bioessays, 2012. **34**(9): p. 721-4.
19. Goehring, N.W. and A.A. Hyman, *Organelle growth control through limiting pools of cytoplasmic components.* Curr Biol, 2012. **22**(9): p. R330-9.
20. Decker, M., et al., *Limiting amounts of centrosome material set centrosome size in C. elegans embryos.* Curr Biol, 2011. **21**(15): p. 1259-67.
21. Katsura, I., *Determination of bacteriophage lambda tail length by a protein ruler.* Nature, 1987. **327**(6117): p. 73-5.
22. Cornelis, G.R., C. Agrain, and I. Sorg, *Length control of extended protein structures in bacteria and bacteriophages.* Curr Opin Microbiol, 2006. **9**(2): p. 201-6.

23. Cox, J.S., R.E. Chapman, and P. Walter, *The unfolded protein response coordinates the production of endoplasmic reticulum protein and endoplasmic reticulum membrane.* Molecular Biology of the Cell, 1997. **8**(9): p. 1805-14.
24. Bernales, S., K.L. McDonald, and P. Walter, *Autophagy counterbalances endoplasmic reticulum expansion during the unfolded protein response.* PLoS Biol, 2006. **4**(12): p. e423.
25. Marshall, W.F., et al., *Flagellar length control system: testing a simple model based on intraflagellar transport and turnover.* Molecular Biology of the Cell, 2005. **16**(1): p. 270-8.
26. Wemmer, K.A. and W.F. Marshall, *Flagellar length control in chlamydomonas--paradigm for organelle size regulation.* Int Rev Cytol, 2007. **260**: p. 175-212.
27. Neumann, F.R. and P. Nurse, *Nuclear size control in fission yeast.* Journal of Cell Biology, 2007. **179**(4): p. 593-600.
28. Ludington, W.B., et al., *Organelle size equalization by a constitutive process.* Curr Biol, 2012. **22**(22): p. 2173-9.
29. Binder, B., et al., *A conceptual mathematical model of the dynamic self-organisation of distinct cellular organelles.* Plos One, 2009. **4**(12): p. e8295.
30. Yamamoto, A., et al., *Novel PI(4)P 5-kinase homologue, Fab1p, essential for normal vacuole function and morphology in yeast.* Molecular Biology of the Cell, 1995. **6**(5): p. 525-39.
31. Goshima, G., S. Saitoh, and M. Yanagida, *Proper metaphase spindle length is determined by centromere proteins Mis12 and Mis6 required for faithful chromosome segregation.* Genes Dev, 1999. **13**(13): p. 1664-77.
32. Gaynor, E.C., et al., *ARF is required for maintenance of yeast Golgi and endosome structure and function.* Molecular Biology of the Cell, 1998. **9**(3): p. 653-70.
33. Ferraro, F., et al., *A two-tier Golgi-based control of organelle size underpins the functional plasticity of endothelial cells.* Developmental Cell, 2014. **29**(3): p. 292-304.
34. Kuchka, M.R. and J.W. Jarvik, *Short-Flagella Mutants of Chlamydomonas reinhardtii.* Genetics, 1987. **115**(4): p. 685-91.
35. Barsel, S.E., D.E. Wexler, and P.A. Lefebvre, *Genetic analysis of long-flagella mutants of Chlamydomonas reinhardtii.* Genetics, 1988. **118**(4): p. 637-48.
36. Palade, G., *Intracellular aspects of the process of protein synthesis.* Science, 1975. **189**(4200): p. 347-58.
37. Bannykh, S.I., T. Rowe, and W.E. Balch, *The organization of endoplasmic reticulum export complexes.* Journal of Cell Biology, 1996. **135**(1): p. 19-35.
38. Droscher, A., *The history of the Golgi apparatus in neurones from its discovery in 1898 to electron microscopy.* Brain Res Bull, 1998. **47**(3): p. 199-203.
39. Farquhar, M.G. and G.E. Palade, *The Golgi apparatus: 100 years of progress and controversy.* Trends Cell Biol, 1998. **8**(1): p. 2-10.
40. Dalton, A.J. and M.D. Felix, *Cytologic and cytochemical characteristics of the Golgi substance of epithelial cells of the epididymis in situ, in homogenates and after isolation.* Am J Anat, 1954. **94**(2): p. 171-207.
41. Sjostrand, F.S. and V. Hanzon, *Ultrastructure of Golgi apparatus of exocrine cells of mouse pancreas.* Exp Cell Res, 1954. **7**(2): p. 415-29.
42. Neutra, M. and C.P. Leblond, *Synthesis of the carbohydrate of mucus in the golgi complex as shown by electron microscope radioautography of goblet cells from rats injected with glucose-H3.* J Cell Biol, 1966. **30**(1): p. 119-36.
43. Jamieson, J.D. and G.E. Palade, *Synthesis, intracellular transport, and discharge of secretory proteins in stimulated pancreatic exocrine cells.* J Cell Biol, 1971. **50**(1): p. 135-58.

44. Fries, E. and J.E. Rothman, *Transport of vesicular stomatitis virus glycoprotein in a cell-free extract.* Proc Natl Acad Sci U S A, 1980. **77**(7): p. 3870-4.
45. Beckers, C.J., D.S. Keller, and W.E. Balch, *Semi-intact cells permeable to macromolecules: use in reconstitution of protein transport from the endoplasmic reticulum to the Golgi complex.* Cell, 1987. **50**(4): p. 523-34.
46. Dunphy, W.G. and J.E. Rothman, *Compartmentation of asparagine-linked oligosaccharide processing in the Golgi apparatus.* J Cell Biol, 1983. **97**(1): p. 270-5.
47. Block, M.R., et al., *Purification of an N-ethylmaleimide-sensitive protein catalyzing vesicular transport.* Proc Natl Acad Sci U S A, 1988. **85**(21): p. 7852-6.
48. Sollner, T., et al., *SNAP receptors implicated in vesicle targeting and fusion.* Nature, 1993. **362**(6418): p. 318-24.
49. Orci, L., B.S. Glick, and J.E. Rothman, *A new type of coated vesicular carrier that appears not to contain clathrin: its possible role in protein transport within the Golgi stack.* Cell, 1986. **46**(2): p. 171-84.
50. Munro, S. and H.R. Pelham, *A C-terminal signal prevents secretion of luminal ER proteins.* Cell, 1987. **48**(5): p. 899-907.
51. Cosson, P. and F. Letourneur, *Coatomer (COPI)-coated vesicles: role in intracellular transport and protein sorting.* Curr Opin Cell Biol, 1997. **9**(4): p. 484-7.
52. Schweizer, A., et al., *Identification, by a monoclonal antibody, of a 53-kD protein associated with a tubulo-vesicular compartment at the cis-side of the Golgi apparatus.* J Cell Biol, 1988. **107**(5): p. 1643-53.
53. Barlowe, C., et al., *COPII: a membrane coat formed by Sec proteins that drive vesicle budding from the endoplasmic reticulum.* Cell, 1994. **77**(6): p. 895-907.
54. Lippincott-Schwartz, J., et al., *Microtubule-dependent retrograde transport of proteins into the ER in the presence of brefeldin A suggests an ER recycling pathway.* Cell, 1990. **60**(5): p. 821-36.
55. Orci, L., et al., *Mammalian Sec23p homologue is restricted to the endoplasmic reticulum transitional cytoplasm.* Proc Natl Acad Sci U S A, 1991. **88**(19): p. 8611-5.
56. Lord, C., S. Ferro-Novick, and E.A. Miller, *The highly conserved COPII coat complex sorts cargo from the endoplasmic reticulum and targets it to the golgi.* Cold Spring Harb Perspect Biol, 2013. **5**(2).
57. Zanetti, G., et al., *COPII and the regulation of protein sorting in mammals.* Nature Cell Biology, 2012. **14**(1): p. 20-8.
58. Okamoto, M., et al., *High-curvature domains of the ER are important for the organization of ER exit sites in Saccharomyces cerevisiae.* Journal of Cell Science, 2012. **125**(Pt 14): p. 3412-20.
59. Hammond, A.T. and B.S. Glick, *Dynamics of transitional endoplasmic reticulum sites in vertebrate cells.* Molecular Biology of the Cell, 2000. **11**(9): p. 3013-30.
60. Stephens, D.J., et al., *COPI-coated ER-to-Golgi transport complexes segregate from COPII in close proximity to ER exit sites.* Journal of Cell Science, 2000. **113 (Pt 12)**: p. 2177-85.
61. Zeuschner, D., et al., *Immuno-electron tomography of ER exit sites reveals the existence of free COPII-coated transport carriers.* Nature Cell Biology, 2006. **8**(4): p. 377-83.
62. Watson, P., et al., *Sec16 defines endoplasmic reticulum exit sites and is required for secretory cargo export in mammalian cells.* Traffic, 2006. **7**(12): p. 1678-87.
63. Hughes, H., et al., *Organisation of human ER-exit sites: requirements for the localisation of Sec16 to transitional ER.* Journal of Cell Science, 2009. **122**(Pt 16): p. 2924-34.

64. Bhattacharyya, D. and B.S. Glick, *Two mammalian Sec16 homologues have nonredundant functions in endoplasmic reticulum (ER) export and transitional ER organization.* Molecular Biology of the Cell, 2007. **18**(3): p. 839-49.
65. Connerly, P.L., et al., *Sec16 is a determinant of transitional ER organization.* Curr Biol, 2005. **15**(16): p. 1439-47.
66. Bharucha, N., et al., *Sec16 influences transitional ER sites by regulating rather than organizing COPII.* Molecular Biology of the Cell, 2013. **24**(21): p. 3406-19.
67. Glick, B.S., *Integrated self-organization of transitional ER and early Golgi compartments.* Bioessays, 2014. **36**(2): p. 129-33.
68. Stephens, D.J., *De novo formation, fusion and fission of mammalian COPII-coated endoplasmic reticulum exit sites.* Embo Reports, 2003. **4**(2): p. 210-7.
69. Aridor, M., et al., *Cargo can modulate COPII vesicle formation from the endoplasmic reticulum.* Journal of Biological Chemistry, 1999. **274**(7): p. 4389-99.
70. Farhan, H., et al., *Adaptation of endoplasmic reticulum exit sites to acute and chronic increases in cargo load.* EMBO J, 2008. **27**(15): p. 2043-54.
71. Shindiapina, P. and C. Barlowe, *Requirements for transitional endoplasmic reticulum site structure and function in Saccharomyces cerevisiae.* Mol Biol Cell, 2010. **21**(9): p. 1530-45.
72. Hughes, H. and D.J. Stephens, *Assembly, organization, and function of the COPII coat.* Histochemistry and Cell Biology, 2008. **129**(2): p. 129-51.
73. Rossanese, O.W., et al., *Golgi structure correlates with transitional endoplasmic reticulum organization in Pichia pastoris and Saccharomyces cerevisiae.* Journal of Cell Biology, 1999. **145**(1): p. 69-81.
74. Nakano, A. and M. Muramatsu, *A novel GTP-binding protein, Sar1p, is involved in transport from the endoplasmic reticulum to the Golgi apparatus.* Journal of Cell Biology, 1989. **109**(6 Pt 1): p. 2677-91.
75. Nakano, A., D. Brada, and R. Schekman, *A membrane glycoprotein, Sec12p, required for protein transport from the endoplasmic reticulum to the Golgi apparatus in yeast.* Journal of Cell Biology, 1988. **107**(3): p. 851-63.
76. Huang, M., et al., *Crystal structure of Sar1-GDP at 1.7 A resolution and the role of the NH2 terminus in ER export.* Journal of Cell Biology, 2001. **155**(6): p. 937-48.
77. Bi, X., R.A. Corpina, and J. Goldberg, *Structure of the Sec23/24-Sar1 pre-budding complex of the COPII vesicle coat.* Nature, 2002. **419**(6904): p. 271-7.
78. Rao, Y., et al., *An open conformation of switch I revealed by Sar1-GDP crystal structure at low Mg2+.* Biochem Biophys Res Commun, 2006. **348**(3): p. 908-15.
79. Bielli, A., et al., *Regulation of Sar1 NH2 terminus by GTP binding and hydrolysis promotes membrane deformation to control COPII vesicle fission.* Journal of Cell Biology, 2005. **171**(6): p. 919-24.
80. Antonny, B., et al., *N-terminal hydrophobic residues of the G-protein ADP-ribosylation factor-1 insert into membrane phospholipids upon GDP to GTP exchange.* Biochemistry, 1997. **36**(15): p. 4675-84.
81. Matsuoka, K., et al., *COPII-coated vesicle formation reconstituted with purified coat proteins and chemically defined liposomes.* Cell, 1998. **93**(2): p. 263-75.
82. Lee, M.C., et al., *Sar1p N-terminal helix initiates membrane curvature and completes the fission of a COPII vesicle.* Cell, 2005. **122**(4): p. 605-17.
83. Miller, E., et al., *Cargo selection into COPII vesicles is driven by the Sec24p subunit.* Embo Journal, 2002. **21**(22): p. 6105-13.
84. Miller, E.A., et al., *Multiple cargo binding sites on the COPII subunit Sec24p ensure capture of diverse membrane proteins into transport vesicles.* Cell, 2003. **114**(4): p. 497-509.

85. Wendeler, M.W., J.P. Paccaud, and H.P. Hauri, *Role of Sec24 isoforms in selective export of membrane proteins from the endoplasmic reticulum.* Embo Reports, 2007. **8**(3): p. 258-64.
86. Demmel, L., et al., *Differential selection of Golgi proteins by COPII Sec24 isoforms in procyclic Trypanosoma brucei.* Traffic, 2011. **12**(11): p. 1575-91.
87. Matsuoka, K., et al., *Surface structure of the COPII-coated vesicle.* Proc Natl Acad Sci U S A, 2001. **98**(24): p. 13705-9.
88. Fath, S., et al., *Structure and organization of coat proteins in the COPII cage.* Cell, 2007. **129**(7): p. 1325-36.
89. Stagg, S.M., et al., *Structure of the Sec13/31 COPII coat cage.* Nature, 2006. **439**(7073): p. 234-8.
90. Gurkan, C., et al., *The COPII cage: unifying principles of vesicle coat assembly.* Nat Rev Mol Cell Biol, 2006. **7**(10): p. 727-38.
91. Stagg, S.M., et al., *Structural basis for cargo regulation of COPII coat assembly.* Cell, 2008. **134**(3): p. 474-84.
92. Zanetti, G., et al., *The structure of the COPII transport-vesicle coat assembled on membranes.* Elife, 2013. **2**: p. e00951.
93. Antonny, B., et al., *Dynamics of the COPII coat with GTP and stable analogues.* Nature Cell Biology, 2001. **3**(6): p. 531-7.
94. Kung, L.F., et al., *Sec24p and Sec16p cooperate to regulate the GTP cycle of the COPII coat.* Embo Journal, 2012. **31**(4): p. 1014-27.
95. Forster, R., et al., *Secretory cargo regulates the turnover of COPII subunits at single ER exit sites.* Curr Biol, 2006. **16**(2): p. 173-9.
96. Futai, E. and R. Schekman, *Purification and functional properties of yeast Sec12 GEF.* Methods Enzymol, 2005. **404**: p. 74-82.
97. McMahon, C., et al., *The structure of Sec12 implicates potassium ion coordination in Sar1 activation.* Journal of Biological Chemistry, 2012. **287**(52): p. 43599-606.
98. Barlowe, C. and R. Schekman, *SEC12 encodes a guanine-nucleotide-exchange factor essential for transport vesicle budding from the ER.* Nature, 1993. **365**(6444): p. 347-9.
99. d'Enfert, C., et al., *Sec12p-dependent membrane binding of the small GTP-binding protein Sar1p promotes formation of transport vesicles from the ER.* Journal of Cell Biology, 1991. **114**(4): p. 663-70.
100. Nishikawa, S. and A. Nakano, *Identification of a gene required for membrane protein retention in the early secretory pathway.* Proc Natl Acad Sci U S A, 1993. **90**(17): p. 8179-83.
101. Budnik, A. and D.J. Stephens, *ER exit sites--localization and control of COPII vesicle formation.* Febs Letters, 2009. **583**(23): p. 3796-803.
102. Soderholm, J., et al., *The transitional ER localization mechanism of Pichia pastoris Sec12.* Developmental Cell, 2004. **6**(5): p. 649-59.
103. Weissman, J.T., H. Plutner, and W.E. Balch, *The mammalian guanine nucleotide exchange factor mSec12 is essential for activation of the Sar1 GTPase directing endoplasmic reticulum export.* Traffic, 2001. **2**(7): p. 465-75.
104. Espenshade, P., et al., *Yeast SEC16 gene encodes a multidomain vesicle coat protein that interacts with Sec23p.* Journal of Cell Biology, 1995. **131**(2): p. 311-24.
105. Gimeno, R.E., P. Espenshade, and C.A. Kaiser, *SED4 encodes a yeast endoplasmic reticulum protein that binds Sec16p and participates in vesicle formation.* Journal of Cell Biology, 1995. **131**(2): p. 325-38.
106. Hardwick, K.G., et al., *Genes that allow yeast cells to grow in the absence of the HDEL receptor.* Embo Journal, 1992. **11**(11): p. 4187-95.

107. Novick, P., C. Field, and R. Schekman, *Identification of 23 complementation groups required for post-translational events in the yeast secretory pathway.* Cell, 1980. **21**(1): p. 205-15.
108. Ivan, V., et al., *Drosophila Sec16 mediates the biogenesis of tER sites upstream of Sar1 through an arginine-rich motif.* Molecular Biology of the Cell, 2008. **19**(10): p. 4352-65.
109. Iinuma, T., et al., *Mammalian Sec16/p250 plays a role in membrane traffic from the endoplasmic reticulum.* Journal of Biological Chemistry, 2007. **282**(24): p. 17632-9.
110. Shaywitz, D.A., et al., *COPII subunit interactions in the assembly of the vesicle coat.* J Biol Chem, 1997. **272**(41): p. 25413-6.
111. Yorimitsu, T. and K. Sato, *Insights into structural and regulatory roles of Sec16 in COPII vesicle formation at ER exit sites.* Mol Biol Cell, 2012. **23**(15): p. 2930-42.
112. Suda, Y. and A. Nakano, *The Yeast Golgi Apparatus.* Traffic, 2012. **13**(4): p. 505-510.
113. Kondylis, V. and C. Rabouille, *The Golgi apparatus: lessons from Drosophila.* Febs Letters, 2009. **583**(23): p. 3827-38.
114. Dupree, P. and D.J. Sherrier, *The plant Golgi apparatus.* Biochimica et Biophysica Acta (BBA) - Molecular Cell Research, 1998. **1404**(1–2): p. 259-270.
115. Farquhar, M.G. and G.E. Palade, *The Golgi apparatus (complex)-(1954-1981)-from artifact to center stage.* Journal of Cell Biology, 1981. **91**(3 Pt 2): p. 77s-103s.
116. Bannykh, S.I. and W.E. Balch, *Membrane dynamics at the endoplasmic reticulum-Golgi interface.* Journal of Cell Biology, 1997. **138**(1): p. 1-4.
117. Hauri, H.P. and A. Schweizer, *The endoplasmic reticulum-Golgi intermediate compartment.* Curr Opin Cell Biol, 1992. **4**(4): p. 600-8.
118. Stanley, P., *Golgi glycosylation.* Cold Spring Harb Perspect Biol, 2011. **3**(4).
119. Anitei, M. and B. Hoflack, *Exit from the trans-Golgi network: from molecules to mechanisms.* Curr Opin Cell Biol, 2011. **23**(4): p. 443-51.
120. Glick, B.S. and A. Nakano, *Membrane traffic within the Golgi apparatus.* Annu Rev Cell Dev Biol, 2009. **25**: p. 113-32.
121. Day, K.J., L.A. Staehelin, and B.S. Glick, *A three-stage model of Golgi structure and function.* Histochemistry and Cell Biology, 2013. **140**(3): p. 239-49.
122. Pfeffer, S.R., *How the Golgi works: a cisternal progenitor model.* Proc Natl Acad Sci U S A, 2010. **107**(46): p. 19614-8.
123. Rothman, J.E., *The golgi apparatus: two organelles in tandem.* Science, 1981. **213**(4513): p. 1212-9.
124. Rothman, J.E. and F.T. Wieland, *Protein sorting by transport vesicles.* Science, 1996. **272**(5259): p. 227-34.
125. Orci, L., et al., *Anterograde flow of cargo across the golgi stack potentially mediated via bidirectional "percolating" COPI vesicles.* Proc Natl Acad Sci U S A, 2000. **97**(19): p. 10400-5.
126. Pelham, H.R. and J.E. Rothman, *The debate about transport in the Golgi--two sides of the same coin?* Cell, 2000. **102**(6): p. 713-9.
127. Orci, L., et al., *Bidirectional transport by distinct populations of COPI-coated vesicles.* Cell, 1997. **90**(2): p. 335-49.
128. Becker, B., B. Bolinger, and M. Melkonian, *Anterograde transport of algal scales through the Golgi complex is not mediated by vesicles.* Trends Cell Biol, 1995. **5**(8): p. 305-7.
129. Bonfanti, L., et al., *Procollagen traverses the Golgi stack without leaving the lumen of cisternae: evidence for cisternal maturation.* Cell, 1998. **95**(7): p. 993-1003.
130. Martinez-Menarguez, J.A., et al., *Peri-Golgi vesicles contain retrograde but not anterograde proteins consistent with the cisternal progression model of intra-Golgi transport.* Journal of Cell Biology, 2001. **155**(7): p. 1213-24.

131. Dahan, S., et al., *Concentration of intracellular hepatic apolipoprotein E in Golgi apparatus saccular distensions and endosomes.* Journal of Cell Biology, 1994. **127**(6 Pt 2): p. 1859-69.
132. Gilchrist, A., et al., *Quantitative proteomics analysis of the secretory pathway.* Cell, 2006. **127**(6): p. 1265-81.
133. Aoe, T., et al., *Modulation of intracellular transport by transported proteins: insight from regulation of COPI-mediated transport.* Proc Natl Acad Sci U S A, 1998. **95**(4): p. 1624-9.
134. Patterson, G.H., et al., *Transport through the Golgi apparatus by rapid partitioning within a two-phase membrane system.* Cell, 2008. **133**(6): p. 1055-67.
135. Cosson, P., et al., *A resident Golgi protein is excluded from peri-Golgi vesicles in NRK cells.* Proc Natl Acad Sci U S A, 2002. **99**(20): p. 12831-4.
136. Kweon, H.S., et al., *Golgi enzymes are enriched in perforated zones of golgi cisternae but are depleted in COPI vesicles.* Molecular Biology of the Cell, 2004. **15**(10): p. 4710-24.
137. Rambourg, A. and Y. Clermont, *Three-dimensional electron microscopy: structure of the Golgi apparatus.* European Journal of Cell Biology, 1990. **51**(2): p. 189-200.
138. Marsh, B.J., et al., *Direct continuities between cisternae at different levels of the Golgi complex in glucose-stimulated mouse islet beta cells.* Proc Natl Acad Sci U S A, 2004. **101**(15): p. 5565-70.
139. Trucco, A., et al., *Secretory traffic triggers the formation of tubular continuities across Golgi sub-compartments.* Nature Cell Biology, 2004. **6**(11): p. 1071-81.
140. San Pietro, E., et al., *Group IV phospholipase A(2)alpha controls the formation of inter-cisternal continuities involved in intra-Golgi transport.* PLoS Biol, 2009. **7**(9): p. e1000194.
141. Lippincott-Schwartz, J. and R.D. Phair, *Lipids and cholesterol as regulators of traffic in the endomembrane system.* Annu Rev Biophys, 2010. **39**: p. 559-78.
142. Glick, B.S. and A. Luini, *Models for Golgi traffic: a critical assessment.* Cold Spring Harb Perspect Biol, 2011. **3**(11): p. a005215.
143. Rink, J., et al., *Rab conversion as a mechanism of progression from early to late endosomes.* Cell, 2005. **122**(5): p. 735-49.
144. Poteryaev, D., et al., *Identification of the switch in early-to-late endosome transition.* Cell, 2010. **141**(3): p. 497-508.
145. Volchuk, A., et al., *Megavesicles implicated in the rapid transport of intracisternal aggregates across the Golgi stack.* Cell, 2000. **102**(3): p. 335-48.
146. Duden, R., et al., *Beta-COP, a 110 kd protein associated with non-clathrin-coated vesicles and the Golgi complex, shows homology to beta-adaptin.* Cell, 1991. **64**(3): p. 649-65.
147. Serafini, T., et al., *A coat subunit of Golgi-derived non-clathrin-coated vesicles with homology to the clathrin-coated vesicle coat protein beta-adaptin.* Nature, 1991. **349**(6306): p. 215-20.
148. Orci, L., et al., *Coatomer-rich endoplasmic reticulum.* Proc Natl Acad Sci U S A, 1994. **91**(25): p. 11924-8.
149. Cosson, P. and F. Letourneur, *Coatomer interaction with di-lysine endoplasmic reticulum retention motifs.* Science, 1994. **263**(5153): p. 1629-31.
150. Misteli, T. and G. Warren, *COP-coated vesicles are involved in the mitotic fragmentation of Golgi stacks in a cell-free system.* Journal of Cell Biology, 1994. **125**(2): p. 269-82.
151. Wu, W.J., et al., *The gamma-subunit of the coatomer complex binds Cdc42 to mediate transformation.* Nature, 2000. **405**(6788): p. 800-4.

152. Hehnly, H., et al., *Cdc42 regulates microtubule-dependent Golgi positioning.* Traffic, 2010. **11**(8): p. 1067-78.
153. Whitney, J.A., et al., *Cytoplasmic coat proteins involved in endosome function.* Cell, 1995. **83**(5): p. 703-13.
154. Lowe, M. and T.E. Kreis, *In vitro assembly and disassembly of coatomer.* Journal of Biological Chemistry, 1995. **270**(52): p. 31364-71.
155. Hara-Kuge, S., et al., *En bloc incorporation of coatomer subunits during the assembly of COP-coated vesicles.* Journal of Cell Biology, 1994. **124**(6): p. 883-92.
156. Reinhard, C., et al., *Receptor-induced polymerization of coatomer.* Proc Natl Acad Sci U S A, 1999. **96**(4): p. 1224-8.
157. Pelham, H.R., *Recycling of proteins between the endoplasmic reticulum and Golgi complex.* Curr Opin Cell Biol, 1991. **3**(4): p. 585-91.
158. Beck, R., et al., *The COPI system: molecular mechanisms and function.* Febs Letters, 2009. **583**(17): p. 2701-9.
159. Nilsson, T., et al., *The membrane spanning domain of beta-1,4-galactosyltransferase specifies trans Golgi localization.* Embo Journal, 1991. **10**(12): p. 3567-75.
160. Wilcox, C.A., et al., *Mutation of a tyrosine localization signal in the cytosolic tail of yeast Kex2 protease disrupts Golgi retention and results in default transport to the vacuole.* Molecular Biology of the Cell, 1992. **3**(12): p. 1353-71.
161. Bos, K., C. Wraight, and K.K. Stanley, *TGN38 is maintained in the trans-Golgi network by a tyrosine-containing motif in the cytoplasmic domain.* Embo Journal, 1993. **12**(5): p. 2219-28.
162. Kornfeld, R. and S. Kornfeld, *Assembly of asparagine-linked oligosaccharides.* Annual Review of Biochemistry, 1985. **54**: p. 631-64.
163. Barlowe, C.K. and E.A. Miller, *Secretory protein biogenesis and traffic in the early secretory pathway.* Genetics, 2013. **193**(2): p. 383-410.
164. Riley, L.G., et al., *The influence of extracellular matrix and prolactin on global gene expression profiles of primary bovine mammary epithelial cells in vitro.* Anim Genet, 2009.
165. Hollmann, K., *Cytology and fine structure of the mammary gland.* . In Lactation: A Comprehensive Treatise (Edited by LARSON B. L. & SMITH V. R.),, 1974: p. 3-95.
166. Mousnier, A., et al., *Human Rhinovirus 16 Causes Golgi Apparatus Fragmentation without Blocking Protein Secretion.* J Virol, 2014. **88**(20): p. 11671-85.
167. Beske, O., et al., *Poliovirus infection blocks ERGIC-to-Golgi trafficking and induces microtubule-dependent disruption of the Golgi complex.* J Cell Sci, 2007. **120**(Pt 18): p. 3207-18.
168. Numata, Y., et al., *Depletion of molecular chaperones from the endoplasmic reticulum and fragmentation of the Golgi apparatus associated with pathogenesis in Pelizaeus-Merzbacher disease.* J Biol Chem, 2013. **288**(11): p. 7451-66.
169. Rendon, W.O., et al., *Golgi fragmentation is Rab and SNARE dependent in cellular models of Parkinson's disease.* Histochem Cell Biol, 2013. **139**(5): p. 671-84.
170. Dupuis, N., et al., *A novel RAB33B mutation in Smith-McCort dysplasia.* Hum Mutat, 2013. **34**(2): p. 283-6.
171. Syx, D., et al., *The RIN2 syndrome: a new autosomal recessive connective tissue disorder caused by deficiency of Ras and Rab interactor 2 (RIN2).* Hum Genet, 2010. **128**(1): p. 79-88.
172. Burman, J.L., J.N. Hamlin, and P.S. McPherson, *Scyl1 regulates Golgi morphology.* Plos One, 2010. **5**(3): p. e9537.
173. Sengupta, D. and A.D. Linstedt, *Control of Organelle Size: The Golgi Complex.* Annu Rev Cell Dev Biol, 2011.

174. Noske, A.B., et al., *Expedited approaches to whole cell electron tomography and organelle mark-up in situ in high-pressure frozen pancreatic islets.* J Struct Biol, 2008. **161**(3): p. 298-313.
175. Kirk, S.J., et al., *Biogenesis of secretory organelles during B cell differentiation.* J Leukoc Biol, 2010. **87**(2): p. 245-55.
176. Becker, B. and M. Melkonian, *The secretory pathway of protists: spatial and functional organization and evolution.* Microbiol Rev, 1996. **60**(4): p. 697-721.
177. Rambourg, A., C.L. Jackson, and Y. Clermont, *Three dimensional configuration of the secretory pathway and segregation of secretion granules in the yeast Saccharomyces cerevisiae*. Journal of Cell Science, 2001. **114**(Pt 12): p. 2231-9.
178. Rambourg, A., et al., *Three-dimensional structure of tubular networks, presumably Golgi in nature, in various yeast strains: a comparative study.* Anat Rec, 1995. **243**(3): p. 283-93.
179. Whitters, E.A., T.P. McGee, and V.A. Bankaitis, *Purification and characterization of a late Golgi compartment from Saccharomyces cerevisiae.* Journal of Biological Chemistry, 1994. **269**(45): p. 28106-17.
180. Towler, D.A., et al., *Amino-terminal processing of proteins by N-myristoylation. Substrate specificity of N-myristoyl transferase.* Journal of Biological Chemistry, 1987. **262**(3): p. 1030-6.
181. Kahn, R.A., et al., *Mutational analysis of Saccharomyces cerevisiae ARF1.* Journal of Biological Chemistry, 1995. **270**(1): p. 143-50.
182. Knoll, L.J., et al., *Analysis of the compartmentalization of myristoyl-CoA:protein N-myristoyltransferase in Saccharomyces cerevisiae.* Journal of Biological Chemistry, 1992. **267**(8): p. 5366-73.
183. Johnson, D.R., et al., *Genetic and biochemical studies of protein N-myristoylation.* Annual Review of Biochemistry, 1994. **63**: p. 869-914.
184. Stearns, T., et al., *ADP ribosylation factor is an essential protein in Saccharomyces cerevisiae and is encoded by two genes.* Molecular and Cellular Biology, 1990. **10**(12): p. 6690-9.
185. Haun, R.S., et al., *Effect of myristoylation on GTP-dependent binding of ADP-ribosylation factor to Golgi.* Journal of Biological Chemistry, 1993. **268**(10): p. 7064-8.
186. Liu, Y., R.A. Kahn, and J.H. Prestegard, *Dynamic structure of membrane-anchored Arf*GTP.* Nature Structural & Molecular Biology, 2010. **17**(7): p. 876-81.
187. Dean, N., Y.B. Zhang, and J.B. Poster, *The VRG4 gene is required for GDP-mannose transport into the lumen of the Golgi in the yeast, Saccharomyces cerevisiae.* Journal of Biological Chemistry, 1997. **272**(50): p. 31908-14.
188. Poster, J.B. and N. Dean, *The yeast VRG4 gene is required for normal Golgi functions and defines a new family of related genes.* Journal of Biological Chemistry, 1996. **271**(7): p. 3837-45.
189. Gao, X.D. and N. Dean, *Distinct protein domains of the yeast Golgi GDP-mannose transporter mediate oligomer assembly and export from the endoplasmic reticulum.* Journal of Biological Chemistry, 2000. **275**(23): p. 17718-27.
190. Wooding, S. and H.R. Pelham, *The dynamics of golgi protein traffic visualized in living yeast cells.* Molecular Biology of the Cell, 1998. **9**(9): p. 2667-80.
191. Spang, A., et al., *The ADP ribosylation factor-nucleotide exchange factors Gea1p and Gea2p have overlapping, but not redundant functions in retrograde transport from the Golgi to the endoplasmic reticulum.* Molecular Biology of the Cell, 2001. **12**(4): p. 1035-45.

192. Chantalat, S., et al., *The Arf activator Gea2p and the P-type ATPase Drs2p interact at the Golgi in Saccharomyces cerevisiae.* Journal of Cell Science, 2004. **117**(Pt 5): p. 711-22.
193. Peyroche, A., S. Paris, and C.L. Jackson, *Nucleotide exchange on ARF mediated by yeast Gea1 protein.* Nature, 1996. **384**(6608): p. 479-81.
194. Deng, Y., et al., *A COPI coat subunit interacts directly with an early-Golgi localized Arf exchange factor.* Embo Reports, 2009. **10**(1): p. 58-64.
195. Chantalat, S., et al., *A novel Golgi membrane protein is a partner of the ARF exchange factors Gea1p and Gea2p.* Molecular Biology of the Cell, 2003. **14**(6): p. 2357-71.
196. Sata, M., et al., *Brefeldin A-inhibited guanine nucleotide-exchange activity of Sec7 domain from yeast Sec7 with yeast and mammalian ADP ribosylation factors.* Proc Natl Acad Sci U S A, 1998. **95**(8): p. 4204-8.
197. Beraud-Dufour, S., et al., *A glutamic finger in the guanine nucleotide exchange factor ARNO displaces Mg2+ and the beta-phosphate to destabilize GDP on ARF1.* Embo Journal, 1998. **17**(13): p. 3651-9.
198. Richardson, B.C. and J.C. Fromme, *Autoregulation of Sec7 Arf-GEF activity and localization by positive feedback.* Small GTPases, 2012. **3**(4): p. 240-3.
199. McDonold, C.M. and J.C. Fromme, *Four GTPases Differentially Regulate the Sec7 Arf-GEF to Direct Traffic at the trans-Golgi Network.* Developmental Cell, 2014. **30**(6): p. 759-67.
200. Franzusoff, A., et al., *Localization of components involved in protein transport and processing through the yeast Golgi apparatus.* Journal of Cell Biology, 1991. **112**(1): p. 27-37.
201. Rossanese, O.W., et al., *A role for actin, Cdc1p, and Myo2p in the inheritance of late Golgi elements in Saccharomyces cerevisiae.* Journal of Cell Biology, 2001. **153**(1): p. 47-62.
202. Bhattacharyya, D. and B.S. Glick, *Two mammalian Sec16 homologues have nonredundant functions in endoplasmic reticulum (ER) export and transitional ER organization.* Mol Biol Cell, 2007. **18**(3): p. 839-49.
203. Soderholm, J., et al., *The transitional ER localization mechanism of Pichia pastoris Sec12.* Dev Cell, 2004. **6**(5): p. 649-59.
204. Sambrook, J. and D.W. Russell, *Calcium-phosphate-mediated Transfection of Eukaryotic Cells with Plasmid DNAs.* CSH Protoc, 2006. **2006**(1).
205. Sambrook, J. and D.W. Russell, *SDS-Polyacrylamide Gel Electrophoresis of Proteins.* CSH Protoc, 2006. **2006**(4).
206. Saito, K., et al., *Concentration of Sec12 at ER exit sites via interaction with cTAGE5 is required for collagen export.* J Cell Biol, 2014. **206**(6): p. 751-62.
207. Montegna, E.A., et al., *Sec12 binds to Sec16 at transitional ER sites.* Plos One, 2012. **7**(2): p. e31156.
208. daSilva, L.L., et al., *Endoplasmic reticulum export sites and Golgi bodies behave as single mobile secretory units in plant cells.* Plant Cell, 2004. **16**(7): p. 1753-71.
209. d'Enfert, C., et al., *Sec12p-dependent membrane binding of the small GTP-binding protein Sar1p promotes formation of transport vesicles from the ER.* J Cell Biol, 1991. **114**(4): p. 663-70.
210. Phillipson, B.A., et al., *Secretory bulk flow of soluble proteins is efficient and COPII dependent.* Plant Cell, 2001. **13**(9): p. 2005-20.
211. Popoff, V., et al., *Several Arf isoforms support COPI vesicle formation.* J Biol Chem, 2011.
212. Monetta, P., et al., *Rab1b interacts with GBF1 and modulates both ARF1 dynamics and COPI association.* Mol Biol Cell, 2007. **18**(7): p. 2400-10.

213. Rose, M.D., et al., *A Saccharomyces cerevisiae genomic plasmid bank based on a centromere-containing shuttle vector.* Gene, 1987. **60**(2-3): p. 237-43.
214. Gietz, R.D. and A. Sugino, *New yeast-Escherichia coli shuttle vectors constructed with in vitro mutagenized yeast genes lacking six-base pair restriction sites.* Gene, 1988. **74**(2): p. 527-34.
215. Boeke, J.D., F. LaCroute, and G.R. Fink, *A positive selection for mutants lacking orotidine-5'-phosphate decarboxylase activity in yeast: 5-fluoro-orotic acid resistance.* Mol Gen Genet, 1984. **197**(2): p. 345-6.
216. Sherman, F., *Getting started with yeast.* Methods Enzymol, 1991. **194**: p. 3-21.
217. *Guide to molecular cloning techniques.* Methods Enzymol, 1987. **152**: p. 1-812.
218. Gietz, R.D. and R.A. Woods, *Transformation of yeast by lithium acetate/single-stranded carrier DNA/polyethylene glycol method.* Methods Enzymol, 2002. **350**: p. 87-96.
219. Rothstein, R., *Targeting, disruption, replacement, and allele rescue: integrative DNA transformation in yeast.* Methods Enzymol, 1991. **194**: p. 281-301.
220. Levi, S.K., et al., *The yeast GRASP Grh1 colocalizes with COPII and is dispensable for organizing the secretory pathway.* Traffic, 2010. **11**(9): p. 1168-79.
221. Shaner, N.C., et al., *Improved monomeric red, orange and yellow fluorescent proteins derived from Discosoma sp. red fluorescent protein.* Nat Biotechnol, 2004. **22**(12): p. 1567-72.
222. Tang, X., J.J. Punch, and W.L. Lee, *A CAAX motif can compensate for the PH domain of Num1 for cortical dynein attachment.* Cell Cycle, 2009. **8**(19): p. 3182-90.
223. Donaldson, J.G. and C.L. Jackson, *ARF family G proteins and their regulators: roles in membrane transport, development and disease.* Nat Rev Mol Cell Biol, 2011. **12**(6): p. 362-75.
224. Wach, A., et al., *New heterologous modules for classical or PCR-based gene disruptions in Saccharomyces cerevisiae.* Yeast, 1994. **10**(13): p. 1793-808.
225. Kukulski, W., et al., *Correlated fluorescence and 3D electron microscopy with high sensitivity and spatial precision.* J Cell Biol, 2011. **192**(1): p. 111-9.
226. Franco, M., et al., *Myristoylation-facilitated binding of the G protein ARF1GDP to membrane phospholipids is required for its activation by a soluble nucleotide exchange factor.* J Biol Chem, 1996. **271**(3): p. 1573-8.
227. Donohoe, B.S., et al., *Cis-Golgi cisternal assembly and biosynthetic activation occur sequentially in plants and algae.* Traffic, 2013. **14**(5): p. 551-67.
228. Bentley, M., et al., *SNARE status regulates tether recruitment and function in homotypic COPII vesicle fusion.* J Biol Chem, 2006. **281**(50): p. 38825-33.
229. Watts, J.L., R.L. Ariagno, and J.P. Brady, *Chronic pulmonary disease in neonates after artificial ventilation: distribution of ventilation and pulmonary interstitial emphysema.* Pediatrics, 1977. **60**(3): p. 273-81.
230. Harris, S.L. and M.G. Waters, *Localization of a yeast early Golgi mannosyltransferase, Och1p, involves retrograde transport.* J Cell Biol, 1996. **132**(6): p. 985-98.
231. Schroder, S., et al., *The Golgi-localization of yeast Emp47p depends on its di-lysine motif but is not affected by the ret1-1 mutation in alpha-COP.* J Cell Biol, 1995. **131**(4): p. 895-912.
232. Spang, A., et al., *The ADP ribosylation factor-nucleotide exchange factors Gea1p and Gea2p have overlapping, but not redundant functions in retrograde transport from the Golgi to the endoplasmic reticulum.* Mol Biol Cell, 2001. **12**(4): p. 1035-45.
233. Renna, L., et al., *Golgi traffic and integrity depend on N-myristoyl transferase-1 in Arabidopsis.* Plant Cell, 2013. **25**(5): p. 1756-73.

234. Ktistakis, N.T., et al., *Evidence that phospholipase D mediates ADP ribosylation factor-dependent formation of Golgi coated vesicles.* J Cell Biol, 1996. **134**(2): p. 295-306.
235. Guo, Y. and A.D. Linstedt, *COPII-Golgi protein interactions regulate COPII coat assembly and Golgi size.* J Cell Biol, 2006. **174**(1): p. 53-63.

Appendix

List of primers:

Amplicon name	Primer name	Sequence 5'to 3'	Dib lab database number	Tm ^{0}C
Sec12 cytoplasmic domain (1.17Kb)	hsec12-bglII-F	GAGCCAGATCTATGGGCCGG CGCCGGGCGCCA	C 57	74
	hsec12-Cyto-R	GTTATAAGCTTCCGTGAGGG CAACAGATGCA	C 58	65
	ycp50-S1	gggatatcgtccattccgac	D10	55
	ycp50AS1	cacctgtcctacgagttgca	D11	57
NMT1 with 5' and 3' UTR (2.07Kb)	NMT1 prom1For	AAGTATAAGCTTGCTATCGTT TACAAATTAAA	B39	55
	NMT1-Term1-R	CGCTGGGTACCATTTTTTCAC TTCGTCAATTGAC	B40	64
nmt1 for integration (1.3Kb)	Intregation 39fwd	AAT CAC AAG CTT ACA CCG GAA GAT ATA TCT GA	C70	58
	NMT1-Term1-R	CGCTGGGTACCATTTTTTCAC TTCGTCAATTGAC	B40	64
NMT1 T400I correction mutagenesis	NMT QC400 T to L B	CAA GAA CAA TGT ATT ATC TTG CGA AGT CAA CGC GTT AAA AAC ATC CAT AT	C52	65
	NMT QC400 T to L T	ATA TGG ATG TTT TTA ACG CGT TGA CTT CGC AAG ATA ATA CAT TGT TCT TG	C51	65
ARF1 with 5' and 3' UTR (1.8Kb)	Arf1 EcoR1 Fw	TGCACAGTTGAATTCTCG	D23	44
	Arf1 Hind3 Rv	GATGAAAGCTTCTGCAGTTGT CAGTCT	D24	58
ARF1 deletion	ARF1 KanMx-F	ATTgAAggTATAAgAAAgAACT CAAACAggTTTAATAgAATTA AAAcgtacgctgcaggtcgac	D17	64
	ARF2 Kan Mx-R	TTCATTTAgTTTATACAAgCgT ATTTgATCCATATTCTAgAATT Tatcgatgaattcgagctcg	D18	62

ARF1 G2A mutagenesis	Arf1 G2A T	AACAGGTTTAATAGAATTAA AAATGGCTTTGTTTGCCTCTA AGTTGTTCAGTA	H58	64
	Arf1 G2A B	TACTGAACAACTTAGAGGCA AACAAAGCCATTTTTAATTCT ATTAAACCTGTT	H59	64
GEA2 C term (2.1Kb)	GEA2 Pst1 fw	ACACAGCTGCAGGACACACA ATCTGTCATG	F63	50
	GEA2 EcoR1 Rv	TTCGAAGAATTCAAGCTTTAT GGACCCTGA	F64	52
Gea2 BamHI NotI mutagenesis	GEA2 BN FW	GAAGTTATCTGATGTAGAAA AGGATAGGGATCCCTAGCGG CCGCAGATGCTAAGAGATAG TGATGATAT	F61	53
	GEA2 BN RV	ATATCATCACTATCTCTTAGC ATCTGCGGCCGCTAGGGATC CCTATCCTTTTCTACATCAGA TAACTTC	F62	53

Publications

© 2014. Published by The Company of Biologists Ltd | Journal of Cell Science (2014) 127, 250–257 doi:10.1242/jcs.140996

RESEARCH ARTICLE

Golgi enlargement in Arf-depleted yeast cells is due to altered dynamics of cisternal maturation

Madhura Bhave[1,*], Effrosyni Papanikou[2,*], Prasanna Iyer[1], Koushal Pandya[1], Bhawik Kumar Jain[1], Abira Ganguly[1], Chandrakala Sharma[1], Ketakee Pawar[1], Jotham Austin II[3], Kasey J. Day[2], Olivia W. Rossanese[2], Benjamin S. Glick[2] and Dibyendu Bhattacharyya[1,‡]

ABSTRACT

Regulation of the size and abundance of membrane compartments is a fundamental cellular activity. In *Saccharomyces cerevisiae*, disruption of the ADP-ribosylation factor 1 (*ARF1*) gene yields larger and fewer Golgi cisternae by partially depleting the Arf GTPase. We observed a similar phenotype with a thermosensitive mutation in Nmt1, which myristoylates and activates Arf. Therefore, partial depletion of Arf is a convenient tool for dissecting mechanisms that regulate Golgi structure. We found that in *arf1Δ* cells, late Golgi structure is particularly abnormal, with the number of late Golgi cisternae being severely reduced. This effect can be explained by selective changes in cisternal maturation kinetics. The *arf1Δ* mutation causes early Golgi cisternae to mature more slowly and less frequently, but does not alter the maturation of late Golgi cisternae. These changes quantitatively explain why late Golgi cisternae are fewer in number and correspondingly larger. With a stacked Golgi, similar changes in maturation kinetics could be used by the cell to modulate the number of cisternae per stack. Thus, the rates of processes that transform a maturing compartment can determine compartmental size and copy number.

KEY WORDS: Organelle size, Organelle number, Golgi, Cisternal maturation, Arf

INTRODUCTION

The mechanisms that control organelle size and number are attracting increasing interest (Goehring and Hyman, 2012; Levy and Heald, 2012; Marshall, 2002; Sengupta and Linstedt, 2011). Apart from being a basic cell biological problem, this topic has clinical relevance because cancer cells display altered organelle structure (Levy and Heald, 2012; Zink et al., 2004). One way to control organelle structure is with fusion and fission events. For example, mitochondrial networks are maintained by a balance between fusion and fission (Chan, 2012; Westermann, 2010). Similarly, endosomes and yeast vacuoles undergo frequent homotypic fusion (Epp et al., 2011). Another way to control organelle structure is to alter the relative rates of membrane influx and efflux (Sengupta and Linstedt, 2011). Many of these membrane remodeling events are controlled by GTPases. Improved understanding of such processes may enable the reprogramming of organelle size in diseased cells (Marshall, 2012).

An organelle that shows great plasticity and variability is the Golgi apparatus, which consists of disk-shaped cisternae that sometimes exhibit fenestrations, tubular extensions and lateral interconnections (Warren and Rothman, 2011). The mammalian Golgi undergoes changes during differentiation or cancer progression (Kellokumpu et al., 2002; Kirk et al., 2010; Lu et al., 2001; Weller et al., 2010; Wu et al., 2000). In most eukaryotes, Golgi cisternae are arranged in polarized stacks, but in some species such as the yeast *Saccharomyces cerevisiae*, Golgi cisternae are dispersed throughout the cell (Mowbrey and Dacks, 2009; Preuss et al., 1992). The dispersed cisternae can be tracked individually by fluorescence microscopy (Wooding and Pelham, 1998). A typical *S. cerevisiae* cell contains about six to ten early Golgi cisternae plus a similar number of late or *trans*-Golgi network (TGN) cisternae (Papanikou and Glick, 2009). Early yeast Golgi cisternae mature to generate late Golgi cisternae, a process that appears to be evolutionarily conserved (Glick and Nakano, 2009; Losev et al., 2006; Matsuura-Tokita et al., 2006).

S. cerevisiae can be used to study the regulation of Golgi structure. In a microscopy-based screen to identify thermosensitive mutants defective in Golgi inheritance, we also identified mutants that contained fewer and larger Golgi cisternae (Rossanese et al., 2001). A similar phenotype had been described for the ADP-ribosylation factor 1 (*ARF1*)-deleted (*arf1Δ*) mutant (Gaynor et al., 1998). *S. cerevisiae* contains the closely related genes *ARF1* and *ARF2*, with *ARF1* accounting for ~90% of the Golgi-associated Arf (Stearns et al., 1990a). *arf1Δ* mutants show abnormal Golgi structure but only mild defects in secretion (Gaynor et al., 1998; Stearns et al., 1990b). We find that a thermosensitive mutant has enlarged Golgi cisternae due to impaired function of the *N*-myristoyl transferase Nmt1 (Johnson et al., 1994), which activates Arf (Donaldson and Jackson, 2011; Kahn, 2009). Thus, separate lines of investigation have pointed to Arf as a key regulator of Golgi size and number.

To clarify the mechanisms that generate enlarged Golgi cisternae, we used four-dimensional (4D) fluorescence microscopy. The results indicate that during Golgi maturation, early Golgi cisternae mature more slowly and less frequently in *arf1Δ* cells than in wild-type cells. By contrast, after the early-to-late Golgi transition, the maturation kinetics in *arf1Δ* cells are

[1]Advanced Centre for Treatment Research & Education in Cancer (ACTREC), Tata Memorial Centre, Kharghar, Navi Mumbai, 410210 MH, India. [2]Department of Molecular Genetics and Cell Biology, The University of Chicago, 920 East 58th Street, Chicago, IL 60637, USA. [3]Electron Microscopy Core Facility, The University of Chicago, Gordon Center for Integrated Science, 929 East 57th Street, Chicago, IL 60637, USA.
*These authors contributed equally to this work

‡Author for correspondence (dbhattacharyya@actrec.gov.in)

Received 28 August 2013; Accepted 17 October 2013

Journal of Cell Science

Journal of Cell Science (2014) 127, 250–257 doi:10.1242/jcs.140996

essentially normal. The consequence of these selective changes is a severe reduction in the number of late Golgi cisternae. Our analysis highlights the importance of kinetic parameters for regulating the size and copy number of dynamic compartments.

RESULTS

A mutation in *NMT1* results in enlarged late Golgi cisternae

We used a thermosensitive yeast mutant that has larger and fewer late Golgi cisternae, as marked by Sec7–GFP (Rossanese et al., 2001). For further analysis, we also labeled the plasma membrane with mCherry–Ras2 (Tang et al., 2009). Late Golgi cisternae were visualized with 2D projections, and with 3D rendering that represented a cisterna as a closed surface (Fig. 1A). Although Golgi cisternae are topologically complex (see below), modeling a cisterna as a closed surface enabled us to use volume as a measure of cisternal size. An alternative measure was the maximal diameter of a cisterna in the X–Y plane. Quantification revealed that on average, late Golgi cisternae in mutant cells had approximately threefold greater volume and approximately twofold greater diameter than in wild-type cells (Fig. 1B,C).

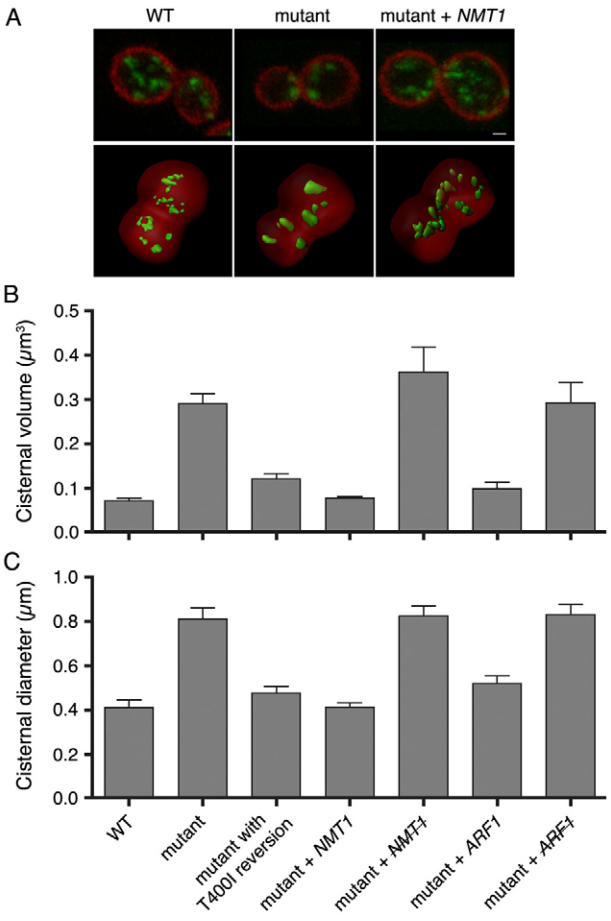

Fig. 1. A conditional mutation in *NMT1* generates enlarged late Golgi cisternae. (A) Representative images of the wild-type (WT) parental strain, the thermosensitive mutant, and the mutant transformed with a centromeric plasmid encoding *NMT1*. The plasma membrane was labeled with mCherry–Ras2 (red), and the late Golgi was labeled with Sec7–GFPx3 (green). The top row shows projected confocal sections of a central portion of the cell, and the bottom row shows 3D renderings. Scale bar: 1 μm. (B,C) Images of the type shown in A were quantified by rendering late Golgi cisternae as closed surfaces. The following strains were examined: the wild-type, the thermosensitive mutant, the mutant in which the *nmt1* T400I mutation was reverted by gene replacement, the mutant transformed with a centromeric plasmid encoding *NMT1*, the mutant transformed with the plasmid encoding *NMT1* and then cured of this plasmid (indicated by the strikethrough), the mutant transformed with a high copy number plasmid encoding *ARF1*, and the mutant transformed with the plasmid encoding *ARF1* and then cured of this plasmid (indicated by the strikethrough). Sizes of the rendered late Golgi elements were quantified by measuring either (B) the average volume or (C) the average X–Y-plane diameter. Error bars indicate s.e.m.

To identify the mutated gene, a genomic library was screened for complementation of the thermosensitive growth defect (Rossanese et al., 2001). Two overlapping clones rescued the growth and Golgi size phenotypes (Fig. 1A–C). The overlapping region contained *NMT1*, which encodes *N*-myristoyl transferase (Johnson et al., 1994). Rescue of the mutant phenotypes was lost if mutant cells were cured of a plasmid carrying *NMT1* (Fig. 1B,C). The *nmt1* allele had a T400I mutation, and the growth and Golgi size phenotypes were rescued by reverting this mutation in the genome (Fig. 1B,C; supplementary material Fig. S1). Thus, a point mutation in *NMT1* leads to enlarged late Golgi cisternae.

Golgi enlargement can be caused by reduced Arf activity

One substrate for Nmt1 is Golgi-associated Arf, a GTPase that recruits multiple effectors, including the COPI coatomer and clathrin adaptors (Donaldson and Jackson, 2011; Kahn, 2009). Because Arf activity depends on N-terminal myristoylation, we suspected that the enlarged Golgi cisternae in the *nmt1* strain were due to reduced myristoylation of Arf.

This hypothesis was tested in two ways. First, we compensated for impaired Nmt1 activity in the mutant strain by overexpressing *ARF1*. Elevated Arf1 levels suppressed the Golgi size phenotype, and this effect was lost if the mutant cells were cured of the plasmid (Fig. 1B,C; supplementary material Fig. S1). Second, we deleted *ARF1* to confirm that reduced Arf levels cause Golgi enlargement in our strain. Indeed, *arf1Δ* cells contained a small number of late Golgi cisternae that were often abnormally large (Fig. 2A,B). Thus, depletion or partial inactivation of Golgi-associated Arf leads to larger and fewer late Golgi cisternae.

It was reported that *arf1*Δ cells also had enlarged endosomes (Gaynor et al., 1998), as judged by labeling the endocytic pathway with the dye FM 4-64 (Vida and Emr, 1995). We observed abnormally large fluorescent compartments after incubating *arf1*Δ cells with FM 4-64 (Fig. 2C). However, FM 4-64 is a bulk membrane marker that moves from the endocytic pathway to the late Golgi/TGN (Lewis et al., 2000), and most of the Sec7–GFP-labeled structures were also labeled with recently internalized FM 4-64 in both wild-type and *arf1*Δ cells (Fig. 2C). We conclude that in *arf1*Δ cells, the enlarged compartments containing FM 4-64 are late Golgi cisternae.

The late Golgi in *arf1Δ* cells consist of fenestrated cisternae

Are the late Golgi structures in *arf1Δ* cells large individual cisternae or clusters of smaller cisternae? To address this question, we combined fluorescence microscopy with electron tomography (Kukulski et al., 2011). While optimizing the procedure, we discovered that embedding yeast cells in Lowicryl K4M resin preserved strong GFP fluorescence while yielding sufficient contrast.

For wild-type cells, we labeled late Golgi cisternae with Sec7–GFP, and prepared ~300-nm sections from plastic-embedded samples. Labeled cisternae were visible by fluorescence microscopy (Fig. 2D). The same structures were then analyzed

Journal of Cell Science (2014) 127, 250–257 doi:10.1242/jcs.140996

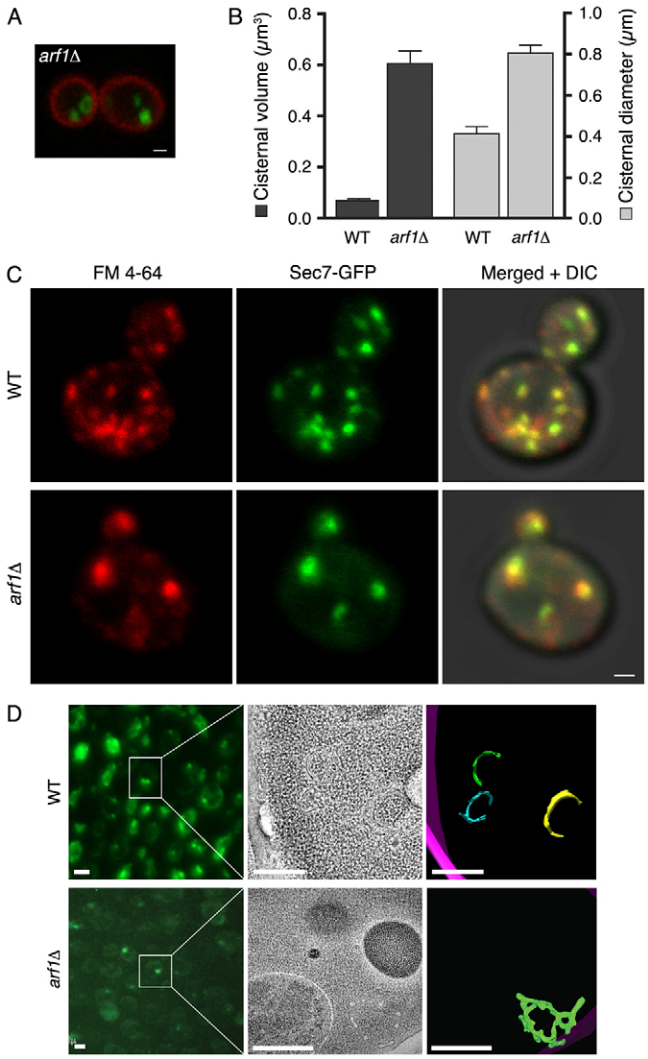

Fig. 2. The *arf1Δ* mutation generates enlarged late Golgi cisternae that label with FM 4-64. (A) *arf1Δ* cells were imaged by fluorescence microscopy as in Fig. 1 to visualize the plasma membrane (red) and late Golgi (green). Scale bar: 1 μm. (B) The average volume and average X–Y-plane diameter of late Golgi cisternae were measured as in Fig. 1 for wild-type and *arf1Δ* strains. Error bars indicate s.e.m. (C) Wild-type or *arf1*Δ cells expressing Sec7-6xGFP were grown in SD medium at 23˚C to an OD_{600} of 0.6, then incubated with 0.8 μM FM 4-64 for 5 minutes. SCAS was added to 4 μM, and cells were compressed beneath a coverslip. Confocal images were captured ~2.5 minutes after SCAS addition. Scale bar: 1 μm. (D) Wild-type or *arf1*Δ cells expressing Sec7-GFPx3 were rapidly frozen, then freeze substituted and embedded in plastic. Left: thick sections were imaged by fluorescence microscopy to identify late Golgi cisternae. Scale bars: 2 μm. Middle: the same sections were analyzed by electron tomography to visualize membranes in tomographic slices. Scale bars: 0.5 μm. Right: membrane contours were traced to model Golgi cisternae (green, blue, yellow) and the plasma membrane (purple). Scale bars: 0.5 μm.

by electron tomography. This method examines a single thick section, so only part of each cisterna was visible, but the results indicated that wild-type late Golgi cisternae were curved and perforated disks (Fig. 2D; supplementary material Movie 1).

For *arf1Δ* cells (Fig. 2D; supplementary material Movies 2, 3), partial reconstructions indicated that mutant late Golgi cisternae were large fenestrated hollow structures, presumably identical to structures previously visualized in *arf1Δ* cells by thin-section electron microscopy (Gaynor et al., 1998). These results confirm that partial depletion of Arf generates abnormally large late Golgi cisternae.

The changes in *arf1Δ* cells are more pronounced for older Golgi cisternae

Late Golgi cisternae are generated by maturation, and we sought to determine where in this pathway the *arf1Δ* mutation exerts its effects. First, we examined transitional endoplasmic reticulum (tER) sites, which produce COPII vesicles (Rossanese et al., 1999; Shindiapina and Barlowe, 2010). Some mutations cause coalescence of these structures (Castillon et al., 2009; Levi et al., 2010; Shindiapina and Barlowe, 2010), but we saw no consistent differences in the tER patterns of wild-type and *arf1Δ* cells (supplementary material Fig. S2), suggesting that the *arf1Δ* mutation acts at the level of the Golgi.

Next, we counted early and late Golgi cisternae by using GFP–Vrg4 as an early Golgi marker, and Sec7–DsRed as a late Golgi marker (Losev et al., 2006). Wild-type cells contained an average of nine early Golgi cisternae and seven late Golgi cisternae (Fig. 3A; Table 1). In the *arf1Δ* strain, early Golgi cisternae tended to be slightly enlarged (supplementary material Fig. S3) and their average number was reduced to five. For the late Golgi, the reduction in the *arf1Δ* strain was more pronounced, with an average of only two cisternae per cell (Fig. 3A and Table 1). Thus, as the Golgi matures, the *arf1Δ* mutation progressively reduces the number of cisternae.

Altered maturation kinetics could explain why *arf1Δ* cells have fewer Golgi cisternae

The effects of the *arf1Δ* mutation on Golgi cisternal number might be due to altered maturation kinetics. To test this idea, we devised a simple quantitative framework in which E is the average number of early Golgi cisternae per cell, L is the average number of late Golgi cisternae per cell, m is the average maturation frequency, p_E is the average persistence time of early Golgi cisternae, and p_L is the average persistence time of late Golgi cisternae. m is defined here as the number of early-to-late Golgi transitions per minute, i.e. the frequency at which early Golgi cisternae disappear and late Golgi cisternae appear. Because the average number of Golgi cisternae is constant at steady-state, m also refers to the frequency at which early Golgi cisternae appear. The average number of early or late Golgi cisternae should be equal to the frequency of appearance multiplied by the persistence time. Thus: $E=m\times p_E$ and $L=m\times p_L$. Combining these equations yields: $E/L=p_E/p_L$.

The implications are that changes in maturation frequency or persistence time could alter the number of cisternae, and that a selective change in one of the persistence times could alter the ratio of early to late Golgi cisternae.

The *arf1Δ* mutation slows maturation of the early Golgi

This model was tested by measuring maturation parameters for wild-type and *arf1*Δ strains. An initial experiment employed *arf1*Δ cells expressing Sec7-GFP. In wild-type cells, Sec7–GFP is present on cisternae and then this marker is lost within ~1.5–2 minutes (Losev et al., 2006). The same phenomenon was observed with *arf1Δ* cells. Because this mutant strain has so few late Golgi cisternae, we could often track every Sec7–GFP-labeled structure in a cell. Fig. 3B shows that in a representative cell over a 10-minute period, Sec7–GFP was present on each cisterna and then lost within ~100 seconds. This result suggests

Journal of Cell Science (2014) 127, 250–257 doi:10.1242/jcs.140996

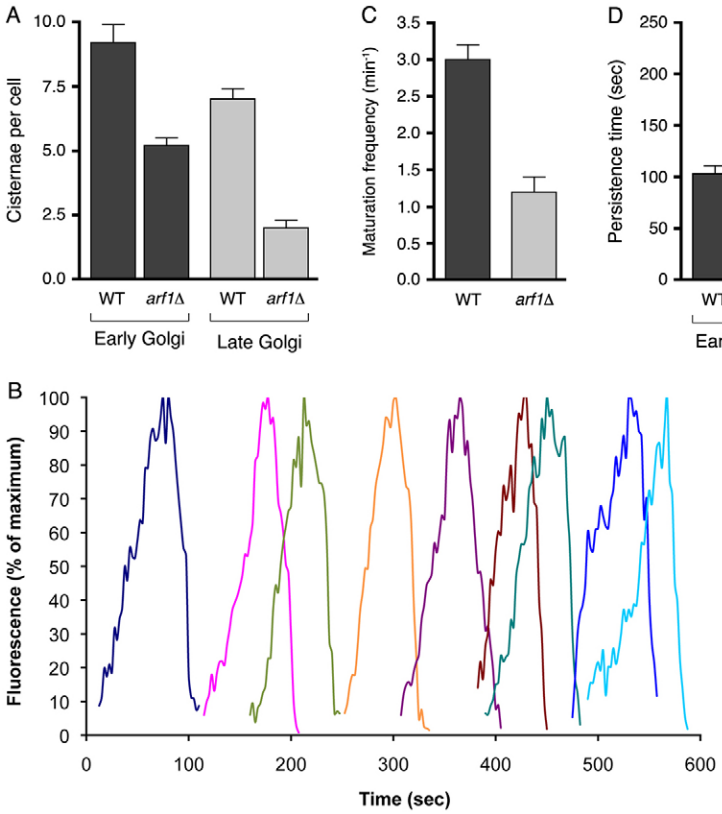

Fig. 3. The *arf1*Δ mutation differentially affects the early and late Golgi. (A) The average numbers of early Golgi cisternae, marked with GFP–Vrg4, or late Golgi cisternae, marked with Sec7–DsRed, in wild-type and *arf1*Δ strains. Error bars indicate s.e.m. (B) A 10-minute 4D movie was generated for an *arf1*Δ cell expressing Sec7-3xGFP. Fluorescence intensities were quantified for each cisterna that appeared and subsequently disappeared during the recording. The different colors represent distinct cisternae. (C) The average frequency of early-to-late Golgi transitions as indicated by loss of GFP–Vrg4 and acquisition of Sec7–DsRed in wild-type and *arf1*Δ strains. Error bars indicate s.e.m. (D) The average persistence time on cisternae of the early Golgi marker GFP–Vrg4 and the late Golgi marker Sec7–DsRed in wild-type and *arf1*Δ strains. Error bars indicate s.e.m.

that late Golgi cisternae function similarly in wild-type and *arf1Δ* cells (Daboussi et al., 2012).

Further analysis was performed with strains expressing GFP-Vrg4 and Sec7-DsRed (supplementary material Movie 4). Dual-color 4D movies were captured for 5 minutes, a period suitable for acquiring closely spaced Z-stacks without excessive photobleaching. To measure the maturation frequency m (Fig. 3C; Table 1), we counted the number of early-to-late Golgi transitions per minute (Losev et al., 2006). To measure the persistence times p_E and p_L (Fig. 3D; Table 1), we identified cisternae that acquired and then lost either GFP–Vrg4 or Sec7–DsRed.

Our analysis revealed a striking effect: the *arf1*Δ mutation selectively increased the early Golgi persistence time p_E. The p_E/p_L ratio was ~1 in wild-type cells but ~2 in *arf1*Δ cells (Table 1). This finding could explain why the number of early Golgi cisternae, E, was similar to the number of late Golgi cisternae, L, in wild-type cells, whereas E was about twice as large as L in *arf1*Δ cells.

Another clear difference between the two strains is the maturation frequency, m, which was ~2.5-fold greater in wild-type cells than in *arf1*Δ cells (Table 1). We infer that the entire early Golgi maturation process is slowed in *arf1*Δ cells, with early Golgi cisternae persisting longer and maturing less frequently than in wild-type cells.

Golgi cisternae undergo homotypic fusion

Table 1 shows a comparison of the measured values E and L, and the corresponding predicted values $m\times p_E$ and $m\times p_L$. The number of late Golgi cisternae, L, agrees reasonably well with the predicted value $m\times p_L$ for both wild-type and *arf1*Δ strains. However, the number of early Golgi cisternae, E, is higher than the predicted value $m\times p_E$ for both strains.

To explore this discrepancy, we re-evaluated the rationale for using $m\times p_E$ as an estimate of E. Because the spatial and temporal resolution of the 4D movies was insufficient for counting early Golgi formation events directly, we assumed that the frequency of early Golgi formation events matched the frequency

Table 1. Parameters for Golgi maturation in wild-type and *arf1*Δ cells

	E	L	m (per minute)	p_E (seconds)	p_L (seconds)	$m\times p_E$	$m\times p_L$
Wild type	9.2±0.7	7.0±0.4	3.0±0.2	103±8	113±10	5.2	5.7
*arf1*Δ	5.2±0.3	2.0±0.3	1.2±0.2	185±19	101±7	3.7	2.0

E, average number of early Golgi cisternae; L, average number of late Golgi cisternae; m, average frequency of Golgi maturation (early-to-late Golgi transitions per minute); p_E, average persistence time of early Golgi cisternae (seconds); and p_L, average persistence time of late Golgi cisternae (seconds).
Values are means ± s.e.m.
As determined by an two-tailed unpaired *t*-test, the following parameters are significantly different for wild-type versus *arf1Δ* cells: E ($P<0.0001$), L ($P<0.0001$), m ($P<0.0001$) and p_E ($P<0.001$).
The last two columns show predicted values of E and L according to the formulas stated in the text.

Journal of Cell Science (2014) 127, 250–257 doi:10.1242/jcs.140996

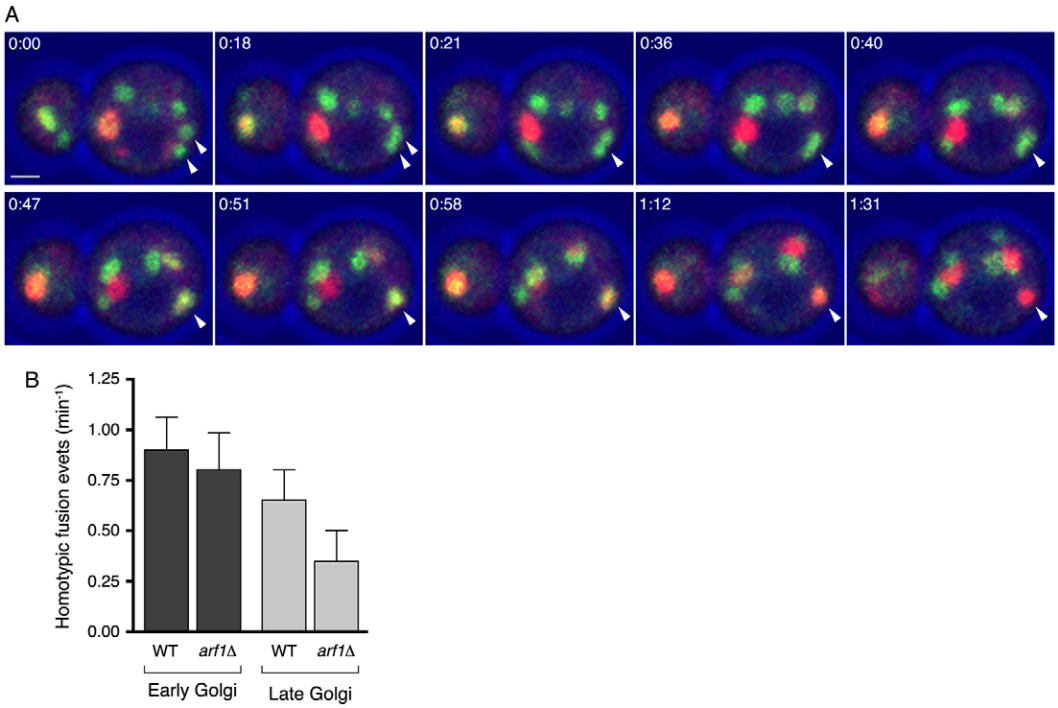

Fig. 4. Golgi cisternae can undergo homotypic fusion. (A) Frames from a 4D movie (supplementary material Movie 4) illustrate a homotypic fusion event in an *arf1*Δ cell. The arrowheads mark two GFP–Vrg4-labeled early Golgi cisternae that fused before maturing into a Sec7–DsRed-labeled late Golgi cisterna. Time is shown in minutes:seconds. Scale bar: 1 μm. (B) The average number of homotypic fusion events per minute for early and late Golgi cisternae in wild-type and *arf1*Δ strains.

of early-to-late Golgi conversion events. This assumption would be incorrect if early Golgi cisternae undergo homotypic fusion. Indeed, such homotypic fusion events take place, as illustrated in Fig. 4A and supplementary material Movie 4. A typical wild-type or *arf1Δ* cell exhibited about one early Golgi homotypic fusion event per minute (Fig. 4B). As a consequence of homotypic fusion, the frequency of early Golgi formation events is higher than the maturation frequency m, so $m \times p_E$ is an underestimate of the number of early Golgi cisternae.

Despite the limitations caused by homotypic fusion, the quantitative framework yields two strong conclusions (supplementary material Fig. S4). First, the reason that *arf1*Δ cells contains more early than late Golgi cisternae is that in these cells, early Golgi cisternae persist longer than late Golgi cisternae. Second, the reason that *arf1*Δ cells have fewer late Golgi cisternae than wild-type cells is that *arf1*Δ cells have an abnormally low frequency of early-to-late Golgi transitions but a normal persistence time for the late Golgi.

DISCUSSION

Rates of membrane influx and efflux can regulate the overall size of the mammalian Golgi (Guo and Linstedt, 2006; Sengupta and Linstedt, 2011), and we find that in *S. cerevisiae*, kinetic parameters can also regulate Golgi copy number. Because Golgi cisternae are constantly turning over, the copy number of a Golgi compartment depends on how often the compartment forms and how long it persists. The total amount of Golgi material is presumably comparable in different strains, so when the number of Golgi cisternae in a strain is abnormally small, the average size of the cisternae is abnormally large. Thus, the rates of processes that transform a maturing compartment can dramatically influence compartmental size and copy number.

Slowed maturation of the early Golgi in *arf1Δ* cells helps to explain the observed delay in secretion (Gaynor et al., 1998), but the mechanism by which partial depletion of Arf alters Golgi maturation remains to be determined. A decrease in Golgi-associated Arf may compromise the recruitment or function of the COPI vesicle coat. In support of this idea, a thermosensitive COPI allele was reported to slow Golgi maturation at the restrictive temperature (Matsuura-Tokita et al., 2006). Another possibility is that Arf depletion perturbs lipid metabolism (Gaynor et al., 1998). Indeed, the *arf1Δ* mutation induces the unfolded protein response (Jonikas et al., 2009), which in turn alters phospholipid biosynthesis and other aspects of the secretory pathway (Travers et al., 2000). Regardless of the specific processes that are affected, it is notable that two previous studies of Golgi cisternal enlargement in *S. cerevisiae* both implicated Arf (Gaynor et al., 1998; Peyroche et al., 2001) and that our identification of the *nmt1* mutant points to Arf as well. These findings support the idea that Arf is a regulator of Golgi maturation (Stalder and Antonny, 2013).

How might our results be relevant to organisms with a stacked Golgi? We propose that changes in the kinetics of Golgi maturation could alter the number of cisternae per stack. Golgi cisternal number is variable between different cell types – in mammals, the number of cisternae per stack ranges from about 3 to 10 depending on the cell type (Rambourg and Clermont, 1997). Large Golgi stacks typically contain multiple COPI-vesicle-producing Golgi cisternae but only one or two clathrin-coated vesicle-producing TGN cisternae (Mogelsvang et al., 2004; Staehelin and Kang, 2008). By analogy to the *arf1Δ* mutant, if the persistence time of Golgi cisternae increased while the persistence time of TGN cisternae remained unchanged, the result would be a selective increase in the number of Golgi cisternae

Journal of Cell Science (2014) 127, 250–257 doi:10.1242/jcs.140996

Fig. 5. Changes in maturation kinetics could alter the number of cisternae in a stacked Golgi. A Golgi stack is represented as consisting of two classes of cisternae: the Golgi itself (green) and the *trans*-Golgi network (TGN; orange). These classes would correspond in *S. cerevisiae* to the early and late Golgi, respectively. If the persistence time of Golgi cisternae were increased without changing other parameters, the stack would contain more Golgi cisternae but the same number of TGN cisternae.

(Fig. 5). Interestingly, when mammalian cells are depleted of the Rab6 GTPase, secretion slows and the number of Golgi cisternae per stack increases (Storrie et al., 2012). It is possible that Rab6 depletion increases the persistence time of Golgi cisternae. Future developments in live-cell microscopy should enable a test of our hypothesis that maturation kinetics regulate the size of Golgi stacks.

MATERIALS AND METHODS

Yeast strains and plasmids

All experiments were performed with derivatives of the haploid *S. cerevisiae* strain JK9-3d, which has the genotype *leu2-3,112 ura3-52 rme1 trp1 his4* (Kunz et al., 1993). A mutant with enlarged late Golgi cisternae (Rossanese et al., 2001) was backcrossed four times to the parental strain, and thermosensitive growth segregated with the enlarged Golgi phenotype as a single-gene mutation through each cross. Yeast were grown in rich glucose medium (YPD) or minimal glucose medium (SD) (Sherman, 1991), with shaking at 200 r.p.m. in baffled flasks. Growth media were obtained from HiMedia Laboratories (Mumbai, India) or Difco Laboratories (Detroit, MI, USA). Wild-type strains were grown at 30°C unless otherwise indicated. Thermosensitive mutants were grown at 25°C, and then shifted to 37°C for 30 minutes before analysis. Molecular biology procedures were simulated and recorded using SnapGene software (GSL Biotech, Chicago, IL, USA; http://www.snapgene.com).

Integrating or centromeric plasmids were transformed into yeast using the lithium acetate method (Gietz and Woods, 2002), and chromosomal gene replacements were performed using the pop-in/pop-out method (Rothstein, 1991). *SEC7* was tagged by gene replacement with three or six tandem copies of monomeric EGFP (mEGFP) (Zacharias et al., 2002) as previously described (Rossanese et al., 2001). Additional integrating constructs were used to overexpress either Sec7-3xmEGFP or Sec7-6xDsRed.M1 (Losev et al., 2006). Vrg4 was tagged at its N-terminus with sGFP by gene replacement (Losev et al., 2006). Sec13 was tagged at its C-terminus with EGFP by gene replacement (Rossanese et al., 1999). Ras2 was tagged at its N-terminus with mCherry (Shaner et al., 2004) as follows. The *RAS2* gene plus flanking sequences were amplified using forward primer 5′-TCGATGAATTCTAGCTCTCGGGCGAATATC-3′ and reverse primer 5′-TCTAAGGGGAAAGAGAAGCTTG-3′. The PCR product was digested with *Eco*RI and *Hin*dIII and subcloned at the same sites in the centromeric *URA3* plasmid YCplac33 (Gietz and Sugino, 1988). A *Bam*HI-*Not*I cassette was then introduced by primer-directed mutagenesis at the *RAS2* start codon. mCherry was amplified with primers 5′-tggtaGGATCCATGGTGAGCAAGGGCGAGGA-3′ and 5′-tgttcGCGGCCGCaCTTGTACAGCTCGTCCATGC-3′, and the PCR product was subcloned as a *Bam*HI–*Not*I fragment. A *Bam*HI–*Hin*dIII fragment encoding mCherry–Ras2 was then subcloned into the *TRP1* integrating plasmid YIplac204-T/C to drive strong constitutive expression from the *TPI1* promoter (Losev et al., 2006). This construct was linearized with *Eco*RV for integration at the *TRP1* locus.

To complement the *nmt1* mutation, the wild-type *NMT1* gene with its 5′ and 3′ control regions was amplified with primers 5′-AAGTATAAGCTTGCTATCGTTTACAAATTAAA-3′ and 5′-CGCTGGGTACCATTTTTTCACTTCGTCAATTGAC-3′, and subcloned as *Hin*dIII–*Kpn*I fragment into YCplac33. To overexpress *ARF1*, this gene with its 5′ and 3′ control regions was amplified with primers 5′-TGCACAGTTGAATTCTCG-3′ and 5′-GATGAAAGCTT-CTGCAGTTGTCAGTC-3′, and subcloned as an *Eco*RI–*Hin*dIII fragment into the high-copy episomal *URA3* plasmid YEplac195 (Gietz and Sugino, 1988). Where indicated, strains were cured of the *URA3* plasmids by growth on plates containing 1 mg/ml 5-fluoroorotic acid (United States Biological, Salem, MA, USA).

To revert the T400I mutation in the *nmt1* mutant, a fragment of the wild-type *NMT1* gene was amplified with primers 5′-GCCACCA-AGCTTACACCGGAAGATATATCTGA-3′ and 5′-CGCTGGGTACC-ATTTTTTCACTTCGTCAATTGAC-3′, and subcloned as a *Hin*dIII–*Kpn*I fragment into a modified *URA3* integrating plasmid YIplac211 (Gietz and Sugino, 1988) that had been mutagenized to remove the *Eco*RI site. One of the two *Eco*RI sites in the *NMT1* fragment was then removed by changing codon 293 from GAA to GAG. The final construct was linearized at the unique *Eco*RI site for integrative gene replacement, and the reverted *NMT1* allele was confirmed by PCR amplification and sequencing of genomic DNA. To delete the *ARF1* gene, the *kanMX* cassette was amplified with the following primers to append sequences that matched the regions flanking the *ARF1* open reading frame: 5′-ATTGAAGGTATAAGAAAGAACTCAAACAGGTTTAATAGAATTA-AAACGTACGCTGCAGGTCGAC-3′ and 5′-TTCATTTAGTTTATA-CAAGCGTATTTGATCCATATTCTAGAATTTATCGATGAATTCGA-GCTCG-3′. The resulting fragment was transformed into cells, which were plated on YPD medium containing 250 µg/ml G418 (Sigma-Aldrich, St. Louis, MO, USA) to select for double-crossover replacement of the *ARF1* open reading frame (Wach et al., 1994).

Fluorescence image capture and processing

To capture static images of fluorescently tagged tER sites, live yeast cells were compressed beneath a coverslip and viewed using a Zeiss Axioplan 2 microscope with a 100× 1.4 NA objective. A single image plane was captured with a Hamamatsu digital camera. To quantify the number of tER sites, Z-stacks were captured with a Zeiss LSM 780 confocal microscope. Each confocal 3D data set was opened with Imaris software (Bitplane, Zurich, Switzerland). The spot detection option was used, with the threshold set to detect even the smallest fluorescent tER sites. The number of spots was then counted in randomly chosen full-size ‘mother’ cells.

To capture static images of cells labeled with FM 4-64, dye in a 1 mM DMSO stock solution was added to a log-phase culture at 23°C. After a brief incubation, non-internalized dye was quenched by adding excess SCAS (4-sulfonato calix[8]arene, sodium salt; Biotium, Hayward, CA, USA) from a 1 mM aqueous stock solution. Cells were then mixed with 3.0 µm polystyrene beads (Polysciences, Warrington, PA, USA), compressed beneath a coverslip that had been siliconized with Sigmacote (Sigma-Aldrich), and viewed with a Zeiss LSM 710. GFP fluorescence was excited with a 488-nm laser and collected between 495 and 550 nm, and simultaneously, FM 4-64 fluorescence was excited with a 561-nm laser and collected between 650 and 760 nm. A 3D image volume spanning an entire cell was captured using a pixel size of 40 nm and Z-stack spacing of 0.47 µm. Image stacks were converted to 16-bit and average projected using ImageJ (http://rsbweb.nih.gov/ij/).

Confocal imaging was performed with either a Leica SP5 or a Zeiss LSM 780 for 4D imaging, or a Zeiss LSM 510 META or LSM 710 for single time-point measurements, equipped with 100× or 63× 1.4 NA objectives. Cells grown to log phase at 25°C or 30°C in nonfluorescent or minimally fluorescent SD medium were immobilized on glass-bottomed dishes (Cell E&G, Houston, TX, USA) using concanavalin A (Sigma-Aldrich) as previously described (Bevis et al., 2002), and were imaged at room temperature. Single- or dual-color data sets were obtained using separate excitation and capture of red and green signals, with a pinhole of 1.0–1.2 AU and with line averaging of 4 to improve the signal-to-noise ratio. Transmitted light images were captured in the blue channel. The pixel size was 70–90 nm. Optical sections were 0.25–0.40 µm apart, and

~15–20 optical sections were collected to span an entire cell. Z-stacks were collected at intervals of 2–4 seconds. To limit photodamage, laser illumination was minimized and confocal scans were carried out as quickly as possible.

Fluorescence micrographs were assembled using Adobe Photoshop, with uniform adjustments of brightness where appropriate. Projected movies of 4D confocal data sets were generated and quantified using ImageJ as follows. To remove shot noise, individual optical sections were processed with a custom plugin that implemented a 3D version of a 3×3 hybrid median filter (Hammond and Glick, 2000). The processed optical sections were then average projected and corrected for exponential photobleaching (Bevis et al., 2002), and the fluorescence and transmitted light channels were merged. Quantification of late Golgi fluorescence intensities was performed as previously described (Losev et al., 2006).

For measurements of cisternal size, a confocal 3D data set was opened with Imaris. After the image was cropped, the surface fill option was used to define a closed surface around each fluorescent structure of average diameter at least 0.5 µm, with objects being smoothed using a filter radius of 0.05 µm. The rendered 3D objects were then analyzed to obtain the desired parameters. To calculate the average volume of late Golgi cisternae, 60 cells were imaged for each strain, and all of the rendered cisternae were measured. The corresponding volume measurements of early Golgi cisternae were performed on 20 cells for each strain. To calculate the average X–Y-plane diameter, 10 cells were imaged for each strain, and the maximal X–Y-plane diameter was measured for three or four representative cisternae from each cell.

For measurements of maturation and homotypic fusion parameters, a confocal 4D data set was opened with Imaris. The image was exported to Fiji (http://fiji.sc/Fiji), and shot noise was removed by processing individual optical sections with a custom plug-in that implemented a 3D version of a 3×3 hybrid median filter with a tight mean. The processed optical sections were then corrected for exponential photobleaching, and the fluorescence and transmitted light channels were merged. This processed image was imported back into Imaris for visual inspection and manual quantification.

Quantitative analysis of maturation and homotypic fusion

All measurements were performed using the same set of 20 dual-color 5-minute 4D movies, with 10 movies each for wild-type and *arf1*Δ strains expressing GFP-Vrg4 and Sec7-DsRed. A single full-size 'mother' cell from each movie was analyzed using Imaris. To count early and late Golgi cisternae in a cell, the numbers of green and red spots in each movie were recorded at 10 successive time points and averaged, with a spot being recorded only if it persisted for at least two consecutive time points. To measure the maturation frequency, the number of maturation events in each movie was counted during each of minutes 2, 3 and 4, with a cisterna being tracked for additional time if needed to verify the maturation event. To measure the persistence times of early and late Golgi cisternae, 20 cisternae that could be seen to acquire and then lose either the early or the late Golgi marker were chosen at random from the 10 movies, and the fluorescence duration for each cisterna was measured. To measure the frequency of homotypic fusion, the number of early or late Golgi fusion events was counted during a 2-minute interval for each movie. Cisternae that underwent homotypic fusion were excluded from the measurements of persistence times.

Correlative fluorescence microscopy and electron tomography

Wild-type or *arf1*Δ strains carried a Sec7-3xmEGFP gene replacement plus an integrating vector that drove mild (~3×) overexpression of Sec7-3xmEGFP (Losev et al., 2006). A 100 ml culture was grown in SD medium at 30℃ to mid-log phase with shaking. Cells were then subjected to high-pressure freezing, freeze substitution, and embedding in plastic as described previously (Levi et al., 2010), except that glutaraldehyde was omitted during freeze substitution and the resin was Lowicryl K4M.

Embedded samples were trimmed and cut with a Leica EM UC6 ultramicrotome to produce ~300 nm sections, which were placed on 200 mesh London Finder Formvar/carbon-coated copper grids (Electron Microscopy Sciences, Hatfield, PA, USA). To provide fiducial markers for both light and electron microscopy, 15 nm colloidal gold was applied to both sides of the grid as described previously (Levi et al., 2010). For light microscopy, a grid was placed on a glass slide with the resin side up, and a 22×22 mm number 1.5 glass coverslip with a 10-µl drop of 500 mM Na^+HEPES, pH 7.5 was inverted onto the grid. After capture of fluorescence and differential interference contrast micrographs on a Zeiss Axioplan 2 with a 1.4 NA objective, the grid was retrieved and blotted dry. For embedded wild-type cells, the samples were post-stained for 8 minutes with 2% uranyl acetate in 70% methanol, followed by a water rinse, followed by 5 minutes with Reynold's lead citrate. Cells that showed promising morphologies and fluorescence patterns were analyzed by electron tomography as described previously (Levi et al., 2010). Golgi membrane contours were traced in the tomograms, and the structures were modeled.

Competing interests

The authors declare no competing interests.

Author contributions

O.W.R. provisionally identified the *nmt1* mutant. M.B. and P.I. created yeast strains and acquired images for the *nmt1* analysis, created the *ARF1* overexpression strain, and re-created and modified *arf1Δ* strains for Golgi maturation studies. M.B., P.I., K. Pandya, B.K.J. and C.S. carried out quantitative analyses of the *nmt1* strains. M.B. performed kinetic studies of Golgi maturation in wild-type and *arf1Δ* cells by collecting 4D movies and analyzing the data. M.B., P.I., K. Pandya, B.K.J., A.G. and K. Pawar measured persistence times, cisternal numbers, and other Golgi parameters. E.P. analyzed tER structure, and worked with K.J.D. on initial kinetic studies of *arf1Δ* cells. E.P. and J.A. performed correlative fluorescence and electron tomography. K.J.D. analyzed FM 4-64 localization. B.S.G. and D.B. supervised the project and assembled the manuscript and figures.

Funding

This work was supported by the Department of Biotechnology [grant number 102/IFD/SAN/2282/2012-2013 to D.B and C.S.]; the Council of Scientific and Industrial Research [doctoral fellowship Ref. no. 20-6/2009 (i) EU-IV to M.B.]; the Council of Scientific and Industrial Research grant [grant number 37(1553)112/EMR-II to K. Pandya]; an Advanced Centre for Treatment, Research and Education in Cancer doctoral fellowship to A.G., B.K.J. and P.I.; the National Institutes of Health [grant numbers R01 GM061156 and R01 GM104010 to B.S.G.]; and a National Institutes of Health training grant [grant number T32 GM007183 to K.J.D. and O.W.R.]. Deposited in PMC for release after 12 months.

Supplementary material

Supplementary material available online at
http://jcs.biologists.org/lookup/suppl/doi:10.1242/jcs.140996/-/DC1

References

Bevis, B. J., Hammond, A. T., Reinke, C. A. and Glick, B. S. (2002). *De novo* formation of transitional ER sites and Golgi structures in Pichia pastoris. *Nat. Cell Biol.* **4**, 750-756.

Castillon, G. A., Watanabe, R., Taylor, M., Schwabe, T. M. and Riezman, H. (2009). Concentration of GPI-anchored proteins upon ER exit in yeast. *Traffic* **10**, 186-200.

Chan, D. C. (2012). Fusion and fission: interlinked processes critical for mitochondrial health. *Annu. Rev. Genet.* **46**, 265-287.

Daboussi, L., Costaguta, G. and Payne, G. S. (2012). Phosphoinositide-mediated clathrin adaptor progression at the *trans*-Golgi network. *Nat. Cell Biol.* **14**, 239-248.

Donaldson, J. G. and Jackson, C. L. (2011). ARF family G proteins and their regulators: roles in membrane transport, development and disease. *Nat. Rev. Mol. Cell Biol.* **12**, 362-375.

Epp, N., Rethmeier, R., Krämer, L. and Ungermann, C. (2011). Membrane dynamics and fusion at late endosomes and vacuoles – Rab regulation, multisubunit tethering complexes and SNAREs. *Eur. J. Cell Biol.* **90**, 779-785.

Gaynor, E. C., Chen, C. Y., Emr, S. D. and Graham, T. R. (1998). ARF is required for maintenance of yeast Golgi and endosome structure and function. *Mol. Biol. Cell* **9**, 653-670.

Gietz, R. D. and Sugino, A. (1988). New yeast-Escherichia coli shuttle vectors constructed with in vitro mutagenized yeast genes lacking six-base pair restriction sites. *Gene* **74**, 527-534.

Gietz, R. D. and Woods, R. A. (2002). Transformation of yeast by lithium acetate/single-stranded carrier DNA/polyethylene glycol method. *Methods Enzymol.* **350**, 87-96.

Glick, B. S. and Nakano, A. (2009). Membrane traffic within the Golgi apparatus. *Annu. Rev. Cell Dev. Biol.* **25**, 113-132.

Goehring, N. W. and Hyman, A. A. (2012). Organelle growth control through limiting pools of cytoplasmic components. *Curr. Biol.* **22**, R330-R339.
Guo, Y. and Linstedt, A. D. (2006). COPII-Golgi protein interactions regulate COPII coat assembly and Golgi size. *J. Cell Biol.* **174**, 53-63.
Hammond, A. T. and Glick, B. S. (2000). Raising the speed limits for 4D fluorescence microscopy. *Traffic* **1**, 935-940.
Johnson, D. R., Bhatnagar, R. S., Knoll, L. J. and Gordon, J. I. (1994). Genetic and biochemical studies of protein N-myristoylation. *Annu. Rev. Biochem.* **63**, 869-914.
Jonikas, M. C., Collins, S. R., Denic, V., Oh, E., Quan, E. M., Schmid, V., Weibezahn, J., Schwappach, B., Walter, P., Weissman, J. S. et al. (2009). Comprehensive characterization of genes required for protein folding in the endoplasmic reticulum. *Science* **323**, 1693-1697.
Kahn, R. A. (2009). Toward a model for Arf GTPases as regulators of traffic at the Golgi. *FEBS Lett.* **583**, 3872-3879.
Kellokumpu, S., Sormunen, R. and Kellokumpu, I. (2002). Abnormal glycosylation and altered Golgi structure in colorectal cancer: dependence on intra-Golgi pH. *FEBS Lett.* **516**, 217-224.
Kirk, S. J., Cliff, J. M., Thomas, J. A. and Ward, T. H. (2010). Biogenesis of secretory organelles during B cell differentiation. *J. Leukoc. Biol.* **87**, 245-255.
Kukulski, W., Schorb, M., Welsch, S., Picco, A., Kaksonen, M. and Briggs, J. A. (2011). Correlated fluorescence and 3D electron microscopy with high sensitivity and spatial precision. *J. Cell Biol.* **192**, 111-119.
Kunz, J., Henriquez, R., Schneider, U., Deuter-Reinhard, M., Movva, N. R. and Hall, M. N. (1993). Target of rapamycin in yeast, TOR2, is an essential phosphatidylinositol kinase homolog required for G1 progression. *Cell* **73**, 585-596.
Levi, S. K., Bhattacharyya, D., Strack, R. L., Austin, J. R. I., 2nd and Glick, B. S. (2010). The yeast GRASP Grh1 colocalizes with COPII and is dispensable for organizing the secretory pathway. *Traffic* **11**, 1168-1179.
Levy, D. L. and Heald, R. (2012). Mechanisms of intracellular scaling. *Annu. Rev. Cell Dev. Biol.* **28**, 113-135.
Lewis, M. J., Nichols, B. J., Prescianotto-Baschong, C., Riezman, H. and Pelham, H. R. B. (2000). Specific retrieval of the exocytic SNARE Snc1p from early yeast endosomes. *Mol. Biol. Cell* **11**, 23-38.
Losev, E., Reinke, C. A., Jellen, J., Strongin, D. E., Bevis, B. J. and Glick, B. S. (2006). Golgi maturation visualized in living yeast. *Nature* **441**, 1002-1006.
Lu, Z., Joseph, D., Bugnard, E., Zaal, K. J. M. and Ralston, E. (2001). Golgi complex reorganization during muscle differentiation: visualization in living cells and mechanism. *Mol. Biol. Cell* **12**, 795-808.
Marshall, W. (2002). Size control in dynamic organelles. *Trends Cell Biol.* **12**, 414-419.
Marshall, W. F. (2012). Organelle size control systems: from cell geometry to organelle-directed medicine. *Bioessays* **34**, 721-724.
Matsuura-Tokita, K., Takeuchi, M., Ichihara, A., Mikuriya, K. and Nakano, A. (2006). Live imaging of yeast Golgi cisternal maturation. *Nature* **441**, 1007-1010.
Mogelsvang, S., Marsh, B. J., Ladinsky, M. S. and Howell, K. E. (2004). Predicting function from structure: 3D structure studies of the mammalian Golgi complex. *Traffic* **5**, 338-345.
Mowbrey, K. and Dacks, J. B. (2009). Evolution and diversity of the Golgi body. *FEBS Lett.* **583**, 3738-3745.
Papanikou, E. and Glick, B. S. (2009). The yeast Golgi apparatus: insights and mysteries. *FEBS Lett.* **583**, 3746-3751.
Peyroche, A., Courbeyrette, R., Rambourg, A. and Jackson, C. L. (2001). The ARF exchange factors Gea1p and Gea2p regulate Golgi structure and function in yeast. *J. Cell Sci.* **114**, 2241-2253.
Preuss, D., Mulholland, J., Franzusoff, A., Segev, N. and Botstein, D. (1992). Characterization of the *Saccharomyces* Golgi complex through the cell cycle by immunoelectron microscopy. *Mol. Biol. Cell* **3**, 789-803.
Rambourg, A. and Clermont, Y. (1997). Three-dimensional structure of the Golgi apparatus in mammalian cells. In *The Golgi Apparatus* (ed. E. G. Berger and J. Roth), pp. 37-61. Basel: Birkhäuser Verlag.
Rossanese, O. W., Soderholm, J., Bevis, B. J., Sears, I. B., O'Connor, J., Williamson, E. K. and Glick, B. S. (1999). Golgi structure correlates with transitional endoplasmic reticulum organization in Pichia pastoris and Saccharomyces cerevisiae. *J. Cell Biol.* **145**, 69-81.
Rossanese, O. W., Reinke, C. A., Bevis, B. J., Hammond, A. T., Sears, I. B., O'Connor, J. and Glick, B. S. (2001). A role for actin, Cdc1p, and Myo2p in the inheritance of late Golgi elements in Saccharomyces cerevisiae. *J. Cell Biol.* **153**, 47-62.
Rothstein, R. (1991). Targeting, disruption, replacement, and allele rescue: integrative DNA transformation in yeast. *Methods Enzymol.* **194**, 281-301.
Sengupta, D. and Linstedt, A. D. (2011). Control of organelle size: the Golgi complex. *Annu. Rev. Cell Dev. Biol.* **27**, 57-77.
Shaner, N. C., Campbell, R. E., Steinbach, P. A., Giepmans, B. N. G., Palmer, A. E. and Tsien, R. Y. (2004). Improved monomeric red, orange and yellow fluorescent proteins derived from Discosoma sp. red fluorescent protein. *Nat. Biotechnol.* **22**, 1567-1572.
Sherman, F. (1991). Getting started with yeast. *Methods Enzymol.* **194**, 3-21.
Shindiapina, P. and Barlowe, C. (2010). Requirements for transitional endoplasmic reticulum site structure and function in Saccharomyces cerevisiae. *Mol. Biol. Cell* **21**, 1530-1545.
Staehelin, L. A. and Kang, B. H. (2008). Nanoscale architecture of endoplasmic reticulum export sites and of Golgi membranes as determined by electron tomography. *Plant Physiol.* **147**, 1454-1468.
Stalder, D. and Antonny, B. (2013). Arf GTPase regulation through cascade mechanisms and positive feedback loops. *FEBS Lett.* **587**, 2028-2035.
Stearns, T., Kahn, R. A., Botstein, D. and Hoyt, M. A. (1990a). ADP ribosylation factor is an essential protein in Saccharomyces cerevisiae and is encoded by two genes. *Mol. Cell. Biol.* **10**, 6690-6699.
Stearns, T., Willingham, M. C., Botstein, D. and Kahn, R. A. (1990b). ADP-ribosylation factor is functionally and physically associated with the Golgi complex. *Proc. Natl. Acad. Sci. USA* **87**, 1238-1242.
Storrie, B., Micaroni, M., Morgan, G. P., Jones, N., Kamykowski, J. A., Wilkins, N., Pan, T. H. and Marsh, B. J. (2012). Electron tomography reveals Rab6 is essential to the trafficking of *trans*-Golgi clathrin and COPI-coated vesicles and the maintenance of Golgi cisternal number. *Traffic* **13**, 727-744.
Tang, X., Punch, J. J. and Lee, W. L. (2009). A CAAX motif can compensate for the PH domain of Num1 for cortical dynein attachment. *Cell Cycle* **8**, 3182-3190.
Travers, K. J., Patil, C. K., Wodicka, L., Lockhart, D. J., Weissman, J. S. and Walter, P. (2000). Functional and genomic analyses reveal an essential coordination between the unfolded protein response and ER-associated degradation. *Cell* **101**, 249-258.
Vida, T. A. and Emr, S. D. (1995). A new vital stain for visualizing vacuolar membrane dynamics and endocytosis in yeast. *J. Cell Biol.* **128**, 779-792.
Wach, A., Brachat, A., Pöhlmann, R. and Philippsen, P. (1994). New heterologous modules for classical or PCR-based gene disruptions in Saccharomyces cerevisiae. *Yeast* **10**, 1793-1808.
Warren, G. and Rothman, J. (2011). *The Golgi*, pp. 322. Cold Spring Harbor, NY: Cold Spring Harbor Laboratory Press.
Weller, S. G., Capitani, M., Cao, H., Micaroni, M., Luini, A., Sallese, M. and McNiven, M. A. (2010). Src kinase regulates the integrity and function of the Golgi apparatus via activation of dynamin 2. *Proc. Natl. Acad. Sci. USA* **107**, 5863-5868.
Westermann, B. (2010). Mitochondrial dynamics in model organisms: what yeasts, worms and flies have taught us about fusion and fission of mitochondria. *Semin. Cell Dev. Biol.* **21**, 542-549.
Wooding, S. and Pelham, H. R. B. (1998). The dynamics of golgi protein traffic visualized in living yeast cells. *Mol. Biol. Cell* **9**, 2667-2680.
Wu, C. C., Yates, J. R., 3rd, Neville, M. C. and Howell, K. E. (2000). Proteomic analysis of two functional states of the Golgi complex in mammary epithelial cells. *Traffic* **1**, 769-782.
Zacharias, D. A., Violin, J. D., Newton, A. C. and Tsien, R. Y. (2002). Partitioning of lipid-modified monomeric GFPs into membrane microdomains of live cells. *Science* **296**, 913-916.
Zink, D., Fischer, A. H. and Nickerson, J. A. (2004). Nuclear structure in cancer cells. *Nat. Rev. Cancer* **4**, 677-687.

OPEN ACCESS Freely available online

PLoS one

Sec12 Binds to Sec16 at Transitional ER Sites

Elisabeth A. Montegna[1], Madhura Bhave[2], Yang Liu[1], Dibyendu Bhattacharyya[2]*, Benjamin S. Glick[1]*

1 Department of Molecular Genetics and Cell Biology, The University of Chicago, Chicago, Illinois, United States of America, **2** Advanced Centre for Treatment Research and Education in Cancer (ACTREC), Tata Memorial Centre, Kharghar, Navi Mumbai, India

Abstract

COPII vesicles bud from an ER domain known as the transitional ER (tER). Assembly of the COPII coat is initiated by the transmembrane guanine nucleotide exchange factor Sec12. In the budding yeast *Pichia pastoris*, Sec12 is concentrated at tER sites. Previously, we found that the tER localization of *P. pastoris* Sec12 requires a saturable binding partner. We now show that this binding partner is Sec16, a peripheral membrane protein that functions in ER export and tER organization. One line of evidence is that overexpression of Sec12 delocalizes Sec12 to the general ER, but simultaneous overexpression of Sec16 retains overexpressed Sec12 at tER sites. Additionally, when *P. pastoris* Sec12 is expressed in *S. cerevisiae*, the exogenous Sec12 localizes to the general ER, but when *P. pastoris* Sec16 is expressed in the same cells, the exogenous Sec12 is recruited to tER sites. In both of these experimental systems, the ability of Sec16 to recruit Sec12 to tER sites is abolished by deleting a C-terminal fragment of Sec16. Biochemical experiments confirm that this C-terminal fragment of Sec16 binds to the cytosolic domain of Sec12. Similarly, we demonstrate that human Sec12 is concentrated at tER sites, likely due to association with a C-terminal fragment of Sec16A. These results suggest that a Sec12–Sec16 interaction has a conserved role in ER export.

Citation: Montegna EA, Bhave M, Liu Y, Bhattacharyya D, Glick BS (2012) Sec12 Binds to Sec16 at Transitional ER Sites. PLoS ONE 7(2): e31156. doi:10.1371/journal.pone.0031156

Editor: Wanjin Hong, Institute of Molecular and Cell Biology, Singapore

Received November 30, 2011; **Accepted** January 3, 2012; **Published** February 8, 2012

Funding: Research in the Glick lab was supported by National Institute of Health grant R01 GM061156 (BSG) and National Institute of Health training grant T32 GM7183 (EAM). Research in the Bhattacharyya lab was supported by startup funds provided by ACTREC (Advanced Centre for Treatment, Research & Education in Cancer) at the Tata Memorial Centre, and by an Indian government fellowship from the Council of Scientific and Industrial Research (MB). The funders had no role in study design, data collection and analysis, decision to publish, or preparation of the manuscript.

Competing Interests: The authors have declared that no competing interests exist.

* E-mail: dbhattacharyya@actrec.gov.in (DB); bsglick@uchicago.edu (BSG)

Introduction

In the secretory pathway, newly synthesized proteins are exported from the ER in COPII coated transport vesicles [1,2,3]. COPII vesicles bud from ribosome-free ER domains known as transitional ER (tER) sites or ER exit sites [4,5,6]. The mechanism that generates tER sites is unknown, but our working model is that tER sites form by a self-organization process that depends on the specific properties of components involved in COPII assembly [7,8]. Therefore, an analysis of tER site formation must build on knowledge of how COPII coat proteins interact with each other and with partner proteins.

The first step in COPII coat assembly is the exchange of GDP for GTP on the small GTPase Sar1. This reaction is catalyzed by the guanine nucleotide exchange factor Sec12, which spans the ER membrane with its catalytic domain facing the cytosol [9]. Sar1-GTP associates with the ER membrane and recruits the Sec23/24 heterodimer. Sec23 acts as a GTPase activating protein for Sar1, while Sec24 functions to capture cargo into the nascent vesicle [2]. Sec23/24 binds the Sec13/31 heterodimer, which polymerizes to form the outer shell of the coat [10]. In all eukaryotes studied to date, Sec23/24 and Sec13/31 localize to punctate ER regions that operationally define tER sites [5].

By contrast, the localization of Sec12 is variable. In the budding yeast *Pichia pastoris*, Sec12 is concentrated at tER sites [11,12], but in *Saccharomyces cerevisiae*, Sec12 is found throughout the ER [11,13]. This variability suggests that Sec12 localization does not establish tER sites, and indeed, mutations that delocalize *P. pastoris* Sec12 (PpSec12) to the general ER do not prevent tER site formation [12]. Instead, PpSec12 is recruited to tER sites by a partner protein that interacts with the PpSec12 cytosolic domain [12]. Overexpression of PpSec12 results in localization to the general ER, indicating that binding by the partner protein is saturable [12]. Identification of the partner protein should help to clarify the functional significance of this novel Sec12 interaction.

A candidate for the PpSec12 partner protein is Sec16, a large peripheral ER membrane protein that functions in ER export and interacts with multiple COPII pathway components [14,15,16]. In previous work, we isolated a thermosensitive *P. pastoris* mutant with fragmented tER sites, and identified the cause of the defect as a missense mutation in *SEC16* [8]. Sec16 colocalizes with COPII coat proteins at tER sites in both *P. pastoris* and *S. cerevisiae* [8]. Mammalian and *Drosophila* cells also contain Sec16 homologs that localize to tER sites and play a key role in tER organization [17,18,19,20,21]. In the *P. pastoris sec16* strain at the nonpermissive temperature, most of the mutant Sec16 protein is displaced from tER sites, and most of the PpSec12 is delocalized to the general ER [8], consistent with the idea that *P. pastoris* Sec16 (PpSec16) recruits PpSec12 to tER sites.

Here, we demonstrate that a C-terminal fragment of PpSec16 binds to PpSec12, and that this interaction recruits PpSec12 to tER sites. Moreover, mammalian Sec12 is concentrated at tER sites, and the cytosolic domain of mammalian Sec12 can bind to a C-terminal fragment of Sec16A, which is the mammalian ortholog of yeast Sec16. Thus, the Sec12–Sec16 interaction may have a conserved role in generating COPII vesicles and tER sites.

Results

Overexpression of PpSec16 in *P. pastoris* restores tER localization to overexpressed PpSec12

When Glu-Glu epitope-tagged PpSec12 (PpSec12-GG) was expressed at normal levels in *P. pastoris*, this protein localized to tER sites, but when untagged PpSec12 was overexpressed in the same cells, most of the PpSec12-GG molecules were found in the general ER [12]. This general ER pattern included partial or complete fluorescent rings representing the nuclear envelope (Fig. 1, top row). We infer that the PpSec12-GG molecules marked the distribution of the combined pool of tagged and untagged PpSec12 molecules, and that this combined pool had saturated the tER-localized partner protein.

Cells expressing PpSec12-GG and overexpressing PpSec12 were engineered to express GFP-tagged PpSec16 (PpSec16-GFP) at either normal or elevated levels. When PpSec16-GFP was expressed at normal levels, it localized to punctate tER sites that contained only a small fraction of the PpSec12-GG (Fig. 1, top row). However, when PpSec16-GFP was overexpressed, it was found in abnormally large punctate structures that also contained most of the PpSec12-GG (Fig. 1, bottom row). The large punctate structures generated by simultaneous overexpression of PpSec12 and PpSec16 were exaggerated tER sites because they also contained the COPII coat protein Sec13 (Fig. S1). These results are consistent with the idea that PpSec12 binds PpSec16, and that overexpressed PpSec16 recruits overexpressed PpSec12 to tER sites.

PpSec16 can recruit PpSec12 to tER sites in *S. cerevisiae*

As a further test of whether PpSec16 can recruit PpSec12 to tER sites, we expressed both proteins in *S. cerevisiae*, which has numerous small tER sites [11,22,23]. When either PpSec12-GG or Glu-Glu epitope-tagged *S. cerevisiae* Sec12 (ScSec12-GG) was expressed alone in *S. cerevisiae*, the tagged Sec12 was found in the general ER (Fig. 2A) as previously observed [12]. When PpSec16-YFP was simultaneously expressed in *S. cerevisiae*, this protein colocalized with CFP-tagged *S. cerevisiae* Sec13 (ScSec13-CFP) at tER sites, and now PpSec12-GG was also concentrated at tER sites (Fig. 2B). By contrast, expression of PpSec16-YFP in *S. cerevisiae* did not change the localization of ScSec12-GG (Fig. 2B), indicating that the recruitment of PpSec12-GG to tER sites was due to a specific interaction with PpSec16-YFP.

A C-terminal region of PpSec16 is required for PpSec12 localization

As shown in Fig. 3A, PpSec16 contains a central conserved domain (CCD) as well as a conserved C-terminal region (CTR) that is essential for life [8,14]. To determine which parts of PpSec16 affect PpSec12 localization, we systematically deleted nonessential regions of PpSec16 by chromosomal gene replacement, and then examined PpSec12 localization in these cells. All of these strains showed normal tER localization of PpSec12-GG (Fig. 3A,B).

S. cerevisiae and its close relatives contain not only Sec12, but also the Sec12-like protein Sed4, which interacts with a C-terminal fragment of *S. cerevisiae* Sec16 (ScSec16) [24,25,26]. Therefore, we suspected that PpSec12 might interact with a C-terminal fragment of PpSec16. To test this hypothesis, we repeated the experiment of simultaneously overexpressing PpSec12 and PpSec16 in *P. pastoris*, except that the overexpressed PpSec16 was truncated. This truncation removed residues 1967–2550, which encompassed the CTR plus a nonconserved stretch between the glutamine-rich region and the CTR. The truncated PpSec16 was found at tER sites, but unlike intact PpSec16 (see Fig. 1), the truncated PpSec16 was unable to restore tER localization to overexpressed PpSec12 (Fig. 4A). We also expressed the truncated version of PpSec16 in *S. cerevisiae* cells that simultaneously expressed PpSec12. Unlike intact PpSec16 (see Fig. 2B), the truncated PpSec16 was unable to recruit PpSec12 to tER sites (Fig. 4B). These results indicate that a C-terminal fragment of PpSec16 is needed for the tER localization of PpSec12.

To determine which parts of the C-terminal fragment of PpSec16 interact with PpSec12, we made deletions within the C-terminal fragment, and then simultaneously overexpressed PpSec12 and a mutant PpSec16 in *P. pastoris*. Two hundred cells

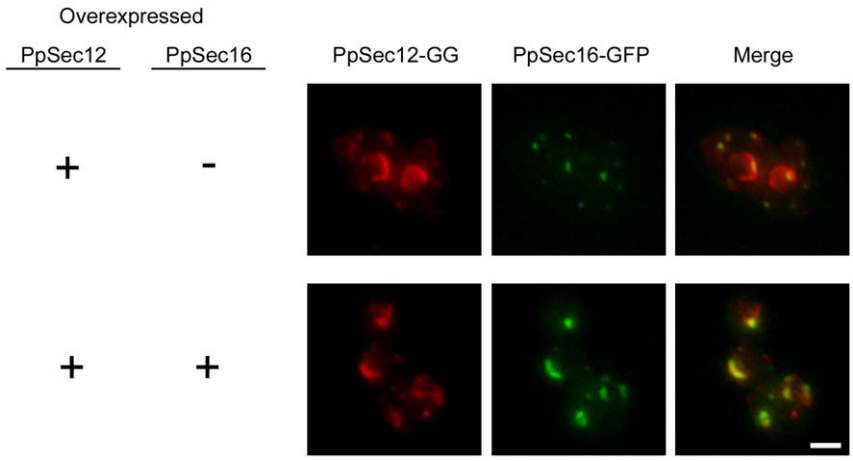

Figure 1. Recruitment of overexpressed PpSec12 to tER sites in *P. pastoris* by simultaneous overexpression of PpSec16. PpSec12 was tagged with the Glu-Glu epitope (PpSec12-GG) by gene replacement, and a second untagged copy of PpSec12 was expressed in the same cells using the methanol-inducible *AOX1* promoter, resulting in a high total level of PpSec12 expression. Top row: in a strain overexpressing PpSec12, PpSec16 was expressed at normal levels after being tagged by gene replacement with GFP. A small fraction of the PpSec12-GG colocalized with PpSec16-GFP, but most of the PpSec12-GG was in the general ER as indicated by the prominent nuclear envelope signal. Bottom row: in a strain overexpressing PpSec12, PpSec16-GFP was overexpressed as a second copy using the *AOX1* promoter. Most of the PpSec12-GG colocalized with PpSec16-GFP in exaggerated tER sites. Scale bar, 2 μm.
doi:10.1371/journal.pone.0031156.g001

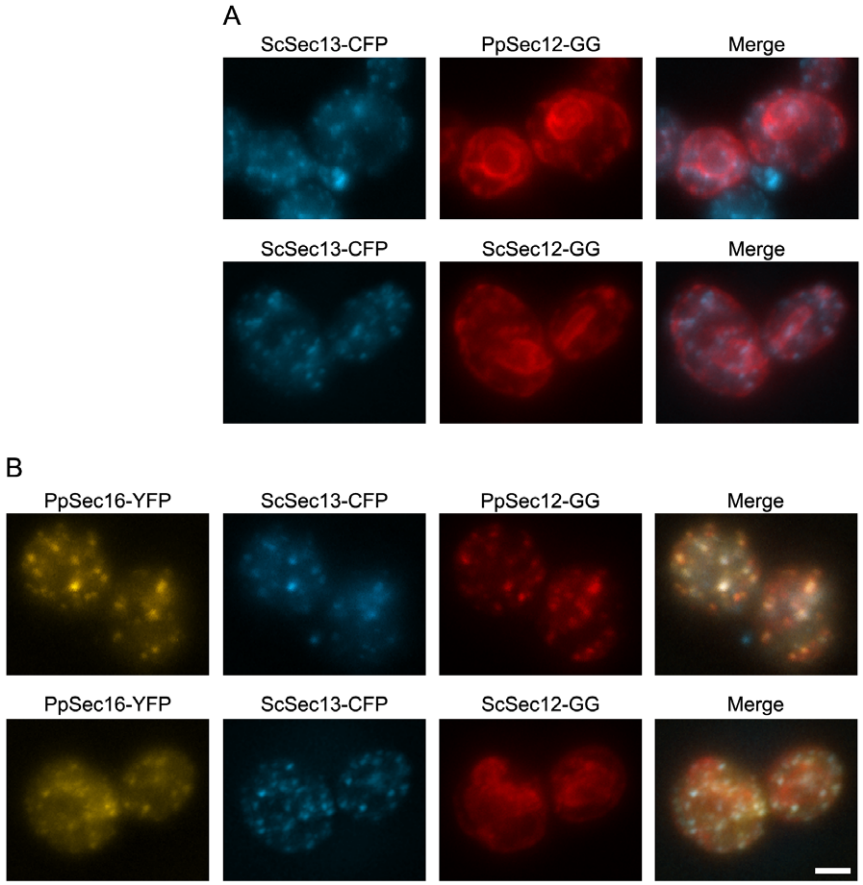

Figure 2. Recruitment of PpSec12 to tER sites in *S. cerevisiae* by simultaneous expression of PpSec16. (A) *S. cerevisiae* cells expressed *S. cerevisiae* Sec13-CFP (ScSec13-CFP) plus either PpSec12-GG (top row) or ScSec12-GG (bottom row). Both versions of Sec12 localized to the general ER. (B) Same as (A), except that the *S. cerevisiae* cells also expressed PpSec16-YFP under control of the inducible *GAL10* promoter. PpSec16-YFP colocalized with ScSec13-CFP at tER sites, and now tER localization was observed for PpSec12-GG but not for ScSec12-GG. Scale bar, 2 μm.
doi:10.1371/journal.pone.0031156.g002

from each strain were scored to determine if PpSec12 was strongly colocalized with PpSec16 at tER sites, or partially colocalized, or not colocalized (Fig. 5). In the control strain overexpressing full-length PpSec16, ~90% of the cells showed strong colocalization of PpSec12 with PpSec16. Deletion of the entire C-terminal fragment of PpSec16 resulted in <1% of the cells showing strong colocalization. Deletion of the nonconserved stretch (residues 1967–2340) had a mild effect, with ~80% of the cells showing strong colocalization, indicating that the nonconserved stretch within the C-terminal fragment plays some role in recruiting PpSec12 to tER sites. Deletion of the CTR (residues 2340–2550) had a dramatic effect, with only ~5% of the cells showing strong colocalization, indicating that the CTR plays a major role in recruiting PpSec12 to tER sites. Smaller deletions that truncated the CTR had intermediate effects. These results indicate that recruitment of PpSec12 to tER sites requires a C-terminal fragment of PpSec16, and that the bulk of this interaction is mediated by the CTR.

A C-terminal fragment of PpSec16 binds the cytosolic domain of PpSec12 *in vitro*

To determine if a C-terminal fragment of PpSec16 interacts directly with the cytosolic domain of PpSec12, we used bacterial expression to produce glutathione S-transferase (GST) fused to residues 1960–2550 of PpSec16. In parallel, we used bacterial expression to produce the cytosolic domain of PpSec12 with a C-terminal hexahistidine tag. Glutathione-agarose beads were incubated with a lysate from cells expressing either GST alone or GST-Sec16(1960–2550), and were subsequently incubated with a lysate from cells expressing PpSec12(cyto)-His6 (Fig. 6, "I"). The unbound material was collected (Fig. 6, "U"), and the bound protein (Fig. 6, "B") was eluted from the beads with glutathione. With GST alone, all of the PpSec12(cyto)-His6 was in the unbound fraction. With GST-PpSec16(1960–2550), none of the PpSec12(cyto)-His6 was in the unbound fraction and a significant amount could be eluted from the beads with glutathione. The remaining PpSec12(cyto)-His6 that had bound to GST-PpSec16(1960–2550) was apparently lost during the wash steps (data not shown), suggesting that this binding is readily reversible. These data provide evidence for a direct interaction between a C-terminal fragment of PpSec16 and the cytosolic domain of PpSec12.

Viability of *S. cerevisiae* does not require strong interaction of a Sec12 family member with Sec16

PpSec12 binds to the CTR of PpSec16, and Sed4 binds to the CTR of ScSec16, and the CTR is essential for life, so we wondered whether the interaction of a Sec12 family member with Sec16 is essential. To answer this question, we took advantage of the finding that PpSec12 can replace ScSec12 in *S. cerevisiae* [12]

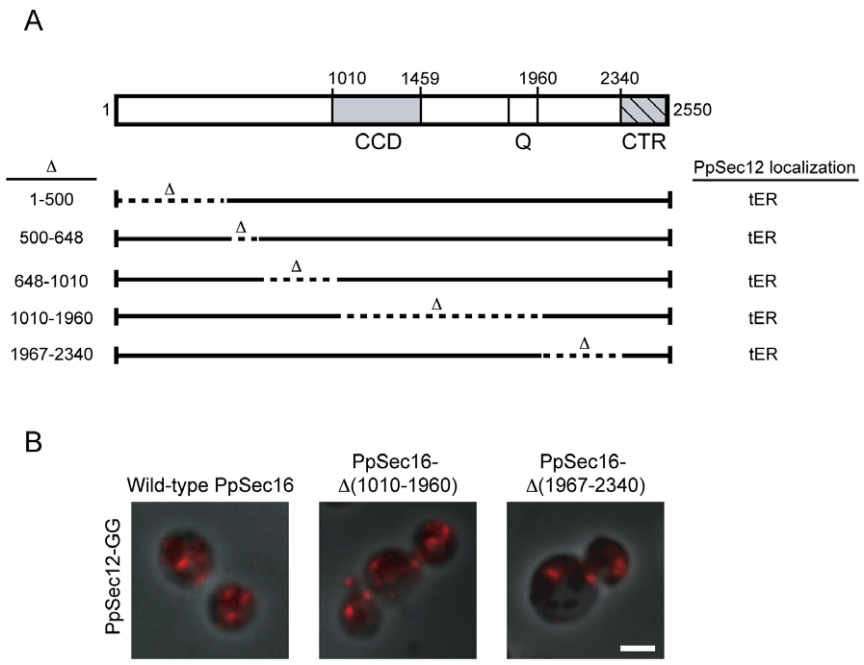

Figure 3. Effect of deleting nonessential PpSec16 regions on PpSec12 localization in *P. pastoris*. (A) Diagram of the domain organization of PpSec16. Shading indicates conserved regions while hatch marks indicate an essential region. CCD, central conserved domain; Q, glutamine-rich region; CTR, C-terminal conserved region. Deletions introduced by gene replacement are indicated. None of these deletions affected PpSec12 localization. (B) Representative images of PpSec12-GG localization in *P. pastoris* cells carrying the indicated deletions in PpSec16. Scale bar, 2 μm.
doi:10.1371/journal.pone.0031156.g003

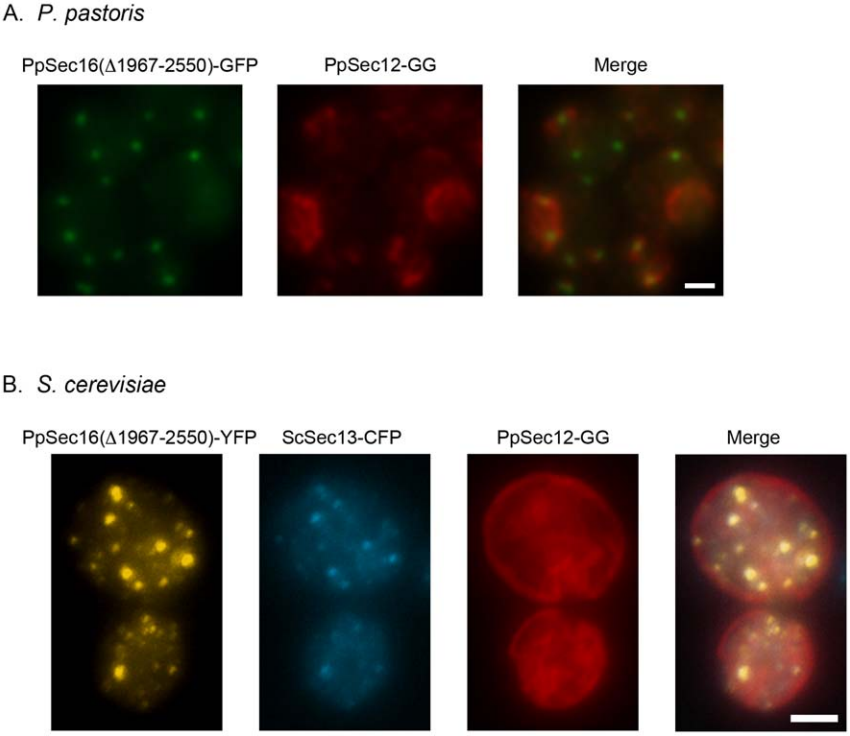

Figure 4. Requirement of the C-terminal portion of PpSec16 for tER localization of PpSec12 in both *P. pastoris* and *S. cerevisiae*. (A) As in Fig. 1, *P. pastoris* cells expressed PpSec12-GG from the endogenous promoter plus untagged Sec12 from the *AOX1* promoter, resulting in a high total level of PpSec12 expression. In the same cells, a truncated version of PpSec16 lacking residues 1967–2550 was tagged with GFP and overexpressed as a second copy using the *AOX1* promoter. PpSec16(Δ1967–2550)-GFP was found in punctate tER sites. By contrast to the result obtained when full-length PpSec16 was expressed (Fig. 1), PpSec12-GG was found in the general ER. (B) *S. cerevisiae* cells expressed the same truncated version of PpSec16 as in (A), except that the protein was tagged with YFP and was expressed under control of the *GAL10* promoter. As in Fig. 2B, ScSec13-CFP and PpSec12-GG were also expressed in these cells. By contrast to the result obtained when full-length PpSec16 was expressed (Fig. 2B), PpSec12-GG was found in the general ER. Scale bars, 2 μm.
doi:10.1371/journal.pone.0031156.g004

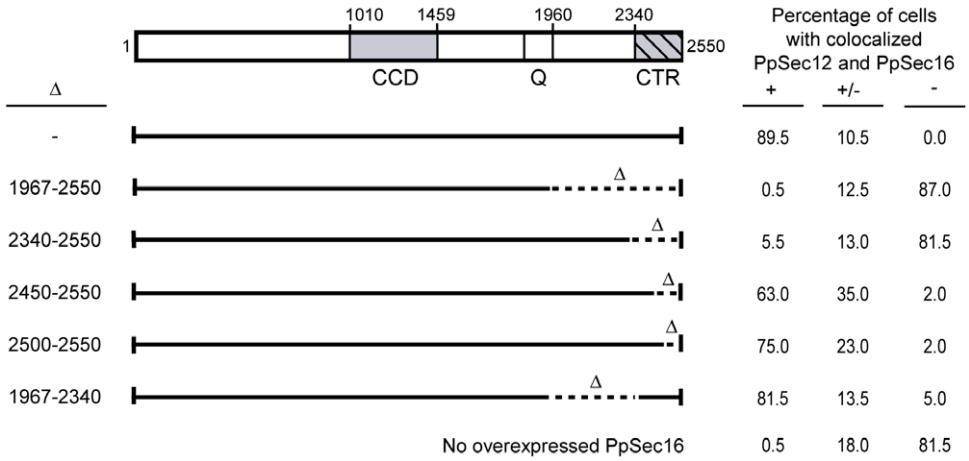

Figure 5. Requirement of the C-terminal portion of PpSec16 for recruiting overexpressed PpSec12 to tER sites. As in Fig. 1, PpSec16-GFP was overexpressed in *P. pastoris* cells overexpressing PpSec12, except that deletions were introduced as indicated near the C-terminus of PpSec16. Two hundred randomly chosen cells from each of the indicated *P. pastoris* strains were examined by immunofluorescence and scored for colocalization of PpSec12-GG with PpSec16-GFP. Cells in which nearly all of the PpSec12-GG overlapped with PpSec16-GFP were scored as having strong colocalization (+). Cells in which PpSec12-GG showed clear concentration in the PpSec16-GFP puncta but also showed prominent staining outside of these puncta were scored as having partial colocalization (+/−). Cells showing no visible concentration of PpSec12-GG in the PpSec16-GFP puncta were scored as having no colocalization (−). Colocalization was virtually abolished by deleting the entire C-terminal portion of PpSec16, and was strongly reduced by deleting only the C-terminal conserved region (CTR).
doi:10.1371/journal.pone.0031156.g005

even though PpSec12 binds to ScSec16 weakly or not at all (see above). The earlier Sec12 replacement was performed with a *SED4* strain of *S. cerevisiae*, but if PpSec12 replaced ScSec12 in a *sed4*Δ strain, there would be no strong interaction of a Sec12 family member with ScSec16. Therefore, the crucial question is whether PpSec12 can still replace ScSec12 in a *sed4*Δ strain of *S. cerevisiae*.

This experiment was performed using a plasmid shuffle approach. The chromosomal *SED4* and *SEC12* genes were deleted, and were replaced using two plasmids: a *URA3* plasmid carrying *SED4*, and a *LEU2* plasmid carrying either *ScSEC12* or *PpSEC12*. 5-fluoroorotic acid (5-FOA) was then used to select for cells that had lost the *URA3 SED4* plasmid. The cells that had lost the *URA3 SED4* plasmid were viable regardless of whether the *LEU2* plasmid carried *ScSEC12* or *PpSEC12* (Fig. 7). Thus, PpSec12 can replace ScSec12 even in a *sed4*Δ strain of *S. cerevisiae*, indicating that a strong interaction of a Sec12 family member with Sec16 is not essential for life in this yeast.

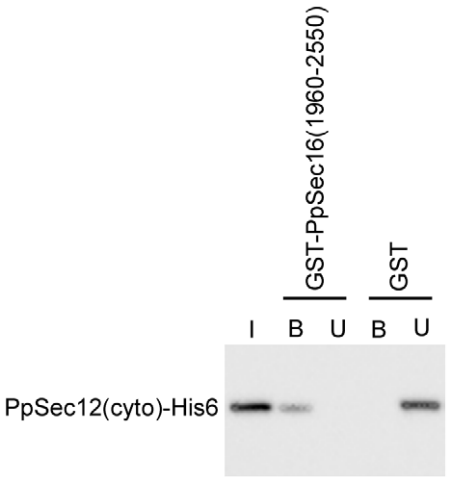

Figure 6. Biochemical interaction of the C-terminal portion of PpSec16 with the cytosolic domain of PpSec12. Glutathione-agarose beads were incubated with a bacterial lysate from cells expressing either GST alone, or GST fused to the C-terminal residues 1960–2550 of PpSec16. Sufficient lysate was used to saturate the binding sites on the glutathione-agarose. A second incubation was then performed with sub-saturating amounts of a bacterial lysate from cells expressing a hexahistidine-tagged version of the cytosolic domain of PpSec12 (PpSec12(cyto)-His6). The beads were centrifuged, and the unbound material in the supernatant was collected. Bound protein was eluted from the beads with 100 mM glutathione. I, input (100% relative to other lanes); U, unbound; B, bound. PpSec12(cyto)-His6 bound to the beads carrying GST-PpSec16(1960–2550) but not to the beads carrying GST alone.
doi:10.1371/journal.pone.0031156.g006

Human Sec12 localizes to tER sites and binds a C-terminal fragment of Sec16A

Concentration of Sec12 at tER sites has only been described in *P. pastoris*, so an obvious question is whether the Sec12–Sec16

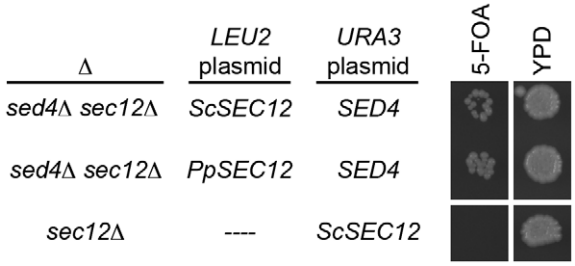

Figure 7. Viability of *S. cerevisiae* cells carrying *PpSEC12* as the only gene from the *SEC12* family. A plasmid shuffle was performed in *sed4*Δ *sec12*Δ cells, with *SED4* in a *URA3* plasmid plus either *ScSEC12* (top row) or *PpSEC12* (middle row) in a *LEU2* plasmid. Both strains grew on rich media (YPD) and also on media containing 5-FOA, indicating that *PpSEC12* could replace *ScSEC12* even in the absence of *SED4*. As a control, *sec12*Δ cells carrying *ScSEC12* on a *URA3* plasmid were plated on the same media, and no growth was seen in the presence of 5-FOA.
doi:10.1371/journal.pone.0031156.g007

interaction in this yeast is of broader significance. To address this issue, we revisited the localization of human Sec12. It was previously reported that human Sec12 was found throughout the ER [27], but the immunofluorescence data were ambiguous. We therefore repeated this experiment using an improved immunofluorescence protocol [28]. The labeling of human Sec12 was consistent with localization to the ER network, but punctate Sec12 labeling was also seen in tER sites (Fig. 8A) that

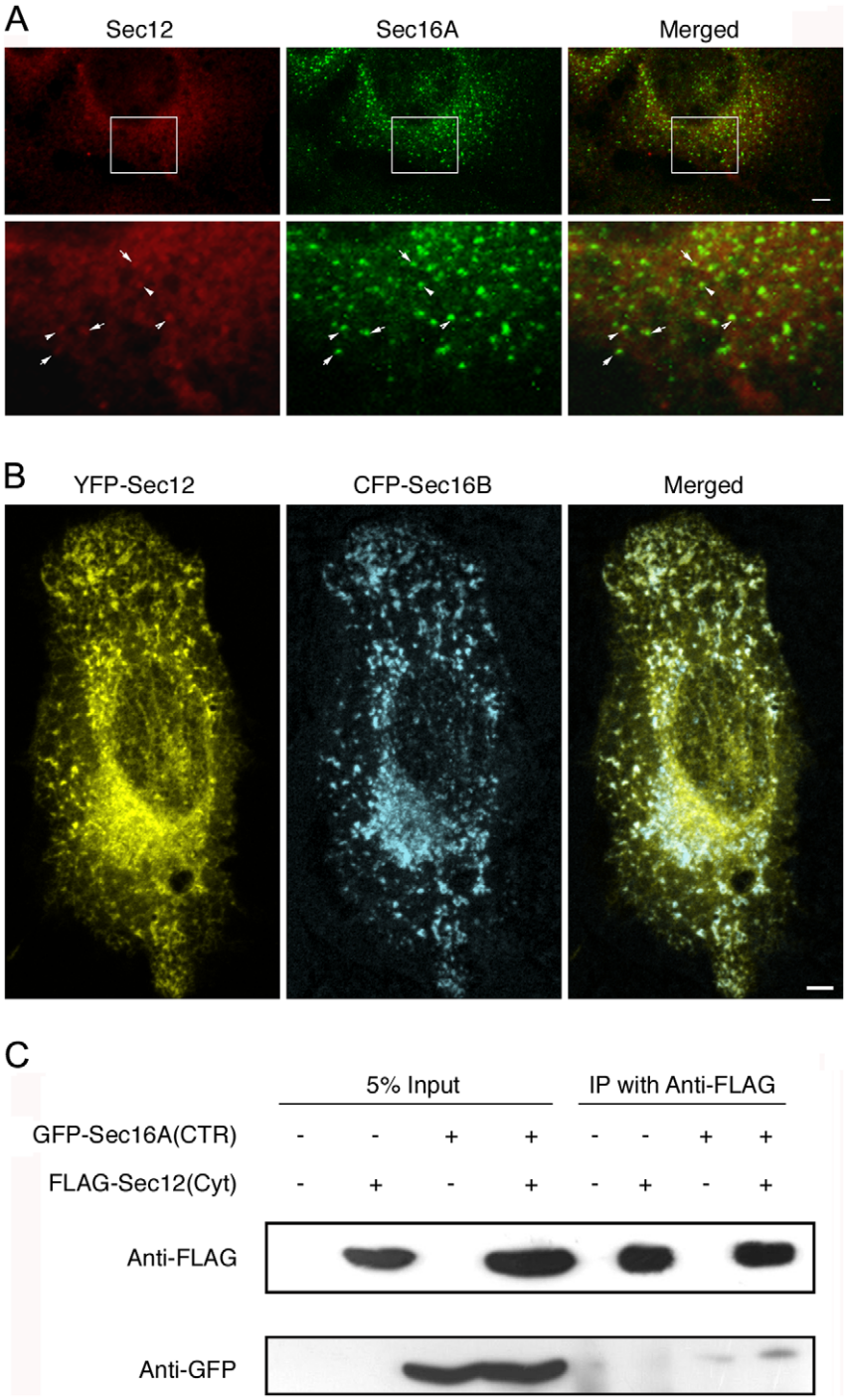

Figure 8. Colocalization of mammalian Sec12 with Sec16A at tER sites. (A) U2OS human osteosarcoma cells were subjected to immunofluorescence as described [28] using commercial antibodies against human Sec12 and Sec16A. Scale bar, 2 μm. (B) Plasmids encoding YFP-tagged full-length human Sec12 and CFP-tagged full-length Sec16B were co-transfected into U2OS cells. The cells were imaged at 16 h post-transfection, a time point that yielded relatively low expression levels. Scale bar, 2 μm. (C) HeLa cells were transfected where indicated with plasmids encoding either monomeric GFP fused to a C-terminal region (''CTR'') of human Sec16A (residues 1909–2332), or an N-terminally triple-FLAG-tagged cytosolic domain (''Cyt'') of human Sec12 (residues 1–386). At 24 h post-transfection, the cells were lysed and the lysate was subjected to immunoprecipitation (''IP'') with anti-FLAG antibody. The immunoprecipitated material and 5% of the lysate (''5% Input'') was subjected to SDS-PAGE followed by immunoblotting with either anti-FLAG or anti-GFP antibody.
doi:10.1371/journal.pone.0031156.g008

contained Sec16A [17], which is the mammalian ortholog of yeast Sec16.

This result was confirmed by expressing GFP-tagged human Sec12. At various expression levels, GFP-Sec12 signal was present in the general ER but punctate structures were also visible (Fig. S2). As the expression level increased, the punctate structures became progressively larger (Fig. S2). This effect is reminiscent of the exaggerated tER sites seen with simultaneous overexpression of PpSec12 and PpSec16 in *P. pastoris* (see Figs. 1 and S1), except that in mammalian cells, overexpression of Sec12 alone suffices to generate enlarged structures. To verify that the punctate structures were tER sites, YFP-tagged Sec12 was co-expressed with CFP-tagged Sec16B, which is a tER-localized Sec16 homolog [17]. A large fraction of the YFP-Sec12 puncta overlapped with the CFP-Sec16B puncta at both low and high expression levels (Fig. 8B, and data not shown). We conclude that Sec12 is concentrated at tER sites in mammalian cells.

Sec16A contains a C-terminal region that appears to be related to the CTR of yeast Sec16 [17], suggesting that this domain of Sec16A may be responsible for recruiting human Sec12 to tER sites. As an initial test of this idea, we expressed in HeLa cells a FLAG-tagged cytosolic domain of human Sec12 together with a GFP-tagged C-terminal region of Sec16A. When the FLAG-tagged Sec12 fragment was immunoprecipitated, we reproducibly observed co-immunoprecipitation of a small amount of the GFP-tagged Sec16A fragment (Figure 8C). This result is consistent with a possible role of the C-terminal region of Sec16A in recruiting human Sec12 to tER sites.

Discussion

The cytosolic domain of PpSec12 interacts with a tER-localized partner protein, and this interaction is readily reversible [12]. A likely candidate for the partner protein was Sec16, which binds to the cytosolic surface of the ER membrane at tER sites [8,14]. Indeed, we have now obtained two lines of evidence that PpSec16 recruits PpSec12 to tER sites. The first line of evidence comes from overexpression studies in *P. pastoris*. When PpSec12 is overexpressed, most of the molecules are delocalized to the general ER because the tER-localized partner protein has been saturated [12]. We showed that simultaneous overexpression of PpSec16 suppresses the delocalization of overexpressed PpSec12, as would be expected if PpSec16 is the saturable partner protein. The second line of evidence comes from heterologous expression studies in *S. cerevisiae*. When PpSec12 is expressed in *S. cerevisiae*, it is found in the general ER, presumably because the interaction with ScSec16 is too weak to confer tER localization. We showed that simultaneous expression of PpSec16 in *S. cerevisiae* results in recruitment of PpSec12 to tER sites, consistent once again with the idea that PpSec16 is the partner protein for PpSec12.

In *S. cerevisiae*, the Sec12-like protein Sed4 binds to a C-terminal fragment of ScSec16 [24]. Similarly, we showed that PpSec12 binds to a C-terminal fragment of PpSec16. When this C-terminal fragment of PpSec16 is deleted, the truncated PpSec16 fails to recruit PpSec12 to tER sites either in *P. pastoris* or in *S. cerevisiae*. Biochemical pull-down experiments with recombinant proteins confirmed that a C-terminal fragment of PpSec16 can interact directly with the cytosolic domain of PpSec12. We found that the conserved C-terminal region (CTR) of PpSec16 is the major site of interaction with PpSec12, although a nonconserved stretch upstream of the CTR contributes to this interaction.

Deletion of the CTR is lethal [14], so an important question is whether the Sec12–Sec16 interaction is essential for life. Although we cannot yet answer this question with certainty, the data suggest that the Sec12–Sec16 interaction is nonessential. We found that PpSec12 binds weakly or not at all to ScSec16, and yet PpSec12 can replace ScSec12 in *S. cerevisiae*, even when *SED4* has been deleted to ensure that PpSec12 is the only Sec12 family member in the cells. Thus, the CTR probably has an essential function apart from binding Sec12. The CTR interacts with Sec23 in both yeast and mammalian cells [14,17], so this Sec23 interaction may be the essential function of the CTR, with the Sec12 interaction playing a secondary role. This idea could be tested by identifying point mutations that selectively disrupt either the Sec12-CTR interaction or the Sec23-CTR interaction.

How conserved is the Sec12–Sec16 interaction? We showed here that Sec12 is concentrated at tER sites in human cells, and that the cytosolic domain of human Sec12 is capable of associating with the C-terminal region of human Sec16A. Recently, a Sec12–Sec16 interaction was also detected in *Caenorhabditis elegans* [29]. The combined data suggest that Sec12 has a conserved interaction with Sec16. This interaction may play a previously unsuspected role in tER organization, because exaggerated tER sites are seen upon simultaneous overexpression of PpSec12 and PpSec16 in *P. pastoris* or upon overexpression of human Sec12 in cultured mammalian cells.

Does the Sec12–Sec16 interaction modulate Sec12 function, or Sec16 function, or both? One possibility is that this interaction boosts the efficiency of COPII vesicle formation by concentrating Sec12 at tER sites, thereby enhancing local activation of Sar1 [30]. On the other hand, *S. cerevisiae* Sed4 binds Sec16 but lacks detectable guanine nucleotide exchange activity for Sar1 [24,31], suggesting that the Sed4–Sec16 interaction serves to modulate Sec16 function. In support of this idea, overexpression of Sed4 suppresses temperature-sensitive *sec16* mutations [24]. We infer that Sed4 and Sec12 may share the ability to influence Sec16 function.

It is noteworthy that the CTR of Sec16 interacts both with Sec12, which is the guanine nucleotide exchange factor for Sar1, and with Sec23, which is the GTPase activating protein for Sar1. An intriguing question is whether the Sec12–Sec16 and Sec23–Sec16 interactions are mutually exclusive and perhaps antagonistic. Further biochemical and structural studies are needed to understand the complex interplay between Sec16 and the COPII pathway.

Materials and Methods

Fluorescence microscopy

Immunofluorescence microscopy was carried out as previously described [11,12] except that the fixed cells were incubated in lyticase for 30 min at 30°C. For the yeast studies, samples were viewed with a Zeiss Axioplan 2 epifluorescence microscope using a 1.4-NA 100X Plan Apo objective, and images were captured with a Hamamatsu digital camera followed by processing in Adobe Photoshop to adjust brightness and contrast. For the mammalian cell studies, samples were viewed with a Zeiss LSM 510 META confocal microscope.

Expression in *P. pastoris*

All *P. pastoris* strains were derivatives of PPY12 [32]. *P. pastoris* cells were transformed with linearized integrating vectors using electroporation [33]. The constructs used in this study are documented with annotated sequence files in Sequence Archive S1. Overexpression in *P. pastoris* was achieved using the strong methanol-inducible *AOX1* promoter as previously described [12]. Briefly, cells were grown overnight at 30°C in 5 mL of glycerol-containing SYG medium. This medium was then removed by

filtration, and the cells were rinsed with methanol-containing SYM medium and then resuspended in SYM. After 8 h of growth with shaking in SYM, cells were either fixed and processed for immunofluorescence, or visualized directly by fluorescence microscopy. We showed previously that under these conditions, PpSec12 is overexpressed ~190-fold [12].

Tagging of endogenous PpSec12 was achieved as follows. A BamHI fragment containing a modified 3′ portion of *PpSEC12* [12] was inserted into the BamHI site of pUC19-HIS4 [33] to create pLY051. This plasmid was then linearized with StyI and integrated at the *SEC12* locus via homologous recombination to tag PpSec12 with a Glu-Glu epitope tag, yielding strain EM19. Regulated expression of PpSec12 was achieved as follows. pEM04 was created from pIB4 [33] by replacing most of *P. pastoris HIS4* with *P. pastoris ARG4*. A gene encoding PpSec12-GG [12] was subcloned between the EcoRI and PstI sites of pEM04 to create pEM13. This plasmid was linearized by partial digestion with PflMI and then integrated at the *SEC12* locus to yield strain EM15, which has two tandem copies of *PpSEC12*: one copy that encodes PpSec12-GG under control of the endogenous promoter, and a second copy that encodes untagged PpSec12 under control of the *AOX1* promoter.

To label endogenous PpSec16 with monomeric enhanced GFP (mEGFP) [34], a PCR fragment spanning from codon 1178 of *PpSEC16* to ~400 bp downstream of the stop codon was PCR amplified and inserted into the SmaI site of pUC19-HIS4 to create pME004. Then a fragment of *PpSEC16* fused to *mEGFP* was excised from pUC19-ARG4-S16C-mEGFP [8] using BspEI and XmnI, and inserted between the BspEI and SfoI sites of pME004 to create pME008. This plasmid was linearized with PshAI and integrated at the *SEC16* locus of strain EM15, yielding strain EM34.

Because full-length *PpSEC16* is toxic to *E. coli*, the *PpSEC16-GFP* overexpression construct was assembled by *in vitro* ligation as previously described [8] using plasmids pEM08, which contains the *AOX1* promoter followed by codons 1022–2550 of *PpSEC16* followed by *mEGFP*, and pEM12, which contains the *AOX1* promoter followed by codons 1–1678 of *PpSEC16*. A ligation product of fragments derived from pEM08 and pEM12 was integrated at the *HIS4* locus of strain EM15, yielding strain EM17. Two methods were used to create pEM08-type plasmids encoding deletions in a C-terminal fragment of PpSec16. In the first method, portions near the 3′ end of *PpSEC16* were deleted in pEM08 by primer-directed mutagenesis to create pEM48 (lacking codons 1967–2340), pEM49 (lacking codons 2341–2550), pEM50 (lacking codons 2501–2550), and pEM55 (lacking codons 2451–2550). In the second method, a pIB4 derivative was created in which codons 1505–1967 of *PpSEC16* were followed by *mEGFP* to create pEM43. pEM43, pEM48, pEM49, pEM50, and pEM55 were each used in an *in vitro* ligation reaction with pEM12, and the products were integrated at the *HIS4* locus of strain EM15, yielding strains EM16, EM25, EM26, EM27, and EM38, respectively.

Deletion of nonessential *PpSEC16* regions was accomplished by integrating linearized deletion constructs at the *PpSEC16* locus of strain EM19. This approach employed derivatives of plasmids pME005 and pLY100, as follows. pME005 was created by inserting codons 1178–2550 of *PpSEC16* plus ~400 bp of downstream sequence into the SmaI site of pUC19-ARG4 [11]. Primer-directed mutagenesis of pME005 deleted codons 1967–2340 to create pEM54, which was linearized with PshAI for integration. Alternatively, a BstEII fragment spanning codons 682–1633 of *PpSEC16* was inserted into the BstEII site of pME005, and then primer-directed mutagenesis deleted codons 1010–1960 to create pLY080, which was linearized by partial digestion with XbaI for integration. pLY100 was created by inserting codons 1–1461 of *PpSEC16* plus ~500 bp of upstream sequence into pUC19-ARG4. Primer-directed mutagenesis of pLY100 deleted either codons 500–648 to create pLY114, or codons 648–1010 to create pLY115, or codons 1–500 to create pLY116. These three plasmids were linearized with BssHII for gene replacement at the *PpSEC16* locus.

A strain expressing Sec13-DsRed as well as overexpressing PpSec12-GG and PpSec16-GFP was made as follows. The *KanMX* gene [35] was PCR amplified and inserted into the SspI site of pUC19 to create pUC19-KanMX. An EcoRI-XmnI fragment encoding a C-terminal portion of Sec13 fused to DsRed-Monomer was subcloned from pUC19-ARG4-Sec13-DsRed.M1 [8] into pUC19-KanMX to create pEM42. This plasmid was then linearized using MscI and integrated into the *SEC13* locus of strain EM17, yielding strain EM30.

Expression in *S. cerevisiae*

All *S. cerevisiae* strains were derivatives of JK9-3d [36]. The constructs used in this study are documented with annotated sequence files in Sequence Archive S1. Overexpression in *S. cerevisiae* was achieved using the strong galactose-indiciuble *GAL10* promoter [37]. Induction was carried out as follows. Cells were grown overnight in synthetic media containing dextrose. When the culture reached an OD_{600} of ~0.4, the cells were transferred to synthetic media containing galactose, grown for 4.5 h, and then fixed and processed for immunofluorescence.

Heterologous expression of *P. pastoris* genes in *S. cerevisiae* was performed as follows. The starting strain carried a deletion of the endogenous *SEC12* gene, with the cells being kept alive by a 2μ *URA3* plasmid [38] encoding a Glu-Glu-tagged Sec12 protein under control of the *ScSEC12* promoter. This plasmid was either YEplac195-ScSec12-GG, which encodes *ScSEC12-GG*, or YEplac195-PpSec12-GG, which encodes *PpSEC12-GG* [12]. The chromosomal *ScSEC13* gene in these strains was then tagged with a triple-CFP cassette using pUC19-URA3-SEC13-CFPx3 that had been linearized with BstEII, yielding strains LY05 and LY06. Additional regulated expression of PpSec16-YFP was achieved using the *GAL10* promoter. Because the full-length *PpSEC16* gene is toxic to *E. coli*, the PpSec16-YFP plasmid was constructed by *in vitro* ligation of fragments from pEM45, which encodes a 5′ portion of *PpSEC16*, and pEM46, which encodes a 3′ portion of *PpSEC16* fused to a triple-YFP cassette. Strains LY03 and LY04 expressed ScSec13-3xCFP, PpSec16-3xYFP, and either ScSec12-GG or PpSec12-GG, respectively.

GST pull-down and immunoblotting

To express GST fused to a C-terminal fragment of PpSec16, codons 1960–2550 of *PpSEC16* were subcloned between the XmaI and XhoI sites of pGEX-4T-1 (GE Healthcare) to create pME107. To express the cytosolic domain of PpSec12 fused to a hexahistidine tag, codons 1–337 of PpSEC12 were amplified by PCR and inserted between the NdeI and XhoI sites of pET21a(+) (Novagen), yielding pET21a(+)-PpSec12(cyto). pME107 and pET21a(+)-PpSec12(cyto) were each transformed into *E. coli* Rosetta cells (Novagen) containing the pLysS plasmid. For protein expression, a 50-mL culture of cells was grown at 37°C with shaking for 5 h, and then protein expression was induced with 1 mM isopropyl-β-D-thiogalactopyranoside for a further 4 h.

Cell lysis and GST pull-down were conducted using the Thermo Scientific Pierce ProFound Pull-Down GST Protein:Protein Interaction kit. A brief protocol follows. All incubations and washes were performed using a 1:1 mixture of ProFound Lysis

Buffer and 1 M Tris-buffered saline. Cell pellets were lysed for 30 minutes in the presence of Benzonase (Novagen), and lysates were clarified by centrifugation at 100,000×g to obtain the Input fraction. Glutathione-agarose beads were incubated for 1 h at 4°C with clarified lysate from cells expressing GST-Sec16(1960–2550). The beads were washed, and then incubated for 1 h at 4°C with clarified lysate from cells expressing PpSec12(cyto)-His6. At this point the beads were spun in a column and the flow-through was collected as the Unbound fraction. The beads were then washed, followed by a 10-minute incubation at room temperature with 100 mM glutathione to elute the Bound fraction.

Equivalent amounts of the Input, Bound, and Unbound fractions were boiled in SDS-PAGE sample buffer and loaded onto an SDS-PAGE gel. Separated proteins were transferred to PVDF membranes, and the hexahistidine-tagged PpSec12 cytosolic domain was detected using a 6-His monoclonal antibody (Covance, catalog no. MMS-156P) and the Supersignal West Femto kit (Pierce).

Plasmid shuffle experiment

pEM60 was made by ligating a PCR product containing *SED4*, including the promoter and terminator, into the *CEN URA3* plasmid YCplac33 [38]. pEM61 and pEM62 were created by subcloning *ScSEC12-GG* or *PpSEC12-GG*, respectively, together with the *ScSEC12* promoter [12] into the 2 μm *LEU2* plasmid YEplac181 [38].

Strains EM59 to EM62 were created by first deleting one copy of the *SED4* coding sequence in a diploid strain in which one copy of *ScSEC12* had been replaced by *KanMX* [12]. To delete *SED4*, the cells were transformed with a PCR product containing a hygromycin B resistance gene [39] flanked by sequences upstream and downstream of the *SED4* coding sequence, with selection on rich medium containing 200 μg/mL hygromycin B (US Biologicals). Next, pEM60 plus either pEM61 or pEM62 were introduced to create strains EM54 and EM55, respectively. These strains were then sporulated and subjected to tetrad dissection. A sporulation defect was observed, with two- and three-spore tetrads outnumbering four-spore tetrads, probably reflecting a role for *SED4* during sporulation [40]. Haploid clones were tested on selective media to assess the presence of plasmids and drug resistance markers.

Survival in the absence of *SED4* was tested as follows. Strains EM59 to EM62, plus a control strain in which a *ScSEC12* deletion was rescued by YEplac195-ScSEC12-GG, were grown to mid-log phase in rich medium overnight to give the cells an opportunity to lose the *URA3* plasmids. Equal numbers of cells were then spotted onto plates containing 1 g/L 5-FOA (US Biologicals). Plates were incubated in the dark at 30°C for several days to allow for growth of colonies lacking the *URA3* plasmids.

Analysis of mammalian Sec12 and Sec16

For immunofluorescence, human Sec12 was detected using an affinity purified goat anti-human PREB antibody from R&D Systems (cat. #AF5557, diluted 1:50), and Sec16A was detected using a rabbit polyclonal anti-KIAA0310 antibody from Bethyl Laboratories (cat. #BL2467, diluted 1:50). These primary antibodies were detected with Alexa Fluor 594 donkey anti-goat and Alexa Fluor 488 chicken anti-rabbit IgG secondary antibodies (Invitrogen), respectively. For immunoblotting, GFP was detected using a rabbit polyclonal antibody (Abcam cat. #ab290, diluted 1:1000), and the FLAG epitope was detected using a mouse monoclonal antibody (Sigma cat. #F1804, diluted 1:2000).

For expression of fluorescently tagged proteins in U2OS cells, full-length human Sec12 was N-terminally tagged with monomeric enhanced GFP (mEGFP) or YFP (mEYFP), and full-length Sec16B was N-terminally tagged with monomeric enhanced CFP (mECFP) [34]. The human Sec12 and Sec16B genes were amplified from cDNAs by PCR and subcloned into pEGFP-C1 (Clontech) downstream of the EGFP gene, followed by replacement of EGFP with either mEGFP or mEYFP or mECFP. Sec16B is identical to the gene that we previously designated Sec16S [17]. These constructs are documented with annotated sequence files in Sequence Archive S1.

For co-immunoprecipitation, tagged fragments of human Sec12 and Sec16A [17] were expressed transiently from the CMV promoter. The cytosolic domain of human Sec12 (codons 1–386) was amplified from a cDNA by PCR and subcloned into pCMV-3FLAG-1A (Stratagene) downstream of a triple-FLAG cassette. A C-terminal region of Sec16A (codons 1909–2332) was amplified from a cDNA by PCR and subcloned into pmEGFP-C1, which is a derivative of pEGFP-C1 (Clontech) carrying the monomerizing A206K mutation [34]. In the case of Sec16A, which we previously designated Sec16L [17], our original description of the gene overlooked the first 178 codons [18], so we added those codons for the numbering used here. Because our cDNA lacks the 75-bp intron between the 28th and 29th exons [17], our numbering for the C-terminal fragment of Sec16A differs by 25 amino acids from the numbering used elsewhere [18]. These constructs are documented with annotated sequence files in Sequence Archive S1. Plasmids were transfected into HeLa cells using calcium phosphate transfection. The cells were harvested at 24 h post-transfection, and lysed in 50 mM Tris-HCl, pH 7.9, 50 mM NaCl, 1 mM phenylmethylsulfonyl fluoride, 0.5% NP-40 supplemented with the Complete mini protease inhibitor cocktail (Roche). Approximately 3 mg of cell lysate was used for each immunoprecipitation. Protein A-agarose beads (Calbiochem) were pre-blocked with 1% bovine serum albumin and then incubated at 4°C with polyclonal rabbit anti-FLAG antibody (Sigma). Immunoprecipitation was performed overnight at 4°C. Then the beads were washed three times with 20 mM Na^+-HEPES, pH 7.9, 100 mM NaCl, 0.1% NP-40. Finally, bound material was eluted by boiling in SDS-PAGE sample buffer, followed by SDS-PAGE, transfer to nitrocellulose, and immunoblotting [17].

Supporting Information

Figure S1 Colocalization of PpSec16 with PpSec13 in *P. pastoris* cells overexpressing both PpSec12 and PpSec16. The method of Fig. 1 was used to achieve simultaneous overexpression of PpSec12 and GFP-tagged PpSec16. In addition, PpSec13 was tagged with DsRed by gene replacement. The overexpressed PpSec16-GFP colocalized with PpSec13-DsRed, confirming that the structures labeled with PpSec16-GFP were exaggerated tER sites. Scale bar, 2 μm.
(TIF)

Figure S2 Localization of GFP-tagged human Sec12 at different expression levels. A plasmid encoding GFP-tagged full-length human Sec12 was transfected into U2OS human osteosarcoma cells. The cells were imaged at either (A) 12 h, (B) 24 h, or (C, D) 36 h post-transfection. Representative images are shown for cells expressing GFP-Sec12 at (A) low, (B) moderate, (C) high, and (D) very high levels. These cells were imaged at different exposure levels according to their fluorescence intensities. As the expression level of GFP-Sec12 increased, the punctate structures became progressively larger. Scale bar, 5 μm.
(TIF)

Sequence Archive S1 Annotated sequence files for the constructs used in this study. A compressed folder contains GenBank-style sequence files for the relevant constructs.
(RAR)

Acknowledgments

We would like to thank members of the Glick and Bhattacharyya laboratories for helpful discussions and advice. Special thanks to Jon Soderholm for plasmid pET21a(+)-PpSec12(cyto), to Masatoshi Esaki for plasmids pME004, pME008, pME010, and pME107, to Rita Strack for assisting with two control experiments, and to the members of the ACTREC Digital Imaging Facility for help with microscopy.

Author Contributions

Conceived and designed the experiments: DB BSG. Performed the experiments: EAM MB YL. Analyzed the data: EAM MB YL DB BSG. Wrote the paper: EAM MB YL DB BSG.

References

1. Hughes H, Stephens DJ (2008) Assembly, organization, and function of the COPII coat. Histochem Cell Biol 129: 129–151.
2. Lee MC, Miller EA (2007) Molecular mechanisms of COPII vesicle formation. Semin Cell Dev Biol 18: 424–434.
3. Lukyanov KA, Serebrovskaya EO, Lukyanov S, Chudakov DM (2010) Fluorescent proteins as light-inducible photochemical partners. Photochem Photobiol Sci 9: 1301–1306.
4. Bannykh SI, Balch WE (1997) Membrane dynamics at the endoplasmic reticulum-Golgi interface. J Cell Biol 138: 1–4.
5. Budnik A, Stephens DJ (2009) ER exit sites–localization and control of COPII vesicle foramtion. FEBS Lett 583: 3796–3803.
6. Palade G (1975) Intracellular aspects of the process of protein synthesis. Science 189: 347–358.
7. Bevis BJ, Hammond AT, Reinke CA, Glick BS (2002) *De novo* formation of transitional ER sites and Golgi structures in *Pichia pastoris*. Nat Cell Biol 4: 750–756.
8. Connerly PL, Esaki M, Montegna EA, Strongin DE, Levi S, et al. (2005) Sec16 is a determinant of transitional ER organization. Curr Biol 15: 1439–1447.
9. Barlowe C, Schekman R (1993) *SEC12* encodes a guanine-nucleotide-exchange factor essential for transport vesicle budding from the ER. Nature 365: 347–349.
10. Russell C, Stagg SM (2010) New insights into the structural mechanisms of the COPII coat. Traffic 11: 303–310.
11. Rossanese OW, Soderholm J, Bevis BJ, Sears IB, O'Connor J, et al. (1999) Golgi structure correlates with transitional endoplasmic reticulum organization in *Pichia pastoris* and *Saccharomyces cerevisiae*. J Cell Biol 145: 69–81.
12. Soderholm J, Bhattacharyya D, Strongin D, Markovitz V, Connerly PL, et al. (2004) The transitional ER localization mechanism of *Pichia pastoris* Sec12. Dev Cell 6: 649–659.
13. Nishikawa S, Nakano A (1993) Identification of a gene required for membrane protein retention in the early secretory pathway. Proc Natl Acad Sci USA 90: 8179–8183.
14. Espenshade P, Gimeno RE, Holzmacher E, Teung P, Kaiser CA (1995) Yeast *SEC16* gene encodes a multidomain vesicle coat protein that interacts with Sec23p. J Cell Biol 131: 311–324.
15. Gimeno RE, Espenshade P, Kaiser CA (1996) COPII coat subunit interactions: Sec24p and Sec23p bind to adjacent regions of Sec16p. Mol Biol Cell 7: 1815–1823.
16. Shaywitz DA, Espenshade PJ, Gimeno RE, Kaiser CA (1997) COPII subunit interactions in the assembly of the vesicle coat. J Biol Chem 272: 25413–25416.
17. Bhattacharyya D, Glick BS (2007) Two mammalian Sec16 homologs have nonredundant functions in ER export and transitional ER organization. Mol Biol Cell 18: 839–849.
18. Hughes H, Budnik A, Schmidt K, Palmer KJ, Mantell J, et al. (2009) Organisation of human ER-exit sites: requirements for the localisation of Sec16 to transitional ER. J Cell Sci 122: 2924–2934.
19. Iinuma T, Shiga A, Nakamoto K, O'Brien MB, Aridor M, et al. (2007) Mammalian Sec16/p250 plays a role in membrane traffic from the endoplasmic reticulum. J Biol Chem 282: 17632–17639.
20. Ivan V, de Voer G, Xanthakis D, Spoorendonk KM, Kondylis V, et al. (2008) *Drosophila* Sec16 mediates the biogenesis of tER sites upstream of Sar1 through an arginine-rich motif. Mol Biol Cell 19: 4352–4365.
21. Watson P, Townley AK, Koka P, Palmer KJ, Stephens DJ (2006) Sec16 defines endoplasmic reticulum exit sites and is required for secretory cargo export in mammalian cells. Traffic 7: 1678–1687.
22. Papanikou E, Glick BS (2009) The yeast Golgi apparatus: insights and mysteries. FEBS Lett 583: 3746–3751.
23. Shindiapina P, Barlowe C (2010) Requirements for transitional endoplasmic reticulum site structure and function in *Saccharomyces cerevisiae*. Mol Biol Cell 21: 1530–1545.
24. Gimeno RE, Espenshade P, Kaiser CA (1995) *SED4* encodes a yeast endoplasmic reticulum protein that binds Sec16p and participates in vesicle formation. J Cell Biol 131: 325–338.
25. Hardwick KG, Boothroyd JC, Rudner AD, Pelham HR (1992) Genes that allow yeast cells to grow in the absence of the HDEL receptor. EMBO J 11: 4187–4195.
26. Payne WE, Kaiser CA, Bevis BJ, Soderholm J, Fu D, et al. (2000) Isolation of *Pichia pastoris* genes involved in ER-to-Golgi transport. Yeast 16: 979–993.
27. Weissman JT, Plutner H, Balch WE (2001) The mammalian guanine nucleotide exchange factor mSec12 is essential for activation of the Sar1 GTPase directing endoplasmic reticulum export. Traffic 2: 465–475.
28. Bhattacharyya D, Hammond AT, Glick BS (2010) High-quality immunofluorescence of cultured cells. In: Economou A, ed. Protein Secretion Methods and Protocols. New York: Humana Press. pp 403–410.
29. Witte K, Schuh AL, Hegermann J, Sarkeshik A, Mayers JR, et al. (2011) TGF-1 function in protein secretion and oncogenesis. Nat Cell Biol 13: 550–558.
30. Kaddoum L, Magdeleine E, Waldo GS, Joly E, Cabantous S (2010) One-step split GFP staining for sensitive protein detection and localization in mammalian cells. Biotechniques 49: 727–728.
31. Cantabous S, Terwilliger TC, Waldo GS (2005) Protein tagging and detection with engineered self-assembling fragments of green fluorescent protein. Nat Biotechnol 23: 102–107.
32. Gould SJ, McCollum D, Spong AP, Heyman JA, Subramani S (1992) Development of the yeast *Pichia pastoris* as a model organism for a genetic and molecular analysis of peroxisome assembly. Yeast 8: 613–628.
33. Sears IB, O'Connor J, Rossanese OW, Glick BS (1998) A versatile set of vectors for constitutive and regulated gene expression in *Pichia pastoris*. Yeast 14: 783–790.
34. Zacharias DA, Violin JD, Newton AC, Tsien RY (2002) Partitioning of lipid-modified monomeric GFPs into membrane microdomains of live cells. Science 296: 913–916.
35. Wach A (1996) PCR-synthesis of marker cassettes with long flanking homology regions for gene disruptions in *S. cerevisiae*. Yeast 12: 259–265.
36. Kunz J, Schneider U, Deuter-Reinhard M, Movva NR, Hall MN (1993) Target of rapamycin in yeast, TOR2, is an essential phosphatidylinositol kinase homolog required for G1 progression. Cell 73: 585–596.
37. Johnston M, Davis RW (1984) Sequences that regulate the divergent *GAL1–GAL10* promoter in *Saccharomyces cerevisiae*. Mol Cell Biol 4: 1440–1448.
38. Gietz RD, Sugino A (1988) New yeast-*Escherichia coli* shuttle vectors constructed with in vitro mutagenized yeast genes lacking six-base pair restriction sites. Gene 74: 527–534.
39. Goldstein AL, McCusker JH (1999) Three new dominant drug resistance cassettes for gene disruption in *Saccharomyces cerevisiae*. Yeast 15: 1541–1553.
40. Deutschbauer AM, Williams RM, Chu AM, Davis RW (2002) Parallel phenotypic analysis of sporulation and postgermination growth in *Saccharomyces cerevisiae*. Proc Natl Acad Sci USA 99: 15530–15535.